RAA 2023 Vol. **23** No. **03**, A02

http://www.raa-journal.org *http://iopscience.iop.org/raa*

***R**esearch in*
***A**stronomy and*
***A**strophysics*

FAST pulsar database: I. Polarization profiles of 682 pulsars

P. F. Wang[1,2], J. L. Han[1,2], J. Xu[1,2], C. Wang[1,2], Y. Yan[1,2], W. C. Jing[1,2], W. Q. Su[1,2], D. J. Zhou[1,2], and T. Wang[1,2]

[1] National Astronomical Observatories, Chinese Academy of Sciences, 20A Datun Road, Chaoyang District, Beijing 100101, China; *pfwang@nao.cas.cn; hjl@nao.cas.cn*

[2] School of Astronomy, University of Chinese Academy of Sciences, Beijing 100049, China;

Received 2022 XXX; accepted 2022 XXX

Abstract Pulsar polarization profiles are very basic database for understanding the emission processes in pulsar magnetosphere. After careful polarization calibration of the 19-beam L-band receiver and verification of beam-offset observation results, we obtain polarization profiles of 682 pulsars from observations by the Five-hundred-meter Aperture Spherical radio Telescope (FAST) during the survey tests for the Galactic Plan Pulsar Snapshot (GPPS) survey and other normal FAST projects. Among them, polarization profiles of about 460 pulsars are observed for the first time. The profiles exhibit diverse features. Some pulsars have a polarization position angle curve with a good S-shaped swing, and some with orthogonal modes; some have components with highly linearly components or strong circularly polarized components; some have a very wide profile, coming from an aligned rotator, and some have an interpulse from a perpendicular rotator; some wide profiles are caused by interstellar scattering. We derive geometry parameters for 190 pulsars from the S-shaped position angle curves or with orthogonal modes. We find that the linear and circular polarization or the widths of pulse profiles have various frequency dependencies. Pulsars with large fraction of linear polarization are more likely to have a large Edot.

Key words: polarization, astronomical data bases: miscellaneous, pulsars: general

1 INTRODUCTION

Pulsars are highly polarized radio sources in the universe. Its highly polarized emission was first noticed about 50 years ago soon after the pulsar discovery (Lyne & Smith 1968). Since then, great efforts have been made to uncover polarization features at a wide range of frequencies by many radio telescopes. The big projects produce large databases. For example at 1.4 GHz, 300 pulsars have been observed with the Lovel telescope (Gould & Lyne 1998), 98 pulsars by Arecibo (Weisberg et al. 1999), initially 45 (Wu et al. 1993) and then 66 (Manchester et al. 1998) and recently 600 pulsars (Johnston & Kerr 2018) by the Parkes telescope. At higher frequencies, 32 pulsars have been observed at 4.9 GHz by the Effelsberg radio telescope (von Hoensbroech et al. 1998a), and 48 pulsars at 3.1 GHz by the Parkes telescope (Karastergiou et al. 2005). At lower frequencies, 100 pulsars were observed at 774 MHz by the Green Bank telescope (Han et al. 2009), 57 pulsars at 430 MHz and the lower frequencies by Arecibo (Hankins & Rankin 2010), 123 pulsars at 333 MHz and/or 618 MHz by GMRT (Mitra et al. 2016), and 20 pulsars below 200 MHz by LOFAR (Noutsos et al. 2015). Recently, Sobey et al. (2021) extended the polarimetric observations to the ultra wide frequency band, from 704 to 4032 MHz, for 40 pulsars by using Parkes. Posselt et al. (2023)measured the polarimetry of 1170 pulsars using MeerKAT in a frequency band from 856 to 1712 MHz.

Pulsar polarization profiles exhibit rich features (e.g. Lyne & Manchester 1988; Rankin et al. 1989; Rankin & Ramachandran 2003). Pulsar polarization is predominantly linear. Some pulsars are highly linearly polarized for the whole or part of the profiles (e.g. Gould & Lyne 1998; Karastergiou et al. 2005; Wang & Han 2016), like PSRs B1259-63, B0355+54 and B1931+24. The degree of linear polarization generally decreases with the increase of observing frequency (e.g. Manchester 1971; Xilouris et al. 1996; Wang et al. 2015). The circular polarization is usually weak, but can be extremely strong for some pulsars like PSR B1702-19 or for some component such as PSR J1920+2650 (Han et al. 2009). The circular polarization has a single sign, or a sign reversal for core or conal components (e.g. Rankin 1983; Lyne & Manchester 1988;

Table 1 FAST observations for pulsar polarization profiles

Projects	PI	Obs. Mode	Beams	Obs. Dates	Obs. Time
GPPS survey	J. L. Han	snapshot	M01–M19	201904–	5 min
		tracking	M01–M19		15 min
		swiftcalibration	M01–M19		15 min
PT2020_0087	P. F. Wang	tracking	M01	202104-202105	30 min
PT2020_0161	P. F. Wang	tracking	M01	202009-202009	180 min
PT2020_0164	J. Xu	tracking	M01	202010-202104	10 min
PT2021_0051	J. Xu	snapshotdec	M01–M19	202109-202111	5 min
PT2022_0169	J. Xu	tracking	M01	202208-202211	15 min

Han et al. 1998). The polarization position angle (PA) curves ideally have an S-shape, such as PSRs B2045-16, J1420-6048, and B0833-45, but not for most pulsars. Some pulsars exhibits the polarization angle jumps of 90 degrees (e.g. Stinebring et al. 1984a; McKinnon & Stinebring 2000), which is called as the orthogonal modes. The polarization features are poorly understood, although polarization profiles of about 1500 pulsars were reported in the literatures.

To understand these diverse polarization features, many theoretical models have been developed, based on pulsar emission geometry, emission mechanisms and propagation effects. The geometry of pulsar emission region can be described by the rotating magnetosphere with a dipole magnetic field, called the rotating vector model (RVM, Radhakrishnan & Cooke 1969). Pulsar radio emission is believed to be coherent radiation generated by relativistic particles streaming along the curved dipole magnetic field lines in the magnetosphere. Curvature radiation is one of the most probable mechanisms, and the radiation of which is highly linearly polarized (e.g. Gangadhara 2010; Wang et al. 2012). Circular polarization produced by relativistic particles can be of one sign or have a sign reversal, depending on the density gradients of the relativistic particles and the geometry of line of sight to the emission magnetic field lines (Wang et al. 2012). The inverse Compton scattering of low frequency waves by relativistical particles in pulsar magnetosphere can also produce similar polarization features (Xu et al. 2000). In addition to the emission processes, propagation effects can also significantly affect the polarization states. The plasma in the pulsar magnetosphere has two orthogonally polarized modes, the ordinary mode (O-mode) and the extraordinary mode (X-mode) (e.g. Melrose & Stoneham 1977; Arons & Barnard 1986; Wang & Lai 2007). The polarized radiation produced by any emission processes has to be coupled to these transverse modes to propagate out in the magnetosphere. During propagation, it will experience 'adiabatic walking', 'wave-mode coupling' and 'cyclotron absorption' (e.g. Cheng & Ruderman 1979; Wang et al. 2010; Beskin & Philippov 2012), and the additional refraction for the O-mode wave (Barnard & Arons 1986; Lyubarskii & Petrova 1998). Moreover, the pulsar rotation not only causes the phase lag between the PA curve and the pulse profile (e.g. Blaskiewicz et al. 1991), but also leads to the separation of the O and X modes (e.g. Wang et al. 2014). Therefore, polarization profiles at different frequencies can be understood only if the dipole geometry, curvature emission process and propagation effects within pulsar magnetosphere are jointly considered (Wang et al. 2014). Up to now, the origins of orthogonal modes, highly linearly polarized emission and its frequency dependency can be naturally explained (Wang et al. 2015; Wang & Han 2016). To further test these theories, much more sensitive observations are needed.

The Five-hundred-meter Aperture Spherical radio Telescope (FAST) gives us a great opportunity to get more details of polarization profiles and more profiles for fainter pulsars, because of its unprecedented sensitivity. In this paper, we present the polarization profiles for 682 pulsars observed by the FAST via several projects, including the test observations during the Galactic Plan Pulsar Snapshot survey (GPPS). The paper is organized as follows. In Section 2, we briefly describe the observations, data reduction procedures and the capability for polarization measurements of the 19 beams of the L-band 19-beam receiver. Observation results with classifications of polarization features are presented in Section 3. Further understanding of the polarization profiles are discussed in Section 4. Conclusions are given in Sections 5.

2 OBSERVATIONS AND DATA REDUCTION

2.1 Observations

The data for pulsar polarization profiles presented in this paper are obtained by the FAST observations from 2019 to 2022 via six projects (see Table 1).

The FAST GPPS survey is one of the five FAST key projects with project numbers as ZD2020_2, ZD2021_2, and ZD2022_2, which is carried out for discovering new pulsars within the Galactic latitude of $\pm 10^{\circ}$ by employing all the 19 beams with the newly invented snapshot observation mode (Han et al. 2021). The observations of nearby 4 pointing can cover a hexagonal sky coverage of about $28'$ in size (see Figure 1) which is called a cover. Any cover with one or more known pulsars in any beam, not necessary

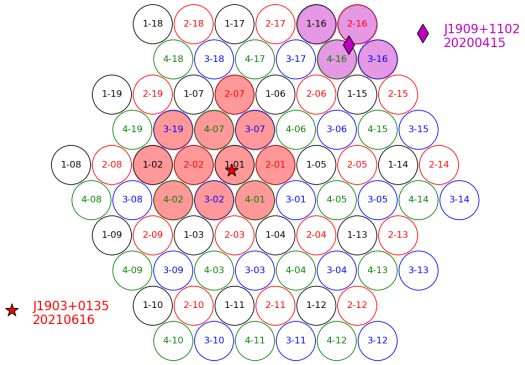

Fig. 1 FAST has a 19-beam L-band receiver, which has been used for a snapshot mode in the GPPS survey (Han et al. 2021). With 4 nearby pointing, each with one color for beams, a sky coverage can be fully covered. The beam number and pointing number are indicated inside each beam (e.g. 2-07 is the beam M07 in the 2nd pointing). A bright pulsar can be detected by a few nearby beams, as illustrated for PSRs J1903+0135 and J1909+1102, which were observed at two different sessions with dates indicated. The polarization results of the targeted pulsar from these beams are surprising consistent (see results below in Figure 4 and listed in Table 2), which implies the excellent polarization characteristics of the 19-beam L-band receiver.

in the beam center (see also Figure 1 and Table 2), was observed as the survey tests with polarization data recorded, which provide a good database for this work but a careful polarization calibration is really desired.

In the last three years, we carried out targeted observations for a dedicated study of polarization features of known pulsars (FAST projects: PT2020_0087 and PT2020_0161), for the general studies of high Galactic latitude pulsars without polarimetry before (FAST projects: PT2020_0164, PT2021_0051 and PT2022_0169).

All these observations have been made with the 19-beam L-band receiver of the FAST. These 19-beam receivers cover 1.0 – 1.5 GHz band (Jiang et al. 2020). Radio signals from two orthogonal linear polarization channels, X and Y, of each beam are sampled. They are channelized for 4096 or 2048 channels, and then correlated for the XX, YY, Re[X*Y] and Im[X*Y] polarization products in a digital backend (see Han et al. 2021, for details). The data are accumulated to a time resolution of 49.152 μs, and then written to fits files. Observations often take 5, 10, 15, 30 minutes in general, depending on objects and projects.

2.2 Data reduction

Offline data processing has many steps. The FAST data in fits files were recorded in the search mode (see e.g. Han et al. 2021), and have to be first folded for each frequency channel and de-dispersed according to the ephemeris of a given pulsar in the pulsar catalog (Manchester et al. 2005) by using the software tool DSPSR (van Straten & Bailes 2011). The frequency channels at two edges of the frequency band are exercised with PSRCHIVE (Hotan et al. 2004) because of the low gain (see Figure 2), so that the frequency coverage is reduced from 1000-1500 MHz to 1048-1452 MHz. Radio frequency interference (RFI) is then exercised both in frequency and time domains.

In general, the calibration signals are recorded for 2 minutes in every observation session, which are didoes signals of a temperature of 1.1 K injected to the feed at an angle of 45^o with respect to the two linear feed receptors. The signals are on for 1 s on and then off for the other 1 s. The data recorded in the 4 polarization channels, are folded to the period of 2 s to get a square wave, so that the gain, differential gain and differential phase of the 19-beam receiver can be obtained, as shown in Figure 2. By employing these system characteristic parameters obtained from the nearest calibration observation session, we get the observed pulsar signals calibrated.

The data for XX, YY, Re[X*Y] and Im[X*Y] are transformed to the Stokes parameters, through $I = \mathrm{XX} + \mathrm{YY}$, $Q = \mathrm{XX} - \mathrm{YY}$, $U = 2\mathrm{Re}[\mathrm{X}^*\mathrm{Y}]$ and $V = 2\mathrm{Im}[\mathrm{X}^*\mathrm{Y}]$. They are integrated over frequency to form 8 frequency subbands with Faraday rotation corrected, and integrated in time so that the polarization profiles can be analyzed for frequency dependence. The final integrated pulse profiles are further integrated from these 8 frequency subbands. The linear polarization for phase bin i is calculated as $L_i = \sqrt{Q_i^2 + U_i^2}$ and its associated PA as $\psi_i = 1/2 \arctan(U_i/Q_i))$. The baseline bias of L_i caused by the quadrature summation is corrected as, $L_{c,i} = \sqrt{|L_i^2 - (\sigma_Q^2 + \sigma_U^2)|}$ if $L_i^2 \geq (\sigma_Q^2 + \sigma_U^2)$, otherwise, $L_{c,i} = -\sqrt{|L_i^2 - (\sigma_Q^2 + \sigma_U^2)|}$. Here, σ_Q and σ_U are the standard deviation of the off pulse Q and U data. The bias for the absolute circulation $|V_i|$ is also corrected, $|V_{c,i}| = \sqrt{|V_i^2 - \sigma_V^2|}$ if $|V_i| \geq \sigma_V$, otherwise, $|V_{c,i}| = -\sqrt{|V_i^2 - \sigma_V^2|}$, and σ_V is estimated from the off-pulse V data. The degrees of linear, circular and absolute circular polarization are calculated as L/I, V/I, and $|V|/I$ with $I = \sum I_i$, $L = \sum L_{c,i}$, $V = \sum V_i$ and $|V| = \sum |V_{c,i}|$ for N_d phase bins with $I_i \geq 3\sigma_I$. Their uncertainties are estimated as, $\sigma_{L/I,m} = \sqrt{N_d[(\sigma_L/I)^2 + (L\sigma_I/I^2)^2]}$, $\sigma_{V/I,m} = \sqrt{N_d[(\sigma_V/I)^2 + (V\sigma_I/I^2)^2]}$ and $\sigma_{|V|/I,m} = \sqrt{N_d[(\sigma_{|V|}/I)^2 + (|V|\sigma_I/I^2)^2]}$. In general, $\sigma_{L/I,m} \geq \sigma_{V/I,m} \geq \sigma_{|V|/I,m}$. Their total uncertainties are calculated as the quadrature sum of these measurement uncertainties and the estimated systematic uncertainty of 3 percent.

The polarization is presented in normal pulsar convention (van Straten et al. 2010). It reads, the PAs are with respect to the North Celestial Pole, they are defined to increase counter-clockwise on the sky, and the left-hand circular polarization is positive. This is set for all FAST observations presented in this paper, though the data are

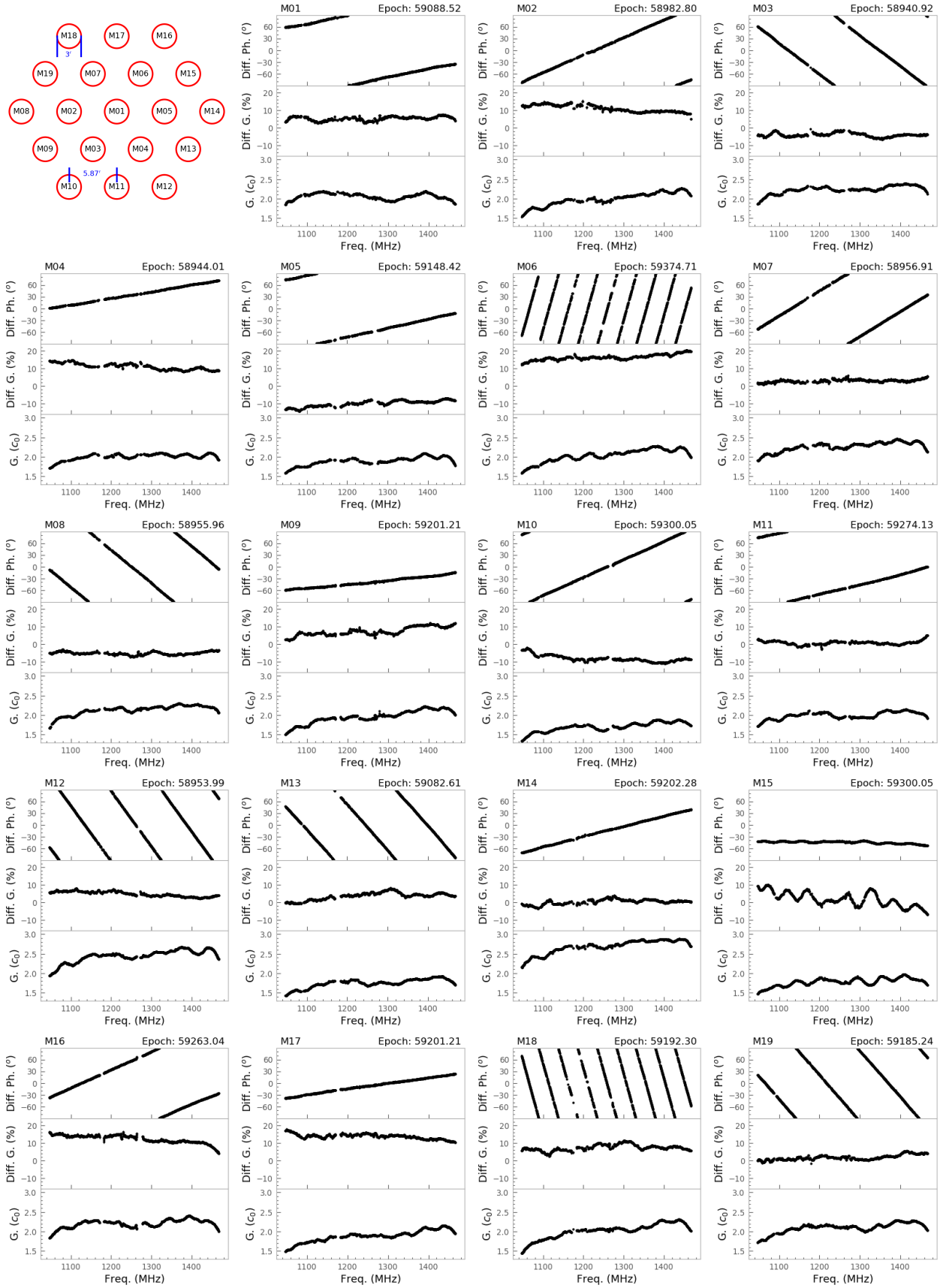

Fig. 2 Instrumental characteristics as a function of observing frequency calculated for 19 beams of the FAST 19-beam L-band receiver. The sky distribution of the 19 beams is shown in the top left panel for beams M01 to M19. For each beam, the gain, differential gain and differential phase are plotted in three sub-panels.

Table 2 No significant differences on polarization measurements observed at or near the center of beam M01 and at a very offset position in other beams.

PSR	Obs. Date	Beam	Offset	Int.	S/N	$\mathrm{RM_{ISM}}$	ΔPA(°)		ΔL/I(%)		ΔV/I(%)	
			(′)	(min)		$(\mathrm{rad/m^2})$	ave.	std.	ave.	std.	ave.	std.
J2113+4644	20220308	P1M01	0.0	120	52096.6	-222.4(3)	0.0		0.0		0.0	
	20200826	P1M01	3.0	15	7802.4	-221.6(3)	-2.9	2.1	1.8	2.8	0.3	1.1
	20200917	P1M12	3.0	15	7835.7	-221.2(2)	-1.0	1.4	1.9	3.0	-1.3	1.1
J0631+1036	20210501	P1M01	0.0	30	2638.8	143.6(2)	0.0		0.0		0.0	
	20200816	P1M02	2.2	15	440.9	145.2(3)	-6.4	1.7	-1.5	10.2	-0.2	2.5
J1915+1606	20191028	P1M01	0.0	30	1472.1	357.2(2)	0.0		0.0		0.0	
	20210422	M03	0.6	5	585.3	356.5(3)	4.3	2.0	-0.4	3.9	-0.3	3.1
J0711+0931	20210111	P1M01	0.0	10	1135.5	60.9(7)	0.0		0.0		0.0	
	20210526	M04	0.5	5	578.7	63.0(5)	2.7	5.4	0.7	4.8	-2.5	3.1
J1844+1454	20210430	P1M01	0.0	30	5171.3	119.1(3)	0.0		0.0		0.0	
	20210606	M10	1.0	5	2824.5	118.1(3)	0.7	1.8	-0.6	3.1	0.1	0.9
J1935+1616	20190919	P1M01	0.0	50	430977.0	-2.8(2)	0.0		0.0		0.0	
	20210119	M11	2.5	5	13216.0	-2.6(3)	3.5	2.6	0.7	4.4	0.0	1.3
J1828+0625	20210118	P1M01	0.0	10	223.0	24(2)	0.0		0.0		0.0	
	20210615	M17	1.6	5	166.8	16(11)	2.6	6.6	0.6	6.5	-	-
J1842+1332	20210115	P1M01	0.0	10	1612.2	130.3(2)	0.0		0.0		0.0	
	20210605	M19	1.2	5	1050.8	129.6(2)	-2.3	3.0	2.1	4.2	0.8	0.3
J1903+0135	20210616	P1M01	0.4	5	13125.7	73.0(4)	0.0		0.0		0.0	
		P3M02	2.5	5	2226.4	72.9(5)	1.1	5.4	1.8	2.3	0.4	1.4
		P2M02	2.7	5	1901.0	72.2(8)	3.5	4.3	0.6	2.5	0.2	1.0
		P4M01	2.8	5	1955.3	70.8(8)	1.1	4.2	1.4	3.1	-0.6	1.4
		P2M01	3.2	5	1138.0	75.3(11)	-0.5	13.7	0.5	2.8	-1.0	2.8
		P4M07	3.2	5	757.8	70.1(22)	-1.8	7.7	1.5	2.9	1.5	2.2
		P3M07	3.4	5	662.1	69.6(14)	5.2	6.2	2.7	4.0	-1.3	1.9
		P4M02	4.7	5	27.0	77(4)	9.9	6.5	11.8	3.8	-	-
		P3M19	5.1	5	90.8	75.2(14)	3.2	8.5	1.2	4.5	-0.5	2.5
		P2M07	5.5	5	42.9	70(5)	11.4	17.6	4.5	5.2	0.7	3.7
		P1M02	5.7	5	37.8	57(9)	25.1	3.4	1.1	1.5	-2.1	2.3
J1909+1102	20200414	P4M16	1.4	5	2450.4	553.3(4)	0.0		0.0		0.0	
		P2M16	1.6	5	2733.1	554.0(4)	-0.5	2.8	-1.0	5.7	-1.2	2.0
		P3M16	2.3	5	767.7	552.4(7)	0.5	3.2	-0.2	5.0	-0.4	1.7
		P1M16	2.8	5	644.2	553.7(7)	0.7	4.6	0.7	8.2	2.4	3.3

taken through the tracking, swiftcalibration and snapshot-dec modes. Note that FAST observations with the snapshot mode are made with respect to the North Galactic pole, i.e., $\mathrm{PA_{snap}}$. A correction of the PA should be made via $\mathrm{PA} = \mathrm{PA_{snap}} - \mathrm{PA_c}$, and

$$\mathrm{PA_c} = \tan^{-1}\left[\frac{\sin(\Delta\mathrm{RA})}{\cos\delta\cot 62.9^\circ - \sin\delta\cos(\Delta\mathrm{RA})}\right]. \quad (1)$$

Here, $\Delta RA = \mathrm{RA_{psr}} - \mathrm{RA_{NGP}}$, and $\mathrm{RA_{psr}}$ and $\mathrm{RA_{NGP}}$ are the right ascensions of a pulsar and the north Galactic pole, δ is the declination of the pulsar, and the inclination angle of the North Galactic pole to the North Celestial pole is 62.9°. After these corrections, the position angles are finally referred to the same frame.

The plane of linear polarization of pulsar radio emission has been rotated during their propagation through the magnetized interstellar medium. Faraday rotation of linearly polarized signals across the observational frequency band has to be corrected to the central frequency 1250 MHz by using the observed rotation measure (RM) of an observation, $\mathrm{RM_{obs}}$. The initial value of RM is first found by searching for the maximum of linearly polarized pulse emission as a function of many trial RMs. The more accurate value is then obtained by iteratively refining the differential PAs of the two halves of the total bandwidth (see Han et al. 2018). These calculations are achieved by employing the program RMFIT in the package of PSRCHIVE. The so-obtained $\mathrm{RM_{obs}}$ includes the RM contribution from the interstellar medium, $\mathrm{RM_{ISM}}$, and the variable RM contribution from the earth ionosphere, $\mathrm{RM_{ion}}$. The $\mathrm{RM_{ion}}$ is modeled by using the vertical total electron content maps of the ionosphere, CODE[1], and the International Geomagnetic Reference Field (IGRF-13)[2] with an updated code of IONFR[3] (Sotomayor-Beltran et al. 2013). The variable RM contribution should be discounted, and then the published RM value is purely from the interstellar medium and is $\mathrm{RM_{obs}} - \mathrm{RM_{ion}}$.

2.3 Polarization characteristics for the 19 beams

In order to understand polarization characteristics of the 19 beams, polarized pulse profiles obtained by the central beam without any offset and by the outer beams with different offsets are carefully examined. The FAST observation results are also compared with those published in the literature.

[1] ftp://ftp.aiub.unibe.ch/CODE/

[2] https://www.ngdc.noaa.gov/IAGA/vmod/igrf.html

[3] https://sourceforge.net/projects/ionfarrot/

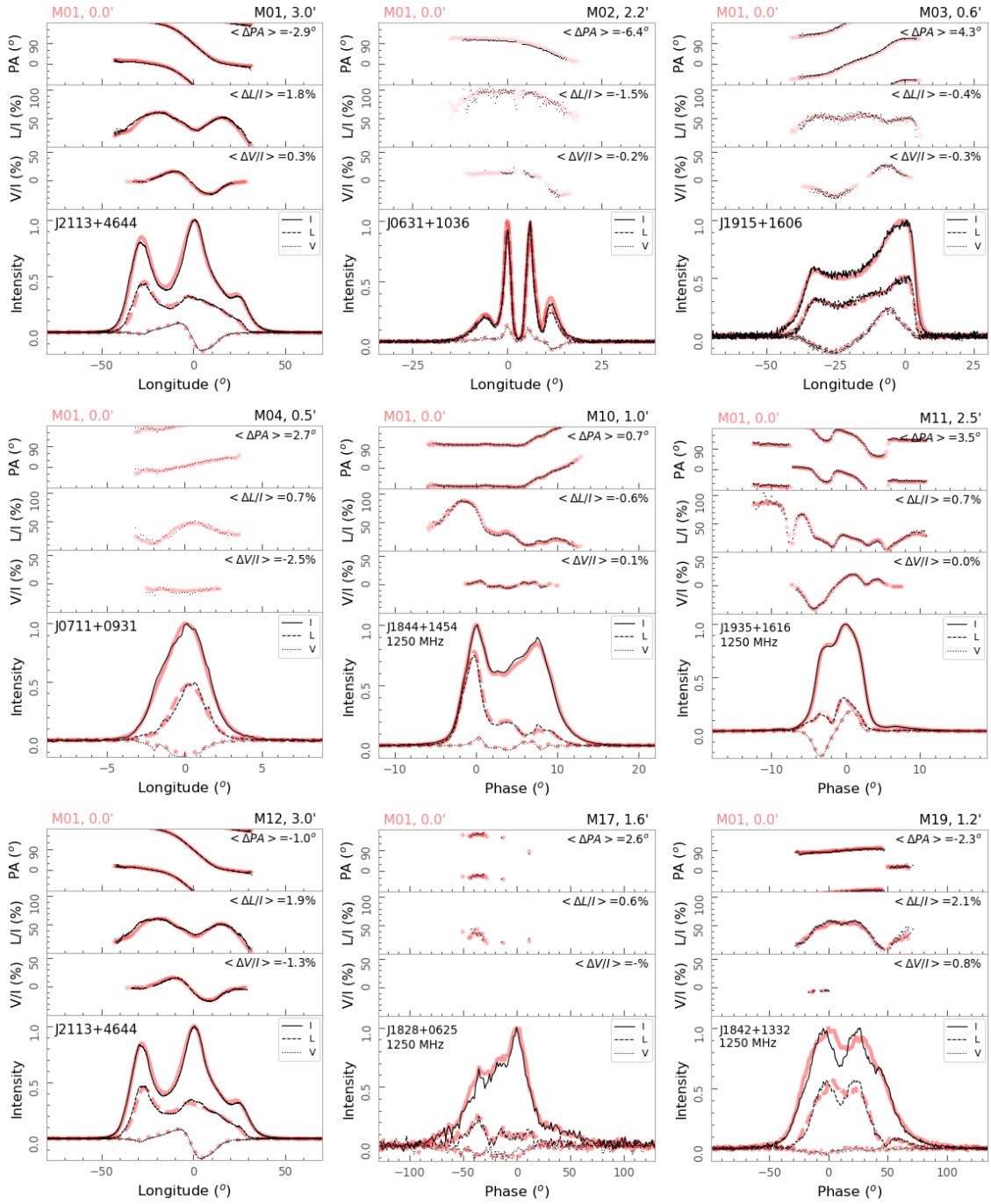

Fig. 3 Comparisons for polarization profiles (thin lines) obtained from data recorded by the outer beams of the 19-beam L-band receiver when a pulsar is very offset from the beam center with the results (thick background lines) observed by the central beam M01 without offset. For each pulsar, in the bottom sub-panel are the total intensity, linear and circular polarization represented by solid, dashed and doted lines; and other sub-panels are the fractional circular and linear polarization and position angle curves of linear polarization with the linear polarized intensities exceeding 5σ, here σ is obtained from the off pulse phase-bins. In general, results from the outer beams are very consistent with that from the central beam M01 in the thick background line, with a small derivations for $\langle \Delta PA \rangle$, $\langle \Delta L/I \rangle$ and $\langle \Delta V/I \rangle$ as indicated in each sub-panel.

First of all, is there any difference between the polarization profiles obtained by the central beam and outer beams? In the PI projects, we do observe some pulsars targeted by the central beam without offset (see the list in Table 2), while the covers with some of these pulsars are also tested in the GPPS survey with a somehow "random" location offset in the outer beams. Figure 3 shows such a comparison of pulse polarization profiles for the cases for offset observations with the beams of M01, M02, M03, M04, M10, M11, M12, M17 and M19. Apparently there

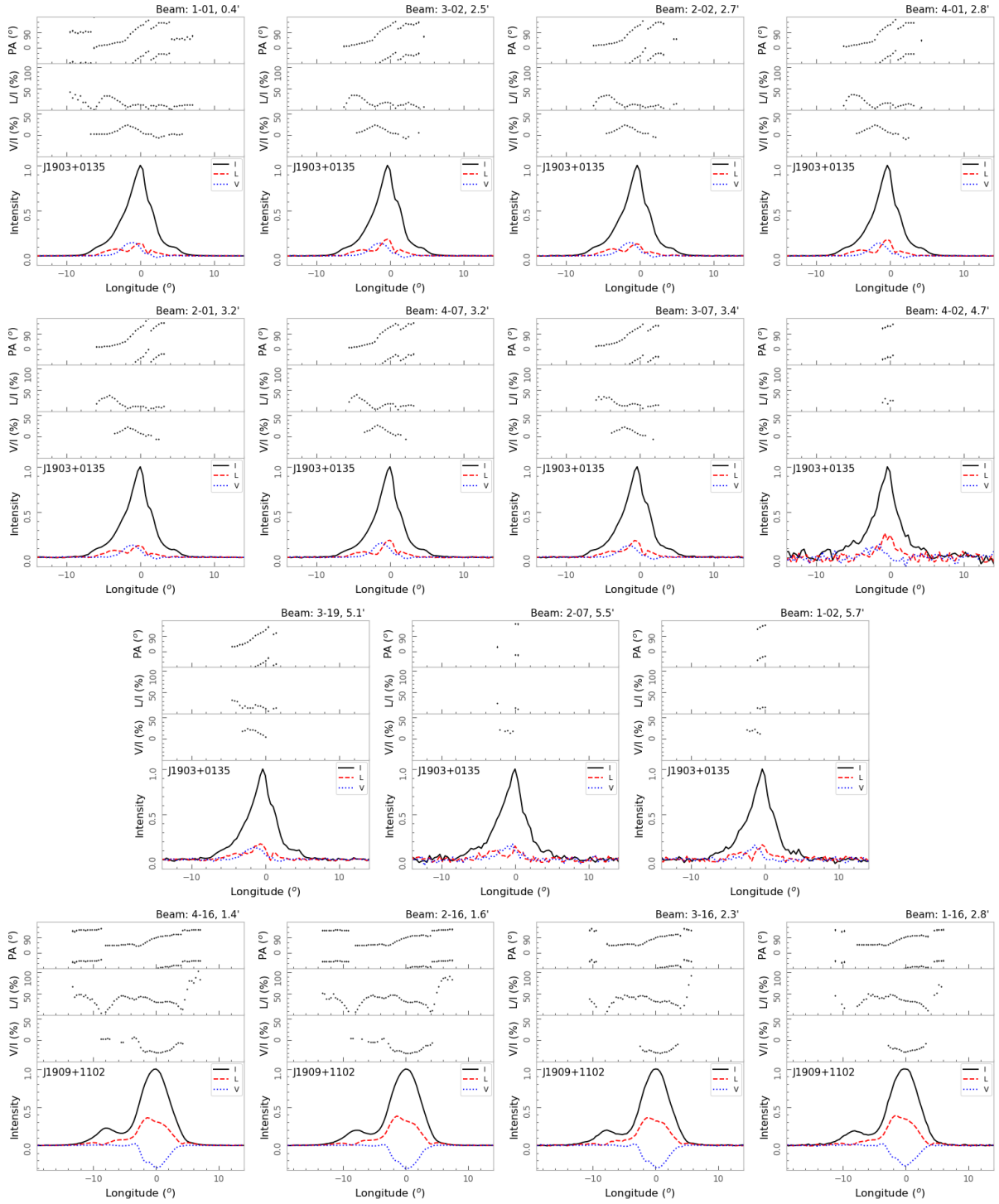

Fig. 4 Polarization profiles of PSRs J1903+0135 and J1909+1102 obtained from the data recorded in the 11 nearby beams and 4 nearby beams, respectively, as illuminated in Figure 1 and listed in Table 2. The total intensity, linear polarization and circular polarization, their fractions, as well as position angle of linear polarization, all are plotted from the bottom to the top sub-panels for each profile. They are all consistent though with very different offsets for different beams, which demonstrates the excellent polarization characteristics of the 19-beam L-band receiver.

are some but not significantly different results from the offset observations. The quantitative differences in PA, linear polarization and circular polarization are obtained as listed in the first part of Table 2 for their averages and standard deviations. The difference in PA can reach 6.4° for an offset of $2.2'$ of a pulsar to the beam center of M02, and 4.3° for an offset of $0.6'$ for a pulsar from the beam center of M03. The difference in the degree of linear polarization

reaches 2.1% in an offset observation of $1.2'$ from the beam center of M19. The data scattering of the fractional linear polarization of PSR J0631+1036 leads to a large standard deviation for the offset observations of beam M02, probably due to the intrinsic data scattering rather than measurements. The maximum difference in fractional circular polarization is only 2.5% from PSR J0711+0931 observed by the beam M04. We therefore conclude that polarization characteristics of 19 beams, even observed with an offset as large as $3'$, are so excellent that polarization profiles have less than 3% difference compared with measurements by the central beam M01 without offset.

Second, we compare the polarization profiles obtained by data recorded quasi-simultaneously by several beams in snapshot observations (see e.g. Figure 1). For 4 nearby beams with various offsets, the polarization profiles in Figure 4 are excellently consistent with each other, see the quantitative comparisons in Table 2. If the observation of a pulsar of the nearest beam is chosen as the references, the average deviations in PA, fractional linear polarization and circular polarization are maximally of 3.5°, 1.8% and 2.4% for beams within $3.0'$. Only for pulsars detected by a very far beam with an offset more than $3.4'$, a slightly large difference emerges with a large uncertainty due to the low S/N. That is to day, the polarization response of these beams even in the very offset positions are so consistent with each other.

Certainly, to understand polarization characteristics of the FAST observations, we have to compare the polarization profiles with published ones, at least one pulsar is chosen for each beam. For beam M01, the polarized pulse profile PSR J1932+1059 obtained by FAST is consistent with the one observed at 1.4 GHz by Stinebring et al. (1984b) and Johnston et al. (2005). The pulsars for the other beams are also compared, such as PSR J0631+1036 (Johnston & Kerr 2018) to that from the FAST beam M02, PSR J1932+1059 (Hankins & Rankin 2010) to that from the beam M03, PSR J0711+0931 (Lommen et al. 2000) to that from the beam M04, PSR J1904+0004 (Johnston & Kerr 2018) to that from the beam M06, PSRs J1954+2923 (Weisberg et al. 1999; Hankins & Rankin 2010) and J2008+2513 (Han et al. 2009) to those from the beam M07, PSR J1932+2220 (Mitra & Rankin 2011) to that from the beam M10, PSR J1935+1616 (Han et al. 2009; Hankins & Rankin 2010) to that from the beam M11, PSR J1909+1102 (Hankins & Rankin 2010) to that from the beam M16, PSR J1946+1805 (Hankins & Rankin 2010; Mitra & Rankin 2011) to that from the beam M17, PSR J1857+0943 (Ord et al. 2004) to that from the beam M18, and PSR J1842+1332 (Johnston & Kerr 2018) to that from the beam M19. All the FAST polarization profiles are consistent with the published ones, albeit at slightly different observing frequencies.

3 FAST PULSAR POLARIZATION PROFILES

Polarization profiles of 682 pulsars are finally obtained from FAST observations, as listed in Table 3. The period and DM are listed after the name, allowing identification of a pulsar with parameters. Then FAST observation dates, FAST observation modes, the beam name and the pulsar offsets from the beam center are given in columns (4), (5), (6) and (7). The profile widths W_{50} and W_{10} at 50% and 10% the peak intensities (only if the 10% peak intensities exceeding three times the standard deviation of off pulse data) are listed in columns (8) and (9). Their uncertainties are estimated as, $\sigma_{W,H} = t_b\sqrt{1+(\sigma_I/H)^2}$, by following Kijak & Gil (1997) . Here, t_b represents the time resolution of the phase bins of a profile, H is 0.5 for W_{50}, and 0.1 for W_{10}. The degrees of linear, circular and absolute circular polarization and their uncertainties are listed in columns (10) - (12). We obtain new RMs (i.e. $\mathrm{RM} = \mathrm{RM_{obs}} - \mathrm{RM_{ion}}$) for 402 pulsars as given in column (13), which have been employed to investigate the magnetic fields in the Galaxy by Xu et al. (2022). The figure number for polarization profile, and the short notes as well as references for profile comparison are given in columns (14)-(16).

The observed polarization profiles exhibit diverse features, such as those with S-shaped PA curves or orthogonal modes, profiles or components with significant linear polarization or circular polarization, profiles of conal double pulsars, profiles with interpulse emission or emission occupying wide ranges of longitudes, and those affected by interstellar scattering. These different features are discussed in the following.

3.1 Polarization profile with a S-shaped PA curve

The S-shaped PA curves are generally deemed to be related to the orientation of the dipolar magnetic field line planes, and are important indicators for pulsar radio emission generated from the poles of dipolar magnetosphere. They are usually employed to determine pulsar geometry as discussed in section 4.2, and can be naturally reproduced by various emission mechanisms and propagation effects (e.g. Xu et al. 2000; Gangadhara 2010; Wang et al. 2012).

Among the integrated pulse profiles of 682 pulsars observed by FAST, we see the S-shaped PA curves for 195 pulsars, as shown for 3 example pulsars in Figure 5 of 96 pulsars in Figure A.1, and 99 pulsars in other figures: 46 pulsars with orthogonal mode jumps in Figure A.2, 14 pulsars with high linear polarization in Figure A.3, one pulsar with high circular polarization in Figure A.4, 22 conal dou-

Table 3 Polarization parameters of 682 pulsars (see notes for the columns at the end, – *to be continued*.)

PSR	P	DM[a]	Date	Mode	Beam	Offset	W_{50}	W_{10}	L/I	V/I	$\|V\|$/I	RM	Fig.	Note.	Ref.
	(s)					($'$)	(°)	(°)	(%)	(%)	(%)	(rad/m^2)			
(1)	(2)	(3)	(4)	(5)	(6)	(7)	(8)	(9)	(10)	(11)	(12)	(13)	(14)	(15)	(16)
J0006+1834	0.693	11.4	20210110	TR	P1M01	0.0	39.9(28)	-	100.0(35)	-6.6(31)	7.5(31)	-19.4(4)	A.3	hiL,S	
J0011+08	2.552	24.9	20210927	SD	P3M02	<1.5	1.8(7)	7.4(7)	39.9(38)	-6.0(34)	6.1(34)	-17.4(27)	A.5	cd	
J0023+0923	0.0030	14.3	20201120	TR	P1M01	0.0	23.1(14)	85.6(14)	24.6(31)	1.8(31)	6.6(31)	-5.5(30)	A.2	ot	
J0050+03	1.366	26.5	20210117	TR	P1M01		10.0(14)	14.1(14)	36.5(33)	-8.5(32)	12.3(32)	-25.6(22)	A.9		
J0058+4950	0.996	66.9	20201120	TR	P1M01	0.0	11.1(7)	16.8(7)	30.6(30)	14.4(30)	15.5(30)	-114.2(5)	A.1	S	
J0103+54	0.354	54.8	20210927	SD	P4M04	<1.5	6.2(7)	–	19.6(36)	6.0(35)	7.4(34)	-74(5)	A.9		
J0107+1322	1.197	21.6	20210124	TR	P1M01	0.0	1.9(7)	9.7(7)	14.6(31)	-7.0(30)	9.0(30)	-13.9(22)	A.9		
J0122+1416	1.389	17.6	20210110	TR	P1M01	0.0	5.4(7)	–	24.1(40)	0.9(38)	4.2(38)	-15(5)	A.9		
J0139+3336	1.248	21.2	20210110	TR	P1M01		5.3(7)	8.7(7)	25.4(31)	-8.4(30)	10.4(30)	-29.1(11)	A.9		
J0146+31	0.938	25.0	20210927	SD	P1M10		4.9(7)	–	22.7(36)	-10.3(35)	11.0(35)	-32(26)	A.9		
J0229+20	0.806	28.4	20210118	TR	P1M01		7.2(7)	–	23.5(39)	-8.9(37)	9.0(37)	-33(9)	A.9		
J0241+16	1.544	20.8	20210927	SD	P1M05	<1.5	5.9(7)	–	20.7(38)	8.6(36)	15.1(36)	-6(4)	A.9		
J0244+14	2.127	31.0	20210927	SD	P2M19		4.8(7)	8.1(7)	21.7(32)	10.4(31)	12.6(31)	-8.1(21)	A.1	S	
J0302+2252	1.207	18.9	20201101	TR	P1M01	0.0	14.1(2)	17.4(2)	25.4(30)	-1.0(30)	7.1(30)	-7.8(4)	A.9		
J0329+1654	0.893	40.8	20201101	TR	P1M01	0.0	7.8(7)	14.9(7)	9.8(31)	-4.1(31)	4.7(31)	3(4)	A.9		
J0335+4555	0.269	47.1	20210524	SS	P4M08	3.1	2.4(4)	10.3(4)	33.5(30)	-2.8(30)	6.4(30)	-2.7(10)	A.9		13
J0337+1715	0.0027	21.3	20201114	TR	P1M01	0.0	149.3(2)	275.2(2)	36.4(30)	-5.6(30)	7.1(30)	26.4(1)	A.7	w,ot	
J0340+4130	0.0032	49.6	20201121	TR	P1M01	0.0	26.2(7)	56.2(7)	15.1(30)	-3.6(30)	4.2(30)	50.5(7)	A.2	ot	
J0349+2340	2.420	62.9	20210427	TR	P1M01	0.0	8.7(7)	–	15.9(36)	-13.1(35)	19.2(35)	97(4)	A.9		
J0358+4155	0.226	46.3	20210108	TR	P1M01	0.0	4.4(7)	19.4(7)	19.3(30)	6.6(30)	6.9(30)	-7.0(2)	A.9		
J0358+5413	0.156	57.1	20191109	TR	P1M01	0.0	17.7(1)	37.8(1)	46.2(30)	-3.7(30)	8.4(30)	81.9(2)	A.3	hiL,ot,S	12,13,15
J0402+4825	0.512	85.2	20220225	SS	P3M16	0.5	15.3(4)	17.1(4)	42.0(30)	-7.5(30)	10.2(30)	-93.1(7)	A.1	S	
J0453+1559	0.045	30.3	20210108	TR	P1M01	0.0	4.1(7)	15.8(7)	20.5(30)	0.8(30)	2.2(30)	-35.2(2)	A.2	ot,S	
J0454+5543	0.340	14.6	20210502	TR	P1M01	0.0	18.0(2)	30.6(2)	27.9(30)	-5.8(30)	6.3(30)	6.5(2)	A.3	hiL,ot,S	7,12,13
J0457+23	0.504	59.0	20210119	TR	P1M01		25.7(14)	37.6(14)	31.4(31)	5.8(30)	16.3(30)	-56.8(7)	A.2	ot,S	
J0502+4654	0.638	42.2	20220917	SC	P1M01		10.7(2)	13.5(2)	14.9(30)	0.3(30)	6.1(30)	-172.5(4)	A.2	ot	13
J0517+2212	0.222	18.3	20210524	SS	P2M08	3.4	43.2(14)	63.7(15)	24.8(31)	18.9(31)	23.3(31)	-27.3(18)	A.9		
J0518+5416	0.340	42.3	20210110	TR	P1M01	0.0	9.5(14)	19.4(14)	9.1(31)	-10.9(31)	12.0(31)	-21(10)	A.9		
J0538+2817	0.143	39.5	20210501	TR	P1M01	0.0	7.2(1)	32.4(1)	98.4(30)	14.8(30)	14.9(30)	38.0(2)	A.3	hiL,ot,S	12
J0543+2329	0.246	77.7	20220308	SS	P2M16	4.7	6.9(4)	24.8(4)	55.5(30)	-9.9(30)	11.6(30)	-2.4(5)	A.1	S	10, 24
J0555+3948	1.146	37.0	20210524	SS	P3M04	<1.5	6.6(4)	12.4(4)	13.4(31)	1.0(30)	2.9(30)	5.8(26)	A.2	ot	
J0605+3757	0.0027	20.9	20210108	TR	P1M01	0.0	23.7(14)	-	38.4(32)	-0.6(32)	4.0(32)	-0.1(27)	A.1	S,hiL	
J0608+1635	0.945	85.6	20220308	SS	P3M10		7.1(4)	11.5(4)	10.7(31)	8.9(30)	9.7(30)	-108(2)	A.1	S	
J0612+37216	0.443	39.2	20210427	TR	P1M01	0.0	9.4(7)	22.6(7)	22.8(31)	-0.1(31)	20.1(31)	36.9(10)	A.2	ot?	
J0613+3731	0.619	18.9	20210110	TR	P1M01	0.0	9.5(7)	19.9(7)	35.6(31)	-4.1(31)	5.5(31)	15.3(5)	A.2	ot,S	
J0621+0336	0.269	72.6	20220307	SS	P3M01	1.4	3.3(2)	7.2(2)	33.0(30)	8.4(30)	11.0(30)	46.2(5)	A.9		
J0625+17	2.518	58.4	20220308	SS	P2M15		4.2(7)	7.4(7)	22.0(34)	3.0(34)	5.7(33)	104(2)	A.9		
J0628+0909	1.241	87.9	20210922	TR	P1M01	0.0	2.5(2)	4.9(2)	28.7(30)	15.7(30)	17.2(30)	127.3(7)	A.9		
J0629+2415	0.476	84.1	20210524	SS	P3M08	3.0	9.4(2)	16.4(2)	25.0(30)	9.9(30)	14.6(30)	64.9(5)	A.2	ot?	13,16,19
J0630-0046	0.680	97.3	20220225	SS	P3M09	1.3	2.7(4)	14.8(4)	29.1(30)	1.5(30)	10.4(30)	37.5(10)	A.1	S	
J0631+1036	0.287	125.3	20210501	TR	P1M01	0.0	8.2(2)	24.5(2)	92.7(30)	6.4(30)	13.5(30)	143.6(2)	A.3	hiL,S	11,22,29
J0647+0913	1.234	157.5	20220226	SS	P4M04	1.0	2.8(4)	9.6(4)	17.3(30)	-16.5(30)	17.0(30)	-121.2(11)	A.2	ot	
J0653+4706	0.0047	25.5	20210130	TR	P1M01	0.0	23.7(14)	193.2(14)	14.7(32)	1.5(32)	4.9(31)	13(5)	A.6	ip,ot	
J0659+1414	0.384	13.9	20210425	TR	P1M01	0.0	13.9(4)	29.7(4)	87.1(30)	-15.3(30)	15.4(30)	23.3(3)	A.3	hiL,ot,S	13,22,24
J0709+0458	0.034	44.2	20210530	SS	P3M17	1.8	9.5(14)	–	19.1(38)	4.6(34)	4.7(34)	88(18)	A.9		
J0711+0931	2.428*	41.7	20210111	TR	P1M01	0.0	3.3(2)	6.1(2)	36.8(30)	-10.3(30)	10.7(30)	60.9(2)	A.1	S	
J0806+08	2.062	46.0	20210928	SD	P1M03	<1.5	9.5(7)	–	16.1(35)	-12.7(34)	14.9(34)	10(5)	A.9		
J0811+37	1.248	14.9	20210928	SD	P4M07	<1.5	6.2(7)	12.3(7)	29.2(33)	9.2(32)	10.1(32)	-0.9(16)	A.9		
J0813+22	0.531	51.1	20210928	SD	P1M01	<1.5	30.9(28)	–	23.8(34)	-1.4(33)	5.2(33)	14(7)	A.9		
J0815+4611	0.434	11.2	20201124	TR	P1M01	0.0	7.7(2)	16.0(2)	41.4(30)	8.1(30)	9.9(30)	2.3(4)	A.9		
J0827+53	0.013	23.1	20210928	SD	P2M19		185.8(28)	–	49.2(45)	14.8(39)	28.1(39)	-15(4)	A.6	ip	
J0848+16	0.904*	38.0	20210928	SD	P4M01	<1.5	4.1(7)	19.7(7)	15.6(31)	4.6(30)	5.7(30)	38.8(16)	A.5	cd,ot	
J0928+06	2.060	50.0	20210928	SD	P2M01		4.8(7)	15.0(7)	9.2(31)	-7.3(31)	9.0(31)	11(6)	A.9		
J0944+4106	2.229	21.4	20201124	TR	P1M01	0.0	8.3(2)	10.5(2)	37.8(30)	0.3(30)	14.4(30)	1.3(8)	A.2	ot,S	
J1017+3011	0.452	27.1	20210124	TR	P1M01	0.0	143.2(28)	157.3(28)	50.8(34)	-1.8(32)	5.3(32)	19.2(8)	A.6	ip?,S,hiL	
J1038+0032	0.028	26.5	20201120	TR	P1M01	0.0	27.5(28)	75.2(29)	27.0(33)	3.1(32)	11.3(32)	14(5)	A.2	ot?	
J1132+25	1.002	23.4	20220904	SD	P1M17		3.5(7)	7.1(7)	32.9(31)	-12.7(31)	13.9(31)	-3.0(10)	A.1	S	
J1142+0119	0.0050	19.1	20210427	TR	P1M01	0.0	25.1(7)	200.3(7)	27.5(30)	10.8(30)	17.8(30)	-5.2(17)	A.7	w,ot	
J1236-0159	3.597	19.0	20201219	TR	P1M01	0.0	8.9(7)	11.3(7)	21.2(30)	-12.0(30)	16.0(30)	1.1(7)	A.2	ot,S	
J1242+39	1.310	28.6	20220901	SC	P1M01		10.1(7)	-	16.8(37)	-2.6(36)	7.1(35)	17(10)	A.9		
J1301+0833	0.0018	13.2	20220921	SC	P1M01	0.0	72.7(14)	124.5(14)	50.0(30)	2.1(30)	3.8(30)	6.4(3)	A.2	ot,S	
J1312+0051	0.0042	15.3	20221005	SC	P1M01	0.0	37.4(14)	187.8(14)	56.8(31)	-1.1(31)	3.0(30)	2.4(5)	A.7	w,ot	
J1312+1810A	0.033	25.0	20221103	SC	P1M01	0.0	32.7(14)	40.3(15)	55.3(32)	-21.6(32)	24.4(31)	-10.7(9)	A.5	cd,S	
J1404+1159	2.650	18.4	20220913	SC	P1M01	0.0	4.8(4)	8.1(4)	8.1(30)	-0.7(30)	0.9(30)	1.2(4)	A.9		
J1411+2551	0.062	12.3	20220915	SC	P1M01	0.0	13.4(7)	25.3(7)	25.0(31)	13.2(31)	15.3(31)	2.5(10)	A.1	S	
J1453+1902	0.0057	14.0	20220902	SC	P1M01	0.0	19.0(14)	135.0(14)	62.8(31)	-3.6(30)	5.4(30)	3.2(5)	A.2	ot	23
J1501-0046	0.464	22.2	20201218	TR	P1M01	0.0	8.2(7)	10.2(7)	17.3(30)	8.1(30)	10.6(30)	-1.9(10)	A.9		
J1518+0204A	0.0055	30.0	20210111	TR	P1M01	0.0	22.8(14)	47.8(14)	18.2(31)	4.0(31)	4.6(31)	2.6(19)	A.2	ot	
J1529+40	0.476	6.6	20210122	TR	P1M01		35.6(14)	68.1(14)	66.3(31)	6.7(30)	9.0(30)	-0.9(3)	A.2	ot	
J1538+2345	3.449	14.9	20201216	TR	P1M01	0.0	7.7(7)	9.5(7)	40.3(30)	-7.7(30)	8.1(30)	10.6(2)	A.5	cd,S	

Table 3 *– continued –*

PSR	P (s)	DM[a]	Date	Mode	Beam	Offset (′)	W_{50} (°)	W_{10} (°)	L/I (%)	V/I (%)	$\|V\|$/I (%)	RM (rad/m^2)	Fig.	Note.	Ref.
(1)	(2)	(3)	(4)	(5)	(6)	(7)	(8)	(9)	(10)	(11)	(12)	(13)	(14)	(15)	(16)
J1544+4937	0.0021	23.2	20201219	TR	P1M01	0.0	20.4(14)	61.6(14)	14.9(31)	-0.3(31)	7.5(31)	10.3(11)	A.9		
J1628+4406	0.181	7.3	20201026	TR	P1M01	0.0	198.6(14)	205.5(14)	36.9(30)	-0.6(30)	4.5(30)	1.6(4)	A.6	ip,hiL	
J1630+3734	0.0033	14.1	20201216	TR	P1M01	0.0	201.8(14)	237.8(14)	36.4(30)	1.5(30)	5.5(30)	1.1(2)	A.7	w,ot,hiL	
J1635+2332	1.208	37.5	20201026	TR	P1M01	0.0	13.4(7)	16.1(7)	22.2(30)	1.0(30)	17.3(30)	25.9(8)	A.9		
J1638+4005	0.767	33.4	20210201	TR	P1M01	0.0	5.9(7)	11.2(7)	18.1(33)	0.8(32)	3.0(32)	17(4)	A.9		
J1641+3627A	0.010	30.4	20210115	TR	P1M01	0.0	41.8(14)	55.6(14)	20.0(33)	-25.8(33)	27.5(33)	10.9(17)	A.5	cd,S	
J1641+3627C	0.0037	30.1	20210115	TR	P1M01	0.0	16.0(14)	–	31.2(37)	-13.5(34)	16.3(34)	6(6)	A.9		
J1641+3627D	0.0031	30.4	20210115	TR	P1M01	0.0	18.2(14)	–	9.1(36)	-1.2(36)	7.0(35)	11(10)	A.9		
J1643+1338	1.099	35.8	20210203	TR	P1M01	0.0	8.4(2)	11.4(2)	10.2(30)	-4.2(30)	8.7(30)	36.0(10)	A.9		
J1656+00	1.497	46.9	20211028	SD	P3M03	<1.5	7.4(7)	–	26.1(35)	1.1(34)	4.4(34)	5(4)	A.9		
J1657+3304	1.570	23.9	20210203	TR	P1M01	0.0	7.0(7)	9.6(7)	22.4(32)	-3.4(32)	13.1(32)	22.2(13)	A.1	S	
J1658+3630	0.033	3.0	20210203	TR	P1M01	0.0	109.0(14)	130.3(14)	22.3(31)	-0.2(30)	3.1(30)	8(32)	A.9		
J1709+2313	0.0046	25.3	20201027	TR	P1M01	0.0	27.8(14)	224.2(14)	35.6(31)	5.6(30)	7.7(30)	39.1(8)	A.7	w,hiL	
J1710+4923	0.0032	7.0	20201013	TR	P1M01	0.0	22.2(14)	274.8(14)	16.5(30)	-0.6(30)	10.3(30)	6.9(8)	A.7	w,ot	
J1715+46	0.548	20.7	20210204	TR	P1M01		10.5(7)	22.2(7)	44.7(31)	0.9(31)	5.6(31)	17.2(6)	A.9		
J1722+35	0.821	22.8	20211030	SD	P4M07	<1.5	6.9(7)	10.9(7)	22.8(31)	-10.8(31)	13.0(31)	35.1(15)	A.9		
J1736+05	0.999	42.0	20210206	TR	P1M01		4.7(7)	8.6(7)	30.1(31)	13.0(31)	14.4(31)	53.9(11)	A.1	S	
J1738+0333	0.0058	33.7	20201013	TR	P1M01	0.0	9.7(7)	82.6(7)	25.7(30)	-2.6(30)	4.5(30)	33.2(3)	A.9		
J1738+04	1.391	23.1	20210206	TR	P1M01		6.9(7)	10.0(7)	28.7(35)	1.2(33)	9.0(33)	26.7(28)	A.9		
J1739+0612	0.234	95.4	20201013	TR	P1M01	0.0	11.4(4)	23.2(4)	26.6(30)	7.6(30)	12.5(30)	26.6(3)	A.9		22,29
J1741+1351	0.0037	24.2	20201013	TR	P1M01	0.0	10.5(14)	134.9(14)	16.4(33)	5.0(32)	5.3(32)	63.2(36)	A.9		
J1743-0339	0.444	30.2	20201114	TR	P1M01	0.0	10.7(7)	17.6(7)	15.8(32)	2.8(32)	5.0(32)	48.2(28)	A.2	ot	13
J1745-0129	1.045	90.1	20201129	TR	P1M01	0.0	2.4(7)	7.1(7)	10.2(30)	9.1(30)	12.1(30)	36.3(9)	A.9		
J1745+1017	0.0026	23.9	20201115	TR	P1M01	0.0	35.7(14)	116.6(14)	51.0(30)	-10.5(30)	13.5(30)	24.2(3)	A.9		
J1745+1252	1.059	66.1	20210207	TR	P1M01	0.0	12.1(14)	24.2(14)	18.9(32)	-2.0(31)	3.4(31)	70.3(31)	A.9		
J1750+07	5.725⋆	55.6	20210208	TR	P1M01		2.5(7)	4.3(7)	20.3(33)	-0.8(32)	3.1(32)	55(3)	A.9		
J1800-0125	0.783	50.0	20201129	TR	P1M01	0.0	12.0(7)	23.7(7)	24.4(30)	-7.2(30)	8.3(30)	41.4(3)	A.1	S	
J1800+5034	0.578	22.7	20201016	TR	P1M01	0.0	7.1(7)	10.9(7)	18.5(30)	-5.6(30)	13.9(30)	22.3(6)	A.9		
J1802+0128	1.108⋆	98.0	20210117	TR	P1M01	0.0	4.2(7)	6.5(7)	8.2(30)	2.2(30)	3.2(30)	18.4(11)	A.9		
J1806+1023	0.484	52.0	20210115	TR	P1M01	0.0	1.8(7)	17.8(7)	29.6(30)	-1.3(30)	6.1(30)	25.9(4)	A.2	ot?	
J1806+2819	0.015	18.7	20210110	TR	P1M01	0.0	27.5(28)	81.9(28)	17.6(31)	3.5(31)	6.5(31)	28(9)	A.2	ot,S	
J1807+04	0.798	52.6	20211123	SD	P1M04	<1.5	9.5(7)	12.4(7)	27.7(31)	4.1(31)	21.5(31)	92.6(13)	A.1	S	
J1807+0756	0.464	89.2	20210117	TR	P1M01	0.0	13.3(7)	20.6(7)	4.2(30)	-4.3(30)	5.7(30)	148.1(19)	A.2	ot,S	
J1808+00	0.425	149.0	20210619	SS	P4M07	<1.5	11.5(7)	21.1(7)	29.7(31)	-2.2(31)	2.6(31)	119.8(6)	A.1	S	
J1809-0119	0.744	140.0	20210118	TR	P1M01	0.0	5.8(7)	11.0(7)	23.8(30)	-31.7(30)	32.8(30)	21.7(3)	A.4	hiC	
J1809+17	2.066	45.5	20211123	SD	P4M07	<1.5	3.5(7)	7.7(7)	22.4(30)	-7.4(30)	8.1(30)	93.0(8)	A.1	S	
J1810+0705	0.307	79.4	20210213	TR	P1M01	0.0	11.3(7)	46.0(7)	18.5(30)	2.8(30)	9.5(30)	158.3(4)	A.9		
J1811-0154	0.924	148.1	20210811	SS	P1M09	1.4	7.7(4)	13.1(4)	27.0(30)	-8.6(30)	16.9(30)	28.1(8)	A.9		22
J1812+0226	0.793	104.1	20201129	TR	P1M01	0.0	6.7(7)	9.2(7)	9.2(30)	3.5(30)	4.2(30)	-22.7(5)	A.9		13,16
J1813+1822	0.336	60.8	20210116	TR	P1M01	0.0	10.5(7)	20.7(7)	26.1(30)	-5.0(30)	6.2(30)	116.6(4)	A.2	ot	
J1814+1130	0.751	65.0	20210116	TR	P1M01	0.0	4.1(7)	8.3(7)	6.6(30)	2.0(30)	2.8(30)	64.3(19)	A.9		
J1814+22	0.253	62.4	20210207	TR	P1M01		5.1(7)	12.0(7)	23.8(33)	-7.6(32)	9.7(32)	118.5(24)	A.9		
J1816+4510	0.0031	38.8	20201230	TR	P1M01	0.0	24.3(14)	228.1(14)	4.5(30)	-14.4(30)	15.6(30)	38(4)	A.7	w	
J1818-0151	0.837	201.0	20210923	SS	P4M02	0.2	5.3(4)	13.0(4)	15.3(31)	-2.8(31)	13.3(31)	127.2(21)	A.9		
J1821+0155	0.033	51.8	20210618	SS	P3M18	0.4	3.6(4)	8.1(4)	27.7(30)	1.2(30)	3.6(30)	109.5(6)	A.9		
J1821-0256	0.414	84.0	20210811	SS	P4M04	0.6	8.6(7)	15.7(7)	9.3(31)	2.4(31)	4.0(31)	75.7(33)	A.9		
J1821+4147	1.261	40.6	20201031	TR	P1M01	0.0	14.1(7)	16.0(7)	29.9(30)	0.7(30)	8.7(30)	35.9(4)	A.2	ot	
J1822+0705	1.362	62.2	20210616	SS	P1M11	1.8	1.8(2)	13.0(2)	16.6(30)	3.1(30)	9.1(30)	158.4(11)	A.9		
J1822+1120	1.786	95.2	20210116	TR	P1M01	0.0	4.9(7)	11.1(7)	27.4(31)	12.4(31)	16.0(31)	108.9(12)	A.9		
J1823-0154	0.759	135.9	20210828	SS	P2M19	0.8	2.4(2)	7.1(2)	19.2(30)	6.9(30)	10.4(30)	106.4(6)	A.2	ot,S	
J1823+0550	0.752	66.7	20210701	SS	P3M12	1.5	22.0(7)	28.9(7)	23.3(30)	4.4(30)	10.9(30)	141.9(4)	A.2	ot	13,24
J1824-0127	2.499	63.2	20210822	SS	P2M16	1.4	1.7(2)	9.8(2)	24.9(32)	-15.2(32)	16.6(32)	74.9(8)	A.2	ot,S	
J1824-0132	0.223	81.0	20211124	SS	P4M09	1.6	12.9(14)	35.3(14)	10.0(32)	0.1(32)	3.2(32)	57(5)	A.2	ot	
J1825+0004	0.779	56.6	20210826	TR	P1M08	1.0	3.9(4)	14.3(4)	24.9(30)	0.7(30)	11.1(30)	19.4(5)	A.9		13,19
J1826-00	0.0045	42.6	20211212	SS	P3M12		9.2(14)	-	25.3(37)	8.4(35)	16.7(35)	2(2)	A.9		
J1827+00	0.375	97.6	20210610	SS	P2M06	<1.5	10.2(28)	–	30.1(45)	-1.3(40)	0.0(39)	-81(8)	A.9		
J1828+0625	0.0036	22.4	20210118	TR	P1M01	0.0	54.5(14)	126.7(14)	14.8(33)	-10.6(33)	12.4(33)	24.4(17)	A.1	S	
J1829+2456	0.041	13.8	20210115	TR	P1M01	0.0	3.6(7)	12.3(7)	67.0(37)	-1.5(34)	2.0(34)	-1.0(9)	A.3	hiL	
J1830-0052	0.345	220.4	20210905	SS	P2M03	0.9	11.0(14)	–	23.8(37)	2.5(36)	5.8(36)	245(6)	A.9		
J1830-0131	0.457⋆	97.3	20210828	SS	P1M08	1.1	8.9(7)	15.0(7)	12.2(30)	3.0(30)	6.2(30)	134.9(15)	A.2	ot	
J1832+27	0.631	47.5	20211123	SD	P4M03	<1.5	8.4(7)	12.1(7)	24.8(31)	15.2(31)	16.2(31)	61.7(18)	A.5	cd,S	
J1833-0209	0.583⋆	326.1	20210928	SS	P3M02	1.1	11.7(7)	15.6(7)	22.9(33)	-11.0(33)	13.4(33)	293.8(19)	A.5	cd,S	
J1834+10	1.172	78.4	20210213	TR	P1M01		3.7(7)	26.5(7)	30.1(31)	7.0(31)	7.8(31)	98.2(6)	A.1	S	
J1835-0114	0.0051	98.2	20210912	SS	P4M11	0.9	31.7(14)	149.0(15)	28.5(31)	-19.0(31)	20.4(31)	116.8(13)	A.7	w,ot	
J1836+09	0.541	36.3	20211221	SS	P2M10		4.0(4)	7.8(4)	27.6(31)	-2.4(31)	4.1(31)	77.3(12)	A.9		
J1837-0045	0.617	86.9	20210912	SS	P3M07	0.9	3.5(4)	17.0(4)	20.2(30)	-1.2(30)	6.0(30)	139.6(8)	A.2	ot	22
J1837+0053	0.473	122.5	20200203	TR	P1M15	2.2	34.1(14)	74.7(14)	20.9(33)	-0.9(32)	8.8(32)	-10.4(34)	A.2	ot,S	
J1837+1221	1.963	100.6	20210701	SS	P2M06	1.1	1.8(2)	7.9(2)	29.2(30)	3.5(30)	6.8(30)	146.7(4)	A.9		22
J1838+0044g	2.203	228.1	20200203	TR	P1M01	<1.5	1.7(4)	17.6(4)	36.6(32)	-4.1(32)	5.1(32)	177.9(7)	A.5	cd,S	
J1838-01	0.183	312.0	20210928	SS	P2M06	<1.5	2.7(4)	6.3(4)	77.7(32)	-8.5(31)	9.5(31)	420.9(5)	A.3	hiL	

Table 3 *– continued –*

PSR	P (s)	DM[a]	Date	Mode	Beam	Offset (′)	W_{50} (°)	W_{10} (°)	L/I (%)	V/I (%)	$\|V\|$/I (%)	RM ($\mathrm{rad/m^2}$)	Fig.	Note.	Ref.
(1)	(2)	(3)	(4)	(5)	(6)	(7)	(8)	(9)	(10)	(11)	(12)	(13)	(14)	(15)	(16)
J1838-0107	0.444	270.1	20210928	SS	P4M15	0.2	3.7(4)	29.9(4)	14.9(30)	-8.5(30)	10.1(30)	412.7(12)	A.5	cd	
J1838+1523	0.549	68.2	20210117	TR	P1M01	0.0	11.9(7)	39.4(7)	38.5(30)	-21.8(30)	23.5(30)	160.4(4)	A.2	ot?	
J1839-0223	1.266	336.8	20210816	SS	P4M18	1.5	12.0(7)	15.4(7)	21.0(33)	-9.8(33)	10.2(33)	147.1(34)	A.5	cd,S	
J1840+0214	0.797	182.4	20210616	SS	P3M11	0.7	4.5(7)	7.6(7)	27.5(31)	-5.3(31)	6.7(31)	108.1(10)	A.9		
J1841-0157	0.663	475.0	20210901	SS	P3M01	1.7	11.5(4)	19.9(4)	16.0(30)	-3.3(30)	3.8(30)	100.7(5)	A.9		
J1841+0912	0.381	49.1	20210630	SS	P1M03	0.5	8.9(2)	13.3(2)	29.4(30)	0.7(30)	5.9(30)	53.3(2)	A.2	ot,S	10,13,24
J1842-0153	1.054	426.8	20210903	TR	P1M15	1.2	8.2(4)	20.2(4)	14.9(30)	4.4(30)	5.3(30)	142.9(8)	A.8	c	
J1842+0257	3.088	148.1	20210215	SS	P4M10	1.1	6.0(2)	10.6(2)	20.6(31)	5.9(31)	6.6(31)	69.4(6)	A.1	S	
J1842+0358	0.233	106.7	20220513	SC	P1M05		5.0(4)	184.7(4)	32.7(30)	-3.1(30)	4.4(30)	32.7(7)	A.6	ip	
J1842+0638	0.313	214.4	20210610	SS	P2M14	1.6	15.3(7)	19.6(7)	34.0(31)	15.4(31)	16.9(31)	335.6(8)	A.2	ot	
J1842+1332	0.471	102.5	20210115	TR	P1M01	0.0	72.1(7)	109.6(7)	38.7(30)	-1.9(30)	2.5(30)	130.3(2)	A.2	ot,S	22,29
J1843-0000	0.880	101.5	20200203	TR	P1M01	0.5	10.4(2)	14.9(2)	15.5(30)	-0.7(30)	2.7(30)	-51.6(3)	A.2	ot	29
J1843-0050	0.782	511.8	20210811	SS	P1M01	1.4	9.5(7)	18.2(7)	2.9(31)	-4.4(31)	5.0(31)	144(5)	A.9		
J1843-0137	0.669	484.8	20220202	TR	P1M12	1.2	10.0(7)	24.2(7)	7.7(31)	5.6(30)	6.6(30)	581(2)	A.9		
J1843-0211	2.027	441.7	20210822	SS	P2M03	0.9	3.1(2)	17.6(2)	55.1(31)	-7.1(31)	7.7(31)	-79.1(2)	A.5	cd,S	
J1843+0119	1.267	250.1	20220720	TR	P1M10		11.6(7)	-	31.9(36)	-7.7(35)	10.1(35)	50(3)	A.1	S	
J1843+04	0.397	267.2	20220423	SS	P2M09		6.0(7)	11.2(7)	11.0(34)	2.5(33)	5.9(33)	187(5)	A.9		
J1843+2024	3.406	85.3	20210116	TR	P1M01	0.0	5.0(7)	6.8(7)	23.2(31)	14.0(31)	15.2(31)	151.9(12)	A.9		
J1844-0030	0.641	604.2	20201219	SS	P1M18	0.1	7.8(7)	15.0(7)	13.7(30)	8.4(30)	9.1(30)	217.7(13)	A.9		
J1844-0244	0.507	424.5	20221120	SS	P4M02		13.8(4)	29.2(4)	12.5(30)	-0.1(30)	1.5(30)	111.2(11)	A.9		13
J1844-0256	0.273	824.8	20221120	SS	P4M05		66.9(28)	-	44.6(34)	-7.8(32)	9.3(32)	239(5)	A.9		22
J1844-0302	1.198	543.8†	20221120	SS	P2M14		7.0(7)	-	17.5(35)	1.7(34)	6.4(34)	955(6)	A.9		
J1844+00	0.460	345.5	20210217	TR	P1M15		4.6(7)	27.6(7)	33.5(30)	-7.4(30)	7.6(30)	328.9(4)	A.2	ot,S	
J1844+0115	0.0041	148.2	20201218	SS	P3M09	1.2	30.0(56)	–	22.8(40)	-4.9(39)	4.1(38)	41(18)	A.9		
J1844+1454	0.375	41.4	20210430	TR	P1M01	0.0	11.1(2)	15.2(2)	37.3(30)	0.4(30)	2.6(30)	119.1(3)	A.3	hiL	8,13,21
J1845+0623	1.421	115.0	20210619	SS	P2M07	0.8	2.7(4)	6.7(4)	18.2(30)	-2.4(30)	4.8(30)	235.3(7)	A.9		23
J1846+0051	0.434	140.8	20200417	SS	P1M07	1.1	10.5(7)	21.3(7)	64.0(35)	-18.8(34)	20.0(34)	-67.6(8)	A.1	S	
J1847-0130	6.707	674.8	20210905	SS	P2M07	1.3	10.3(7)	14.9(7)	35.3(31)	-2.3(31)	4.0(31)	-376.5(11)	A.2	ot	
J1847+01	0.0034	20.1	20200901	SS	P1M01	<1.5	18.5(28)	–	41.4(37)	-6.8(34)	9.6(34)	24(5)	A.9		
J1847+0133g	2.846	193.8	20200902	TR	P1M01	<1.5	3.2(7)	5.0(7)	53.2(38)	19.7(35)	21.3(35)	11.3(18)	A.9		
			20200910	TR	P1M01										
J1847+0614g	1.662	273.0	20210220	TR	P1M01	<1.5	6.9(7)	12.6(7)	28.8(33)	19.4(33)	22.9(33)	98.5(14)	A.1	S	
J1848-0023	0.537	35.0	20210119	SS	P3M03	1.2	2.6(4)	16.1(4)	15.8(31)	0.7(31)	5.2(31)	20.4(26)	A.9		
J1848-0055	0.274	1162.8	20211024	SS	P2M17	0.7	57.2(28)	-	27.6(34)	9.0(34)	10.0(34)	-433(4)	A.8	c	
J1848-0123	0.659	159.5	20210816	SS	P3M12	0.4	9.2(2)	20.3(2)	16.4(30)	1.5(30)	2.3(30)	514.6(3)	A.2	ot	13,16,24
J1848+0127g	0.534	77.7	20200811	TR	P1M01	<1.5	9.0(7)	24.8(7)	43.7(34)	0.9(33)	2.6(33)	-49.1(12)	A.9		20
			20200829	TR	P1M01										
J1848+0150g	3.290	503.3	20201004	TR	P1M01	<1.5	6.6(7)	–	27.4(45)	-7.5(42)	9.3(42)	211(11)	A.9		
J1848+0351	0.191	336.6	20210609	SS	P1M15	0.6	14.0(14)	–	14.9(34)	-11.0(34)	15.8(33)	181(4)	A.9		
J1848+0604	2.218	242.7	20210428	SS	P1M16	1.6	4.6(7)	8.7(7)	17.7(32)	-12.0(31)	16.8(31)	-119.9(18)	A.1	S	23
J1848+0826	0.328	90.3	20210608	SS	P3M07	0.7	20.1(14)	38.7(14)	26.9(34)	-1.4(34)	2.0(34)	272.4(10)	A.1	S	
J1848+12	0.754	128.5	20210714	TR	P1M17		57.1(7)	77.4(7)	35.3(32)	-3.0(32)	6.1(32)	216.9(3)	A.2	ot,S	
J1848+1516	2.233	73.4	20211202	SS	P1M13	1.0	24.7(7)	48.5(7)	41.4(30)	-4.0(30)	17.3(30)	238.4(8)	A.9		
J1849+0001g	0.525	189.4	20200415	TR	P1M01	<1.5	10.5(14)	–	17.2(35)	2.0(34)	8.2(34)	-251(10)	A.9		
			20200902	TR	P1M01										
J1849-0014g	0.491	346.5	20200401	TR	P1M01	<1.5	24.0(14)	74.2(14)	20.8(31)	-1.6(31)	3.1(31)	-107(2)	A.8	c	30
			20200815	TR	P1M01										
J1849-0040	0.672	1282.9	20210130	SS	P4M15	0.9	55.2(28)	–	5.0(33)	8.2(32)	8.8(32)	-427(15)	A.9		
J1849+0106	1.832	216.8	20211014	SC	P1M01		1.2(4)	10.1(4)	29.5(31)	-5.7(30)	6.5(30)	106.9(10)	A.5	cd,S	
J1849+0127	0.542	203.3	20200326	SS	P4M15	1.0	7.1(7)	19.2(7)	15.0(31)	-1.3(31)	4.6(31)	-145.8(12)	A.2	ot,S	
J1849+0225g	1.474	267.7	20201002	TR	P1M01	<1.5	4.7(7)	8.3(7)	5.5(34)	-12.1(33)	13.6(33)	186(12)	A.9		
J1849+0340g	1.666	350.0	20210318	TR	P1M01	<1.5	14.7(7)	18.0(7)	29.0(35)	3.9(34)	9.6(34)	256.3(13)	A.1	S	
J1849+0409	0.761	63.7	20210609	SS	P1M19	3.2	177.5(14)	–	38.3(41)	6.7(38)	15.6(38)	15.7(32)	A.6	ip	30
J1849+0430	0.421	189.0	20200203	TR	P1M01		17.4(28)	–	23.6(36)	-4.1(34)	3.5(33)	148(9)	A.9		
J1849+2559	0.519	75.0	20210427	TR	P1M01	0.0	3.6(7)	14.9(7)	20.5(31)	-9.9(31)	14.0(31)	60.1(11)	A.9		
J1850-0006	2.191	630.0	20200821	TR	P1M13	1.2	28.6(28)	67.0(28)	19.2(30)	-0.4(30)	1.6(30)	685.0(7)	A.9		
J1850-0020g	1.574	602.3	20200402	TR	P1M01	<1.5	7.5(7)	17.9(7)	14.4(32)	1.6(32)	6.3(31)	89(7)	A.9		
			20200801	TR	P1M01										
			20200819	TR	P1M01										
J1850-0026	0.166	947.0	20200402	TR	P1M03	1.4	42.7(28)	112.8(28)	49.0(30)	-12.3(30)	13.6(30)	664.3(3)	A.8	c	
J1850-0031	0.734	895.0	20200402	SS	P1M10	0.4	22.3(14)	59.0(14)	27.7(31)	-4.0(30)	4.5(30)	-212.5(25)	A.8	c	
J1850+0423	0.290	265.8	20210506	SS	P3M15	1.0	30.7(14)	54.0(14)	33.5(31)	11.8(31)	14.4(31)	25.8(9)	A.9		
J1850+1335	0.345	60.1	20210618	SS	P4M09	1.7	5.5(2)	11.5(2)	62.7(30)	-9.1(30)	9.5(30)	154.8(4)	A.1	S	13,16,21
J1850+15	1.383	21.1	20210806	SS	P4M05		8.0(7)	-	36.7(42)	-23.4(39)	23.6(38)	63(4)	A.9		
J1851-0029	0.518	522.0	20210306	SS	P1M17	0.3	9.5(7)	19.8(7)	13.2(31)	1.9(31)	2.9(31)	653.9(12)	A.1	S	
J1851-0053	1.409	24.0	20210822	SS	P2M04	1.3	3.8(2)	7.9(2)	11.2(30)	-8.7(30)	9.2(30)	-17.7(4)	A.9		
J1851-0114	0.953	427.2	20210923	SS	P2M03	1.1	8.0(7)	18.4(7)	20.4(31)	5.5(31)	6.4(31)	375.1(9)	A.1	S	
J1851+0118	0.907	420.4	20211012	SS	P2M03	0.4	5.8(14)	12.4(14)	72.9(33)	34.7(31)	36.7(31)	-331.8(8)	A.6	ip.hiC	
J1851+0241	4.491	524.3	20200528	SS	P1M17	1.2	3.5(4)	–	25.3(37)	2.8(35)	6.3(35)	422(6)	A.9		
J1851+0418	0.284	115.5	20200509	SS	P2M08	1.3	89.7(7)	204.7(7)	9.9(30)	3.4(30)	4.0(30)	96.9(7)	A.7	w	13,16

Table 3 *– continued –*

PSR	P (s)	DM[a]	Date	Mode	Beam	Offset (′)	W_{50} (°)	W_{10} (°)	L/I (%)	V/I (%)	$\|V\|$/I (%)	RM ($\mathrm{rad/m^2}$)	Fig.	Note.	Ref.
(1)	(2)	(3)	(4)	(5)	(6)	(7)	(8)	(9)	(10)	(11)	(12)	(13)	(14)	(15)	(16)
J1851+1259	1.205	70.2	20210605	SS	P3M19	2.7	3.2(7)	6.0(7)	21.5(31)	2.9(31)	5.1(31)	147(2)	A.9		13,16
J1852-0024g	0.355	292.0	20200905	TR	P1M01	<1.5	6.5(7)	14.0(7)	24.7(32)	1.4(32)	9.5(32)	95.9(24)	A.9		31
J1852-0054g	0.164	211.3	20210408	TR	P1M01	<1.5	28.7(28)	–	46.4(37)	-1.8(34)	6.4(34)	166(3)	A.9		
J1852-0118	0.451	286.4	20211113	TR	P1M04	1.5	142.0(7)	154.9(7)	65.1(30)	-6.1(30)	11.2(30)	708.4(6)	A.3	hiL,S	
J1852+0008	0.467	254.9	20200404	TR	P1M06	1.9	11.9(14)	24.2(15)	58.4(34)	1.1(32)	7.3(32)	-1(1)	A.9		
J1852+0013	0.957	545.0	20200826	TR	P1M03	0.7	7.3(7)	14.9(7)	21.7(30)	4.0(30)	5.2(30)	460.1(12)	A.8	c	13,16
J1852+0018g	0.318	455.4	20200826	TR	P1M01	<1.5	13.6(14)	–	74.7(37)	-4.5(34)	5.6(34)	74.6(11)	A.3	hiL	
			20200915	TR	P1M01										
J1852+0031	2.180	787.0	20200816	TR	P1M06	0.2	54.6(7)	156.9(7)	6.3(30)	0.2(30)	1.1(30)	313.4(7)	A.8	c,ot	16,29
J1852+0056g	1.177	881.9	20200404	TR	P1M01	<1.5	15.4(28)	213.5(29)	52.1(34)	-30.4(34)	30.0(33)	-92.3(11)	A.6	ip,c,hiC	
			20200819	TR	P1M01										
J1852+0158g	0.185	608.9	20200812	TR	P1M01	<1.5	22.6(28)	–	33.7(39)	6.5(38)	7.3(37)	91(4)	A.9		
J1852+0305	1.326	320.0	20210211	SS	P3M09	1.1	10.7(7)	21.1(7)	43.5(32)	-2.4(31)	14.0(31)	245.3(8)	A.9		
J1852+0857g	3.771	86.5	20210306	TR	P1M01	<1.5	3.7(7)	8.7(7)	19.5(32)	8.7(32)	10.3(31)	321.3(22)	A.9		
J1853-0004	0.101	437.5	20200404	TR	P1M09	1.3	7.7(7)	50.0(7)	92.3(31)	2.9(30)	3.7(30)	633.9(4)	A.3	hiL	29
J1853+0009	0.033	192.4	20200401	TR	P1M13	0.8	12.6(14)	29.3(14)	13.3(32)	1.1(32)	5.0(32)	162(2)	A.2	ot	
J1853+0023g	0.576	206.6	20200405	TR	P1M01	<1.5	13.4(14)	–	21.0(36)	0.6(34)	11.4(34)	19(9)	A.9		
			20200418	TR	P1M01										
			20200827	TR	P1M01										
J1853+0029	1.876	226.7	20200920	TR	P1M07	2.0	13.2(7)	16.9(7)	28.8(30)	7.6(30)	15.8(30)	58.2(9)	A.2	ot	
J1853+0056	0.275	180.9	20201026	SS	P3M11	1.2	15.9(14)	29.1(14)	78.7(34)	-33.6(33)	36.7(33)	67.2(8)	A.1	S,hiL,hiC	
J1853+0259	0.585	290.2	20200509	SS	P3M14		39.9(14)	–	34.9(37)	-8.5(37)	13.6(37)	132.0(21)	A.1	S	
J1853+0312g	0.438	342.0	20200818	TR	P1M01	<1.5	4.9(7)	–	26.6(42)	8.5(41)	13.4(40)	115(4)	A.9		
J1853+0427	1.320	550.1	20211004	TR	P1M01		2.3(7)	23.9(7)	31.0(30)	14.6(30)	16.2(30)	380.3(7)	A.2	ot,S	
J1853+0505	0.905	260.0†	20210422	SS	P2M11	1.2	47.5(14)	136.5(14)	17.7(30)	-5.0(30)	6.1(30)	10.3(4)	A.8	c	
J1853+0545	0.126	198.7	20200801	SS	P4M06	1.1	30.3(7)	75.8(7)	6.7(30)	7.1(30)	8.3(30)	83.5(11)	A.8	c,ot	29
J1853+0853	3.914	235.6	20210208	SS	P2M05	2.0	4.0(7)	7.0(7)	9.0(32)	1.5(31)	8.2(31)	599(6)	A.2	ot?	
J1853+1303	0.0040	30.5	20210607	SS	P3M15	1.4	50.9(14)	191.8(14)	20.5(31)	4.0(31)	19.6(31)	78.2(15)	A.7	w,ot	23
J1854-00	0.716	492.8	20220306	TR	P1M14		9.2(14)	25.1(14)	37.9(34)	-3.5(33)	6.6(33)	563.4(15)	A.9		
J1854-0033g	0.361	615.9	20200909	TR	P1M01	<1.5	14.3(28)	–	33.5(43)	-1.9(40)	2.0(40)	481(6)	A.9		
J1854-01	0.680	570.0	20210919	TR	P1M07		33.7(14)	-	19.0(33)	9.1(32)	15.7(32)	1100(7)	A.2	ot	
J1854+0050	0.767	525.0	20200401	TR	P1M01		7.4(14)	23.8(14)	20.8(33)	11.6(33)	13.0(33)	238(6)	A.9		
J1854+0306	4.557	192.4	20200509	SS	P1M12	1.6	1.8(4)	6.0(4)	50.6(32)	-7.1(32)	8.7(32)	-54.7(10)	A.1	S	
J1854+0317	1.366	390.0	20200522	SS	P2M15	1.4	7.7(7)	12.3(7)	30.0(32)	-4.1(31)	5.6(31)	145.7(15)	A.9		
J1854+0319	0.628	480.2	20200509	SS	P2M09	1.2	7.6(7)	31.9(7)	36.4(33)	15.8(32)	17.2(32)	225.1(11)	A.5	cd,S	
J1854+0704g	0.450	10.5	20210126	TR	P1M01	<1.5	14.0(14)	–	14.2(36)	6.0(34)	9.2(34)	-16(4)	A.2	ot?	
J1854+1050	0.573	207.2	20210608	SS	P4M09	1.8	5.8(4)	31.6(4)	38.7(30)	11.6(30)	14.6(30)	501.1(5)	A.2	ot	
J1855+0139g	0.444	405.5	20200404	TR	P1M01	<1.5	21.4(28)	–	62.0(37)	-26.3(36)	31.8(36)	123.0(21)	A.3	hiL,hiC,S	
			20200828	TR	P1M01										
J1855+0235g	0.983	104.1	20210111	TR	P1M01	<1.5	3.2(7)	7.0(7)	16.3(38)	12.5(37)	18.1(37)	-23(9)	A.9		
J1855+0306	1.633	634.0	20201206	SS	P3M16	1.3	6.9(14)	–	58.4(71)	-39.2(61)	44.8(61)	3(18)	A.4	hiC	
J1855+0307	0.845	402.5	20201206	SS	P2M16	3.1	6.0(14)	–	62.7(47)	18.0(42)	19.8(41)	33.1(22)	A.9		
J1855+0511g	1.421	292.1	20200820	TR	P1M01	<1.5	25.3(28)	–	14.8(45)	-12.9(40)	16.2(40)	67(19)	A.9		
J1855+0527	1.393	358.8	20210608	SS	P3M06	1.1	11.3(7)	33.8(7)	64.1(32)	41.8(31)	45.5(31)	121.6(9)	A.8	c,hiC	
J1855+0700	0.258	247.2	20201222	SS	P3M10	0.5	6.0(14)	10.3(14)	20.6(32)	-1.4(31)	3.5(31)	528(3)	A.6	ip,S	
J1856+0011g	0.928	454.2	20200807	TR	P1M01	<1.5	3.2(7)	–	41.3(44)	12.8(40)	14.7(39)	616.4(23)	A.9		
J1856+0102	0.620	554.4	20220329	TR	P1M15		9.6(7)	16.3(7)	9.3(30)	3.7(30)	4.3(30)	560.5(17)	A.1	S	
J1856+0211g	9.889	127.4	20210113	TR	P1M01	<1.5	1.1(2)	–	52.0(43)	32.4(40)	43.0(40)	-175(3)	A.4	hiC	31
J1856+0243g	0.546	181.4	20201120	TR	P1M01	<1.5	7.9(7)	23.7(7)	49.8(32)	-6.0(32)	7.4(32)	75.3(8)	A.5	cd,S,hiL	
J1856+0245	0.080	623.5	20201104	SS	P4M03	1.3	82.2(28)	–	56.4(37)	20.9(36)	22.5(36)	259.2(11)	A.1	S	30
J1856+0404	0.420	344.5	20200528	SS	P2M07	1.3	14.5(7)	35.4(7)	16.8(31)	-0.8(31)	3.8(31)	-123.6(13)	A.9		
J1856+0615g	0.327	335.7	20200806	TR	P1M01	<1.5	7.4(7)	13.9(7)	20.7(31)	5.4(31)	6.8(31)	871(2)	A.9		
J1856+0912	2.170	192.6	20211009	SC	P1M01		6.9(4)	9.3(4)	37.0(30)	0.8(30)	10.1(30)	617.9(7)	A.1	S?	
J1857+0057	0.356	82.3	20200830	TR	P1M03	2.9	25.1(7)	35.8(7)	43.8(31)	-13.1(31)	14.0(31)	91.1(5)	A.1	S	13,16,19
J1857+0210	0.630	783.0	20210113	TR	P1M08	0.6	9.7(7)	25.2(7)	9.9(30)	-2.1(30)	2.6(30)	110.8(23)	A.9		
J1857+0212	0.415	506.7	20211107	SS	P3M19	1.1	11.5(4)	18.8(4)	16.1(30)	2.0(30)	2.6(30)	420.4(7)	A.2	ot	13
J1857+0224g	0.875	399.0	20200822	TR	P1M01	<1.5	14.9(14)	–	18.4(37)	8.2(35)	10.6(34)	76(4)	A.9		
J1857+0300	0.772	691.0	20200519	SS	P2M17	1.1	7.3(14)	–	33.3(41)	-3.3(39)	1.6(38)	883.0(26)	A.9		
J1857+0526	0.349	466.4	20200514	SS	P1M02	1.5	10.1(7)	29.3(7)	45.0(31)	-15.6(30)	17.2(30)	956.4(8)	A.8	c	18
J1857+0809	0.502	281.6	20211111	TR	P1M07	1.3	10.0(7)	17.5(7)	7.8(31)	-1.9(30)	1.8(30)	667(4)	A.2	ot?	
J1857+0943	0.0053	13.3	20210424	SS	P1M18	2.3	36.3(7)	206.1(7)	10.3(30)	0.9(30)	6.0(30)	21.6(12)	A.6	ip	6,26,28
J1858-0024g	0.400	190.6	20200829	TR	P1M01	<1.5	31.8(28)	–	43.2(42)	-13.0(41)	17.8(40)	486(5)	A.3	hiL	
			20200917	TR	P1M01										
J1858-02	1.462	182.6	20211022	SS	P2M07		5.8(4)	7.9(4)	26.6(30)	-2.8(30)	10.6(30)	240.6(9)	A.1	S	
J1858+0215	0.745	702.0	20200418	SS	P2M16	1.0	16.8(14)	40.7(14)	37.8(32)	5.7(32)	7.9(32)	-4.2(15)	A.9		
J1858+0239	0.197	492.7	20200606	TR	P1M01		20.7(14)	31.6(14)	74.9(32)	0.4(31)	2.7(31)	93.9(5)	A.1	S,hiL	
J1858+0241	4.693	324.0	20200806	TR	P1M02	1.2	6.0(4)	8.3(4)	25.5(31)	-2.3(31)	3.4(31)	-51.2(10)	A.1	S	
J1858+0310g	0.372	703.4	20201112	TR	P1M01	<1.5	124.0(28)	–	89.4(40)	5.2(37)	12.8(36)	406.4(10)	A.3	hiL,S	
J1858+0319	0.867	284.0	20201026	SS	P1M11	1.0	4.2(7)	–	26.4(38)	12.0(36)	12.7(36)	-161(5)	A.9		
J1858+0346	0.256	386.0	20201209	SS	P2M03	0.9	55.6(28)	–	90.8(39)	7.5(34)	9.3(34)	-555.3(10)	A.3	hiL	

Table 3 *– continued –*

PSR	P (s)	DM[a]	Date	Mode	Beam	Offset (′)	W_{50} (°)	W_{10} (°)	L/I (%)	V/I (%)	$\|V\|$/I (%)	RM (rad/m^2)	Fig.	Note.	Ref.
(1)	(2)	(3)	(4)	(5)	(6)	(7)	(8)	(9)	(10)	(11)	(12)	(13)	(14)	(15)	(16)
J1859+00	0.559	420.0	20200513	SS	P3M15		34.8(7)	61.9(7)	24.4(30)	-4.2(30)	4.9(30)	581.6(4)	A.2	ot,S	
J1859+0126g	0.957	529.2	20200815	TR	P1M01	<1.5	13.4(14)	–	57.4(38)	6.4(37)	8.4(37)	358.0(12)	A.1	S	
J1859+0430g	0.336	785.4	20200402	TR	P1M01	<1.5	18.8(28)	–	24.5(39)	17.9(38)	19.6(37)	1554(9)	A.9		
			20200404	TR	P1M01										
			20200816	TR	P1M01										
J1859+0434g	0.458	321.8	20200404	TR	P1M01	<1.5	12.5(14)	–	96.9(49)	0.1(39)	6.4(39)	-103.9(14)	A.3	hiL	
			20200815	TR	P1M01										
J1859+0601	1.044	276.0	20200821	TR	P1M01	1.7	10.5(14)	49.6(14)	28.1(32)	3.2(32)	5.5(32)	76.6(16)	A.8	c	
J1859+1526	0.934	97.4	20210806	SS	P1M04	1.6	3.0(7)	12.1(7)	29.0(32)	-9.8(32)	12.7(32)	334.3(22)	A.9		23
J1900-0051	0.385	136.0	20220420	TR	P1M16		4.6(7)	13.9(7)	32.7(34)	-0.6(33)	1.4(33)	236(2)	A.9		
J1900-0134	1.832	177.7	20211022	SS	P1M16		9.1(7)	11.8(7)	24.7(31)	9.1(30)	10.5(30)	18.8(12)	A.5	cd,S	
J1900+0227	0.374	202.3	20200901	SS	P2M01	0.6	14.6(4)	26.1(4)	15.9(30)	-4.3(30)	5.2(30)	-52.1(7)	A.1	S	23
J1900+0405g	0.072	636.9	20200402	TR	P1M01	<1.5	33.4(28)	–	53.9(38)	-3.7(36)	6.7(35)	132(3)	A.9		
			20200817	TR	P1M01										
J1900+0634	0.389	323.4	20200328	SS	P3M02	1.3	6.0(4)	10.0(4)	29.3(32)	-10.0(32)	11.8(32)	641.3(18)	A.1	S	
J1900+0715g	0.970	263.2	20200904	TR	P1M01	<1.5	15.7(7)	21.7(7)	32.5(31)	21.0(31)	22.5(31)	444.7(16)	A.9		
			20200906	TR	P1M01										
			20200911	TR	P1M01										
			20201001	TR	P1M01										
J1900+30	0.602	71.8	20210211	TR	P1M01		5.6(7)	10.0(7)	15.9(31)	-19.8(31)	20.5(31)	127.8(22)	A.9		
J1901+00	0.777	340.3	20200509	SS	P3M07	<1.5	9.7(4)	13.0(4)	15.1(30)	12.6(30)	19.3(30)	227.3(8)	A.9		
J1901+0020g	0.214	239.1	20201002	TR	P1M01	<1.5	9.3(7)	17.8(7)	42.9(32)	-1.7(32)	2.3(32)	185.5(9)	A.1	S	
J1901+0124	0.318	314.8	20201218	SS	P3M07	2.1	8.4(7)	16.0(7)	59.0(31)	20.0(31)	21.8(31)	365.5(7)	A.1	S	23
J1901+0156	0.288	105.4	20200528	SS	P4M11	3.4	6.7(7)	18.8(7)	31.5(33)	-3.5(32)	6.6(32)	-30.7(17)	A.2	ot	13,16
J1901+0234	0.885	404.8	20200901	SS	P1M09	2.0	6.6(7)	13.2(7)	37.7(34)	7.7(33)	8.7(33)	-34.5(13)	A.1	S	
J1901+0254	1.299	185.0	20200514	SS	P1M03	0.7	18.3(4)	27.5(4)	19.0(30)	-3.9(30)	5.4(30)	-120.8(9)	A.2	ot	
J1901+0320	0.636	396.0	20200403	TR	P1M01	1.2	31.1(14)	58.6(14)	26.7(30)	-7.6(30)	9.3(30)	6.6(7)	A.2	ot,S	
J1901+0331	0.655	401.2	20211208	TR	P1M17		4.8(7)	18.7(7)	32.8(35)	3.6(34)	17.9(34)	-235.6(21)	A.9		13,24
J1901+0355	0.554	547.4	20200418	SS	P1M08	1.2	7.7(7)	11.8(7)	47.9(32)	0.2(31)	4.3(31)	684.3(12)	A.9		
J1901+0413	2.662	347.5	20200401	TR	P1M18	2.5	12.9(7)	17.2(7)	37.2(32)	-10.7(32)	12.1(32)	213.3(7)	A.2	ot,S	18,29
J1901+0510	0.614	435.0	20201219	SS	P4M08	1.1	37.8(14)	60.1(14)	44.6(31)	-8.6(30)	10.5(30)	1301.9(8)	A.1	S	
J1901+0511	4.600	410.0	20210826	TR	P1M03	0.8	1.0(2)	6.5(2)	24.4(30)	-1.3(30)	3.9(30)	824.3(11)	A.2	ot,S	
J1901+0621	0.831	105.2†	20210211	SS	P2M17	0.4	28.8(14)	79.3(14)	14.5(30)	-3.7(30)	6.7(30)	-265.1(10)	A.2	ot,S	
J1901+0716	0.643	252.8	20200607	TR	P1M07	1.2	8.0(2)	22.1(2)	19.7(30)	1.2(30)	5.3(30)	271.9(4)	A.2	ot	13,19
J1901+1306	1.830	75.0	20210208	SS	P3M14	0.7	9.4(7)	13.8(7)	37.1(32)	-1.2(31)	12.5(31)	233.1(11)	A.9		
J1902+0248	1.223	268.8	20210119	SS	P4M08	1.4	2.8(7)	17.2(7)	22.8(32)	4.7(31)	5.3(31)	-172.0(20)	A.9		
J1902+0615	0.673	502.9	20200817	TR	P1M01	1.1	2.1(2)	6.1(2)	10.8(30)	3.7(30)	4.2(30)	546.3(6)	A.9		13,16
J1902+0723	0.487	105.0	20200327	SS	P4M13	0.7	10.8(7)	24.9(7)	18.2(31)	17.9(30)	19.7(30)	-259.1(16)	A.1	S	
J1902+0809g	0.190	436.8	20210320	TR	P1M01	<1.5	3.7(7)	–	84.4(49)	-2.4(43)	2.5(42)	779(2)	A.3	hiL	
J1903+0135	0.729	245.2	20210615	SS	P1M01	0.4	3.7(2)	10.2(2)	13.3(30)	9.5(30)	10.3(30)	73.0(4)	A.2	ot	2,13,16
J1903+0327	0.0021	297.5	20220606	TR	P1M17		57.2(14)	134.4(14)	11.2(30)	-11.5(30)	13.0(30)	234.1(24)	A.8	c	
J1903+0851g	1.231	81.9	20200907	TR	P1M01	<1.5	6.5(14)	–	35.4(40)	9.9(40)	14.0(38)	181(4)	A.1	S	
J1903+0912	0.166	363.1	20201219	SS	P3M14		12.5(28)	–	28.5(43)	-5.9(40)	10.7(39)	627(20)	A.9		
J1903+0925	0.357	162.0	20210317	TR	P1M15		38.7(14)	200.4(14)	25.6(30)	-4.4(30)	7.9(30)	398.1(8)	A.7	w	
J1903+2225	0.651	109.2	20210716	SS	P3M14	1.5	6.5(7)	14.6(7)	25.7(32)	-2.0(31)	5.4(31)	54.6(16)	A.1	S	23
J1904-0150	0.379	158.2	20210828	SS	P3M17	1.3	4.3(4)	13.7(4)	42.4(31)	-2.1(31)	4.9(31)	201.4(9)	A.9		
J1904+0004	0.139	233.6	20210422	SS	P1M06	0.9	18.4(2)	38.5(2)	25.6(30)	14.1(30)	15.4(30)	299.9(4)	A.9		22,29
J1904+0358g	0.751	531.3	20200920	TR	P1M01	<1.5	4.1(7)	–	53.1(45)	-12.6(41)	15.1(41)	991.4(25)	A.9		
J1904+0412	0.071	186.7	20200529	SS	P4M02	1.3	8.6(14)	60.5(14)	7.1(32)	3.8(31)	11.3(31)	112(6)	A.9		
J1904+0415g	0.231	522.6	20200807	TR	P1M01	<1.5	26.9(14)	–	7.7(33)	0.3(33)	5.3(33)	949(15)	A.9		
J1904+0519g	1.680	72.7	20200827	TR	P1M01	<1.5	14.1(7)	26.1(7)	37.7(31)	6.3(31)	10.0(30)	-147.1(8)	A.3	hiL	
			20200910	TR	P1M01										
J1904+0738	0.208	278.3	20200321	SS	P1M12	1.6	5.2(14)	13.6(14)	25.9(32)	3.4(31)	3.8(31)	146.8(17)	A.9		
J1904+0800	0.263	438.8	20210608	SS	P2M12	1.0	10.1(4)	21.7(4)	30.3(30)	6.2(30)	7.1(30)	748.7(7)	A.1	S	
J1904+0823g	1.507	59.4	20200915	TR	P1M01		1.1(4)	–	33.4(41)	4.9(37)	17.9(37)	-2(4)	A.9		
J1904+1011	1.856	137.0	20200419	SS	P2M05	1.1	27.5(7)	34.0(7)	43.4(30)	8.0(30)	9.8(30)	-106.3(4)	A.5	cd,S	
J1905-0056	0.643	229.1	20220210	TR	P1M10	1.2	1.9(2)	5.2(2)	21.8(30)	-5.9(30)	6.9(30)	136.7(5)	A.9		13, 16
J1905+0400	0.0037	25.6	20210428	SS	P3M19	1.5	49.2(14)	113.3(14)	29.8(31)	5.7(31)	9.8(31)	36.9(9)	A.9		
J1905+0600	0.441	728.9	20221109	TR	P1M11		9.2(4)	28.2(4)	7.2(30)	-3.9(30)	5.0(30)	1091.1(30)	A.9		
J1905+0616	0.989	256.0	20201225	SS	P1M03	0.4	3.6(2)	7.7(2)	53.2(30)	-20.0(30)	20.8(30)	148.6(8)	A.1	S	
J1905+0656g	2.511	23.1	20200205	TR	P1M01	<1.5	6.6(4)	12.1(4)	17.8(30)	17.4(30)	19.1(30)	-9.5(11)	A.9		
			20200607	TR	P1M01										
			20200826	TR	P1M01										
J1905+0709	0.648	245.3	20201204	SS	P2M15	1.4	18.8(7)	34.6(7)	31.3(30)	-0.2(30)	1.2(30)	277.2(5)	A.1	S	13,29
J1905+0758g	1.192	197.6	20200829	TR	P1M01	<1.5	7.8(7)	10.8(7)	19.9(32)	4.7(32)	8.6(32)	432(6)	A.2	ot	
			20200911	TR	P1M01										
J1905+0902	0.218	433.8	20211230	SC	P1M16	0.2	6.7(7)	16.5(7)	19.3(31)	0.2(31)	3.3(31)	524(2)	A.2	ot,hiL	
J1905+0936g	1.634	417.4	20210126	TR	P1M01	<1.5	3.1(4)	11.9(4)	19.6(31)	7.2(31)	14.6(31)	694(2)	A.9		
J1906+0414	1.043	348.6	20210506	SS	P4M19	3.5	4.0(7)	24.7(7)	35.9(31)	12.2(31)	14.9(31)	794.5(11)	A.1	S	23
J1906+0641	0.267	472.8	20200402	TR	P1M03	1.5	23.2(2)	34.9(2)	33.1(30)	-2.5(30)	5.8(30)	375.3(4)	A.2	ot,S	13,16

Table 3 *– continued –*

PSR	P (s)	DM[a]	Date	Mode	Beam	Offset (′)	W_{50} (°)	W_{10} (°)	L/I (%)	V/I (%)	$\|V\|$/I (%)	RM (rad/m^2)	Fig.	Note.	Ref.
(1)	(2)	(3)	(4)	(5)	(6)	(7)	(8)	(9)	(10)	(11)	(12)	(13)	(14)	(15)	(16)
J1906+0649	1.286	249.0	20200418	SS	P4M06	1.5	10.7(4)	16.0(4)	42.9(30)	11.3(30)	12.5(30)	-17.5(5)	A.2	ot,S	23
J1906+0724	1.536	475.2	20220210	SC	P1M01		5.0(7)	-	22.5(42)	-4.5(40)	12.6(40)	665(18)	A.9		
J1906+0746	0.143	218.4	20200901	SS	P2M02	1.4	8.0(14)	17.0(14)	58.1(36)	-6.3(35)	7.5(34)	157.1(17)	A.1	S	
J1906+1854	1.019	155.6	20210802	SS	P1M02	1.4	25.9(14)	46.2(14)	9.3(31)	1.8(31)	4.6(31)	398(8)	A.2	ot	23
J1907+0249	0.351	261.0	20210617	SS	P3M15	0.6	19.3(7)	30.9(7)	29.4(30)	0.4(30)	4.0(30)	334.3(9)	A.3	hiL,ot	
J1907+0255	0.618	260.6	20210621	SS	P1M09	0.6	16.6(14)	40.0(14)	10.0(31)	-8.6(31)	11.7(31)	171(7)	A.9		
J1907+0345	0.240	311.7	20210707	TR	P1M18	0.4	2.5(4)	15.4(4)	73.5(31)	29.8(30)	30.9(30)	433.1(6)	A.3	hiL,hiC	23
J1907+0534	1.138	526.0	20200514	SS	P4M14	0.9	4.9(4)	12.5(4)	5.5(31)	-4.8(31)	6.7(31)	614(8)	A.9		
J1907+0555	0.168	457.5	20201101	ArcTR	P1M19		14.1(14)	37.8(14)	8.7(32)	-7.5(32)	9.0(32)	474(6)	A.9		
J1907+0631	0.323	428.6	20200907	TR	P1M10	2.4	24.9(28)	–	70.8(51)	-11.8(45)	9.6(43)	435(44)	A.3	hiL,S	30
J1907+0709g	0.344	279.4	20201107	TR	P1M01	<1.5	6.4(4)	20.6(4)	11.5(31)	-2.3(31)	5.9(31)	1361.9(20)	A.1	S	
J1907+0740	0.574	332.0	20200523	SS	P3M14	1.5	8.4(7)	14.6(7)	14.2(30)	-2.2(30)	3.1(30)	561.8(24)	A.2	ot	
J1907+0918	0.226	357.7	20221107	TR	P1M15		3.6(4)	-	64.5(36)	40.7(35)	43.4(34)	689.6(10)	A.4	hiC,S	
J1907+1149	1.420	207.2	20210211	SS	P3M05	0.7	3.5(4)	6.7(4)	9.5(30)	7.0(30)	7.9(30)	915.8(18)	A.9		
J1907+1247	0.827	257.0	20210130	SS	P2M16	0.3	7.1(7)	11.7(7)	17.5(32)	8.3(32)	9.7(32)	1155(3)	A.9		
J1908+0128	0.0047	75.1	20211230	TR	P1M12		27.4(28)	90.9(28)	40.2(32)	-3.6(32)	3.3(31)	-35.6(13)	A.1	S	
J1908+0457	0.846	349.2†	20210703	TR	P1M05	2.1	9.6(2)	23.3(2)	47.9(30)	0.3(30)	1.6(30)	959.0(2)	A.1	S	
J1908+0500	0.291	201.4	20210615	SS	P3M16	1.5	2.9(7)	6.5(7)	14.0(30)	-2.5(30)	3.6(30)	132.4(12)	A.2	ot,S	
J1908+0811g	0.181	298.3	20200402	TR	P1M01	<1.5	18.2(28)	–	68.6(59)	-6.1(49)	12.6(48)	822(12)	A.9		
			20200830	TR	P1M01										
J1908+0839	0.185	513.3	20201026	SS	P1M05	1.6	12.8(14)	33.6(14)	3.0(31)	0.2(31)	2.5(30)	808(9)	A.8	c	
J1908+0909	0.336	465.9	20221107	TR	P1M01		6.6(4)	20.9(4)	42.5(32)	5.2(31)	6.5(31)	366.8(11)	A.9		
J1908+1351	3.174	178.8	20211210	SC	P1M01		1.7(4)	7.0(4)	21.9(30)	-7.4(30)	11.5(30)	634.1(12)	A.9		
J1908+2351	0.377	101.6	20210801	SS	P1M11	1.4	4.5(7)	11.3(7)	9.9(33)	4.1(32)	8.2(32)	53(5)	A.9		
J1909+0007	1.016	112.7	20210701	SS	P1M11	0.9	2.0(2)	7.0(2)	8.7(30)	2.5(30)	6.8(30)	7.8(8)	A.2	ot	13,16
J1909+0254	0.989	171.7	20210617	SS	P2M19	1.4	2.8(4)	12.1(4)	12.4(30)	-3.2(30)	10.8(30)	268.4(8)	A.9		13,16
J1909+0616	0.755	346.8†	20200509	SS	P2M11	1.5	16.8(4)	21.2(4)	23.1(30)	6.2(30)	7.6(30)	15.9(6)	A.2	ot,S	23
J1909+0641	0.741	36.7	20220210	TR	P1M10	1.0	3.7(4)	15.8(4)	8.7(30)	-1.4(30)	10.2(30)	-27(3)	A.9		
J1909+0657g	1.245	62.4	20201120	TR	P1M01	<1.5	3.2(4)	6.9(4)	51.8(31)	9.1(31)	10.6(31)	-59.7(9)	A.9		
J1909+0749	0.237	539.3	20200523	SS	P3M10	2.6	191.4(14)	–	64.0(40)	2.9(36)	8.9(36)	-239.1(19)	A.6	ip,S,ot,hiL	30
J1909+0912	0.222	421.5	20210307	TR	P1M16	2.6	20.4(14)	–	64.5(38)	-10.8(36)	12.5(36)	244.7(15)	A.3	hiL	29
J1909+1102	0.283	149.9	20200414	SS	P4M16	1.4	5.4(4)	14.6(4)	34.1(30)	-16.9(30)	18.5(30)	553.3(4)	A.2	ot	8,13,24
J1909+1148	0.448	199.8	20201104	SS	P4M02	1.3	3.6(7)	10.5(7)	21.8(33)	-6.1(33)	7.0(32)	687.7(20)	A.9		
J1909+1205	1.229	302.5	20201206	SS	P3M03	2.4	11.5(7)	25.7(7)	40.9(32)	-9.5(32)	12.0(31)	784.2(12)	A.1	S	
J1909+1450	0.996	119.5	20210301	SS	P4M11	0.9	9.6(14)	–	45.0(37)	9.6(36)	9.8(35)	414(3)	A.9		23
J1909+1859	0.542	64.5	20210802	SS	P2M14	0.8	8.0(4)	18.0(4)	25.9(30)	7.3(30)	17.0(30)	217.0(5)	A.9		23
J1910-0112	1.360	155.6†	20210907	SS	P1M02	0.5	12.6(7)	15.3(7)	33.5(32)	5.6(31)	22.9(31)	135.0(13)	A.9		
J1910+0534	0.452	479.4	20210621	SS	P3M05	1.0	19.5(7)	33.1(7)	31.9(30)	11.6(30)	14.9(30)	347.8(7)	A.2	ot	
J1910+0714	2.712	123.3	20210806	SS	P4M10	1.2	2.5(2)	6.0(2)	22.2(30)	-4.9(30)	12.8(30)	146.8(8)	A.9		
J1910+0728	0.325	283.7	20200327	SS	P2M17	0.5	15.7(7)	22.0(7)	15.1(30)	10.3(30)	10.9(30)	566.7(8)	A.5	cd,S	
J1910+1026	0.531	715.3	20201123	TR	P1M16	0.7	8.1(14)	–	83.8(51)	-2.2(41)	4.7(40)	209(3)	A.3	hiL	
J1910+1117g	1.321	297.4	20200818	TR	P1M01	<1.5	2.3(7)	13.2(7)	13.8(36)	11.6(34)	13.2(34)	1019(8)	A.9		
J1910+1231	1.441	258.6	20210126	TR	P1M04	2.0	3.5(2)	9.7(2)	27.3(30)	15.0(30)	19.0(30)	1000.5(12)	A.9		19
J1910+1256	0.0049	38.0	20220312	SC	P1M18	3.2	12.4(14)	34.6(14)	8.9(33)	-2.0(32)	17.0(32)	60(9)	A.9		
J1911+0101A	0.0036	202.6	20201202	SS	P2M12	1.2	43.1(28)	–	25.0(32)	18.6(31)	22.0(31)	123.7(14)	A.9		
J1911+0751g	0.796	220.6	20200823	TR	P1M01	<1.5	13.7(7)	27.6(7)	17.7(31)	3.8(31)	6.2(31)	239.0(22)	A.9		
			20200825	TR	P1M01										
J1911+0921	0.273	340.7	20200806	TR	P1M01		27.1(28)	74.1(29)	10.6(33)	-3.7(32)	7.9(32)	188(7)	A.9		
J1911+0939g	0.365	597.0	20200820	TR	P1M01	<1.5	114.0(57)	–	40.2(42)	0.9(41)	6.5(39)	-20(3)	A.3	hiL	
J1911+1301	1.010	388.8	20210316	TR	P1M17	1.6	6.0(7)	8.3(7)	20.2(33)	-10.6(33)	13.4(33)	1388(3)	A.9		
J1911+1347	0.0046	30.9	20210417	SS	P4M08	2.0	9.3(28)	32.9(29)	39.5(35)	26.0(32)	31.9(31)	-7.2(12)	A.2	ot	
J1911+1758	0.460	48.9	20210301	SS	P1M17	0.8	6.8(7)	12.6(7)	30.9(32)	0.1(31)	3.4(31)	154.3(16)	A.9		23
J1912+1036	0.409	147.0	20201209	SS	P1M16	1.7	12.3(14)	27.2(14)	61.5(32)	-17.3(32)	19.0(31)	154.7(11)	A.1	S	23
J1912+1105g	0.670	151.4	20200827	TR	P1M01	<1.5	6.8(7)	–	14.1(34)	1.6(33)	4.1(33)	540(14)	A.9		
			20200910	TR	P1M01										
J1912+2104	2.232	88.5	20210621	SS	P2M10	1.3	1.6(2)	13.9(2)	41.2(30)	-8.4(30)	10.5(30)	149.0(2)	A.2	ot	8,13,24
J1912+2525	0.622	38.2	20210822	SS	P1M17	0.7	4.5(4)	7.8(4)	11.3(30)	-5.3(30)	7.8(30)	32.3(14)	A.2	ot,S	23
J1913+0446	1.616	109.1	20210628	SS	P1M11	0.4	3.5(2)	11.4(2)	36.3(30)	2.1(30)	2.6(30)	-100.1(6)	A.2	ot	
J1913+0657	1.257	142.0	20210422	SS	P1M06	1.0	5.6(7)	7.5(7)	18.4(34)	8.6(33)	11.2(32)	10(5)	A.1	S	
J1913+0832	0.134	356.4	20200514	SS	P2M02	1.4	18.4(7)	198.3(7)	61.0(30)	-3.9(30)	5.8(30)	491.2(4)	A.6	ip,S,hiL	29
J1913+0904	0.163	96.9	20200417	SS	P1M08	0.4	2.6(4)	16.2(4)	72.3(31)	6.1(30)	7.6(30)	-3.8(8)	A.1	S,hiL	29
J1913+1000	0.837	422.8	20210113	TR	P1M02	1.7	14.7(7)	23.7(7)	12.3(30)	-4.6(30)	6.0(30)	496.9(10)	A.2	ot	
J1913+1011	0.035	178.4	20201206	SS	P1M01	0.3	16.9(7)	41.6(7)	21.0(30)	-1.2(30)	4.4(30)	210.2(6)	A.2	ot,S	29
J1913+1037g	0.434	436.8	20201231	TR	P1M01	<1.5	6.8(14)	–	41.7(55)	35.1(50)	39.8(50)	465(6)	A.4	hiC	
J1913+1050	0.190	231.1	20201228	TR	P1M13	1.3	9.2(14)	183.9(14)	18.7(33)	0.2(33)	6.2(33)	674(9)	A.6	ip,S	
J1913+1054g	0.450	335.5	20201231	TR	P1M01	<1.5	19.2(28)	–	91.0(55)	10.4(45)	14.0(44)	711.5(18)	A.3	hiL	
J1913+1145	0.306	641.5	20200523	SS	P4M05	0.7	12.1(7)	28.8(7)	14.4(30)	-0.9(30)	2.2(30)	920.3(11)	A.8	c	
J1913+1400	0.521	145.0	20210211	SS	P3M12	1.5	3.6(2)	14.0(2)	30.2(30)	-13.9(30)	14.7(30)	603.5(5)	A.2	ot	8,13,16
J1913+3732	0.851	72.3	20201128	TR	P1M01	0.0	3.3(7)	11.6(7)	55.4(30)	5.5(30)	7.1(30)	-0.4(2)	A.2	ot,S	
J1914+0219	0.457	233.8	20210628	SS	P3M04	1.7	11.9(7)	17.8(7)	44.6(30)	-3.5(30)	6.4(30)	283.0(2)	A.1	S	

Table 3 *– continued –*

PSR	P (s)	DM[a]	Date	Mode	Beam	Offset (′)	W_{50} (°)	W_{10} (°)	L/I (%)	V/I (%)	$\|V\|$/I (%)	RM (rad/m^2)	Fig.	Note.	Ref.
(1)	(2)	(3)	(4)	(5)	(6)	(7)	(8)	(9)	(10)	(11)	(12)	(13)	(14)	(15)	(16)
J1914+0625	0.878	204.8	20210507	SS	P4M04	<1.5	19.8(7)	22.3(7)	25.6(33)	-2.5(32)	8.8(32)	-49.3(27)	A.9		
J1914+0631	0.693	58.0	20210507	SS	P3M09	1.3	7.2(4)	11.6(4)	21.8(31)	-5.7(30)	6.3(30)	-98.3(15)	A.2	ot	
J1914+0838	0.440	290.6	20200829	TR	P1M15		3.5(7)	8.5(7)	9.3(30)	8.8(30)	10.5(30)	357(2)	A.9		
J1914+1029g	2.485	65.9	20200821	TR	P1M01	<1.5	3.0(2)	5.4(2)	68.1(33)	-2.6(32)	3.6(31)	18.0(9)	A.3	hiL	
			20200914	TR	P1M01										
J1914+1122	0.600	100.8	20220513	TR	P1M10		11.6(4)	14.0(4)	42.2(30)	15.5(30)	16.7(30)	365.1(6)	A.2	ot,S	13,16
J1914+1228g	2.277	311.5	20201001	TR	P1M01	<1.5	2.8(7)	12.5(7)	13.9(34)	4.2(33)	8.4(33)	1400(7)	A.9		
J1915+0227	0.317	192.2	20210628	SS	P4M10	1.4	7.6(4)	31.8(4)	12.8(30)	7.5(30)	12.2(30)	162.6(7)	A.2	ot?	
J1915+0639	0.644	212.5	20211009	TR	P1M01		3.2(4)	9.6(4)	15.8(33)	-0.8(33)	16.4(33)	199(4)	A.9		
J1915+0738	1.542	38.6	20210417	SS	P1M07	1.5	1.7(2)	4.3(2)	36.9(30)	-17.2(30)	17.9(30)	-5.5(6)	A.1	S	23
J1915+0752	2.058	104.1	20210320	TR	P1M01	0.0	2.8(2)	6.3(2)	17.5(30)	-6.8(30)	8.4(30)	214.8(7)	A.9		23
J1915+0832g	2.710	45.6	20200829	TR	P1M01	<1.5	1.7(2)	6.5(2)	31.7(32)	0.1(32)	8.6(32)	-18.1(15)	A.2	ot	
J1915+0838	0.342	358.0	20200829	TR	P1M07	1.4	13.9(7)	26.1(7)	21.1(30)	5.0(30)	6.1(30)	417.2(10)	A.2	ot	
J1915+1145	0.173	337.5	20220113	TR	P1M01		10.0(7)	27.0(7)	21.9(31)	3.4(31)	12.4(31)	1195.2(14)	A.2	ot?	
J1915+1150	0.100	699.7	20220113	TR	P1M01	2.1	20.8(14)	-	74.7(38)	-3.6(35)	7.6(34)	740.8(11)	A.3	hiL	
J1915+1410	0.297	273.7	20200802	SS	P1M06	1.5	16.0(14)	27.8(14)	27.5(33)	-3.9(33)	9.2(33)	587.6(24)	A.1	S	
J1915+1606	0.059	168.7	20191028	TR	P1M01	0.0	38.9(7)	49.0(7)	49.7(30)	1.3(30)	14.9(30)	357.2(2)	A.9		10,13, cal
J1915+1647	1.616	62.5	20201202	SS	P2M13	0.8	7.3(2)	10.3(2)	35.2(30)	7.4(30)	12.3(30)	180.9(4)	A.2	ot,S	8,13,19
J1916+0748	0.541	304.0	20210306	TR	P1M17		86.2(7)	253.1(7)	15.3(30)	-3.3(30)	3.9(30)	366.3(4)	A.7	w,S,ot	
J1916+0748g	0.867	153.4	20210306	TR	P1M01	<1.5	5.6(14)	–	30.3(53)	1.1(48)	15.8(47)	358(8)	A.9		
J1916+0844	0.440	337.4	20201215	SS	P4M04	1.0	6.9(4)	19.7(4)	23.0(30)	-0.3(30)	1.8(30)	602.8(7)	A.8	c	
J1916+0852	2.182	295.0	20201215	SS	P2M09	1.4	6.8(4)	11.9(4)	4.2(31)	16.2(31)	18.1(31)	425(43)	A.9		
J1916+0951	0.270	60.9	20200418	SS	P1M08	1.2	12.2(2)	16.2(2)	28.6(30)	7.7(30)	8.7(30)	96.6(8)	A.2	ot	3,13,16
J1916+1023	1.618	343.3	20220202	TR	P1M01	2.5	16.8(7)	24.4(7)	30.4(31)	-2.9(31)	6.2(31)	390.5(11)	A.1	S	
J1916+1030	0.628	388.4	20220202	TR	P1M16	0.1	12.5(4)	20.5(4)	16.4(30)	0.7(30)	4.3(30)	394.1(8)	A.2	ot	
J1916+1030g	0.349	520.7	20201230	TR	P1M01	<1.5	20.6(28)	–	99.5(79)	5.2(62)	4.2(59)	433(6)	A.3	hiL	
J1916+1312	0.281	237.0	20211107	SS	P1M07	1.9	7.8(2)	12.5(2)	24.0(30)	-15.3(30)	16.6(30)	276.1(6)	A.2	ot	10,13,16
J1916+3224	1.137	84.1	20210212	TR	P1M01	0.0	1.9(7)	10.1(7)	18.2(30)	-0.7(30)	7.3(30)	55.6(8)	A.9		
J1917+0834	2.129	28.4	20201123	TR	P1M08	1.2	9.2(2)	10.9(2)	36.3(30)	-5.4(30)	6.2(30)	-53.4(10)	A.5	cd,S	
J1917+1353	0.194	94.5	20200405	SS	P4M01	0.9	7.7(2)	15.4(2)	49.5(30)	-9.4(30)	9.5(30)	229.4(2)	A.1	S	10,13,24
J1917+2224	0.425	134.7	20210621	SS	P2M11	1.5	16.3(7)	27.8(7)	18.0(30)	-1.6(30)	4.2(30)	191.6(12)	A.2	ot	19
J1917+24	0.0043	82.0	20220502	SS	P4M07		29.5(28)	-	23.9(36)	8.5(37)	15.2(37)	122(6)	A.2	ot	
J1918+1340g	0.232	573.4	20200807	TR	P1M01	<1.5	19.8(28)	-	62.1(36)	-12.9(33)	14.9(33)	738.4(13)	A.9		
J1918+1444	1.181	27.2	20200528	SS	P1M11	1.6	1.9(2)	7.6(2)	53.3(30)	12.8(30)	13.1(30)	-36.7(4)	A.1	S,hiL	10,13,16
J1918+1541	0.370	11.8	20210101	SS	P2M02	1.0	4.8(14)	206.4(14)	58.5(33)	-1.8(32)	3.6(32)	-1.0(13)	A.6	ip,S,hiL	30
J1919+0021	1.272	90.3	20210702	SS	P3M08	1.5	1.8(2)	10.1(2)	15.5(30)	4.6(30)	7.1(30)	123.4(6)	A.9		13
J1919+04	0.0039	142.7	20211202	SS	P4M19		33.3(14)	48.6(15)	67.2(32)	4.1(31)	4.6(31)	103.8(8)	A.9		
J1919+0134	1.603	191.5	20210701	SS	P4M07	1.7	10.2(2)	17.1(2)	28.3(30)	-11.3(30)	12.1(30)	54.0(5)	A.9		22
J1919+1314	0.571	613.4	20211012	SS	P2M10	0.5	9.4(7)	23.4(7)	26.6(31)	-3.6(31)	4.5(31)	1977.4(12)	A.9		
J1919+1645	0.562	208.0	20201219	SS	P3M11	0.7	5.2(7)	14.4(7)	7.2(32)	5.3(32)	7.8(31)	583(6)	A.9		
J1919+1745	2.081	141.5	20210709	SS	P4M10	0.5	11.0(2)	12.9(2)	39.3(30)	2.5(30)	4.6(30)	518.1(5)	A.5	cd,S	
J1919+23	0.0046	38.4†	20220502	SS	P4M05		15.4(7)	74.8(7)	22.4(31)	-3.1(30)	6.2(30)	53(1)	A.9		
J1919+2621	0.651	96.5	20210801	SS	P2M05	1.5	4.0(4)	10.0(4)	30.2(30)	-3.9(30)	8.2(30)	64.7(7)	A.9		
J1920+1040	2.215	308.8	20210130	SS	P1M01	1.6	7.2(4)	13.1(4)	17.7(30)	2.3(30)	3.2(30)	778.2(7)	A.1	S	
J1920+1110	0.509	182.0	20200509	SS	P1M12	1.0	11.5(14)	30.2(14)	15.9(30)	-14.3(30)	15.6(30)	665.0(16)	A.8	c	
J1920+1515g	1.602	646.5	20200811	TR	P1M01	<1.5	7.7(7)	–	13.9(35)	4.5(33)	5.1(33)	859(20)	A.9		
J1920+2650	0.785	27.7	20210717	SS	P1M11	1.3	6.3(2)	11.8(2)	24.1(30)	21.9(30)	22.7(30)	26.9(5)	A.2	ot	13,16,23
J1921+0137	0.0024	104.9	20210806	SS	P1M04	0.5	202.0(28)	–	41.0(35)	-0.1(34)	0.1(33)	91(6)	A.6	ip,S	
J1921+0812	0.210	82.8†	20210215	SS	P3M01	0.9	2.5(2)	5.7(2)	80.8(30)	10.2(30)	10.7(30)	208.6(4)	A.1	S,hiL	
J1921+1419	0.618	91.6	20200330	SS	P1M10	1.8	13.0(4)	23.4(4)	44.6(30)	-7.9(30)	8.8(30)	162.0(3)	A.1	S	8,13,24
J1921+1505g	0.611	514.9	20200812	TR	P1M01	<1.5	7.6(14)	–	14.4(42)	-18.6(40)	19.8(39)	189(21)	A.9		
J1921+1540	0.143	484.2	20200415	SS	P3M12	5.9	13.4(7)	22.4(7)	30.1(33)	-9.0(32)	12.7(32)	307.4(17)	A.5	cd,S	
J1921+1630	0.936	190.3	20211004	TR	P1M14		4.7(14)	-	27.0(42)	-3.4(38)	9.8(38)	505(4)	A.9		
J1921+1929	0.0026	64.7	20210301	SS	P1M12	0.5	19.5(14)	180.6(14)	28.1(31)	28.2(31)	33.5(31)	117.6(11)	A.4	hiC	
J1921+1948	0.820	154.2	20210301	SS	P4M19	1.3	23.2(7)	56.7(7)	18.9(30)	-4.5(30)	5.4(30)	142.4(4)	A.2	ot	13,16,24
J1921+2003	0.760	98.2†	20210208	SS	P2M10	0.6	2.3(4)	18.5(4)	21.6(30)	-18.6(30)	20.5(30)	135.9(6)	A.9		19,23
J1921+2153	1.337	12.4	20200419	SS	M02		9.1(2)	11.6(2)	13.8(30)	4.1(30)	5.9(30)	-15.4(5)	A.9		13,21,24
J1922+1131	0.562	335.0	20201215	SS	P1M13	1.1	14.7(14)	32.5(15)	8.3(32)	0.5(32)	2.7(32)	1073(9)	A.9		
J1922+1733	0.236	234.0†	20200513	SS	P3M18	0.4	4.8(7)	18.1(7)	70.4(30)	-18.1(30)	18.5(30)	525.0(3)	A.1	S	
J1922+2018	1.172	203.3	20210208	SS	P4M17	1.2	15.8(7)	19.4(7)	41.8(30)	8.1(30)	9.4(30)	313.0(4)	A.1	S	13,19
J1922+2110	1.077	217.0	20210706	SS	P4M07	1.0	5.4(2)	17.4(2)	20.7(30)	5.4(30)	9.8(30)	278.2(5)	A.2	ot	13,16
J1923+1706	0.547	141.7	20220415	SS	P4M07		13.4(4)	17.2(4)	18.1(30)	11.2(30)	17.1(30)	592(1)	A.1	S	19
J1923+4243	0.595	52.9	20210106	TR	P1M01	0.0	7.6(7)	14.2(7)	23.3(30)	-12.8(30)	13.8(30)	-40.8(2)	A.2	ot?,S	
J1924+1509g	0.239	297.4	20200824	TR	P1M01	<1.5	5.0(7)	–	94.0(45)	-6.5(39)	5.2(38)	313.9(13)	A.3	hiL	
J1924+1510g	0.498	113.7	20200830	TR	P1M01	<1.5	4.4(7)	–	26.5(44)	8.6(42)	7.2(41)	228(15)	A.9		
J1924+1628	0.375	542.1	20200810	TR	P1M01	1.3	12.8(14)	–	25.5(34)	-2.5(33)	11.2(33)	643.5(26)	A.9		
J1924+1917	1.277	322.3	20210608	SS	P4M08		9.1(7)	11.1(7)	27.7(33)	-0.1(33)	13.3(33)	675.5(21)	A.9		
J1924+1923g	0.689	384.2	20191110	TR	P1M01	<1.5	5.3(7)	–	20.6(39)	1.2(38)	14.1(37)	395(20)	A.9		
J1924+1932g	0.388	279.1	20200204	TR	P1M01	<1.5	3.5(7)	12.6(7)	73.3(40)	-1.9(36)	4.3(35)	460.9(11)	A.3	hiL	
J1924+2040	0.237	226.6	20201120	TR	P1M01	3.1	17.1(4)	29.2(4)	9.4(30)	1.4(30)	2.3(30)	338.7(17)	A.9		13,19,23

Table 3 *– continued –*

PSR	P (s)	DM[a]	Date	Mode	Beam	Offset (′)	W_{50} (°)	W_{10} (°)	L/I (%)	V/I (%)	$\|V\|$/I (%)	RM (rad/m^2)	Fig.	Note.	Ref.
(1)	(2)	(3)	(4)	(5)	(6)	(7)	(8)	(9)	(10)	(11)	(12)	(13)	(14)	(15)	(16)
J1925+1720	0.075	223.3	20200404	SS	P1M09	1.2	14.7(28)	–	81.2(51)	12.2(42)	14.2(41)	437(3)	A.3	hiL	30
J1926+0431	1.074	101.8	20210702	SS	P2M19	1.3	4.5(2)	9.1(2)	16.2(30)	0.8(30)	5.2(30)	-21.0(6)	A.9		13,16
J1926+0737	0.318	159.0	20201226	SS	P2M09	1.2	171.5(7)	177.1(7)	13.0(31)	0.3(31)	4.4(31)	352(7)	A.6	ip	
J1926+1434	1.324	211.4	20210317	TR	P1M15	1.5	3.3(7)	40.3(7)	30.4(30)	-7.3(30)	9.9(30)	252.9(7)	A.5	cd,ot,S	13,16,23
J1926+1631g	0.678	197.0	20200818	TR	P1M01	<1.5	12.1(7)	14.9(7)	18.1(31)	4.7(31)	8.3(31)	555(2)	A.9		
J1926+1648	0.579	176.8	20201026	SS	P1M12	1.4	5.1(2)	12.3(2)	70.9(30)	10.8(30)	11.2(30)	317.5(3)	A.1	S,hiL	10,13,25
J1926+1857g	0.278	424.0	20200401	TR	P1M01	<1.5	12.1(7)	–	75.2(36)	11.0(33)	14.2(33)	267.0(10)	A.3	hiL,S	31
			20200811	TR	P1M01										
J1926+2016	0.299	249.4	20210619	SS	P2M09	1.4	4.0(7)	17.0(7)	37.9(31)	-9.0(31)	10.8(31)	183.8(7)	A.1	S	
J1927+0911	0.290	202.7	20201220	SS	P3M10	1.4	3.6(4)	8.7(4)	10.9(31)	-1.3(31)	5.4(31)	488(2)	A.9		
J1927+1852	0.482	264.5	20200401	TR	P1M03	0.9	13.0(2)	21.0(2)	27.8(30)	9.5(30)	10.1(30)	253.3(6)	A.2	ot,S	19
J1927+1856	0.298	97.5	20200811	TR	P1M02	0.3	4.0(4)	40.3(4)	18.3(30)	-1.2(30)	4.6(30)	90.5(4)	A.2	ot,S	
J1927+2234	1.431	180.0	20210608	SS	P3M04	1.6	15.1(7)	20.4(7)	6.5(30)	0.8(30)	4.0(30)	218(5)	A.9		16,23
J1928-0108	2.365	125.0	20211216	SS	P1M03	1.1	9.7(7)	13.0(7)	38.0(31)	0.3(31)	6.7(31)	-26.5(14)	A.9		
J1928+1245	0.0030	179.3	20211225	SS	P1M15	0.4	32.5(28)	-	14.6(36)	-1.4(34)	3.2(34)	73(9)	A.9		
J1928+1443	1.010	98.6	20200803	SS	P2M06	2.5	15.5(14)	–	34.7(40)	-1.3(35)	2.9(34)	35(7)	A.9		
J1928+1809g	0.294	431.9	20200811	TR	P1M01	<1.5	142.5(56)	–	41.9(39)	2.0(34)	5.9(35)	456(3)	A.3	hiL,S	
J1928+1923	0.817	476.0	20200803	SS	P1M17	1.1	13.6(14)	38.0(14)	15.9(30)	-8.7(30)	10.0(30)	344.2(10)	A.2	ot	
J1929+0132	0.0064	53.4	20210802	SS	P1M06	0.7	29.0(28)	75.6(29)	6.1(32)	-11.1(31)	13.2(31)	-69(13)	A.9		
J1929+1615g	0.044	309.1	20200815	TR	P1M01	<1.5	13.3(14)	–	37.5(50)	-4.3(43)	8.0(42)	145(24)	A.9		
J1929+1731g	3.995	435.0	20201120	TR	P1M01	<1.5	5.9(14)	–	54.0(46)	-9.2(42)	10.3(41)	176.4(25)	A.9		
J1929+1844	1.220	111.6	20210126	TR	P1M19	0.4	6.2(2)	12.4(2)	18.2(30)	6.5(30)	10.6(30)	173.0(5)	A.2	ot	16,19
J1929+1905	0.339	528.4	20201121	TR	P1M03	0.5	41.2(14)	83.8(14)	4.5(30)	1.6(30)	2.4(30)	412(8)	A.9		
J1929+1937g	0.563	459.1	20210306	TR	P1M01	<1.5	10.5(14)	–	71.5(43)	11.9(39)	13.9(39)	675.8(17)	A.3	hiL	
J1929+2121	0.723	63.2†	20210213	SS	P3M06	1.5	2.2(2)	4.6(2)	25.4(30)	5.3(30)	7.3(30)	107.1(18)	A.2	ot	
J1929+3817	0.814	92.6	20201231	TR	P1M01	0.0	9.0(7)	29.6(7)	21.3(30)	1.9(30)	8.2(30)	102.6(6)	A.9		
J1930+1316	0.760	213.1†	20210507	SS	P1M03	1.9	2.8(4)	9.4(4)	27.1(32)	-7.8(32)	11.7(31)	16.5(23)	A.2	ot	16,19,23
J1930+1408	0.425	213.6	20200401	TR	P1M17		6.8(14)	–	38.9(60)	16.0(55)	20.2(54)	42(7)	A.9		
J1930+1722	1.609	201.0	20201104	SS	P2M15	1.8	12.3(14)	18.1(14)	34.3(33)	16.7(32)	17.5(32)	362.5(16)	A.1	S	
J1930+2441	0.0057	69.5	20220508	SS	P4M05		13.5(14)	47.4(14)	18.9(32)	-19.9(31)	24.2(31)	87(4)	A.9		
J1931-0144	0.593	37.1	20221120	SS	P3M10		12.2(7)	21.8(7)	25.5(32)	2.0(31)	3.3(31)	-42.2(34)	A.9		
J1931+1439	1.779	239.4†	20210622	SS	P4M01	2.0	13.2(4)	16.7(4)	48.4(30)	12.3(30)	13.6(30)	15.8(4)	A.5	cd,S	
J1931+1536	0.314	140.0	20210130	SS	P2M02	1.4	8.2(4)	24.9(4)	25.7(30)	2.6(30)	5.5(30)	194.4(7)	A.9		23
J1932+1059	0.226	3.1	20210106	TR	P1M01	0.0	11.2(2)	21.1(2)	76.1(30)	-5.1(30)	6.4(30)	-6.6(2)	A.7	w,ot,hiL	3,10,24
J1932+1500	1.864	90.1	20210605	SS	P3M18	0.6	9.1(7)	11.4(7)	33.9(31)	-1.7(31)	3.6(31)	-84.0(10)	A.1	S	
J1932+2020	0.268	211.1	20200802	SS	P3M05	1.0	6.0(2)	10.7(2)	8.8(30)	4.6(30)	6.5(30)	5.6(10)	A.9		8,13,16
J1932+2220	0.144	219.2	20201209	SS	P3M10	1.1	4.0(2)	11.7(2)	74.5(30)	8.0(30)	8.6(30)	141.8(4)	A.1	S,hiL	10,13,25
J1933+0758	0.437	165.0	20210701	SS	P3M06	0.9	5.7(7)	10.7(7)	17.7(33)	-6.4(32)	8.1(32)	304(7)	A.9		
J1933+1304	0.928	176.6	20201220	SS	P2M18	1.3	10.4(7)	12.3(7)	30.7(30)	-4.5(30)	11.8(30)	-119.4(6)	A.5	cd	16,23
J1933+2038g	0.040	302.7	20200909	TR	P1M01	<1.5	5.4(7)	–	26.2(42)	2.4(39)	7.9(39)	195(8)	A.9		
J1933+5335	2.052	33.5	20210101	TR	P1M01	0.0	7.5(7)	9.6(7)	20.0(32)	1.7(32)	13.6(32)	1(3)	A.5	cd	
J1934+09	0.0046	72.4	20211212	SS	P4M13		16.0(14)	91.8(14)	32.3(32)	-3.2(31)	11.7(31)	15.4(16)	A.2	ot	
J1934+2352	0.178	355.5	20210609	SS	P3M15	1.1	8.7(14)	17.3(14)	72.5(31)	-3.4(31)	6.2(31)	-37.0(8)	A.6	ip,S	30
J1934+5219	0.568	71.9	20201219	TR	P1M01	0.0	16.1(7)	34.0(7)	11.7(31)	-11.6(31)	13.3(31)	7(3)	A.9		
J1935+1159	1.939	188.4	20210617	SS	P4M19	2.1	5.5(14)	-	25.2(38)	4.7(35)	15.0(34)	-98(7)	A.9		
J1935+1616	0.358	158.5	20210119	SS	P1M11	1.9	6.5(2)	9.2(2)	23.5(30)	-1.2(30)	16.4(30)	-2.8(2)	A.2	ot	8,13,23
J1935+1726	0.0042	61.6	20220113	SC	P1M03	2.6	57.5(14)	219.9(14)	15.4(31)	4.5(31)	8.6(30)	-0.9(14)	A.6	ip,ot	
J1935+1745	0.654	214.2	20201219	SS	P4M18	0.5	4.0(7)	7.9(7)	12.2(30)	-2.5(30)	5.5(30)	43.0(16)	A.9		16
J1935+1829	0.843	345.1	20210826	TR	P1M09	0.3	7.5(7)	–	28.6(38)	0.1(37)	21.6(36)	230(3)	A.9		
J1935+2025	0.080	181.4	20201026	SS	P3M02	0.7	7.6(7)	181.6(7)	93.7(30)	-14.4(30)	15.2(30)	22.7(4)	A.6	ip,S,hiL	29
J1936+1536	0.967	189.4†	20210215	SS	P1M15	0.9	6.6(7)	11.9(7)	19.8(30)	22.0(30)	22.5(30)	196.0(9)	A.2	ot	16,23
J1936+2042	1.390	194.7	20200910	TR	P1M01		7.2(7)	9.1(7)	10.6(32)	3.8(32)	9.7(32)	89(5)	A.9		
J1936+21	0.642	262.4	20200405	SS	P4M04	<1.5	8.9(7)	16.7(7)	46.5(32)	28.3(32)	31.0(32)	270.8(11)	A.4	hiC	
J1937-00	0.240	68.3	20211123	SD	P3M03	<1.5	7.6(7)	16.4(7)	31.1(31)	1.7(31)	4.1(31)	-15.4(8)	A.1	S	
J1937+1505	2.872	237.0	20201226	SS	P1M17	1.0	4.6(7)	8.7(7)	13.3(30)	6.9(30)	11.1(30)	-20.0(25)	A.9		
J1937+1658	0.0039	105.8	20211227	SS	P1M03	1.8	39.8(56)	-	39.4(37)	0.3(36)	8.5(35)	-3(3)	A.9		
J1937+2544	0.200	53.2	20210623	SS	P4M10	1.7	24.3(2)	31.7(2)	29.6(30)	-2.8(30)	3.8(30)	27.1(4)	A.5	cd,ot,S	13,16,23
J1937+2950	1.657	113.9	20210324	SS	P3M05	0.6	4.1(4)	15.8(4)	15.1(30)	1.5(30)	10.4(30)	-205.0(8)	A.2	ot	
J1938+0650	1.121	70.8	20210702	SS	P1M04	1.0	4.1(2)	7.6(2)	9.1(30)	4.0(30)	4.7(30)	77.8(10)	A.1	S	
J1938+14	2.902	75.4	20201226	SS	P1M02	<1.5	6.6(4)	12.4(4)	13.8(30)	0.3(30)	2.3(30)	31.2(14)	A.9		
J1938+14A	1.661	113.6	20210814	TR	P1M01		1.3(4)	10.5(4)	21.7(30)	8.2(30)	9.9(30)	4.0(9)	A.5	cd,ot,S	
J1938+2213	0.166	92.8	20200404	SS	P3M03	0.8	5.7(2)	18.2(2)	46.6(30)	2.6(30)	3.9(30)	142.1(6)	A.2	ot,S	30
J1938+2659	0.883	191.4	20210619	SS	P4M13		13.8(7)	16.4(7)	30.7(32)	5.3(31)	16.4(31)	165.4(17)	A.1	S	
J1939+10	2.308	73.9†	20210702	SS	P2M08		2.4(4)	12.9(4)	39.4(30)	2.2(30)	5.7(30)	-104.5(7)	A.1	S	
J1939+2134	0.0015	71.0	20211221	SS	P4M03	0.6	184.5(2)	205.1(2)	29.5(30)	0.8(30)	1.2(30)	11.0(3)	A.6	ip	9
J1939+2449	0.645	142.8	20210514	TR	P1M11	0.5	9.7(2)	18.0(2)	32.3(30)	4.6(30)	6.2(30)	75.4(2)	A.2	ot,S	23
J1939+2609	0.466	47.3	20210208	SS	P2M02	0.7	2.0(2)	8.4(2)	35.0(30)	-15.9(30)	18.6(30)	12.9(8)	A.2	ot	
J1940+0239	1.232	86.0	20210116	TR	P1M01		2.1(7)	15.0(7)	11.5(31)	-8.5(31)	9.0(31)	-22.2(30)	A.9		
J1941+1026	0.905	138.5	20210806	SS	P3M15	1.4	3.9(7)	11.8(7)	16.7(31)	-7.3(31)	9.4(31)	-125(2)	A.9		23
J1941+1341	0.559	144.7	20210324	SS	P1M10	1.5	4.6(4)	15.8(4)	24.1(30)	-3.2(30)	12.3(30)	-93.2(11)	A.2	ot	

Table 3 *– continued –*

PSR	P (s)	DM[a]	Date	Mode	Beam	Offset (′)	W_{50} (°)	W_{10} (°)	L/I (%)	V/I (%)	$\|V\|$/I (%)	RM (rad/m^2)	Fig.	Note.	Ref.
(1)	(2)	(3)	(4)	(5)	(6)	(7)	(8)	(9)	(10)	(11)	(12)	(13)	(14)	(15)	(16)
J1941+2525	2.306	314.4	20200419	SS	P2M03	1.6	5.4(4)	9.7(4)	22.6(31)	-1.5(31)	3.2(31)	-100.3(21)	A.2	ot	
J1941+4320	0.840	79.3	20201215	TR	P1M01	0.0	6.5(7)	10.9(7)	13.6(30)	-1.6(30)	5.3(30)	23.7(14)	A.9		
J1942+3941	1.353	95.5	20210801	SS	P2M01	1.3	12.0(4)	28.2(4)	14.0(30)	-5.3(30)	10.4(30)	1.7(5)	A.9		
J1943+0609	0.446	70.7	20210717	SS	P1M13	0.7	2.4(2)	16.3(2)	21.1(30)	-1.4(30)	4.6(30)	-34.6(3)	A.2	ot	20,22
J1943+28	0.737	231.6	20220508	SS	P3M09		7.0(7)	12.4(7)	26.1(32)	-2.5(31)	6.7(31)	37.0(16)	A.9		
J1944+0907	0.0051	24.3	20210802	SS	P1M14	1.0	106.8(14)	218.9(14)	15.0(30)	7.4(30)	9.9(30)	-41.6(18)	A.7	w,ot	
J1944+16	0.0024	170.9	20220502	SS	P1M15		39.4(28)	-	25.6(38)	16.6(36)	21.5(36)	-113(12)	A.9		
J1945+1211	4.756	94.7	20210807	SS	P4M16	2.2	25.0(2)	31.0(2)	47.1(30)	2.1(30)	6.8(30)	-22.0(3)	A.1	S	
J1945+1834	1.068	214.5	20201226	SS	P3M01	1.4	7.7(14)	12.7(15)	13.5(34)	14.4(34)	15.0(33)	62(23)	A.9		23
J1946+14	2.282	49.5	20210803	SS	P3M07		4.6(4)	5.9(4)	11.9(31)	7.1(31)	10.6(31)	-65(3)	A.5	cd,ot	
J1946+1805	0.440	16.1	20210201	TR	P1M17	1.8	24.9(7)	40.3(7)	37.9(30)	-9.2(30)	9.4(30)	-40.6(4)	A.2	ot,S	13,16,25
J1946+2244	1.334	140.0	20200328	SS	M02	<1.5	5.1(7)	15.9(7)	46.1(32)	-5.6(31)	9.0(31)	2.0(10)	A.2	ot	16,19,25
J1946+2535	0.515	249.2	20210130	SS	P3M16	1.1	6.5(2)	14.4(2)	23.9(30)	2.8(30)	4.4(30)	61.8(5)	A.1	S	
J1946+2611	0.435	165.0	20200415	SS	P1M12	0.8	7.9(2)	17.6(2)	39.4(30)	-12.7(30)	13.4(30)	-83.0(4)	A.9		23
J1946+3417	0.0031	110.2	20210324	SS	P4M10	1.0	31.7(7)	180.8(7)	19.4(30)	-4.8(30)	6.4(30)	2.8(9)	A.7	w,ot	
J1947+0915	1.480	86.5†	20210118	TR	P1M01	0.0	6.5(7)	14.6(7)	24.7(30)	-4.4(30)	4.9(30)	-114.7(2)	A.2	ot	22,29
J1947+10	1.110	129.0†	20210806	SS	P2M10		10.2(4)	15.3(4)	17.4(30)	-6.3(30)	18.5(30)	-125.9(8)	A.9		
J1947+1957	0.157	185.8	20220508	SS	P3M15		13.7(7)	23.8(7)	10.1(31)	1.4(31)	3.3(31)	-185(3)	A.9		
J1948+1808	0.394	255.5	20210803	SS	P3M07		14.6(4)	35.0(4)	32.0(30)	18.2(30)	20.5(30)	-132.0(7)	A.9		
J1948+2551	0.196	289.3	20210130	SS	P4M08	2.7	16.9(14)	31.3(14)	29.3(32)	3.8(31)	7.3(31)	72(2)	A.3	hiL,ot	
J1948+3540	0.717	129.3	20210626	SS	P4M04	1.7	4.9(2)	15.7(2)	20.9(30)	6.9(30)	7.2(30)	119.2(2)	A.2	ot	13,16
J1949+2306	1.319	195.9	20201202	SS	P2M07	1.2	4.9(4)	14.0(4)	22.6(31)	-0.5(31)	7.1(31)	146.2(17)	A.9		
J1949+2516g	0.410	424.7	20200909	TR	P1M01	<1.5	14.4(14)	–	33.8(45)	2.1(40)	10.6(40)	-39(10)	A.9		
			20201004	TR	P1M01										
J1949+3426	0.388	227.8	20220508	SS	P3M13		6.8(7)	19.8(7)	24.2(31)	-9.3(30)	13.0(30)	-156(1)	A.9		
J1950+05	0.455	61.4†	20210213	TR	P1M01		13.8(14)	37.6(14)	63.4(33)	-10.6(32)	12.5(31)	-59.3(7)	A.1	S	
J1950+3001	2.788	247.0	20210607	SS	P3M16		8.1(7)	11.2(7)	39.4(31)	3.5(31)	4.0(31)	-142.4(11)	A.9		
J1951+1123	5.094	29.3	20210710	SS	P1M18	1.7	1.8(2)	3.4(2)	16.4(30)	3.8(30)	5.5(30)	-42.0(14)	A.9		23
J1952+1410	0.275	31.5	20210702	SS	P4M16	1.1	5.9(4)	13.8(4)	17.3(30)	-8.4(30)	10.9(30)	-24.2(9)	A.9		23
J1952+2630	0.020	315.3	20200402	SS	P3M06	2.2	22.9(28)	–	63.1(47)	-0.8(43)	11.0(42)	-151(4)	A.3	hiL	
J1952+3021	1.665	189.4	20211009	TR	P1M01		5.0(4)	8.8(4)	9.7(30)	-2.8(30)	3.5(30)	-11.4(18)	A.9		
J1952+3252	0.039	45.0	20210326	SS	P3M15	1.0	26.1(7)	49.0(7)	41.7(30)	-3.3(30)	4.1(30)	-187.8(5)	A.1	S,hiL	13,19,24
J1953+1149	0.851	140.0	20210116	TR	P1M01	0.0	5.7(7)	10.0(7)	5.0(30)	-1.2(30)	1.8(30)	-46(4)	A.9		
J1953+1846A	0.0048	117.4	20211108	SS	P3M07		38.7(14)	-	17.7(33)	-0.6(33)	4.7(33)	-486.1(45)	A.9		
J1953+2732	1.333	194.6	20200528	SS	P3M18	1.4	6.9(7)	17.7(7)	34.1(33)	9.6(32)	15.0(32)	-74.5(17)	A.9		
J1953+2819	1.011	198.8	20210903	TR	P1M08		5.1(4)	9.2(4)	33.1(30)	11.9(30)	15.6(30)	108.2(9)	A.9		
J1954+1021	2.099	81.5	20210117	TR	P1M01	0.0	4.3(7)	8.6(7)	39.8(30)	2.6(30)	4.5(30)	-18.6(3)	A.9		
J1954+2407	0.193	80.5	20210301	SS	P2M11	0.9	2.6(7)	9.9(7)	66.2(37)	-7.9(34)	12.1(34)	-6.7(12)	A.3	hiL	
J1954+2923	0.426	7.9	20200607	TR	P1M07	2.0	17.0(4)	29.1(4)	30.4(30)	-20.4(30)	23.2(30)	-14.1(3)	A.9		8,13,24
J1954+3852	0.352	65.4	20211024	SS	P3M04	1.4	2.3(4)	6.7(4)	90.4(32)	-3.3(31)	3.1(31)	112.9(10)	A.3	hiL	
J1954+4357	1.387	130.3	20210109	TR	P1M01	0.0	12.9(7)	26.3(7)	19.1(30)	-9.2(30)	10.1(30)	-140.1(5)	A.2	ot	
J1955+2527	0.0048	209.9	20210215	SS	P4M13	0.6	45.1(14)	73.7(14)	4.7(30)	-5.9(30)	7.2(30)	-154(19)	A.9		
J1955+2908	0.0061	104.5	20200607	TR	P1M03	1.0	91.1(4)	123.9(4)	24.6(30)	-7.5(30)	23.8(30)	14.4(4)	A.7	w,ot	9,14
J1955+2912g	0.279	189.0	20201006	TR	P1M01	<1.5	4.3(7)	–	43.0(62)	-4.3(55)	7.2(54)	-40(23)	A.9		
J1955+2930	1.073	210.0	20191110	TR	P1M01		3.2(7)	13.6(7)	12.9(32)	3.3(32)	10.2(32)	12(7)	A.9		
J1956+2826g	0.071	111.8	20200820	TR	P1M01	<1.5	14.1(14)	–	11.4(36)	-29.3(36)	31.6(35)	51(18)	A.4	hiC	
J1957-0002	0.965	38.4	20210427	TR	P1M01	0.0	6.0(7)	–	39.6(37)	6.0(35)	6.2(35)	-8(3)	A.9		
J1957+2831	0.307	139.0	20200820	TR	P1M19	2.3	12.9(7)	20.4(7)	29.2(30)	-0.4(30)	8.1(30)	-44.1(8)	A.3	hiL,ot,S	23
J1958+2213	1.050	84.2	20211212	SS	P4M05	1.9	7.4(7)	-	40.3(40)	4.8(38)	8.0(37)	-176(3)	A.9		
J1958+3033	1.098	200.1	20211009	TR	P1M01		1.6(4)	11.2(4)	10.4(32)	-1.6(32)	10.2(31)	-18(4)	A.9		
J1959+2048	0.0016	29.1	20210311	SS	P4M01	1.1	250.4(28)	274.2(29)	25.1(31)	10.9(31)	13.9(31)	-70.1(13)	A.7	w	9
J1959+3620	0.406	316.5†	20210327	SS	P3M02	0.8	35.9(14)	75.0(14)	32.1(30)	-1.4(30)	2.2(30)	63.8(4)	A.2	ot,S	
J2000+2920	3.073	131.3	20211009	TR	P1M01		1.9(2)	7.7(2)	21.3(30)	-4.4(30)	5.9(30)	62.3(5)	A.9		
J2001+4258	0.719	54.9	20210809	SS	P4M12	1.7	4.7(7)	15.1(7)	14.6(31)	3.1(31)	4.5(31)	-20.9(17)	A.2	ot	
J2002+1637	0.276	94.6	20210807	SS	P4M10	1.2	5.3(4)	20.1(4)	20.4(30)	-0.3(30)	2.6(30)	-43.1(9)	A.1	S	23
J2002+30	0.421	184.0	20210507	SS	P2M03	1.3	7.0(4)	14.5(4)	9.6(31)	-8.6(31)	10.4(31)	-46.2(24)	A.2	ot	
J2002+4050	0.905	131.4	20210717	SS	P4M05	1.2	7.0(2)	19.6(2)	24.9(30)	0.8(30)	4.0(30)	-112.5(5)	A.2	ot	13
J2003+2916	1.009	208.3	20211227	SS	P3M14	0.9	9.0(4)	14.8(4)	21.9(31)	-5.8(30)	8.1(30)	105.1(9)	A.9		
J2004+2653	0.665	160.4	20210615	SS	P1M01	1.0	9.3(28)	–	74.5(49)	12.9(42)	13.1(41)	-308.3(18)	A.3	hiL	
J2004+3429	0.240	355.0†	20200419	SS	P3M18	2.1	6.7(14)	210.4(14)	76.4(32)	0.6(31)	4.7(31)	-162.6(7)	A.6	ip,hiL	
J2005+3411g	0.651	484.5	20200808	TR	P1M01	<1.5	19.4(7)	37.9(7)	19.3(31)	5.0(31)	5.8(31)	207(2)	A.9		
J2005+3547	0.615	401.6	20210627	SS	P3M11	1.4	14.3(7)	26.2(7)	29.3(30)	8.8(30)	10.0(30)	21.1(7)	A.9		
J2005+3552	0.307	448.6†	20210626	SS	P1M18	1.4	10.9(4)	27.1(4)	79.8(30)	-13.4(30)	14.9(30)	208.7(3)	A.1	S,hiL	
J2005+38	2.461	191.6	20211225	SS	P1M01		5.0(4)	-	33.1(37)	0.1(35)	5.7(35)	608.5(22)	A.9		
J2006+22	1.741	129.4	20220502	SS	P2M13		4.9(4)	8.2(4)	23.4(31)	8.7(31)	14.0(31)	-193.7(16)	A.9		
J2006+3102	0.163	106.8	20221111	SC	P1M05		23.9(4)	33.2(4)	81.4(31)	26.1(31)	32.3(31)	-30.8(6)	A.1	S, hiL, hiC	
J2006+4058	0.499	257.4	20210324	SS	P2M19		6.7(7)	17.1(7)	10.1(31)	3.3(30)	6.5(30)	-288.4(27)	A.9		
J2007+2722	0.024	127.0	20210311	SS	P1M04	1.1	203.3(7)	295.4(7)	66.7(30)	-5.9(30)	7.3(30)	-233.3(2)	A.7	w	
J2008+2513	0.589	60.5	20210501	TR	P1M01	0.0	7.0(4)	16.5(4)	28.8(30)	-4.6(30)	5.2(30)	-116.8(5)	A.3	hiL,ot,S	23
J2008+3139	0.226	223.5	20221205	SS	P4M19		3.3(7)	6.7(7)	13.1(34)	0.5(33)	1.8(33)	-179(7)	A.9		

Table 3 *– continued –*

PSR	P (s)	DM[a]	Date	Mode	Beam	Offset (′)	W_{50} (°)	W_{10} (°)	L/I (%)	V/I (%)	$\|V\|$/I (%)	RM (rad/m^2)	Fig.	Note.	Ref.
(1)	(2)	(3)	(4)	(5)	(6)	(7)	(8)	(9)	(10)	(11)	(12)	(13)	(14)	(15)	(16)
J2008+3758	4.352	140.5	20211225	SS	P1M19	1.0	2.8(4)	4.6(4)	24.0(32)	0.5(31)	5.1(31)	270(2)	A.9		
J2009+3326	1.438	263.6	20200816	TR	P1M04	2.3	6.4(7)	22.7(7)	19.5(30)	-4.5(30)	10.9(30)	9.5(16)	A.2	ot,S	
J2010+2845	0.565	112.5	20210619	SS	P1M04	1.3	9.2(4)	15.2(4)	18.4(30)	-12.1(30)	19.1(30)	-230.7(9)	A.9		
J2010+31	1.551	251.4	20221205	SS	P2M08		5.3(4)	10.2(4)	24.5(35)	-5.3(33)	15.7(33)	-43.8(17)	A.9		
J2010+3230	1.442	371.8	20200812	TR	P1M03	2.1	7.4(4)	12.8(4)	32.4(31)	12.7(31)	14.8(31)	-644.7(15)	A.9		
J2011+3006g	2.505	6.1	20201123	TR	P1M01	<1.5	13.3(4)	47.2(4)	35.2(30)	3.1(30)	12.8(30)	-31.8(3)	A.9		
J2011+3331	0.931	299.0	20200816	TR	P1M08	3.4	11.8(7)	15.2(7)	11.7(32)	-7.5(31)	15.0(31)	234(4)	A.9		
J2013+3058	0.276	148.7	20220608	SC	P1M05		3.7(4)	11.2(4)	15.7(30)	-3.6(30)	4.8(30)	-146.5(12)	A.2	ot	
J2013+3100g	0.368	158.0	20210318	TR	P1M01	<1.5	5.3(7)	8.2(7)	6.2(33)	-0.7(33)	6.1(33)	-135(10)	A.9		
J2013+3845	0.230	238.2	20210706	SS	P1M12	1.4	22.9(2)	40.4(2)	62.0(30)	-4.8(30)	5.4(30)	66.1(2)	A.1	S	13
J2015+2524	2.303	10.2	20210618	SS	P1M06	0.6	1.5(4)	6.4(4)	16.7(31)	-4.2(30)	9.7(30)	-25.3(18)	A.9		
J2016+1948	0.064	33.8	20201110	TR	P1M01	0.0	5.8(7)	13.0(7)	46.3(30)	17.4(30)	19.8(30)	-123.2(2)	A.3	hiL,ot	
J2017+0603	0.0028	23.9	20201108	TR	P1M01	0.0	12.9(14)	168.6(14)	34.4(30)	-2.3(30)	4.8(30)	-57.4(6)	A.7	w,S,ot	
J2017+2043	0.537	60.4	20210710	SS	P3M03	0.7	10.8(2)	13.4(2)	16.2(30)	-0.2(30)	12.0(30)	-163.5(4)	A.2	ot	23
J2017+2819g	1.832	67.2	20200401	TR	P1M01	<1.5	9.8(4)	11.8(4)	25.5(30)	-1.1(30)	20.6(30)	-170.8(7)	A.9		
			20200820	TR	P1M01										
J2018+2839	0.557	14.2	20200914	TR	P1M18	2.5	8.2(4)	14.5(4)	10.4(30)	-5.5(30)	6.0(30)	-33.7(3)	A.2	ot,S	13,19,24
J2019+2425	0.0039	17.2	20210623	SS	P1M14	1.5	59.5(28)	–	36.7(38)	4.3(35)	8.5(35)	-49(10)	A.9		17
J2021+24	0.879	58.9	20220508	SS	P2M05		6.3(14)	-	33.8(39)	1.1(36)	8.5(36)	-137(3)	A.9		
J2021+4024g	0.370	680.5	20200812	TR	P1M01	<1.5	38.5(28)	107.1(29)	12.2(31)	-1.7(31)	4.3(31)	-763(13)	A.8	c	
J2022+2854	0.343	24.6	20210513	TR	P1M05	3.2	11.7(2)	15.4(2)	29.6(30)	-9.0(30)	9.9(30)	-69.2(6)	A.2	ot	4,13,24
J2022+3845g	1.008	490.0	20200808	TR	P1M01	<1.5	25.6(28)	92.6(29)	10.5(33)	-4.0(32)	6.8(32)	332(16)	A.8	c	
J2022+5154	0.529	22.6	20221120	SS	P4M11		8.1(2)	16.5(2)	48.7(30)	2.7(30)	3.3(30)	-8.3(3)	A.1	S	1,12,13
J2023+5037	0.372	33.0	20220508	SS	P2M16		3.4(2)	184.8(2)	26.8(30)	-3.5(30)	5.2(30)	43.8(4)	A.6	ip,ot	13,23
J2025+2133	0.623	71.6	20210803	SS	P1M02	1.5	8.6(7)	–	15.7(36)	-11.8(35)	14.1(35)	-114(9)	A.9		
J2027+2146	0.398	97.0	20201111	TR	P1M01	0.0	4.1(7)	17.4(7)	21.2(30)	0.3(30)	9.8(30)	-211.1(8)	A.2	ot	3
J2027+4557	1.099	229.5	20210327	SS	P2M10	0.9	5.9(2)	20.3(2)	38.2(30)	1.8(30)	18.9(30)	335.5(3)	A.2	ot,S	
J2030+2228	0.630	71.9	20210619	SS	P2M18	0.4	11.1(2)	13.7(2)	21.9(30)	2.4(30)	4.5(30)	-193.5(3)	A.1	S	13,16,24
J2030+3641	0.200	246.0	20200328	SS	P1M08	0.4	30.0(7)	43.7(7)	51.0(31)	3.3(31)	4.0(30)	511.4(8)	A.3	hiL	27
J2030+3929g	1.718	493.4	20201120	TR	P1M01	<1.5	16.9(14)	33.1(15)	13.3(33)	-9.0(32)	10.2(32)	-103(7)	A.9		
			20210126	TR	P1M01										
J2030+3944g	0.306	940.8	20200811	TR	P1M01	<1.5	62.4(28)	165.2(29)	3.9(31)	-1.5(31)	7.0(31)	-12(7)	A.8	c	
J2032+4127	0.143	114.6	20200402	SS	P2M17	1.4	15.6(14)	212.4(14)	81.7(32)	-2.1(31)	3.1(31)	212.9(6)	A.6	ip,S,hiL	
J2033+0042	5.013	36.3	20211122	TR	P1M01	0.0	5.6(2)	10.0(2)	14.7(30)	-2.3(30)	3.9(30)	-71.9(4)	A.9		
J2033+1734	0.0059	25.1	20201111	TR	P1M01	0.0	14.3(7)	38.6(7)	35.2(30)	-1.7(30)	15.3(30)	-72.5(3)	A.2	ot,hiL	
J2036+2835	1.358	83.8	20210616	SS	P2M07	0.9	5.5(4)	7.9(4)	29.4(30)	-8.1(30)	10.0(30)	-155.5(4)	A.1	S	
J2038+5319	1.424	159.4	20221122	SS	P1M07		4.9(2)	11.8(2)	15.5(30)	-10.7(30)	14.4(30)	-108.7(14)	A.9		13,23
J2040+1657	0.865	50.6	20201110	TR	P1M01	0.0	6.2(7)	34.6(7)	17.8(30)	4.1(30)	4.9(30)	-100.9(3)	A.9		
J2041+46	1.159	308.0	20220502	SS	P4M13		5.8(2)	13.9(2)	27.4(30)	13.6(30)	15.1(30)	-237.8(5)	A.8	c	
J2042+0246	0.0045	9.2	20210111	TR	P1M01	0.0	11.1(28)	181.4(28)	43.2(36)	-7.2(34)	8.7(33)	-25.6(28)	A.6	ip?,S	
J2043+2740	0.096	21.0	20210618	SS	P1M11	0.7	8.0(2)	17.4(2)	75.4(30)	-3.4(30)	3.7(30)	-95.9(2)	A.1	S,hiL	30
J2044+4614	1.392	315.4	20210324	SS	P1M09	1.0	6.2(4)	35.5(4)	31.7(30)	1.8(30)	12.4(30)	112.8(4)	A.2	ot,S	23
J2045+3633	0.031	129.5	20200404	SS	P4M04	1.3	23.7(7)	32.7(7)	39.6(30)	-7.3(30)	13.7(30)	-263.5(2)	A.9		
J2047+5029	0.445	107.6	20210327	SS	P4M15	1.5	2.0(14)	184.9(14)	37.1(33)	22.6(32)	27.9(32)	-126.5(18)	A.6	ip,S	
J2048+2255	0.283	70.6	20210111	TR	P1M01	0.0	4.9(7)	11.1(7)	15.6(30)	-5.7(30)	11.3(30)	-169.5(7)	A.2	ot?	
J2051+1248	0.553	43.4	20210110	TR	P1M01	0.0	32.1(28)	62.1(29)	3.8(31)	2.3(31)	2.7(31)	-69(12)	A.9		
J2051+4434g	1.303	617.8	20200808	TR	P1M01	<1.5	67.1(7)	89.8(7)	42.9(30)	-1.7(30)	3.2(30)	-99.7(3)	A.5	cd,S	
J2051+50	0.0016	61.0[†]	20221120	SS	P2M19		14.5(14)	-	76.9(52)	0.8(46)	1.8(45)	32.1(22)	A.3	hiL	
J2052+4421g	0.375	547.0	20200607	TR	P1M01	<1.5	39.5(14)	123.4(14)	65.7(30)	12.4(30)	13.6(30)	-275.8(3)	A.8	c	31
			20200812	TR	P1M01										
J2053+4650	0.012	98.0	20200514	SS	P3M05	0.8	26.5(7)	194.5(7)	14.5(30)	-2.8(30)	4.0(30)	-166.3(6)	A.6	ip,ot	
J2053+4718	4.910	323.3	20200607	SS	P1M10		3.2(2)	6.0(2)	15.1(30)	0.2(30)	4.8(30)	-797.7(10)	A.9		
J2055+3630	0.221	97.4	20210621	SS	P1M06	1.4	4.9(2)	12.4(2)	23.7(30)	-14.3(30)	15.2(30)	-61.5(2)	A.2	ot	13,16
J2055+3829	0.0020	91.8	20211216	SS	P3M13	1.4	16.5(7)	34.1(7)	18.8(31)	0.7(30)	2.5(30)	-65.8(13)	A.9		
J2102+38	1.189	86.2	20210605	SS	P3M19		9.9(7)	11.8(7)	17.7(30)	-0.6(30)	11.0(30)	-75.2(10)	A.9		
J2105+07	3.746	52.6	20210118	TR	P1M01		10.0(7)	14.2(7)	32.8(30)	-6.9(30)	11.3(30)	10.6(5)	A.1	S	
J2108+41	1.511	133.9	20211216	SS	P1M10		15.3(14)	-	25.8(43)	-6.3(39)	8.9(39)	-44(4)	A.9		
J2112+4058	4.061	127.2	20211129	SS	P1M06	5.4	3.6(4)	7.8(4)	16.8(30)	-2.7(30)	10.6(30)	-57.3(5)	A.9		
J2113+4644	1.014	141.2	20220308	SC	P1M01	0.0	44.5(7)	73.1(7)	42.6(30)	-2.9(30)	8.9(30)	-222.4(3)	A.2	ot,S	7,13,15
J2122+2426	0.541	8.5	20210427	TR	P1M01	0.0	10.5(7)	24.0(7)	56.8(30)	4.2(30)	4.7(30)	-28.8(2)	A.1	S	
J2129+1210A	0.110	67.3	20200902	TR	P1M01	0.0	6.9(2)	21.8(2)	15.4(30)	-0.6(30)	4.8(30)	-71.3(4)	A.2	ot,S	
J2129+1210B	0.056	67.6	20200902	TR	P1M01	0.1	17.3(14)	55.4(14)	24.8(31)	2.6(30)	10.6(30)	-73.8(9)	A.2	ot	
J2129+1210C	0.030	67.1	20200902	TR	P1M01	0.9	14.2(57)	–	48.9(87)	1.6(76)	10.4(74)	-74(6)	A.9		
J2129+1210D	0.0048	67.3	20200902	TR	P1M01	0.0	54.3(56)	123.8(58)	16.8(32)	5.9(33)	10.1(33)	-71(3)	A.9		
J2129+1210E	0.0046	66.5	20200902	TR	P1M01	0.1	30.3(56)	71.0(59)	21.5(36)	-1.9(34)	4.8(34)	-69(4)	A.9		
J2129+4119	1.687	34.2	20210616	SS	P2M03	0.8	10.0(4)	14.0(4)	71.5(30)	-2.7(30)	9.7(30)	-51.5(4)	A.1	S,hiL	
J2138+4911	0.696	167.6	20200402	SS	P1M11	2.2	6.1(2)	11.1(2)	28.6(30)	0.3(30)	2.0(30)	-145.7(6)	A.2	ot,S	
J2139+4738g	0.557	142.0	20200907	TR	P1M01	<1.5	8.0(14)	–	21.0(41)	36.0(40)	41.0(39)	35(15)	A.4	hiC	
J2150+5247	0.332	148.9	20221120	SS	P2M01		10.4(2)	16.7(2)	18.4(30)	-0.2(30)	3.7(30)	-24.1(6)	A.2	ot	13
J2204+2700	0.084	34.8	20210109	TR	P1M01	0.0	13.7(7)	22.2(7)	9.0(30)	5.5(30)	6.7(30)	-29.8(20)	A.9		

Table 3 – *end.*

PSR	P (s)	DM[a]	Date	Mode	Beam	Offset (′)	W_{50} (°)	W_{10} (°)	L/I (%)	V/I (%)	$\|V\|$/I (%)	RM (rad/m^2)	Fig.	Note.	Ref.
(1)	(2)	(3)	(4)	(5)	(6)	(7)	(8)	(9)	(10)	(11)	(12)	(13)	(14)	(15)	(16)
J2208+4056	0.636	11.8	20201018	TR	P1M01	0.0	16.3(7)	202.2(7)	76.2(30)	-8.0(30)	8.9(30)	-41.7(2)	A.6	ip,S,ot,hiL	
J2208+4610	0.642	61.8	20211124	SS	P4M09		20.6(7)	27.1(7)	19.8(30)	-2.7(30)	6.1(30)	-51.9(11)	A.2	ot	
J2209+22	1.777	45.4	20210129	TR	P1M01		3.4(7)	7.4(7)	23.2(30)	19.2(30)	20.4(30)	-90.1(6)	A.9		
J2215+5135	0.0026	69.2	20210626	SS	P2M10	1.5	15.6(28)	–	49.4(38)	-4.3(36)	2.0(34)	-53.5(12)	A.7	w	
J2219+4754	0.538	43.4	20210608	SS	P1M10	2.0	5.5(2)	10.9(2)	14.8(30)	3.6(30)	5.2(30)	-36.4(4)	A.9		13,25
J2227+3038	0.842	19.0	20210126	TR	P1M01		8.1(7)	-	30.5(34)	1.3(33)	16.5(33)	-60.7(25)	A.9		
J2229+2643	0.0029	22.7	20201027	TR	P1M01	0.0	56.5(14)	80.9(14)	15.6(30)	4.2(30)	7.1(30)	-60.0(7)	A.9		14
J2234+0611	0.0035	10.7	20201020	TR	P1M01	0.0	10.8(14)	23.6(14)	27.3(32)	2.7(32)	2.7(32)	5.6(31)	A.9		
J2234+0944	0.0036	17.8	20201021	TR	P1M01	0.0	26.1(7)	167.0(7)	23.4(30)	5.6(30)	6.6(30)	-10.4(2)	A.7	w,S?	
J2243+1518	0.596	39.9	20201109	TR	P1M01	0.0	9.5(7)	16.5(7)	15.5(31)	3.4(31)	5.0(31)	-39.0(17)	A.9		
J2306+31	0.341	45.9	20210126	TR	P1M01		10.6(7)	33.2(7)	27.5(32)	-1.3(31)	2.2(31)	-79.0(11)	A.9		
J2329+4743	0.728	44.0	20201028	TR	P1M01	0.0	2.8(7)	26.7(7)	38.5(30)	10.8(30)	19.8(30)	-3.9(4)	A.9		
J2340+08	0.303	22.9†	20210125	TR	P1M01		18.2(7)	41.9(7)	12.5(30)	-2.9(30)	3.3(30)	-4.7(25)	A.2	ot,S	
J2355+2246	1.841	23.1	20201101	TR	P1M01	0.0	11.1(14)	23.3(14)	44.9(33)	9.6(31)	12.1(31)	-49.1(11)	A.9		

Columns (1)-(3): pulsar name, period and DM as identification of a pulsar. [a] DM has units of pc/cm^3, ⋆ period updated, † DM updated by FAST observations compared to the pulsar catalog (Manchester et al. 2005); Columns (4)-(7): FAST observation dates, observation modes, the beam name and the pulsar offsets from the beam center. Observation modes: TR – tracking, SS – snapshot, SD - snapshotdec, SC – swiftcalibration; Columns (8)-(12): the profile properties: pulse widths W_{50} and W_{10} at 50% and 10% the peak intensities, degree (and uncertainty on the last digit) of linear, circular and absolute circular polarization L/I, V/I and $|V|/I$; Column (13): FAST measured RM (and uncertainty), i.e. $\mathrm{RM_{ISM}} = \mathrm{RM_{obs}} - \mathrm{RM_{ion}}$; columns (14)-(16): figure number for polarization profile, notes and the references for profile comparison. Notes: S: S-shaped position angle; ot: orthogonal modes; hiL: highly linearly polarized; hiC: highly circularly polarized; cd: conal double pulsar; ip: interpulse; w: wide profile; c: scattering. References for profile comparison: 1 = Manchester (1971); 2 = McCulloch et al. (1978); 3 = Rankin & Benson (1981); 4 = Stinebring et al. (1984a); 5 = Stinebring et al. (1984b); 6 = Segelstein et al. (1986); 7 = Lyne & Manchester (1988); 8 = Rankin et al. (1989); 9 = Thorsett & Stinebring (1990); 10 = Blaskiewicz et al. (1991); 11 = Zepka et al. (1996); 12 = von Hoensbroech & Xilouris (1997); 13 = Gould & Lyne (1998); 14 = Xilouris et al. (1998); 15 = von Hoensbroech et al. (1998a); 16 = Weisberg et al. (1999); 17 = Nice et al. (2001); 18 = Bhat et al. (2002); 19 = Weisberg et al. (2004); 20 = Karastergiou et al. (2005); 21 = Johnston et al. (2008); 22 = Weltevrede & Johnston (2008); 23 = Han et al. (2009); 24 = Hankins & Rankin (2010); 25 = Mitra & Rankin (2011); 26 = Yan et al. (2011); 27 = Camilo et al. (2012); 28 = Dai et al. (2015); 29 = Johnston & Kerr (2018); 30 = Serylak et al. (2021); 31 = Han et al. (2021).

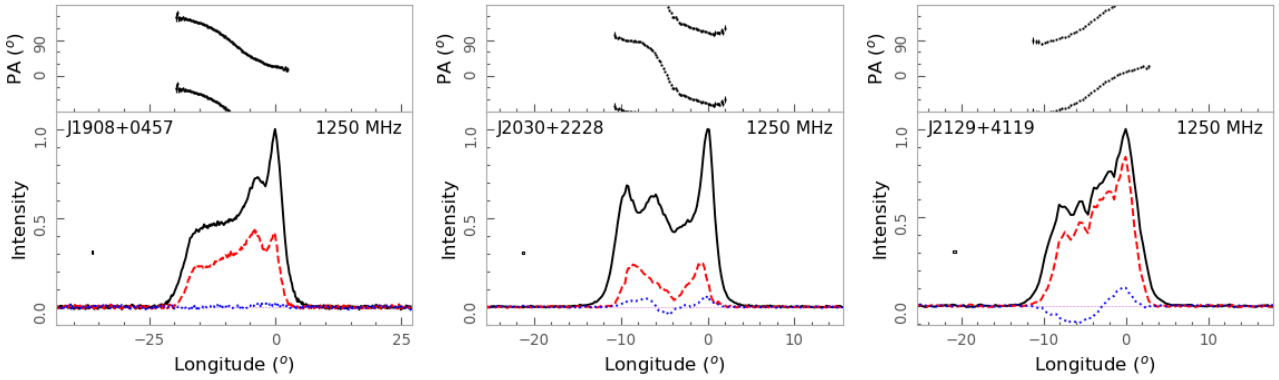

Fig. 5 Polarization profiles with S-shaped PA curves for 3 pulsars as examples of 96 pulsars in Figure A.1 and also 99 pulsars in other figures of Appendix A. For each pulsar, the total intensity, linear and circular polarization are represented by black solid, red dashed and blue doted lines in the bottom sub-panel. The left-hand circular polarization is defined to be positive. The bin size and 3σ are marked inside the sub-panel, here σ is the standard deviation of off-pulse bins. In the top panel, dots with error-bar are measurements of polarization position angles for linear polarization intensity exceeding 3σ.

ble pulsars in Figure A.5, 13 pulsars with an interpulse in Figure A.6, and 3 pulsars with wide pulses in Figure A.7, as denoted by the "Note" column in Table 3.

These S-shaped PA curves are simple and represent the monotonic variation of the PAs of a series of radiating sources, regardless of the complexity of the source arrangement. This behavior is manifested by the intensity profiles with a single component (e.g. PSRs J0711+0931 and J1900+0227 in Figure A.1), double (e.g. PSRs J1312+1810 and J1931+1439 in Figure A.5), triple (e.g. PSRs J1843+0119 in Figure A.1 and J2113+4644 in Figure A.2), or multiple components (e.g. PSRs J1908+0457 and J2129+4119 in Figure 5), and even the 'partial cone' components (e.g. PSRs J1917+1353 and J2013+3845 in Figure A.1), as defined in Lyne & Manchester (1988). More interesting is the S-shaped PA curves detected from 7 millisecond pulsars: PSRs J0605+3757, J1641+3627A, J1828+0625, J1908+0128, J1921+0137, J2042+0246, and J2234+0944. It demon-

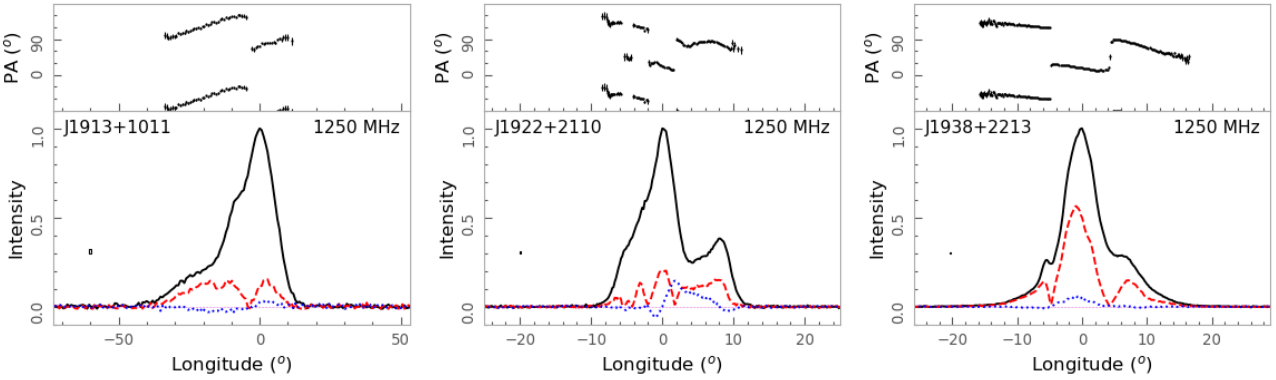

Fig. 6 The same as Figure 5 but for polarization profiles with orthogonal modes for 3 pulsars as examples of 136 pulsars in Figure A.2, and also 35 pulsars in other figures of the Appendix A.

strates that the PA swings of MSPs are not very different from those of normal pulsars.

3.2 Polarization profiles with orthogonal modes

Orthogonal modes have been observed as two populations of PAs of individual pulses, and they manifest as a sudden 90^o jump in PA curves of integrated pulse profiles, often accompanied by a great reduction of linear polarization intensity. Among the polarization profiles we observed by FAST, the PA jumps have been detected for 171 pulsars, as shown in Figure 6 for 3 pulsars as examples of 136 pulsars in Figure A.2 and 35 pulsars in other figures: 9 pulsars with highly linearly polarized components in Figure A.3, 5 conal double pulsar in Figure A.5, 6 pulsars with interpulse emission in Figure A.6, 13 pulsars with wide profiles in Figure A.7, and 2 pulsars affected by interstellar scattering in Figure A.8, as denoted by the "Note" column in Table 3.

The orthogonal PA jumps can happen at one, or two, or multiple phases within the pulse window. Among the total of 171 pulsars with orthogonal modes, 90 pulsars show one PA jump, e.g. PSR J1913+1011 in Figure 6. 60 pulsars exhibit two PA jumps, e.g. PSR J1938+2213 in Figure 6. Multiple jumps are detected for about 21 pulsars, e.g. PSR J1922+2110 in Figure 6.

Apparently the PA jumps from the orthogonal modes can take place at any phases inside the pulse window, e.g. at the profile center for PSR J1913+1011 in Figure 6, or at the profile wings for PSRs J1859+00 and J1946+1805 in Figure A.2. Because of FAST sensitive observations, weak emission has been detected in the wings far away from previously known profiles, such as for PSRs J2113+4644 and J1935+1616 in Figure A.2, which often exhibit significant orthogonal modes.

Millisecond pulsars also exhibit orthogonal modes, such as MSPs J0340+4130 and J1518+0204A in Figure A.2, indicating similar magnetosphere conditions for emission production and wave propagation as those for normal pulsars (e.g. Wang et al. 2014).

Despite these 90^o jumps, some non-orthogonal jumps have been detected, e.g. for PSRs J1946+2244 and J2018+2839 in Figure A.2. Such non-orthogonal jumps can be caused by intrinsic mixture of emission of two modes near the transition phase, e.g. the modes originating from different heights of pulsar magnetosphere (e.g. Xu et al. 1997), or the suppositions of the emission from different propagation paths as seen for pulsars with strong interstellar scattering for PSRs J1852+0031 and J1853+0545 shown in Figure A.8.

3.3 Polarization profiles with highly linearly polarized components

Highly linearly polarized profiles or components have been detected for 73 pulsars in our FAST observations, as shown in Figure 7 for 4 pulsars as examples of 45 pulsars in Figure A.3, and also 28 pulsars in other figures, including 13 pulsars with S-shaped position angles in Figure A.1, 2 pulsars with orthogonal modes in Figure A.2, 9 pulsars with interpulse emission in Figure A.6, 3 pulsars with wide profiles in Figure A.7 and one conal double pulsar in Figure A.5, as denoted by the "Note" column in Table 3.

For most of these pulsars, highly linearly polarized emission is detected for the whole pulse profiles with a polarization degree larger than 70%. These pulsars can have a single component such as PSR J1838-01 in Figure A.3, or double components, e.g., PSRs J0006+1834 in Figure A.3 and J0538+2817 in Figure 7, or multiple components, e.g., PSR J0631+1036 in Figure 7. For some pulsar, the highly linearly polarized emission is only detected from the leading component such as PSRs J0538+5413 in Figure 7, or the trailing component such as PSRs J1911+0939g and J1928+1809g in Figure A.3, or both such as PSRs J1907+0249 and J1957+2831 in Figure A.3. These highly

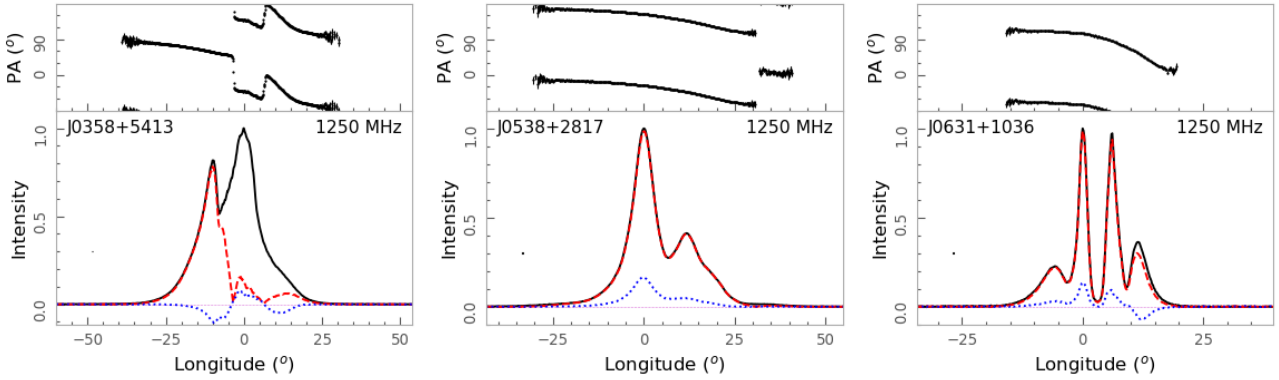

Fig. 7 The same as Figure 5 but for profiles with highly linearly polarized emission for 3 pulsars as examples of 45 pulsars in Figure A.3, and also 28 pulsars in other figures of the Appendix A. The highly linearly polarized emission can appear for the whole profile, the leading component, and/or the trailing component.

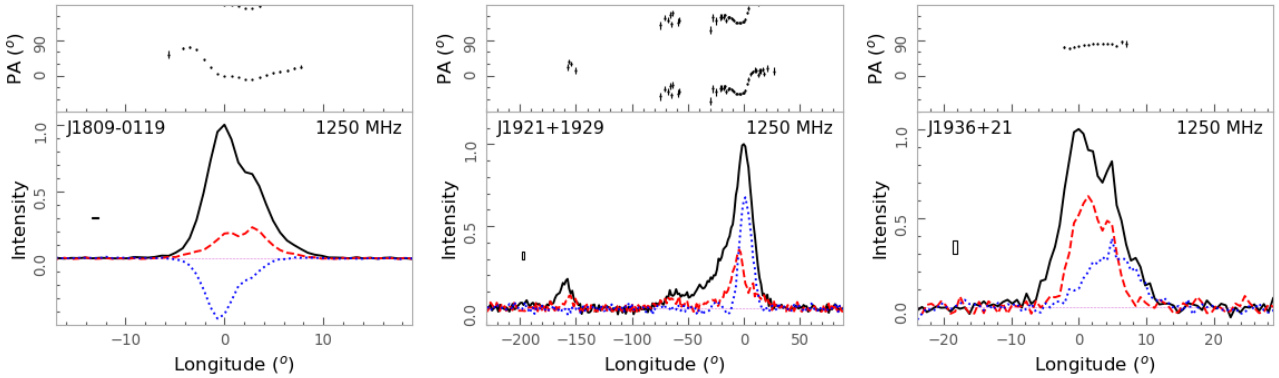

Fig. 8 The same as Figure 5 but for profiles with highly circularly polarized emission for 3 pulsars as examples of 9 pulsars in Figure A.4, and also 7 pulsars in other figures of the Appendix. The significant circularly polarized emission can be of left and/or right hand senses.

linearly polarized emission generally has flat PAs compared with those less polarized ones.

One possible explanation for such highly linearly polarized emission is by considering the emission process and propagation effects within pulsar magnetosphere. As discussed by Wang & Han (2016), the highly linearly polarization can appear in anywhere inside the emission beam, e.g. the leading part, the trailing part or the entire beam, depending on the plasma conditions in pulsar magnetosphere. When the sight lines cut across the emission beam with different impact angles, one can detect highly linearly polarized component at different parts of pulse profiles.

3.4 Polarization profiles with highly circularly polarized components

Most pulsar polarization profiles have a low degree of circular polarization (Han et al. 1998). Among our FAST results, polarization profiles of 16 pulsars have highly circularly polarized components with the degree of circular polarization greater than 30%, as shown for 3 pulsars in Figure 8 as examples of 9 pulsars in Figure A.4 and PSRs J1853+0056 and J2006+3102 with S-shaped PA curves in Figure A.1, PSRs J1855+0139g and J1907+0345 with highly linearly polarized emission in Figure A.3, PSRs J1851+0118 and J1852+0056g with interpulse emission in Figure A.6, and PSR J1855+0527 affected by interstellar scattering in Figure A.8. The strong circular polarization can be of the left hand such as PSR J1921+1929 or the right hand such as PSR J1809-0119 in Figure 8.

Circular polarization can be natural produced by curvature emission mechanism in pulsar magnetosphere. For example, Gangadhara (2010) showed that the circular polarization with a sense reversal correlates with the swing of PA in curvature radiation. Wang et al. (2012) explored the polarization features for curvature radiation for the entire pulsar emission beam, and demonstrated that the density gradient of the relativistic particles result in net circular polarization, and the sense or sense reversal can vary across the emission beam depending on the density distribution of the relativistic particles and the geometry with respect of the line of sight. Moreover, non symmetric cyclotron absorption of emission in the higher magnetosphere can also

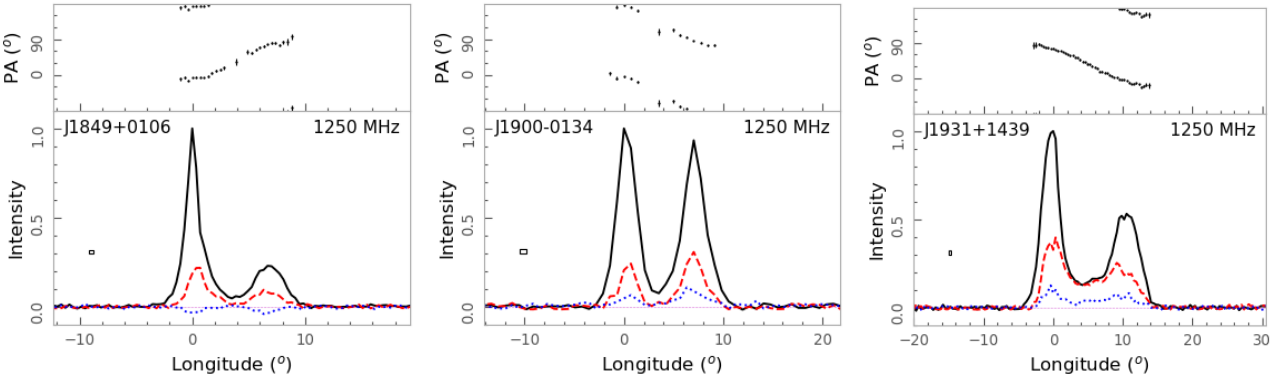

Fig. 9 The same as Figure 5 but for 3 conal double pulsars as examples of 28 pulsars in Figure A.5.

Table 4 Circular polarization of 28 conal-double pulsars.

PSR	PA swing	Sense of V Comp 1	Comp 2
J0011+08	Increase	–	?
J0848+16	Increase	?	?
J1312+1810	Increase	–	–
J1538+2345	Increase	–	–
J1641+3627A	Increase	–	–
J1833-0209	Increase	–	–
J1838+0044g	Increase	?	?
J1839-0223	Increase	–	–
J1843-0211	Increase	–	–
J1849+0106	Increase	–	–
J1910+0728	Increase	?	+
J1917+0834	Increase	–	–
J1919+1745	Increase	+	+
J1926+1434	Increase	–	?
J1933+1304	?	–	–
J1933+5335	Increase	–	+
J1946+14	Increase	+	+
J2051+4434g	Increase	?	?
J1832+27	Decrease	+	+
J1838-0107	Decrease	–	?
J1854+0319	Decrease	+	+
J1856+0243g	Decrease	–	?
J1900-0134	Decrease	+	+
J1904+1011	Decrease	+	+
J1921+1540	Decrease	–	–
J1931+1439	Decrease	+	+
J1937+2544	Decrease	?	–
J1938+14A	Decrease	+	+

Note: ? = not very clear

lead to circular polarization of pulsar emission (Wang et al. 2010).

3.5 Conal-double pulsars

Conal-double pulsars are defined as two distinct components likely from a conal beam. They generally exhibit S-shaped PA curves, as shown in Figure 9 as examples. . Han et al. (1998) found that the senses of PA swing and the senses of circular polarization are related. The decrease of PA swing usually accompanies with the left-hand (+ values) circular polarization, and the increase of PA swing with the right-hand (− values) circular polarization. Such a sense correlation was strengthened by You & Han (2006) using a large dataset.

Using the newly measured polarization profiles, we list the senses of PA swing and circular polarization for 28 conal-double pulsars in Table 4. Among them, 18 pulsars exhibit clear PA changes and the sense of circular polarization, in which 14 of them follow the correlation found by Han et al. (1998), while 4 pulsars (PSRs J1919+1745,J1946+14, J1933+5335 and J1921+1540) do not. .

3.6 Polarization profiles with an interpulse component

The interpulse represents a pulse component located at a longitude separated by about 180° from the main one, which usually indicates that the main pulse and interpulse come from the two opposite poles of pulsar magnetosphere. Among the FAST pulsar database, we get polarization profiles of 27 pulsars most likely to have an interpulse component, as shown in Figure 10 for 3 pulsars as examples of the 27 ones in Figure A.6. More than half of them have good quality so that polarization profiles of the weak interpulse have been well measured. For PSRs J1909+0749 and J2208+4056 in Figure 10, the main pulse and interpulse have the different emission mode so that their PA curves have an offset of 90° in the rotating vector model fitting. The orthogonal mode is clearly seen in the main pulse of PSR J2023+5037 in Figure 10.

For these pulsars with interpulses, the highly linear polarization is often detected for the main pulse such as PSR J1017+3011 in Figure A.6, or for the interpulses such as PSRs J1909+0749 and J1913+0832 in Figure A.6, or both such as PSRs J1935+2025, J2004+3429, J2032+4127 and J2208+4056 in Figure A.6. The leading part of the main pulse of PSR J1628+4406 in Figure A.6 and the trailing part of the main pulse of J1918+1541 in Figure A.6 are also highly linearly polarized. Significant circular polarization is detected from the main pulses of PSRs J1852+0056g and J2047+5029 or the interpulse of PSR J1913+0832 in

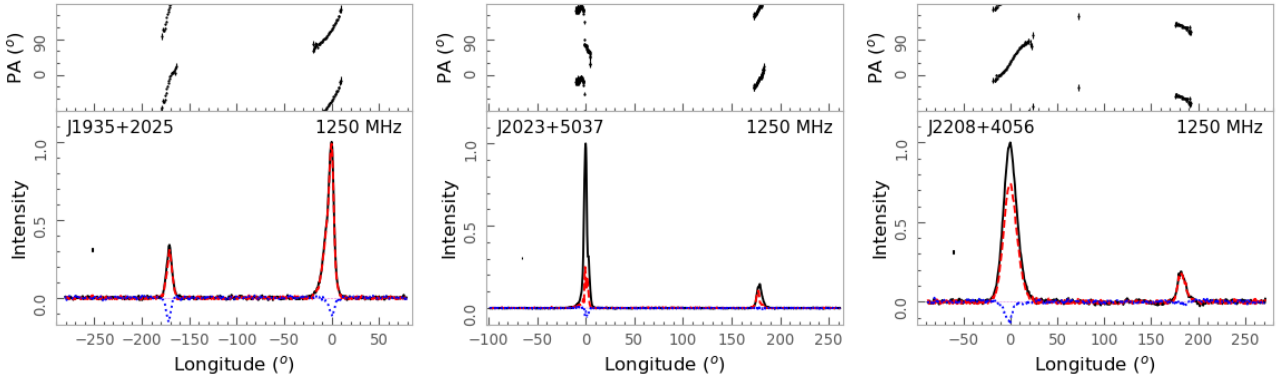

Fig. 10 The same as Figure 5 but for 3 pulsars with interpulse emission as examples of 27 pulsars in Figure A.6.

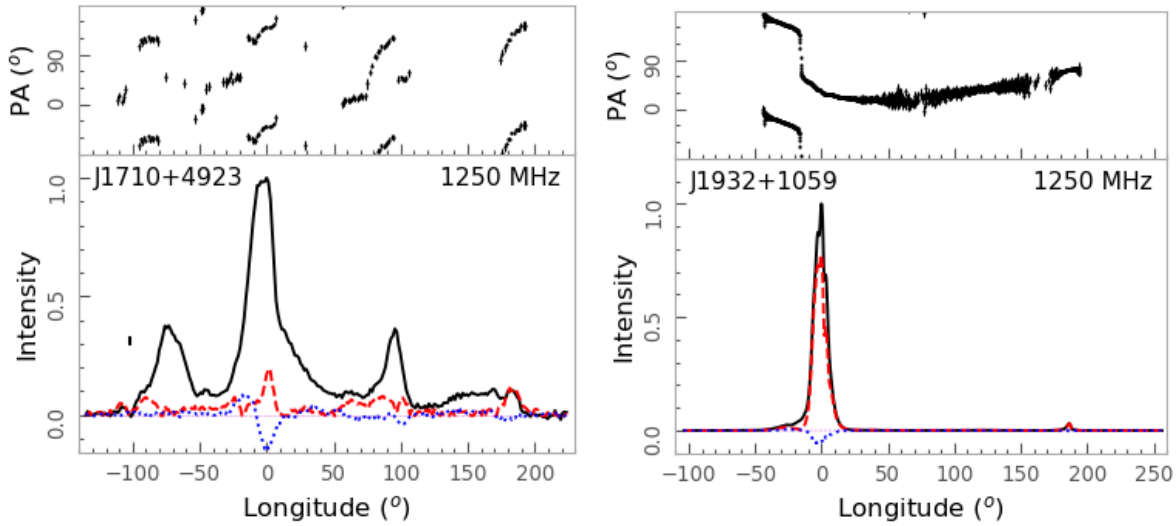

Fig. 11 The same as Figure 5 but for two pulsars with extremely wide profiles as examples of 21 pulsars in Figure A.7. Note that PSR J1932+1059 has a very weak emission between the two peaks detected by FAST.

Figure A.6, and both the main pulse and interpulse of PSR J1935+2025 in Figure 10.

Based on high quality polarization profiles of 5 interpulse pulsars, Johnston & Kramer (2019) found that the polarization properties of main pulse and interpulse are related, so that the signs of circular polarization should be the same when the PA swings in the same trend. We get new data for another 5 pulsars in Figure A.6 which can be used to verify the conclusion. The main pulse and interpulse of PSR J1935+2025 have the same PA swing and the same sign of circular polarization, and PSRs J1934+2352 and J2047+5029 have different PA swings and the opposite signs for circular polarization. The polarization data of these 3 pulsars are consistent with the conclusion of Johnston & Kramer (2019). However, the PA swing of the main pulse and interpulse for PSR J2208+4056 is different, while the circular polarization has the same sign.

3.7 Very wide pulse profiles

Pulsar profiles generally occupy a few percent of a period, i.e. 10° to 30° in the rotation phase. Sensitive observations can reveal the weak emission components (e.g. PSR J2124-3358 in Manchester & Han 2004). From our FAST observations, we get very wide profiles for 21 pulsars (see Figure A.7), occupying the rotation phase by more than 180°, as shown in Figure 11 for 2 pulsars as examples. Emission occupies almost all rotation phase for PSR J1710+4923 in Figure 11, and PSRs J1916+0748 and J2007+2722 in Figure A.7. Most of the pulsars are millisecond pulsars, but there do have 4 normal ones, PSRs J1851+0418, J1903+0925, J1916+0748 and J1932+1059 in Figure A.7.

These pulsars exhibit diverse polarization features, regardless of normal pulsars or millisecond ones. Some of them show S-shaped PA curves, e.g., PSR J2234+0944 in Figure A.7. The rotating vector model can fit some of PA curves very well. About half of them show orthogo-

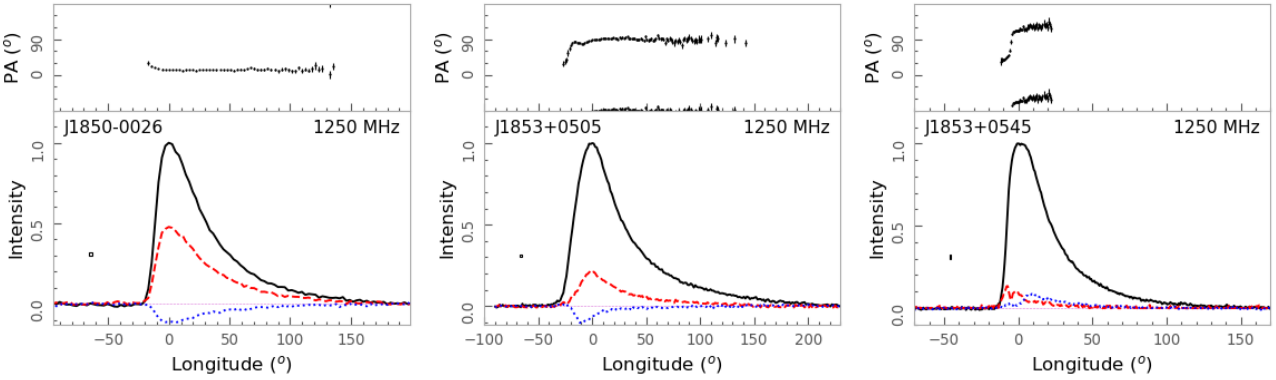

Fig. 12 The same as Figure 5 but for 3 pulsars with scattering tails as examples of 22 pulsars in Figure A.8.

nal modes, such as PSRs J0337+1715 and J1916+0748 in Figure A.7. The orthogonal modes and PA swing of PSR J1710+4923 in Figure 11 regularly repeats 4 times within one rotation. Highly linear polarized components appear in PSRs J1630+3734 and J1709+2313 in Figure A.7. Strong circular polarization is detected for some components of PSRs J1835-0114 and J1955+2908 in Figure A.7.

The profile morphology and polarization are very much complicated for these very wide profiles. For normal pulsars, the wide profiles mean that inclination angles are small, and the sight line remains within the emission beam. Much more discrete radiating sources can be detected inside the beam, and hence the profiles have the complexity. This can be also the case for MSPs, but with much larger polar caps. It means that wide profiles are much more likely to be detected, even for large inclination angles. The wide profiles might also result from emission from both poles, such as PSR J1932+1059 in Figure A.7.

3.8 Profiles with scattering tails

Distant pulsars with large dispersion measures tend to suffer from interstellar scattering, showing not only a long tail of the pulse profile but also a flat PA curve in the tail part (Li & Han 2003).

In our FAST pulsar database, we observed a large number of pulsars with scattering features, as presented by Jing et al (2023, in preparing). Here we present the polarization profiles for 3 pulsars in Figure 12 as examples of the 22 ones in Figure A.8. Apparently all polarization profiles tend to have flat PA curves in the tail part, confirming the conclusion first proposed by Li & Han (2003). In the leading wing before the profile peak, diverse polarization features can be seen, such as orthogonal modes for PSRs J1852+0031 and J1853+0545 in Figure A.8, which means no significant depolarization from the scattered signals in these phase bins. Circular polarization of these profiles generally has one sense. Although affected by scattering, the circular polarization of PSR J1855+0527 in Figure A.8 is the most prominent among all the pulsars presented in this paper, reaching 45.5%.

3.9 Other Pulsars

Polarization profiles of the other 298 pulsars are shown in Figure A.9, which are about 44% of all pulsars reported in this paper. Most of our FAST observations give an unprecedented S/N of profiles. The diverse polarization features may be caused by complicated emission beam structures, such as multiple emission patches from different parts or different heights in pulsar magnetosphere. Superposition of radio emission from the emission of various patches leads to depolarization or complicated polarization behaviors.

4 FURTHER UNDERSTANDING OF PULSAR PROFILES

Diverse profile morphology and different polarization properties of these pulsars need to be further understood in pulsar physics. Here, we first do statistic analysis on profile widths, linear and circular polarization. With the large sample of pulsars with S-shaped PA curves, we then work on the emission geometry. Finally, frequency dependencies of profile width, linear and circular polarization are also explored for some pulsars with the sensitive FAST data.

4.1 Statistics on pulse profile properties

4.1.1 Polarization properties versus fundamental parameters of pulsars

To investigate if the profile properties are related to the period and period derivative, we mark pulsars with different properties on the period-period derivative diagram, as shown in Figure 13. Pulsars with S-shaped PA curves or orthogonal modes have Edots over a wide range with no preference. These features are clearly demonstrated in the histograms of Edot for different types of pulsars in Figure 14.

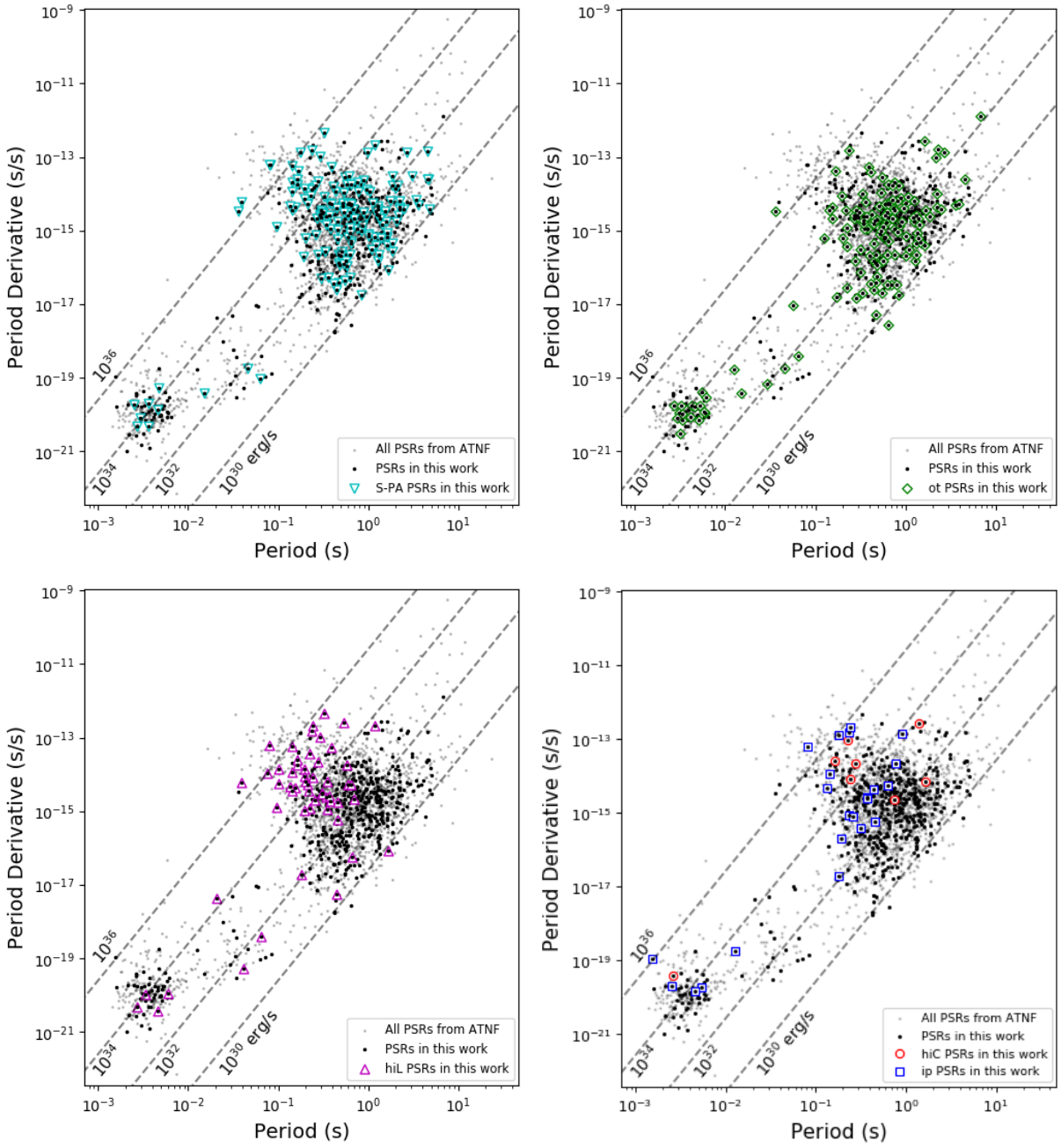

Fig. 13 Pulsars with different polarization properties in the period and period derivative diagram. Grey dots are plotted for the known pulsars taken from the ATNF pulsar catalogue (Manchester et al. 2005), blank dots are for 502 of the 682 pulsars reported in the current work, which have both period and period derivative available. Pulsars with S-shaped PA curve are indicated by "▽" in the top left panel, pulsars with orthogonal modes by the "◇" in the top right panel, pulsars with highly linear polarization by "△" in the lower left panel, and pulsars with highly circular polarization by "○" and inter pulses by "□" in the lower right panel.

MSPs exhibit all the types of polarization features as the normal pulsars. Such results imply that pulsar profiles are fundamentally related to the energy lose of rotating pulsars.

4.1.2 Statistics on profile width

Our FAST observations provide accurate measurements of profile widths for a large number of pulsars. The distributions of pulse profile widths are obtained in Figure 15. The typical widths are 9.1° for W_{50} and 17.4° for W_{10}.

Pulse width in principle is related to the emission geometry and beam width. The beam width should be the

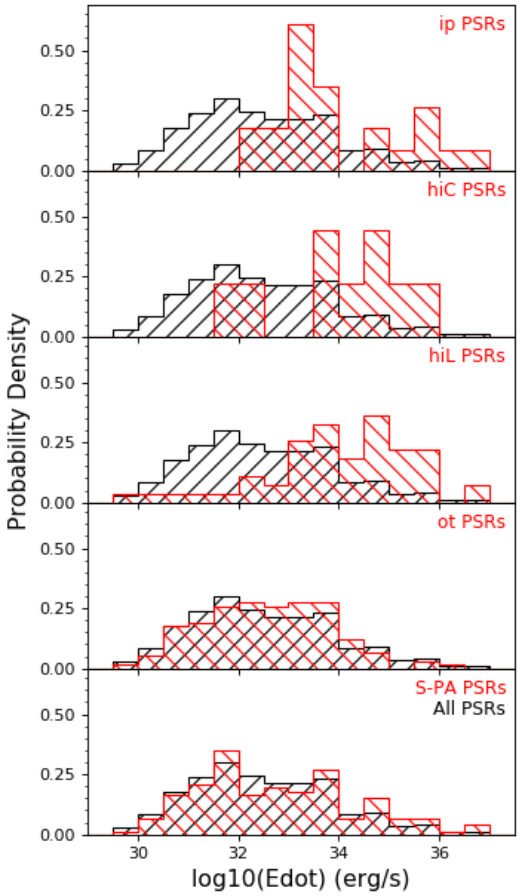

Fig. 14 Distribution of pulsars with different properties against the Edot. Grey histogram is made for 502 pulsars in the current work with available Edot. From bottom to top panels, red steps are for pulsars with S-shaped PA curve, with orthogonal modes, with highly linear polarization or circular polarization, and with inter pulses.

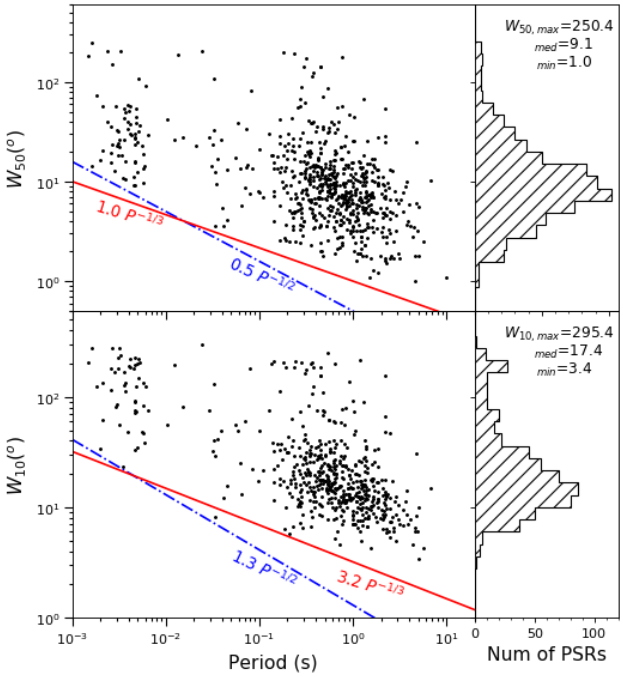

Fig. 15 Distributions of profile widths W_{10} and W_{50} of 682 pulsars. They have the lower boundaries with $P^{-1/2}$ and $P^{-1/3}$. Histograms of profile widths are shown in the right subpanels with indications of the maximum, median and minimum of pulse widths.

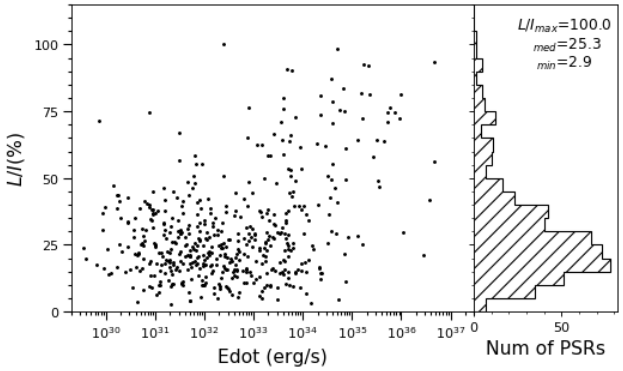

Fig. 16 Distribution of the fractional linear polarization and its correlations with Edot and pulsar age.

lower limit of pulse width in the case of central cut of the line of sight on the beam. As shown in Figure 15, the lower boundary of pulse widths was plotted with power-law relation, $0.5^\circ P^{-1/2}$ for W_{50} or $1.3^\circ P^{-1/2}$ for W_{10}, similar to that for core components (Rankin 1990) and/or conal components (e.g. Maciesiak et al. 2012; Mitra et al. 2016). The scaling relations with $P^{-1/2}$ are understandable for the dipole opening angles of the magnetic field lines by assuming a constant emission height (e.g. Biggs 1990; Kramer et al. 1998). Actually, pulsar emission at a given frequency is not produced at the same height of pulsar magnetosphere. With the data set of 682 pulsars, the lower boundary of observed profile width W_{10} follow $3.2^\circ P^{-1/3}$ or $1.0^\circ P^{-1/3}$ for W_{50}, as shown in Figure 15. These dependencies have a slope less steeper than $P^{-1/2}$, which meet with those from Johnston & Karastergiou (2019).

4.1.3 Linear polarization

The pulsars have a fractional linear polarization of around 25.3% as observed by FAST at 1250 MHz, as shown in the right panel of Figure 16.

The young pulsars with large Edots tend to have a large fraction of linear polarization at 4.9GHz and 1.4GHz (von Hoensbroech et al. 1998b; Crawford et al. 2001), but not at lower frequencies of 408 MHz and 774 MHz (von Hoensbroech et al. 1998b; Han et al. 2009). The gradual transition of highly linear polarization is at Edot of about $10^{34}-10^{35}$ erg/s (Weltevrede & Johnston 2008; Mitra et al. 2016; Johnston & Kerr 2018). Our observation results at

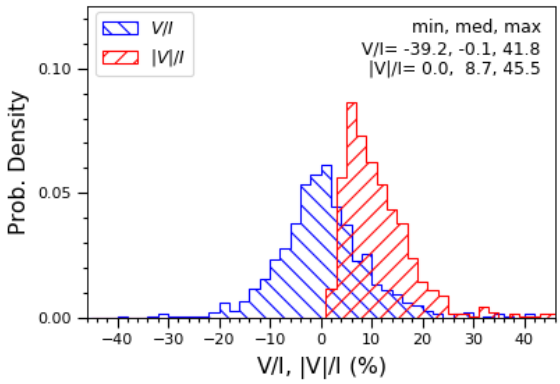

Fig. 17 The distribution of the fraction of circular polarization observed by the FAST in this paper.

1250 MHz by FAST confirm the correlation and transition, as shown in Figure 16. The linear polarization is about 25% for pulsars with a low Edot. When Edot increases to about 10^{33} erg/s, more pulsars tend to have higher linear polarization. When Edot further increases to about 10^{35} erg/s, the linear polarization is more likely to be higher.

4.1.4 Circular polarization

Pulsar radio emission at 1250 MHz usually has an absolute circular polarization of about 8.7%. There is no preference for the handness of circular polarization, as shown by the symmetric distribution of V/I in Figure 17. No significant correlation of $|V|/I$ with pulsar period, period derivative, Edot and age has been found from our observation data.

4.2 Pulsar geometry

The geometry of a pulsar can be described by an inclination angle α that is the angle between the magnetic axis and its rotation axis, and an impact angle β that is the minimum angle of a sight line with respect to the magnetic axis. The line of sight then has an angle of $\zeta = \alpha + \beta$ from the rotation axis. For the geometry, one can find that the polarization position angle ψ swings with respect to the rotation phase ϕ by following (Radhakrishnan & Cooke 1969),

$$\tan(\psi - \psi_0) = \frac{\sin\alpha \sin(\phi - \phi_0)}{\sin(\zeta)\cos\alpha - \cos(\zeta)\sin\alpha\cos(\phi - \phi_0)}. \quad (2)$$

This is called the rotating vector model (RVM). Here, ϕ_0 and ψ_0 represent the phase and position angle where the PA swing has the largest gradient.

4.2.1 Analysis methods

Pulsar geometries can be derived through RVM fitting. Considering that the PAs are defined to increase clockwise in the normal RVM but counter-clockwise in practical observations, we therefore relate α and β in the model to the original α_0 and β_0 (Everett & Weisberg 2001) via $\alpha = 180^\circ - \alpha_0$ and $\beta = -\beta_0$.

Instead of fitting to the PA curves, two-dimensional fitting is performed directly to Stokes Q and U by using PSRMODEL program of PSRCHIVE. We first search a 61×61 grid with α_0 extending from 0° to 180°, and β_0 extending from 0° to 60° or -60° to 0° depending the sense of PA curve. That is to say, the increase PA corresponds to a negative β_0, and vise versa. With the fitting result of each grid point, a 2-D χ^2 surface is plotted. According to which, the region for β_0 and occasionally that for α_0 are adjusted for a second search over much finer 181×181 grids. In general, the searching region for β_0 is reduced in the second iteration, but it is extended to 0° to 90° or -90° to 0° for some pulsars with flat PA curves. Then, the 2-D χ^2 surface is obtained, which is smoothed to avoid the lock down to $\alpha_0 \to 180^\circ$ or 0° and $\beta_0 \to 0^\circ$. Finally, a continuous region containing the minimum of χ^2 (i.e., χ^2_ν) is found, as shown in the right plots of Figure 18. The optimal α_0 and β_0 are then obtained for the minimum χ^2_ν. With the α_0 and β_0 fixed, a new fitting can give ϕ_0 and ψ_0.

Uncertainties of α_0 and β_0 are estimated from the 2-D χ^2 surface. The regions lying at $\Delta\chi^2$=1, 4 and 9 above the minimum χ^2_ν are indicated by the solid, dashed and doted contour lines, respectively, as shown in Figure 18. Its projection on α_0 and β_0 axes forms one-dimensional intervals. The intervals for $\Delta\chi^2$=1, instead of the 2-D region, contain 68.3% of normally distributed data. These confidence intervals around the minimum are employed to estimate the lower and upper boundaries for the uncertainties in α_0 and β_0. With these tangential α_0 and β_0 fixed in new RVM fittings, 4 pairs (occasionally 2 or 3) of ϕ_0 and ψ_0 are obtained. Their maximum offsets from the optimal ϕ_0 and ψ_0, i.e. the one estimated at χ^2_ν, are used to estimate the lower and upper boundaries for the uncertainties in ϕ_0 and ψ_0.

During the fitting, 90° discontinuities are inserted for the orthogonal modes. But the discontinuities are not 90° for 12 pulsars, e.g. PSR J0358+5413 in Figure B.1, and the range of longitudes of the minor mode is unweighed. The best fitted PA curves are represented by the dashed lines in the PA subpanel of Figure 18.

4.2.2 The RVM solutions

The so-obtained geometry parameters of all the 190 pulsars are listed in Table 5, with their fittings shown in Figure B.1. It is obvious that α_0 can not be well constrained for most of the pulsars with a value in the range of 0° to 180°, and only 69 of them have uncertainties less than 90°, as listed in Table 5. Nevertheless, β_0 is much better constrained.

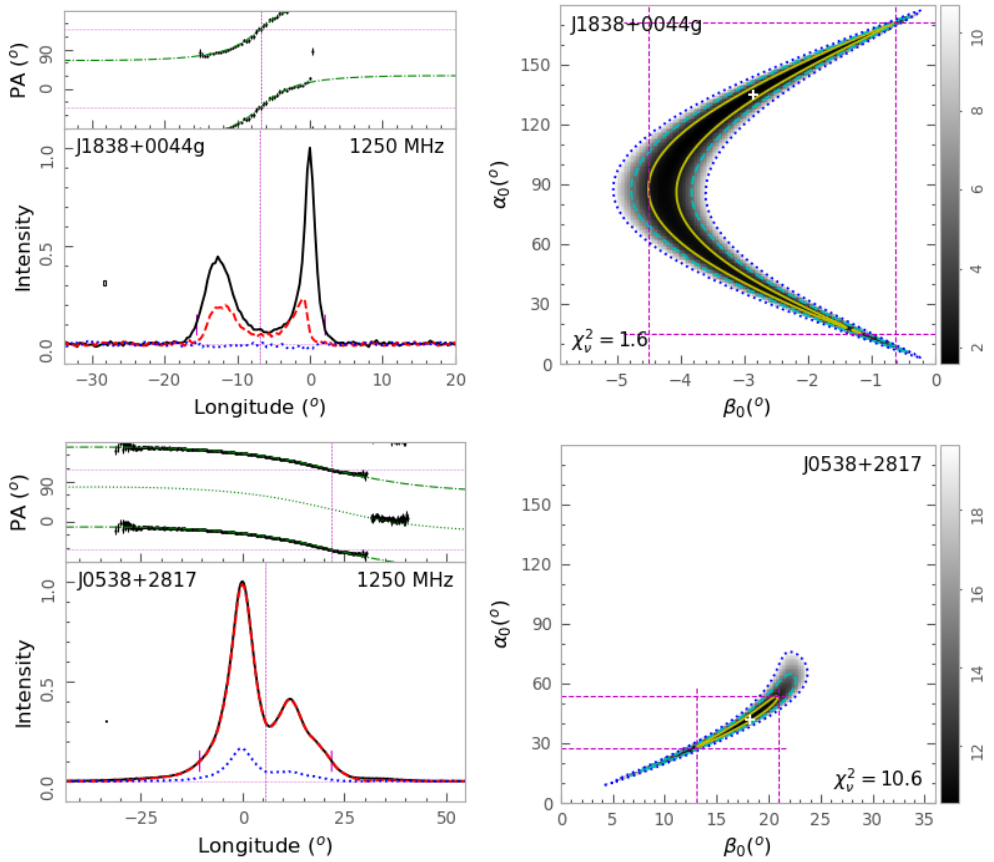

Fig. 18 The RVM fittings for PSRs J1838+0044g and J0538+2817 as two examples. *Left plots:* Polarized pulse profiles with S-shaped PA curve and orthogonal modes. For each pulsar, the total intensity, linear and circular polarization are represented by black solid, red dashed and blue doted lines in the bottom sub-panel. The bin size and 3σ are marked inside the sub-panel, here σ is the standard deviation of off-pulse bins. The short doted vertical lines represent the boundaries for 10% the peak intensity and the long vertical line for the profile center. In the top panel, dots with error-bar are measurements of polarization position angles for linear polarization intensity exceeding 3σ. The dash-doted line indicates the RVM solution, and the doted green one for the orthogonal mode with a 90° shift. The vertical and horizonal doted lines in this subpanel are for the phase and position angle of the steepest position of the PA curve, i.e., ϕ_0 and ψ_0. *Right plots:* χ^2 distribution of the RVM fitting. For each pulsar, the position at the minimum of χ^2 is indicated by "+" with a value of χ^2_ν marked in the panel. The solid, dashed and doted contour lines are for $\Delta\chi^2$=1.0, 4.0, and 9.0, respectively. Projection of the red line bounded region (1-sigma region) on the α_0 and β_0 axes is indicated by the horizonal and vertical dashed lines.

Figure 19 shows the distributions of α_0, β_0 and ϕ_0 for these 190 pulsars. Apparently, magnetic axes are most probably inclined at angles of about 25° or 155° with respect to the rotation axes. There is also a good number of orthogonal rotators, i.e., those around $\alpha_0 \sim 90^\circ$. Our sight lines most likely detect pulsars with $|\beta_0| < 5^\circ$, as shown by the significant overstep in the histogram of β_0. Some pulsars have very flat PA curves, whose β_0 are generally large and can not be well constrained. For example, it extends from 13° to 90° for PSR J1852-0118, -89° to 5° for PSR J1916+0748 and -90° to -18° for PSR J2017+0603, as listed in Table 5 and shown in Figure B.1. The minimum of $|\beta_0|$ is only 0.053° for PSR J2113+4644 in Figure B.1, indicating the sweep of sight line nearly across the magnetic axis. We get β_0 only -0.002 for PSR J1856+09, but it has a large uncertainty since the discontinuity in PA might be caused by orthogonal emission modes.

The offsets of the PA curves with respect to profile peaks are demonstrated by the histogram of ϕ_0 in Figure 19. PA curves lag the profile peaks for 120 of the 190 pulsars. The majority of pulsars exhibiting the lag can be explained by the underlying physics of rotation induced abberation, which leads the profiles to be shifted to an early phases and the PAs lately (e.g. Blaskiewicz et al. 1991; Wang et al. 2012). For some pulsars, the offsets are larger than 60°, e.g., PSR J1852-0118 in Figure B.1. It means that the emission regions are far away from the meridional plane.

4.2.3 Emission heights

With these geometry parameters and the measured profile widths, beam radii ρ are estimated for the pulsars, $\rho = 2\arcsin[\sin^2(W_{10}/4)\sin\alpha\sin(\zeta) + \sin^2(\beta/2)]^{1/2}$, as listed in column (8) of Table 5. Its correlation with pul-

Table 5 Geometry parameters for 190 pulsars. – *to be continued* –

PSR	P	α_0	β_0	ϕ_0	ψ_0	χ^2_ν	ρ	$r_{\rm geo}$	$r_{\rm delay}$	Note
	(s)	(°)	(°)	(°)	(°)		(°)	(km)	(km)	
(1)	(2)	(3)	(4)	(5)	(6)	(7)	(8)	(9)	(10)	(11)
J0006+1834	0.693	9.3	32.8	-16.1	82.2	2.5	-	-	-	l.un
J0058+4950	0.996	21^{+60}_{-16}	$1.7^{+3.0}_{-1.3}$	$3.7^{+0.2}_{-0.2}$	$-17.2^{+1.9}_{-2.1}$	7.0	$3.5^{+6.0}_{-2.7}$	82^{+516}_{-77}	231^{+70}_{-67}	
J0244+14	2.127	52^{+123}_{-47}	$1.5^{+0.7}_{-1.3}$	$-1.4^{+0.3}_{-0.2}$	$88.3^{+4.7}_{-7.9}$	1.4	$3.5^{+1.1}_{-3.1}$	176^{+121}_{-174}	neg	
J0358+5413	0.156	175	0.7	9.3	-16.5	169.2	1.7	3	401	wo.ot, s.un
J0402+4825	0.512	159^{+17}_{-122}	$-2.4^{+1.9}_{-5.3}$	$8.6^{+1.2}_{-0.6}$	$-16.7^{+6.7}_{-5.6}$	3.6	$4.0^{+7.5}_{-3.2}$	55^{+394}_{-53}	192^{+126}_{-71}	
J0453+1559	0.045	23^{+38}_{-14}	$0.7^{+0.8}_{-0.4}$	$-5.6^{+0.1}_{-0.1}$	$86.4^{+1.2}_{-0.7}$	26.0	$3.2^{+3.9}_{-1.9}$	3^{+12}_{-3}	neg	
J0454+5543	0.340	$8.0^{+9.5}_{-2.5}$	$0.7^{+0.8}_{-0.2}$	$7.6^{+0.1}_{-0.1}$	$61.6^{+0.1}_{-0.4}$	460.2	$2.3^{+2.7}_{-0.7}$	12^{+43}_{-6}	570^{+4}_{-1}	wo.ot
J0457+23	0.504	20^{+61}_{-15}	$2.7^{+5.2}_{-2.0}$	$16.7^{+1.2}_{-0.2}$	$70.6^{+0.9}_{-7.6}$	5.8	$7.3^{+13.0}_{-5.4}$	178^{+1177}_{-166}	862^{+227}_{-191}	
J0538+2817	0.143	42^{+11}_{-14}	$18.2^{+2.6}_{-5.0}$	$21.8^{+1.7}_{-1.6}$	$-62.5^{+3.5}_{-4.2}$	10.6	$22.0^{+3.1}_{-6.0}$	460^{+141}_{-218}	482^{+50}_{-46}	
J0543+2329	0.246	154	2.5	26.1	68.3	1.7	5.7	54	1087	l.un
J0605+3757	0.0027	11	-2.3	31.9	-87.2	0.9	-	-	-	no.w, l.un
J0608+1635	0.945	131^{+43}_{-126}	$2.5^{+2.5}_{-2.3}$	$-3.3^{+1.6}_{-0.4}$	-85^{+4}_{-25}	0.7	$4.9^{+2.7}_{-4.3}$	151^{+212}_{-149}	neg	
J0613+3731	0.619	18^{+70}_{-13}	$2.6^{+5.8}_{-1.8}$	$-3.5^{+0.6}_{-1.1}$	$-76.9^{+7.5}_{-4.5}$	15.5	$4.2^{+8.8}_{-3.0}$	71^{+620}_{-65}	neg	
J0631+1036	0.287	16^{+9}_{-8}	$2.3^{+1.1}_{-1.0}$	$11.2^{+0.1}_{-0.1}$	$54.8^{+0.8}_{-1.2}$	35.2	$4.3^{+2.2}_{-2.0}$	35^{+45}_{-24}	508^{+9}_{-6}	
J0659+1414	0.384	17^{+17}_{-8}	$5.7^{+4.9}_{-2.7}$	$12.8^{+0.8}_{-0.3}$	$17.2^{+1.0}_{-2.9}$	5.6	$7.5^{+6.5}_{-3.5}$	143^{+355}_{-103}	1172^{+67}_{-23}	wo.ot
J0711+0931	2.428	136^{+31}_{-119}	$-2.8^{+1.9}_{-1.4}$	$0.5^{+0.3}_{-0.2}$	$13.7^{+4.3}_{-3.0}$	3.7	$3.6^{+1.7}_{-2.4}$	206^{+238}_{-183}	309^{+153}_{-113}	
J0944+4106	2.229	133^{+40}_{-31}	$0.20^{+0.05}_{-0.17}$	$-3.7^{+0.1}_{-0.1}$	$-12.8^{+0.4}_{-0.3}$	41.5	$3.8^{+1.3}_{-3.2}$	217^{+172}_{-211}	neg	
J1017+3011	0.452	12^{+101}_{-9}	$-1.5^{+1.0}_{-51.0}$	139^{+15}_{-33}	23^{+105}_{-1}	2.0	-	-	-	
J1236-0159	3.597	120^{+51}_{-113}	$1.7^{+0.4}_{-1.5}$	$-4.3^{+0.2}_{-0.1}$	$20.9^{+1.4}_{-4.3}$	8.1	$5.1^{+0.9}_{-4.4}$	630^{+231}_{-617}	neg	
J1312+1810A	0.033	91^{+58}_{-84}	$-7.4^{+6.3}_{-0.7}$	$16.0^{+0.6}_{-0.7}$	$-66.8^{+3.8}_{-3.5}$	1.6	$21.5^{+2.1}_{-18.9}$	102^{+10}_{-100}	$13.3^{+13.1}_{-13.2}$	
J1538+2345	3.449	171^{+6}_{-19}	$-0.4^{+0.3}_{-0.8}$	$-3.0^{+0.1}_{-0.1}$	$55.5^{+0.5}_{-0.5}$	44.6	$0.9^{+1.7}_{-0.6}$	17^{+134}_{-15}	neg	
J1641+3627A	0.010	166^{+13}_{-164}	$-3.9^{+3.9}_{-17.2}$	$5.9^{+6.0}_{-2.5}$	60^{+18}_{-7}	1.0	9^{+26}_{-8}	5^{+75}_{-5}	25^{+13}_{-6}	
J1657+3304	1.570	28^{+147}_{-24}	$-1.5^{+1.3}_{-2.1}$	$-0.2^{+0.8}_{-0.3}$	$-18.1^{+13.9}_{-5.1}$	2.2	$2.7^{+3.3}_{-2.3}$	73^{+300}_{-71}	neg	
J1736+05	0.999	167^{+12}_{-165}	$-0.9^{+0.9}_{-4.0}$	$-2.0^{+0.9}_{-0.3}$	$89.1^{+13.0}_{-2.4}$	2.9	$1.3^{+5.1}_{-1.2}$	13^{+263}_{-11}	neg	
J1800-0125	0.783	125^{+51}_{-120}	$11.3^{+4.0}_{-10.4}$	$4.5^{+2.5}_{-3.0}$	56^{+12}_{-10}	1.2	14^{+5}_{-13}	1078^{+849}_{-1070}	617^{+405}_{-495}	
J1806+2819	0.015	33^{+143}_{-29}	$13.5^{+26.4}_{-11.7}$	$19.9^{+6.5}_{-4.8}$	$25.1^{+5.6}_{-11.7}$	1.9	29^{+26}_{-26}	83^{+218}_{-82}	3^{+21}_{-3}	
J1807+04	0.798	21^{+81}_{-16}	$-0.8^{+0.6}_{-1.4}$	$0.7^{+0.1}_{-0.2}$	$36.6^{+2.6}_{-3.0}$	16.9	$2.3^{+4.1}_{-1.7}$	28^{+189}_{-26}	neg	
J1807+0756	0.464	17^{+158}_{-13}	$2.2^{+8.8}_{-2.1}$	$-0.8^{+2.0}_{-2.7}$	-49^{+18}_{-14}	3.1	$3.9^{+11.2}_{-3.0}$	46^{+648}_{-44}	neg	
J1808+00	0.425	150^{+21}_{-76}	$3.7^{+3.8}_{-2.6}$	$1.1^{+0.3}_{-0.6}$	$-49.1^{+3.9}_{-1.6}$	7.1	$6.2^{+6.6}_{-4.3}$	108^{+355}_{-97}	192^{+30}_{-54}	
J1809+17	2.066	166^{+12}_{-164}	$1.2^{+6.1}_{-1.0}$	$2.1^{+0.4}_{-2.7}$	74^{+28}_{-3}	3.4	$1.5^{+6.7}_{-1.3}$	31^{+895}_{-30}	1213^{+179}_{-1156}	
J1823-0154	0.759	36^{+65}_{-23}	$0.8^{+0.6}_{-0.5}$	$1.0^{+0.1}_{-0.1}$	$-9.5^{+0.7}_{-1.4}$	13.4	$2.3^{+1.5}_{-1.4}$	25^{+47}_{-22}	190^{+8}_{-5}	wo.ot
J1824-0127	2.499	151^{+21}_{-144}	$-1.1^{+0.8}_{-1.4}$	$4.8^{+0.1}_{-0.2}$	$-50.2^{+1.2}_{-3.0}$	2.7	$2.6^{+2.8}_{-2.0}$	116^{+378}_{-109}	822^{+50}_{-98}	wo.ot
J1828+0625	0.0036	13^{+65}_{-10}	$4.4^{+18.2}_{-3.2}$	$2.8^{+9.2}_{-2.2}$	$-71.5^{+4.3}_{-20.7}$	1.5	16^{+50}_{-12}	$6.3^{+97.8}_{-6.0}$	$8.9^{+1.3}_{-1.1}$	
J1832+27	0.631	146^{+32}_{-142}	$4.2^{+4.6}_{-3.9}$	$4.3^{+4.2}_{-2.0}$	-65^{+14}_{-34}	1.2	$5.3^{+5.4}_{-4.9}$	116^{+359}_{-115}	130^{+554}_{-130}	
J1833-0209	0.583	146^{+30}_{-141}	$-1.7^{+1.4}_{-1.9}$	$-4.1^{+0.5}_{-0.5}$	$-49.3^{+5.8}_{-6.1}$	1.6	$4.7^{+3.8}_{-4.1}$	87^{+194}_{-86}	neg	
J1834+10	1.172	17^{+60}_{-11}	$-2.1^{+1.3}_{-4.6}$	$-8.0^{+0.3}_{-1.8}$	$-43.8^{+1.5}_{-6.6}$	6.1	$4.2^{+10.1}_{-2.7}$	135^{+1451}_{-117}	532^{+90}_{-439}	
J1837+0053	0.473	123^{+50}_{-89}	$-11.2^{+9.8}_{-6.4}$	$-30.9^{+1.9}_{-4.8}$	-76^{+5}_{-15}	1.4	35^{+5}_{-30}	3786^{+1173}_{-3701}	neg	
J1838+0044g	2.203	135^{+36}_{-120}	$-2.9^{+2.2}_{-1.6}$	$-6.8^{+0.3}_{-0.2}$	$-42.2^{+1.6}_{-1.1}$	1.6	$7.0^{+2.8}_{-5.4}$	709^{+691}_{-674}	34^{+145}_{-34}	
J1839-0223	1.266	153^{+25}_{-151}	$-2.6^{+2.3}_{-4.7}$	$-7.2^{+1.7}_{-0.9}$	20^{+12}_{-7}	1.0	$4.5^{+6.1}_{-4.1}$	167^{+772}_{-166}	neg	
J1841+0912	0.381	114^{+32}_{-58}	$2.3^{+0.3}_{-0.9}$	$0.12^{+0.03}_{-0.03}$	$-18.5^{+0.7}_{-0.5}$	43.0	$6.5^{+0.7}_{-2.5}$	105^{+23}_{-66}	17^{+5}_{-5}	wo.ot
J1842+0257	3.088	44^{+127}_{-36}	$3.8^{+2.3}_{-3.1}$	$-0.2^{+0.4}_{-0.3}$	$-41.8^{+3.1}_{-3.8}$	5.4	$5.4^{+2.7}_{-4.3}$	590^{+730}_{-568}	neg	
J1842+1332	0.471	164^{+12}_{-14}	-43^{+33}_{-47}	21^{+2}_{-55}	-86^{+1}_{-24}	2.4	50^{+50}_{-39}	7910^{+23330}_{-7487}	336^{+221}_{-336}	
J1843-0211	2.027	158^{+18}_{-65}	$-0.8^{+0.7}_{-1.7}$	$7.7^{+0.6}_{-0.2}$	$46.4^{+2.2}_{-2.2}$	1.6	$3.5^{+5.7}_{-2.8}$	160^{+966}_{-155}	512^{+250}_{-87}	
J1843+0119	1.267	28^{+148}_{-25}	$-0.8^{+0.7}_{-1.2}$	$5.2^{+0.2}_{-0.3}$	$2.7^{+2.7}_{-5.4}$	1.7	-	-	-	no.w
J1843-0000	0.880	34^{+13}_{-12}	$3.3^{+0.9}_{-1.1}$	$0.1^{+0.1}_{-0.1}$	$2.5^{+0.3}_{-0.2}$	27.4	$5.4^{+1.6}_{-1.8}$	171^{+115}_{-94}	298^{+12}_{-9}	
J1844+00	0.460	89^{+41}_{-77}	$12.6^{+2.3}_{-9.0}$	$22.8^{+1.8}_{-4.1}$	7^{+20}_{-13}	5.9	19^{+2}_{-14}	1056^{+182}_{-986}	1304^{+176}_{-390}	
J1846+0051	0.434	147^{+26}_{-142}	$5.8^{+6.2}_{-4.9}$	$2.6^{+0.8}_{-2.4}$	80^{+12}_{-4}	0.9	8^{+8}_{-7}	177^{+559}_{-172}	302^{+106}_{-229}	
J1847+0614g	1.662	144^{+30}_{-138}	$2.3^{+2.1}_{-1.9}$	$2.2^{+0.3}_{-0.7}$	$98.1^{+8.4}_{-3.4}$	2.0	$4.3^{+3.4}_{-3.5}$	202^{+448}_{-195}	352^{+164}_{-263}	
J1848+0604	2.218	32^{+141}_{-28}	$-1.4^{+1.2}_{-1.5}$	$1.0^{+0.2}_{-0.5}$	$55.1^{+3.1}_{-8.9}$	4.0	$2.7^{+2.6}_{-2.3}$	103^{+294}_{-101}	336^{+102}_{-225}	
J1848+0826	0.328	57^{+37}_{-51}	$-8.8^{+7.7}_{-3.6}$	$7.5^{+2.0}_{-3.6}$	52^{+10}_{-17}	1.1	18^{+5}_{-16}	676^{+411}_{-666}	244^{+145}_{-246}	
J1848+12	0.754	153^{+20}_{-30}	-11^{+8}_{-12}	$24.6^{+1.4}_{-0.7}$	$82.0^{+2.9}_{-1.2}$	4.2	23^{+19}_{-17}	2715^{+6376}_{-2506}	1385^{+258}_{-162}	
J1849+0106	1.832	151^{+22}_{-145}	$-1.6^{+1.2}_{-2.2}$	$4.5^{+0.2}_{-0.5}$	$42.8^{+1.5}_{-5.4}$	2.7	$3.0^{+3.3}_{-2.3}$	108^{+368}_{-103}	389^{+110}_{-182}	
J1849+0127	0.542	94^{+81}_{-87}	$-5.1^{+4.7}_{-0.8}$	$2.0^{+0.2}_{-0.4}$	$-32.1^{+2.5}_{-4.2}$	2.1	$10.9^{+0.2}_{-9.9}$	424^{+16}_{-421}	neg	
J1849+0340g	1.666	86^{+90}_{-82}	$1.6^{+0.3}_{-1.5}$	$6.8^{+0.2}_{-0.1}$	$97.3^{+1.1}_{-3.1}$	3.2	$9.1^{+0.1}_{-8.5}$	915^{+12}_{-910}	289^{+174}_{-166}	
J1850+1335	0.345	82^{+53}_{-51}	$11.6^{+0.5}_{-5.6}$	$0.5^{+0.9}_{-0.7}$	$-80.2^{+3.6}_{-4.2}$	2.4	$12.9^{+0.5}_{-6.1}$	381^{+27}_{-275}	neg	
J1851-0029	0.518	159^{+17}_{-153}	$-2.4^{+1.9}_{-5.6}$	$0.5^{+1.1}_{-0.9}$	$-49.3^{+8.7}_{-6.8}$	4.1	$4.4^{+8.2}_{-3.5}$	67^{+482}_{-64}	neg	
J1851-0114	0.953	17^{+157}_{-13}	$1.4^{+5.1}_{-1.1}$	$-6.6^{+0.2}_{-1.1}$	-18^{+16}_{-9}	2.8	$3.1^{+8.0}_{-2.4}$	61^{+711}_{-58}	neg	

Notes: neg: negative phase shift; ip: interpulse; wo.ot: without orthogonal mode in fitting; no.w: no W_{10}; l.un: large uncertainty; s.un: small uncertainty.

Table 5 *– continued –*

PSR	P	α_0	β_0	ϕ_0	ψ_0	χ^2_ν	ρ	$r_{\rm geo}$	$r_{\rm delay}$	Note
	(s)	(°)	(°)	(°)	(°)		(°)	(km)	(km)	
(1)	(2)	(3)	(4)	(5)	(6)	(7)	(8)	(9)	(10)	(11)
J1852-0118	0.451	27^{+11}_{-18}	90^{+0}_{-77}	66^{+69}_{-28}	-62^{+6}_{-58}	1.7	-	-	-	
J1853+0056	0.275	26^{+152}_{-23}	$5.2^{+10.6}_{-4.8}$	$6.5^{+5.1}_{-0.6}$	77^{+5}_{-35}	1.2	$8.7^{+12.7}_{-8.1}$	137^{+698}_{-136}	614^{+302}_{-83}	
J1853+0259	0.585	73^{+77}_{-64}	$-5.9^{+4.8}_{-0.8}$	$-10.4^{+0.4}_{-0.3}$	$-43.7^{+2.8}_{-1.4}$	2.1	-	-	-	no.w
J1853+0427	1.320	154^{+18}_{-51}	$-1.1^{+0.7}_{-1.5}$	$-10.0^{+0.1}_{-0.1}$	$-47.6^{+0.8}_{-1.2}$	4.8	$5.4^{+6.5}_{-3.7}$	257^{+992}_{-231}	neg	
J1854+0306	4.557	85^{+88}_{-78}	$-2.0^{+1.8}_{-0.2}$	$0.6^{+0.2}_{-0.4}$	$-83.4^{+5.1}_{-9.8}$	0.2	$3.6^{+0.1}_{-3.2}$	394^{+25}_{-388}	227^{+349}_{-227}	
J1854+0319	0.628	30^{+146}_{-25}	$8.4^{+12.0}_{-7.2}$	$-11.5^{+2.9}_{-11.0}$	88^{+42}_{-9}	1.6	12^{+14}_{-11}	621^{+2150}_{-612}	neg	
J1855+0139g	0.444	17^{+162}_{-15}	$11.5^{+68.0}_{-11.0}$	-5^{+11}_{-41}	-59^{+15}_{-134}	0.7	-	-	-	no.w
J1855+0700	0.258	93^{+2}_{-2}	$-3.3^{+0.5}_{-2.6}$	$1.8^{+0.4}_{-3.1}$	56^{+8}_{-41}	2.7	-	-	-	ip
J1856+0102	0.620	25^{+73}_{-20}	$-0.4^{+0.3}_{-0.6}$	$-0.3^{+0.1}_{-0.2}$	$34.4^{+1.3}_{-1.7}$	2.6	$3.4^{+4.7}_{-2.7}$	49^{+223}_{-47}	neg	
J1856+0243g	0.546	22^{+154}_{-18}	$4.2^{+9.5}_{-3.5}$	$-1.0^{+1.0}_{-4.0}$	58^{+20}_{-5}	1.4	$6.4^{+11.7}_{-5.4}$	147^{+1030}_{-144}	neg	
J1856+0245	0.080	16^{+50}_{-10}	15^{+66}_{-10}	19^{+31}_{-3}	-67^{+2}_{-31}	1.2	-	-	-	no.w
J1856+0912	2.170	6^{+30}_{-3}	$-0.002^{+0.001}_{-0.013}$	$-2.2^{+0.01}_{-0.01}$	$19.2^{+0.4}_{-0.5}$	16.7	$0.5^{+2.2}_{-0.2}$	3^{+104}_{-3}	369^{+30}_{-30}	
J1857+0057	0.356	94^{+65}_{-80}	$-9.5^{+7.1}_{-0.5}$	$2.7^{+0.5}_{-0.5}$	$54.2^{+2.5}_{-2.4}$	1.2	20^{+1}_{-16}	963^{+48}_{-913}	277^{+57}_{-55}	
J1858-02	1.462	75^{+96}_{-68}	$-1.2^{+1.0}_{-0.1}$	$3.3^{+0.1}_{-0.1}$	$22.1^{+1.1}_{-3.1}$	1.0	$4.0^{+0.1}_{-3.5}$	154^{+10}_{-152}	216^{+41}_{-48}	
J1858+0239	0.197	158^{+18}_{-155}	$-6.6^{+5.6}_{-14.8}$	$2.3^{+4.7}_{-2.8}$	59^{+13}_{-9}	1.8	$9.5^{+16.9}_{-8.3}$	117^{+790}_{-115}	401^{+197}_{-121}	
J1858+0241	4.693	48^{+128}_{-44}	$-3.2^{+2.8}_{-1.7}$	$1.4^{+1.2}_{-1.2}$	25^{+15}_{-15}	1.6	$4.4^{+2.0}_{-3.9}$	591^{+668}_{-586}	315^{+1187}_{-315}	
J1858+0310g	0.372	144^{+32}_{-33}	-71^{+66}_{-19}	61^{+98}_{-17}	116^{+69}_{-6}	1.0	-	-	-	no.w
J1859+00	0.559	158^{+17}_{-34}	-23^{+18}_{-41}	-16^{+3}_{-16}	-13^{+4}_{-14}	1.3	28^{+42}_{-21}	2866^{+15426}_{-2712}	neg	
J1859+0126g	0.957	107^{+68}_{-103}	$-12.0^{+11.1}_{-3.2}$	$0.5^{+2.3}_{-3.1}$	-14^{+10}_{-14}	0.7	-	-	-	no.w
J1900-0134	1.832	49^{+118}_{-37}	$2.6^{+1.1}_{-1.9}$	$3.6^{+0.4}_{-0.5}$	$-52.0^{+3.8}_{-3.5}$	2.4	$5.2^{+1.7}_{-3.8}$	331^{+253}_{-305}	neg	
J1900+0227	0.374	25^{+151}_{-21}	$4.4^{+8.2}_{-3.6}$	$2.1^{+1.3}_{-1.3}$	$41.4^{+6.4}_{-5.1}$	1.5	$7.4^{+10.7}_{-6.3}$	136^{+677}_{-133}	241^{+105}_{-106}	
J1900+0634	0.389	21^{+147}_{-16}	$0.6^{+1.4}_{-0.4}$	$-3.1^{+0.1}_{-0.2}$	-33^{+4}_{-5}	3.4	$1.9^{+3.4}_{-1.4}$	$9.3^{+64.0}_{-8.8}$	neg	
J1901+0020g	0.214	86^{+91}_{-81}	$10.5^{+2.5}_{-10.0}$	$0.6^{+5.4}_{-2.9}$	-29^{+15}_{-34}	1.1	14^{+2}_{-13}	270^{+84}_{-269}	83^{+243}_{-83}	
J1901+0124	0.318	39^{+139}_{-37}	$-4.1^{+3.8}_{-4.8}$	$7.0^{+0.3}_{-2.4}$	88^{+2}_{-21}	1.3	$6.5^{+5.7}_{-6.1}$	89^{+222}_{-88}	316^{+25}_{-159}	
J1901+0234	0.885	70^{+107}_{-67}	$12.5^{+7.5}_{-12.0}$	$-4.3^{+5.7}_{-7.7}$	38^{+39}_{-24}	0.8	14^{+7}_{-13}	1152^{+1439}_{-1150}	neg	
J1901+0320	0.636	145^{+31}_{-93}	$13.0^{+12.4}_{-11.3}$	$-20.4^{+5.2}_{-7.8}$	-19^{+20}_{-12}	1.0	19^{+19}_{-16}	1480^{+4592}_{-1458}	neg	
J1901+0413	2.662	144^{+28}_{-131}	$-3.0^{+2.3}_{-2.6}$	$6.6^{+0.5}_{-0.5}$	$-53.6^{+3.7}_{-3.8}$	1.8	$6.0^{+4.2}_{-4.6}$	642^{+1193}_{-604}	991^{+304}_{-304}	
J1901+0510	0.614	82^{+95}_{-80}	24^{+27}_{-23}	40^{+6}_{-18}	-11^{+38}_{-42}	1.4	38^{+20}_{-37}	5936^{+8016}_{-5927}	4064^{+753}_{-2312}	
J1901+0511	4.600	139^{+36}_{-132}	$-1.5^{+1.3}_{-1.0}$	$-2.5^{+0.3}_{-0.4}$	$49.9^{+5.4}_{-6.9}$	1.6	$2.6^{+1.5}_{-2.3}$	209^{+302}_{-205}	neg	
J1901+0621	0.831	20	25.5	-12.2	-0.7	0.7	32	5693	1928	l.un
J1902+0723	0.487	142^{+34}_{-82}	$3.5^{+2.6}_{-3.1}$	$7.4^{+0.4}_{-0.4}$	$14.5^{+3.7}_{-3.2}$	1.6	8^{+6}_{-7}	214^{+397}_{-211}	136^{+57}_{-59}	
J1903+0851g	1.231	96^{+80}_{-92}	$3.1^{+0.5}_{-2.9}$	$-1.5^{+0.9}_{-0.6}$	-16^{+8}_{-12}	0.5	-	-	-	no.w
J1903+2225	0.651	163^{+14}_{-160}	$-2.1^{+1.6}_{-7.0}$	$-4.1^{+5.0}_{-0.8}$	29^{+35}_{-5}	1.5	$3.2^{+8.4}_{-2.3}$	43^{+532}_{-40}	neg	
J1904+0800	0.263	98^{+78}_{-94}	$-5.4^{+5.1}_{-2.4}$	$10.7^{+1.1}_{-0.9}$	-71^{+12}_{-10}	2.4	$12.1^{+1.2}_{-11.3}$	254^{+52}_{-253}	245^{+60}_{-52}	
J1904+1011	1.856	25^{+40}_{-15}	$3.7^{+4.8}_{-2.2}$	$12.0^{+0.2}_{-0.2}$	$-51.7^{+0.7}_{-0.8}$	2.6	9^{+10}_{-5}	888^{+3097}_{-736}	314^{+150}_{-148}	
J1905+0616	0.989	133^{+37}_{-123}	$3.9^{+1.8}_{-2.9}$	$1.2^{+0.2}_{-0.6}$	$51.8^{+6.5}_{-1.6}$	9.2	$4.7^{+2.1}_{-3.6}$	145^{+160}_{-137}	237^{+36}_{-123}	
J1905+0709	0.648	58^{+51}_{-41}	$-9.6^{+6.2}_{-1.8}$	$-0.4^{+0.2}_{-0.2}$	$-17.2^{+0.9}_{-1.1}$	1.7	$16.8^{+3.5}_{-11.1}$	1209^{+548}_{-1071}	415^{+36}_{-36}	
J1906+0414	1.043	29^{+145}_{-25}	$2.5^{+3.5}_{-2.1}$	$10.9^{+0.8}_{-0.6}$	$-70.0^{+5.0}_{-6.4}$	1.1	$6.7^{+7.0}_{-5.7}$	308^{+991}_{-302}	720^{+191}_{-150}	
J1906+0641	0.267	42^{+29}_{-28}	$-7.3^{+4.7}_{-2.8}$	$-3.9^{+0.2}_{-0.4}$	$5.2^{+1.0}_{-1.9}$	30.5	$13.0^{+5.8}_{-8.4}$	299^{+329}_{-261}	45^{+13}_{-23}	
J1906+0649	1.286	154^{+24}_{-152}	-12^{+11}_{-23}	$-0.1^{+23.8}_{-3.6}$	-70^{+69}_{-8}	2.6	12^{+23}_{-11}	1270^{+8982}_{-1267}	neg	wo.ot
J1906+0746	0.144	28^{+148}_{-25}	$-6.0^{+5.6}_{-9.6}$	$0.0^{+11.9}_{-6.6}$	68^{+64}_{-28}	0.8	7^{+11}_{-6}	46^{+251}_{-45}	102^{+361}_{-102}	
J1907+0631	0.323	103^{+73}_{-99}	$18.5^{+8.0}_{-17.5}$	$5.0^{+9.9}_{-8.7}$	25^{+25}_{-34}	1.3	-	-	-	no.w
J1907+0709g	0.344	150^{+25}_{-144}	$-1.1^{+0.9}_{-1.5}$	$-4.3^{+0.3}_{-0.2}$	$20.0^{+6.1}_{-4.5}$	1.5	$5.3^{+5.1}_{-4.4}$	65^{+181}_{-63}	neg	
J1908+0128	0.0047	32	37	11.6	-77	0.7	49.4	76	21	l.un
J1908+0457	0.846	104^{+46}_{-37}	$5.2^{+0.2}_{-2.4}$	$-8.9^{+0.1}_{-0.1}$	$86.2^{+1.0}_{-0.9}$	1.4	$12.3^{+0.5}_{-6.1}$	847^{+74}_{-630}	neg	
J1908+0500	0.291	150^{+27}_{-146}	$1.7^{+2.8}_{-1.5}$	$2.2^{+0.2}_{-0.8}$	-83^{+16}_{-6}	6.4	$2.3^{+3.2}_{-2.0}$	10^{+48}_{-9}	185^{+10}_{-47}	
J1909+0616	0.755	28^{+147}_{-23}	$4.2^{+6.1}_{-3.3}$	$-5.2^{+1.4}_{-0.7}$	$-32.4^{+4.5}_{-6.8}$	1.2	$6.7^{+8.0}_{-5.6}$	227^{+854}_{-220}	254^{+217}_{-119}	
J1909+0749	0.237	82	15.6	180.1	-5.0	0.7	-	-	-	ip
J1909+1205	1.229	112^{+63}_{-107}	$-3.5^{+3.2}_{-1.0}$	$10.8^{+0.6}_{-0.4}$	$-9.9^{+2.4}_{-3.1}$	0.9	$12.5^{+0.6}_{-11.4}$	1278^{+133}_{-1267}	369^{+175}_{-141}	
J1910+0728	0.325	145^{+26}_{-134}	$-5.0^{+3.6}_{-4.8}$	$-0.9^{+0.6}_{-0.8}$	$21.4^{+3.8}_{-3.4}$	3.4	$8.3^{+6.3}_{-6.0}$	150^{+312}_{-138}	254^{+38}_{-53}	
J1912+1036	0.409	31^{+147}_{-28}	$12.0^{+24.5}_{-11.5}$	$11.6^{+12.8}_{-8.2}$	0^{+19}_{-52}	1.5	15^{+24}_{-14}	566^{+3501}_{-564}	988^{+1095}_{-702}	
J1912+2525	0.622	167^{+9}_{-161}	$-0.4^{+0.3}_{-1.8}$	$2.4^{+0.3}_{-0.2}$	$36.6^{+10.8}_{-4.8}$	4.3	$1.0^{+3.5}_{-0.7}$	4^{+79}_{-3}	289^{+39}_{-23}	
J1913+0657	1.257	28^{+143}_{-22}	$-0.4^{+0.3}_{-0.7}$	$-1.2^{+0.2}_{-0.3}$	$47.8^{+3.8}_{-11.1}$	2.8	$1.8^{+2.0}_{-1.4}$	27^{+94}_{-26}	141^{+65}_{-99}	
J1913+0832	0.134	$85.3^{+0.5}_{-1.0}$	$9.3^{+2.1}_{-1.2}$	$-161.2^{+1.4}_{-0.6}$	$-42.6^{+0.4}_{-2.7}$	1.8	-	-	-	ip
J1913+0904	0.163	162^{+16}_{-107}	$-1.3^{+1.2}_{-3.4}$	$13.2^{+1.1}_{-0.6}$	$93.7^{+15.1}_{-5.6}$	1.3	$2.9^{+6.4}_{-2.6}$	$9.1^{+85}_{-9.0}$	337^{+37}_{-20}	
J1913+1011	0.035	26^{+147}_{-24}	$-10.7^{+9.8}_{-18.0}$	$-20.0^{+8.0}_{-1.5}$	$-57.0^{+17.8}_{-3.1}$	1.0	13^{+22}_{-12}	39^{+244}_{-38}	neg	
J1913+1050	0.190	72^{+15}_{-65}	$15.6^{+12.4}_{-13.6}$	$2.3^{+2.6}_{-5.5}$	$-52.2^{+17.9}_{-11.3}$	1.2	-	-	-	ip
J1913+3732	0.851	$13.5^{+0.0}_{-5.0}$	$-0.6^{+0.2}_{-0.0}$	$2.1^{+0.1}_{-0.1}$	$9.6^{+0.1}_{-0.1}$	815.1	$1.5^{+0.0}_{-0.5}$	12^{+0}_{-7}	61^{+5}_{-5}	
J1914+0219	0.457	63^{+44}_{-30}	$6.0^{+0.9}_{-2.4}$	$4.3^{+0.1}_{-0.1}$	$-67.0^{+0.7}_{-0.9}$	8.7	$10.1^{+1.1}_{-3.9}$	309^{+73}_{-191}	28^{+13}_{-10}	
J1914+1122	0.600	35^{+129}_{-24}	$2.2^{+1.8}_{-1.4}$	$-3.8^{+0.2}_{-0.1}$	$67.8^{+1.6}_{-2.6}$	2.0	$4.7^{+3.4}_{-3.1}$	86^{+173}_{-77}	63^{+42}_{-34}	

Table 5 *– continued –*

PSR	P	α_0	β_0	ϕ_0	ψ_0	χ^2_ν	ρ	$r_{\rm geo}$	$r_{\rm delay}$	Note
	(s)	(°)	(°)	(°)	(°)		(°)	(km)	(km)	
(1)	(2)	(3)	(4)	(5)	(6)	(7)	(8)	(9)	(10)	(11)
J1915+0738	1.542	162^{+15}_{-126}	$-0.4^{+0.4}_{-1.1}$	$2.9^{+0.2}_{-0.2}$	$-10.0^{+5.6}_{-3.4}$	20.3	$0.8^{+1.8}_{-0.7}$	$6.1^{+61.8}_{-6.0}$	832^{+62}_{-56}	
J1915+1410	0.297	118^{+54}_{-108}	$1.6^{+0.5}_{-1.3}$	$11.5^{+0.4}_{-0.7}$	$21.2^{+5.9}_{-3.2}$	0.5	$12.3^{+1.8}_{-10.4}$	296^{+90}_{-289}	174^{+40}_{-50}	
J1915+1647	1.616	168^{+10}_{-38}	$0.4^{+1.0}_{-0.3}$	$2.78^{+0.02}_{-0.02}$	$-23.7^{+0.4}_{-0.4}$	17.9	$1.1^{+3.0}_{-0.9}$	$13.3^{+168.8}_{-12.9}$	neg	
J1916+0748	0.541	162^{+16}_{-6}	-85^{+80}_{-4}	39^{+10}_{-29}	$-87.8^{+1.7}_{-7.3}$	1.5	-	-	-	
J1916+1023	1.618	43^{+132}_{-36}	$7.1^{+4.7}_{-6.1}$	$-6.0^{+1.0}_{-3.9}$	$71.0^{+19.6}_{-4.3}$	1.2	$11.3^{+5.6}_{-10.0}$	1374^{+1702}_{-1354}	neg	
J1917+0834	2.129	128^{+31}_{-59}	$-0.9^{+0.5}_{-0.3}$	$-3.2^{+0.1}_{-0.1}$	$-40.5^{+0.6}_{-0.4}$	5.9	$4.4^{+1.2}_{-2.4}$	274^{+162}_{-218}	111^{+34}_{-26}	
J1917+1353	0.194	19^{+0}_{-5}	$2.2^{+0.0}_{-0.6}$	$5.9^{+0.1}_{-0.1}$	$-31.9^{+0.2}_{-0.1}$	102.5	$3.4^{+0.0}_{-0.9}$	15^{+0}_{-7}	188^{+2}_{-2}	
J1918+1444	1.181	165^{+2}_{-13}	$-0.3^{+0.1}_{-0.2}$	$0.26^{+0.01}_{-0.01}$	$-68.1^{+0.1}_{-0.1}$	211.9	$1.0^{+0.8}_{-0.1}$	8^{+19}_{-2}	15^{+9}_{-9}	
J1918+1541	0.370	98^{+34}_{-7}	-27^{+12}_{-63}	$-186.1^{+4.1}_{-2.8}$	69^{+20}_{-23}	1.5	-	-	-	ip
J1919+1745	2.081	127^{+42}_{-107}	$-3.1^{+2.3}_{-1.0}$	$4.3^{+0.2}_{-0.1}$	$38.5^{+1.1}_{-1.5}$	1.8	$6.1^{+1.5}_{-4.6}$	508^{+284}_{-478}	neg	
J1920+1040	2.215	135^{+39}_{-129}	$-6.4^{+5.4}_{-4.5}$	$-0.6^{+1.7}_{-0.8}$	$72.8^{+11.0}_{-4.6}$	2.9	$8.0^{+4.6}_{-6.9}$	948^{+1402}_{-927}	neg	
J1921+0137	0.0024	116	28	-128	-32	1.0	-	-	-	ip?
J1921+0812	0.210	152^{+26}_{-149}	$-2.4^{+2.2}_{-10.8}$	$8.7^{+3.7}_{-0.1}$	$-5.5^{+16.6}_{-20.2}$	1.3	$2.8^{+10.7}_{-2.5}$	11^{+243}_{-10}	358^{+164}_{-5}	
J1921+1419	0.618	29^{+142}_{-21}	$6.0^{+7.4}_{-4.4}$	$6.2^{+3.5}_{-0.4}$	$-44.6^{+2.0}_{-16.4}$	0.9	$8.6^{+9.2}_{-6.2}$	303^{+988}_{-279}	422^{+451}_{-65}	
J1921+1540	0.143	140^{+35}_{-134}	$4.1^{+3.3}_{-3.5}$	$5.0^{+1.1}_{-1.3}$	$90.2^{+10.9}_{-8.4}$	1.2	$8.0^{+5.4}_{-6.9}$	61^{+110}_{-60}	neg	
J1922+1733	0.236	12^{+4}_{-5}	$1.2^{+0.4}_{-0.5}$	$0.2^{+0.1}_{-0.1}$	$28.4^{+0.2}_{-0.3}$	261.0	$2.3^{+0.8}_{-1.0}$	8^{+6}_{-5}	246^{+4}_{-3}	
J1922+2018	1.172	7^{+16}_{-2}	$-0.3^{+0.1}_{-0.7}$	$-3.5^{+0.1}_{-0.1}$	$76.9^{+0.6}_{-0.5}$	21.3	$1.2^{+2.7}_{-0.3}$	11^{+104}_{-5}	238^{+35}_{-34}	
J1923+1706	0.547	8^{+55}_{-5}	$-0.2^{+0.1}_{-0.9}$	$2.2^{+0.1}_{-0.1}$	$-48.8^{+1.2}_{-0.9}$	12.3	$1.1^{+6.5}_{-0.7}$	5^{+208}_{-4}	neg	
J1923+4243	0.595	140^{+23}_{-77}	$-2.3^{+1.2}_{-1.4}$	$2.0^{+0.1}_{-0.1}$	$74.1^{+0.8}_{-1.7}$	51.8	$5.2^{+2.8}_{-2.8}$	106^{+144}_{-84}	123^{+10}_{-18}	
J1926+1434	1.324	158^{+17}_{-47}	$-1.6^{+1.2}_{-3.2}$	$18.3^{+0.3}_{-0.7}$	$66.3^{+1.6}_{-1.5}$	2.1	$7.9^{+11.7}_{-6.1}$	551^{+2835}_{-521}	643^{+95}_{-199}	wo.ot
J1926+1648	0.579	52^{+118}_{-48}	$-10.7^{+9.8}_{-4.3}$	$6.0^{+1.4}_{-3.5}$	$109.9^{+6.7}_{-14.8}$	1.1	$11.6^{+4.6}_{-10.6}$	512^{+488}_{-509}	830^{+170}_{-425}	
J1926+1857g	0.278	138^{+39}_{-135}	11^{+13}_{-10}	$3.6^{+6.8}_{-8.7}$	13^{+28}_{-36}	0.7	-	-	-	no.w
J1926+2016	0.299	28^{+147}_{-23}	$5.2^{+7.8}_{-4.3}$	$4.5^{+3.1}_{-2.1}$	$-7.7^{+9.9}_{-15.8}$	1.7	$6.8^{+8.8}_{-5.6}$	90^{+386}_{-88}	171^{+194}_{-130}	
J1927+1852	0.482	119^{+55}_{-111}	$13.3^{+3.3}_{-11.9}$	$6.7^{+1.6}_{-6.1}$	$-26.3^{+24.0}_{-5.9}$	5.1	$15.8^{+3.7}_{-14.1}$	795^{+422}_{-785}	59^{+164}_{-59}	
J1927+1856	0.298	168^{+8}_{-45}	$-3.3^{+2.3}_{-10.0}$	$15.8^{+3.1}_{-0.4}$	$-56.0^{+8.4}_{-2.0}$	2.4	$5.7^{+16.2}_{-3.9}$	65^{+886}_{-58}	393^{+191}_{-32}	
J1928+1809g	0.294	112	-15.5	-8.8	10.1	1.2	-	-	-	ip
J1930+1722	1.609	27^{+128}_{-21}	$1.7^{+2.3}_{-1.3}$	$5.7^{+0.5}_{-0.4}$	$77.0^{+3.9}_{-5.4}$	3.0	$4.5^{+5.3}_{-3.5}$	220^{+818}_{-208}	313^{+321}_{-300}	
J1931+1439	1.779	80^{+84}_{-65}	$5.8^{+0.4}_{-4.3}$	$5.6^{+0.2}_{-0.3}$	$31.5^{+2.3}_{-1.1}$	1.4	$10.1^{+0.3}_{-7.4}$	1206^{+69}_{-1119}	92^{+67}_{-92}	
J1932+1500	1.864	84^{+88}_{-78}	$1.8^{+0.2}_{-1.6}$	$4.2^{+0.1}_{-0.1}$	$63.7^{+1.5}_{-2.0}$	1.7	$5.9^{+0.1}_{-5.3}$	434^{+11}_{-429}	193^{+76}_{-70}	
J1932+2220	0.144	23^{+99}_{-18}	$-2.5^{+2.0}_{-4.7}$	$6.6^{+0.3}_{-1.1}$	$-26.1^{+6.1}_{-9.4}$	3.7	$3.3^{+6.0}_{-2.6}$	11^{+71}_{-10}	137^{+8}_{-32}	
J1934+2352	0.178	101^{+4}_{-2}	$-12.7^{+4.5}_{-5.2}$	$8.0^{+1.0}_{-1.9}$	$75.9^{+12.8}_{-13.1}$	0.8	-	-	-	
J1935+2025	0.080	87^{+1}_{-1}	$-6.2^{+0.7}_{-0.6}$	$-174.3^{+0.3}_{-0.7}$	$-40.9^{+0.7}_{-4.2}$	4.0	-	-	-	ip
J1937-00	0.240	28^{+150}_{-26}	$-3.7^{+3.3}_{-16.3}$	$7.5^{+0.8}_{-9.0}$	55^{+3}_{-51}	1.7	$5.1^{+16.3}_{-4.7}$	42^{+689}_{-41}	473^{+43}_{-449}	
J1937+2544	0.200	18^{+63}_{-15}	$1.6^{+3.3}_{-1.3}$	$14.4^{+1.0}_{-0.4}$	$81.5^{+2.5}_{-8.9}$	1.8	$5.3^{+11.0}_{-4.4}$	38^{+317}_{-37}	215^{+42}_{-17}	wo.ot
J1938+0650	1.121	21^{+153}_{-16}	$-0.5^{+0.4}_{-1.2}$	$0.7^{+0.2}_{-0.2}$	$44.0^{+7.4}_{-8.4}$	2.1	$1.5^{+2.7}_{-1.1}$	16^{+113}_{-15}	193^{+44}_{-54}	
J1938+14A	1.661	147^{+22}_{-68}	$1.0^{+0.9}_{-0.7}$	$3.5^{+0.3}_{-0.2}$	$-73.9^{+1.1}_{-2.1}$	16.3	$3.0^{+2.6}_{-1.9}$	99^{+243}_{-87}	neg	
J1938+2213	0.166	133^{+41}_{-32}	$8.1^{+2.7}_{-6.9}$	$12.4^{+0.8}_{-0.9}$	$-33.2^{+3.8}_{-6.5}$	7.6	$10.2^{+3.7}_{-8.7}$	114^{+98}_{-112}	376^{+28}_{-33}	
J1938+2659	0.883	146.5	-0.7	-6.9	-84.4	4.2	4.6	125	neg	
J1939+10	2.308	151^{+18}_{-97}	$-1.5^{+0.9}_{-1.9}$	$5.2^{+0.3}_{-0.2}$	$-7.6^{+2.6}_{-1.7}$	14.7	$3.5^{+3.7}_{-2.1}$	190^{+602}_{-160}	neg	
J1939+2449	0.645	15^{+6}_{-3}	$-1.6^{+0.3}_{-0.6}$	$1.5^{+0.1}_{-0.1}$	$-4.2^{+0.1}_{-0.1}$	15.1	$2.7^{+1.0}_{-0.5}$	31^{+29}_{-11}	neg	wo.ot
J1945+1211	4.756	147^{+21}_{-60}	$5.5^{+4.6}_{-3.3}$	$12.9^{+0.1}_{-0.9}$	$44.9^{+4.4}_{-0.4}$	9.8	$9.5^{+8.8}_{-5.9}$	2848^{+7745}_{-2433}	1684^{+156}_{-928}	
J1946+1805	0.440	158^{+17}_{-47}	-16^{+12}_{-15}	$-21.8^{+3.1}_{-12.0}$	-33^{+6}_{-25}	44.4	19^{+17}_{-14}	1019^{+2793}_{-963}	neg	
J1946+2535	0.515	152^{+23}_{-147}	$-4.1^{+3.4}_{-5.7}$	$-0.3^{+0.7}_{-2.8}$	$4.6^{+4.8}_{-19.0}$	1.9	$5.4^{+6.6}_{-4.5}$	100^{+392}_{-98}	neg	
J1950+05	0.455	64^{+111}_{-58}	$-18.8^{+17.0}_{-5.0}$	$8.8^{+3.1}_{-4.7}$	25^{+10}_{-13}	1.6	24^{+5}_{-22}	1753^{+874}_{-1733}	400^{+334}_{-400}	
J1952+3252	0.039	19^{+114}_{-16}	$-6.7^{+5.9}_{-25.9}$	$27.4^{+0.7}_{-16.5}$	7^{+11}_{-41}	2.1	9^{+30}_{-8}	22^{+384}_{-21}	259^{+7}_{-136}	
J1957+2831	0.307	28^{+150}_{-26}	14^{+28}_{-13}	$-13.5^{+9.0}_{-14.8}$	-69^{+10}_{-36}	1.0	15^{+28}_{-14}	465^{+3372}_{-464}	neg	
J1959+3620	0.406	154^{+15}_{-37}	$-16.8^{+9.6}_{-22.2}$	$-14.3^{+2.1}_{-1.6}$	$-14.7^{+3.1}_{-1.8}$	1.9	26^{+27}_{-15}	1868^{+5765}_{-1511}	neg	
J2002+1637	0.276	112^{+66}_{-109}	$14.7^{+8.0}_{-14.3}$	$4.9^{+2.0}_{-17.5}$	-16^{+85}_{-7}	1.4	17^{+8}_{-16}	532^{+587}_{-531}	260^{+117}_{-260}	
J2005+3552	0.307	27^{+71}_{-18}	$8.0^{+11.0}_{-5.4}$	$-9.1^{+0.2}_{-2.8}$	$48.5^{+8.2}_{-0.5}$	1.8	11^{+13}_{-7}	228^{+877}_{-202}	neg	
J2006+3102	0.163	147^{+26}_{-82}	$-6.9^{+5.2}_{-7.8}$	$-3.4^{+0.9}_{-2.3}$	$-62.3^{+4.8}_{-6.7}$	2.0	12^{+6}_{-11}	156^{+208}_{-155}	250^{+43}_{-38}	
J2008+2513	0.589	14^{+32}_{-7}	$-1.0^{+0.6}_{-2.0}$	$10.6^{+0.2}_{-0.4}$	$38.0^{+2.3}_{-2.5}$	52.4	$2.2^{+4.3}_{-1.1}$	18^{+147}_{-14}	907^{+20}_{-43}	
J2009+3326	1.438	152^{+24}_{-147}	$-2.7^{+2.3}_{-4.3}$	$9.9^{+0.7}_{-0.7}$	$-20.6^{+5.0}_{-5.7}$	1.0	$6.2^{+7.0}_{-5.2}$	365^{+1295}_{-356}	1461^{+279}_{-282}	wo.ot
J2013+3845	0.230	52^{+32}_{-40}	$20.1^{+3.3}_{-13.1}$	$30.6^{+2.5}_{-5.4}$	90^{+15}_{-21}	1.8	$26.7^{+2.5}_{-18.0}$	1086^{+209}_{-970}	1545^{+119}_{-259}	
J2017+0603	0.0028	139^{+31}_{-29}	-87^{+69}_{-3}	17^{+20}_{-58}	6^{+25}_{-34}	2.0	-	-	-	
J2018+2839	0.557	159^{+3}_{-3}	$-3.0^{+0.3}_{-0.4}$	$-3.8^{+0.3}_{-0.1}$	$51.9^{+2.4}_{-0.5}$	561.0	$4.1^{+0.5}_{-0.5}$	61^{+17}_{-13}	neg	
J2022+5154	0.529	140^{+10}_{-30}	$-9.1^{+1.9}_{-4.4}$	$-1.7^{+0.1}_{-0.5}$	$20.6^{+0.6}_{-2.4}$	11.9	$10.8^{+5.0}_{-2.2}$	407^{+461}_{-152}	226^{+12}_{-59}	
J2027+4557	1.099	102^{+18}_{-20}	$1.1^{+0.1}_{-0.1}$	$8.9^{+0.1}_{-0.1}$	$66.7^{+0.3}_{-0.2}$	226.8	$10.0^{+0.2}_{-1.2}$	722^{+36}_{-159}	187^{+10}_{-10}	
J2030+2228	0.630	143^{+14}_{-13}	$0.6^{+0.2}_{-0.2}$	$-5.0^{+0.1}_{-0.1}$	$12.1^{+0.1}_{-0.1}$	14.1	$4.1^{+1.1}_{-1.5}$	71^{+44}_{-41}	neg	
J2032+4127	0.143	54	40.5	17.7	32.4	1.1	-	-	-	ip, ot?
J2036+2835	1.358	57^{+89}_{-35}	$1.8^{+0.4}_{-1.0}$	$0.9^{+0.1}_{-0.1}$	$-43.8^{+0.8}_{-1.6}$	11.9	$3.8^{+0.7}_{-2.1}$	131^{+53}_{-105}	221^{+22}_{-13}	

Table 5 *– continued –*

PSR	P	α_0	β_0	ϕ_0	ψ_0	χ^2_ν	ρ	$r_{\rm geo}$	$r_{\rm delay}$	Note
	(s)	(°)	(°)	(°)	(°)		(°)	(km)	(km)	
(1)	(2)	(3)	(4)	(5)	(6)	(7)	(8)	(9)	(10)	(11)
J2042+0246	0.0045	166^{+11}_{-77}	$-2.6^{+2.2}_{-20.4}$	$6.5^{+2.3}_{-5.1}$	39^{+10}_{-26}	1.5	-	-	-	
J2043+2740	0.096	121^{+50}_{-88}	$8.3^{+3.4}_{-7.0}$	$13.1^{+0.7}_{-2.8}$	$-14.5^{+17.1}_{-7.9}$	2.3	$10.9^{+3.6}_{-9.1}$	76^{+59}_{-74}	207^{+14}_{-55}	
J2044+4614	1.392	68^{+25}_{-30}	$2.5^{+0.4}_{-1.0}$	$14.4^{+0.2}_{-0.1}$	$30.1^{+1.7}_{-1.8}$	9.0	$16.8^{+1.1}_{-5.6}$	2585^{+364}_{-1434}	1662^{+72}_{-69}	wo.ot
J2047+5029	0.445	143^{+32}_{-134}	$-1.5^{+1.2}_{-1.2}$	$-1.4^{+0.3}_{-0.4}$	$-28.6^{+3.4}_{-4.3}$	3.2	-	-	-	
J2051+4434g	1.303	160^{+13}_{-27}	$-9.1^{+5.6}_{-12.5}$	$-26.5^{+0.5}_{-0.4}$	$38.6^{+0.7}_{-0.7}$	3.1	20^{+23}_{-13}	3481^{+12445}_{-3012}	neg	
J2105+07	3.746	149^{+22}_{-63}	$1.6^{+1.5}_{-1.0}$	$-3.3^{+0.2}_{-0.2}$	$-58.7^{+3.6}_{-2.6}$	7.4	$3.9^{+3.8}_{-2.7}$	375^{+1105}_{-340}	313^{+210}_{-243}	
J2113+4644	1.014	179.5	0.053	-1.9	-84.0	73014	0.3	0.6	461	s.un
J2122+2426	0.541	47^{+103}_{-35}	$-13.3^{+9.5}_{-5.3}$	$-1.0^{+2.1}_{-0.4}$	$35.3^{+6.6}_{-1.4}$	1.7	15^{+7}_{-11}	847^{+892}_{-778}	neg	
J2129+1210A	0.110	123^{+47}_{-54}	$-1.8^{+1.5}_{-0.6}$	$0.6^{+0.1}_{-0.1}$	$45.7^{+2.2}_{-1.4}$	11.8	$9.4^{+1.7}_{-7.5}$	65^{+26}_{-62}	72^{+3}_{-3}	
J2129+4119	1.687	104^{+30}_{-27}	$-3.5^{+1.0}_{-0.2}$	$-3.8^{+0.1}_{-0.1}$	$-35.7^{+0.6}_{-0.4}$	3.6	$7.7^{+0.2}_{-1.9}$	654^{+26}_{-287}	27^{+30}_{-27}	
J2138+4911	0.696	25^{+147}_{-19}	$4.5^{+7.5}_{-3.3}$	$2.8^{+0.5}_{-1.3}$	$-46.2^{+7.3}_{-2.5}$	3.0	$5.2^{+8.1}_{-3.8}$	123^{+681}_{-114}	435^{+71}_{-194}	
J2208+4056	0.636	120^{+46}_{-11}	$-12.8^{+9.3}_{-1.5}$	$0.8^{+0.3}_{-0.3}$	$36.2^{+1.1}_{-1.1}$	1.5	-	-	-	ip?
J2340+08	0.303	161^{+15}_{-149}	$4.5^{+13.1}_{-3.7}$	$-0.3^{+3.0}_{-3.1}$	-46^{+14}_{-12}	0.8	$7.5^{+19.4}_{-5.9}$	112^{+1337}_{-107}	neg	

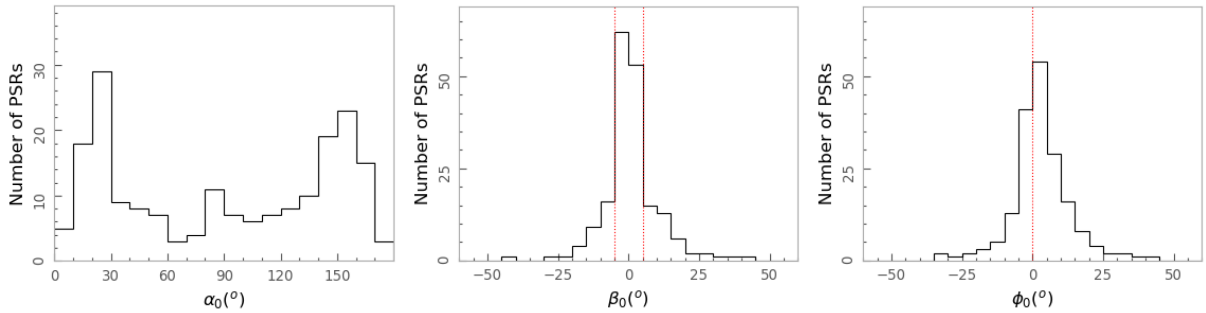

Fig. 19 Histograms of the inclination angles α_0, the impact angles β_0 and the phases of PA curves with the steepest gradients ϕ_0 for the 190 pulsars.

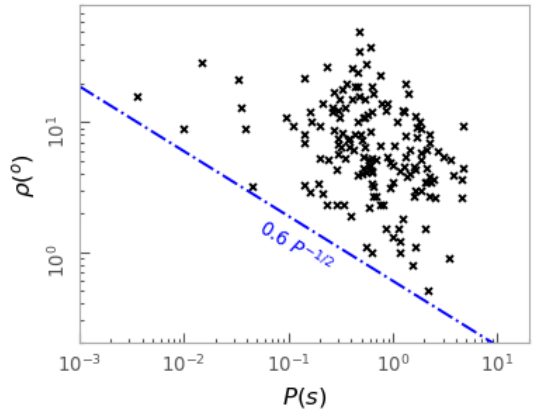

Fig. 20 The beam radius ρ in Table 5 against pulsar period. The lower boundary is indicated by a power-law $0.6P^{-1/2}$.

sar period is shown in Figure 20. It is apparent that the beam radii vary a lot even for pulsars with similar periods, as caused by the emission originated from different heights of pulsar magnetosphere. However, there is a clear low boundary for the beam radii versus period, which can be described by a power-law of $0.6P^{-1/2}$.

Pulsar radio emission is generated at a finite height above the polar cap. By assuming dipole magnetosphere and a circular emission beam, Kijak & Gil (1997) found that

$$r_{\rm geo} \simeq R_\star P(\rho/1.24^\circ)^2 s^{-2}, \quad (3)$$

here $R_\star$ is the neutron star radius. The parameter s describes the relative location of the footpoint of a magnetic field line. It is within the range of 0 to 1, with $s = 0$ for the magnetic axis and $s = 1$ for the polar cap boundary. Simply assuming that the profile edges at 10% the peak intensity originate from the beam boundary, $r_{\rm geo}$ can be estimated, as listed in column (9) of Table 5. 29 ones of them are not determined due to the lack of measurable W_{10}.

As caused by the rotation induced aberration, a pulse profile is shifted towards an early rotation phase, while the PA curve is shifted laterlly (e.g. Blaskiewicz et al. 1991; Wang et al. 2012). The phase offset between a pulse profile and its PA curve reads, $\Delta\phi = \phi_0 - \phi_{\rm prof}$. Here, $\phi_{\rm prof}$ represents the central phase of the profile. We take the midpoint of the longitudes defining W_{10} as the profile center. The emission height, $r_{\rm delay}$, is then estimated as being,

$$r_{\rm delay} = \Delta\phi R_{LC}/4, \quad (4)$$

here, $R_{LC} = cP/2\pi$ is the light-cylinder radius. $r_{\rm delay}$ for these pulsars are listed in column (10) of Table 5. The abberation effect cannot be figured out for 84 pulsars, with

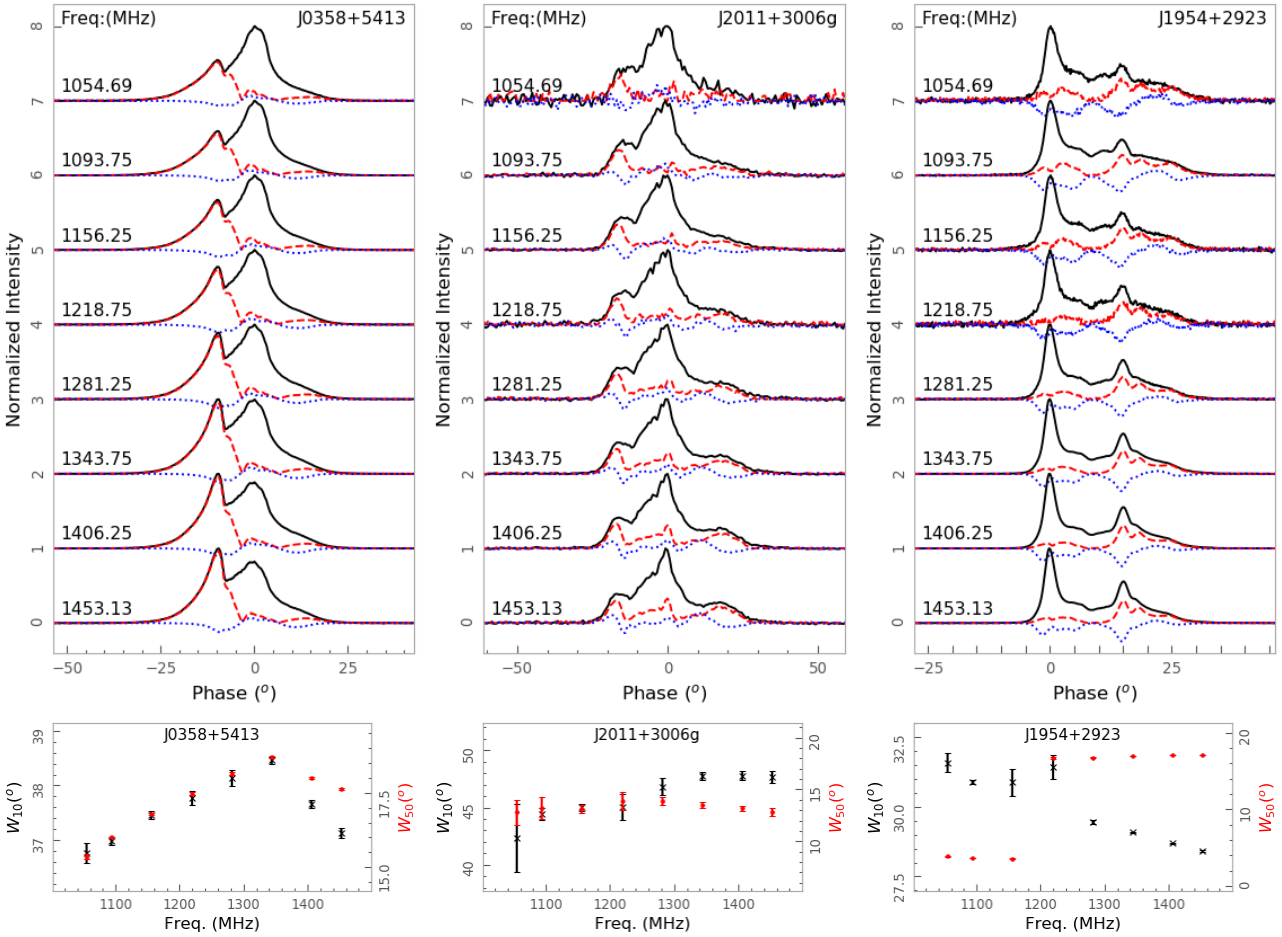

Fig. 21 The frequency evolution of polarization profiles (*upper panels*) for PSRs J0358+5413, J2011+3006g and J1954+2923, and the variations of pulse width W_{10} and W_{50} (*lower panels*). The evolution and variation are caused by the different spectral indexes for different profile components.

55 ones having $\Delta\phi < 0$ and 29 ones lacking midpoint of pulse profiles.

108 pulsars have measurements for both $r_{\rm geo}$ and $r_{\rm delay}$. They are consistent within the uncertainties for 75 ones. $r_{\rm geo}$ is smaller than $r_{\rm delay}$ for 26 pulsars. It is reasonable, since $r_{\rm geo}$ represents only the lower limit of the emission height, which is calculated with s=1 in Equation 3. If the profile edges originate from the inner magnetic field lines, i.e., $s < 1$, the so estimated $r_{\rm geo}$ will be larger. While $r_{\rm geo}$ is larger than $r_{\rm delay}$ for 6 pulsars, J1841+0912, J1901+0621, J1908+01,J1914+0219, J2027+4557 and J2129+4119. It results from the small phase offset $\Delta\phi$ in Equation 4. These small phase offsets together with those negative ones might be caused by the asymmetry of emission regions around the meridional plane. Moreover, if propagation effects dominate, the phase offsets will also be negative (Wang et al. 2010).

4.3 Frequency evolution of pulse profiles

Pulse profiles can evolve with frequency by several reasons. It can be caused by the geometric change of emission region. The radius-to-frequency mapping (Ruderman & Sutherland 1975; Cordes 1978) tells that pulsar emission of a lower frequency is generated from a higher altitude in pulsar magnetosphere with a beam of broader opening angle. Therefore pulse profiles should evolve with frequency, and the pulse width decreases with frequency as described by a power-law relation, $W = a\nu^k + W_0$ (Thorsett 1991). Simulations show that the index k in this radius-frequency-mapping depends on the density and energy distributions of relativistic particles within pulsar magnetosphere (Wang et al. 2013). In many pulsars, however, one can see that profiles may evolve together with the emerge of new components (e.g. Noutsos et al. 2015).

For some bright pulsars observed by the FAST, we examine the frequency evolution of polarization profiles. Profiles of most pulsars do not show clear evolution in such a small frequency range of 1.0 – 1.5 GHz of our

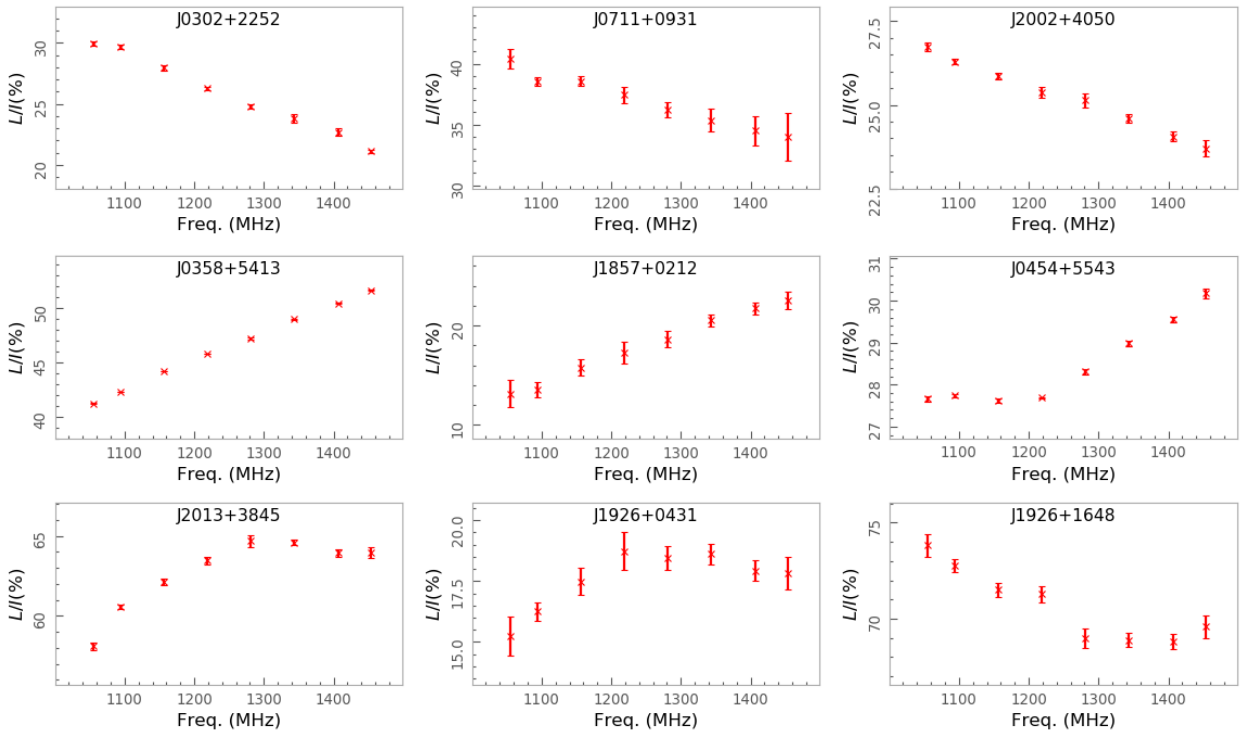

Fig. 22 Frequency dependencies of the fractional linear polarization, L/I.

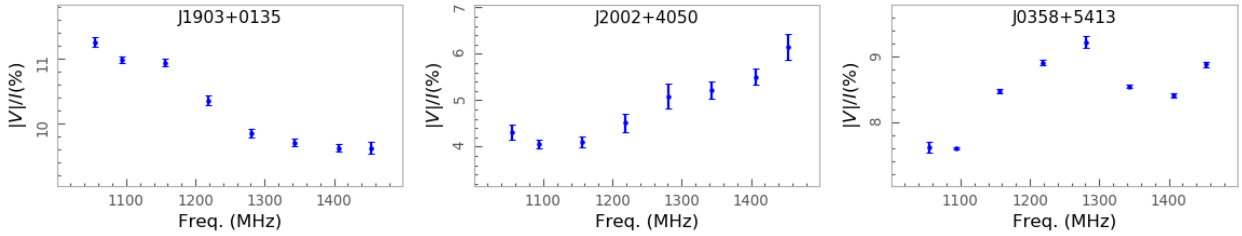

Fig. 23 Frequency dependencies of the fractional circular polarization, $|V|/I$.

FAST observations. However, we do see the evolution of a few pulsars, such as PSRs J0358+5413, J2011+3006g and J1954+2923 in Figure 21. The evolution is caused by the enhancement of leading component of PSR J0358+5413 and trailing component of J2011+3006g towards higher frequency, while the tail of PSR J1954+2923 is diminishing at higher frequency. These evolution can lead to the variation of pulse width W_{10} and/or W_{50} with frequency. Therefore, the different spectral indexes of different profile components should be investigated to understand the frequency evolution of pulse profiles.

We have also examined the frequency evolution of linear polarization and circular polarization for the pulse profile we observed. Again, for most pulsars within the observation frequency range of 1.0-1.5 GHz, significant evolution is not found for almost all pulsars. However, we do see the evolution of linear polarization percentage of several pulsars (see Figure 22). For example, The significant decreases of linear polarization percentage have been observed for PSRs J0302+2252, J0711+0931 and J2002+4050, while the percentage of linear polarization increase with frequency for PSRs J0358+5413 and J1857+0212. More complicated cases are also found for PSRs J0454+5542, J2013+3845, J1926+0431 and J1926+1648. By jointly considering the curvature emission mechanism and propagation effects within pulsar magnetosphere, the fractional linear polarization should decreases with the increase of observing frequency (Wang et al. 2015). Because emission at a higher frequency is usually generated from a lower altitude of pulsar magnetosphere, where the pulsar rotation induced the separation of the two orthogonal modes, the O-mode and X-mode, is less significant and depolarization is serious. When the two orthogonal modes are almost separated above certain heights of pulsar magnetosphere, the fractional linear polarization remains almost unchanged with frequency. When the emis-

sion is generated from the lower magnetosphere, O-mode refraction becomes serious, which reduces the depolarization for the emission at higher frequencies (Wang et al. 2015). Hence, the fractional linear polarization will increase with frequency.

We noticed that circular polarization of a small number of pulsar profiles evolve with frequency, as shown in Figure 23. The circular polarization can increase, or decrease or vary irregularly with frequency. The physical processes for such complicated behaviors are unclear.

5 CONCLUSIONS

We report in this paper the database for polarization profiles of 682 pulsars observed by FAST with unprecedent sensitivity. Polarization profiles for about 460 pulsars are obtained for the first time. The profiles exhibit diverse features. About 194 pulsars have S-shaped PA curves and 171 pulsars exhibit orthogonal modes. The profiles can be highly linearly polarized for its leading and/or trailing or the whole part, and a few of them have high circular polarization. 28 pulsars are probably "conal double", whose sense of circular polarization interplays with their PA variations. Some 27 pulsars show interpulse emission, and 21 pulsars have extremely wide profiles. Profiles of about 22 pulsars are seriously affected by interstellar scattering.

At 1250 MHz, the typical width of pulsar profiles is about 17.4° for W_{10}. In general, profile widths increase with the decrease of pulsar period. Young pulsars with a large Pdot and Edot tend to have a higher fraction of linear polarization.

For 190 pulsars with either S-shaped PA curves or the ones superposed with orthogonal modes, geometry parameters are investigated through RVM fitting. The inclination angle, α_0, has a value in a wide range from about 0° to 180°. Pulsars are most likely to be detected within an impact angle of $|\beta_0| < 5^\circ$ by sight lines. The emission heights estimated from these phase lags are generally larger than or consistent with the geometric ones.

DATA AVAILABILITY

All the polarized pulse profiles presented in this paper are available on the webpage http://zmtt.bao.ac.cn/psr-fast/.

Acknowledgements FAST is a Chinese national mega-science facility built and operated by the National Astronomical Observatories, Chinese Academy of Sciences. J. L. Han is supported by the National Natural Science Foundation of China (No. 11988101 and 11833009). P. F. Wang is supported by the National Key R&D Program of China (No. 2021YFA1600401 and 2021YFA1600400), National Natural Science Foundation of China (No. 11873058, 12133004) and the National SKA program of China (No. 2020SKA0120200). J. Xu is supported by the National Natural Science Foundation of China (No. U2031115).

References

Arons, J., & Barnard, J. J. 1986, ApJ, 302, 120
Barnard, J. J., & Arons, J. 1986, ApJ, 302, 138
Beskin, V. S., & Philippov, A. A. 2012, MNRAS, 425, 814
Bhat, N. D. R., Camilo, F., Cordes, J. M., et al. 2002, Journal of Astrophysics and Astronomy, 23, 53
Biggs, J. D. 1990, MNRAS, 245, 514
Blaskiewicz, M., Cordes, J. M., & Wasserman, I. 1991, ApJ, 370, 643
Camilo, F., Kerr, M., Ray, P. S., et al. 2012, ApJ, 746, 39
Cheng, A. F., & Ruderman, M. A. 1979, ApJ, 229, 348
Cordes, J. M. 1978, ApJ, 222, 1006
Crawford, F., Manchester, R. N., & Kaspi, V. M. 2001, AJ, 122, 2001
Dai, S., Hobbs, G., Manchester, R. N., et al. 2015, MNRAS, 449, 3223
Everett, J. E., & Weisberg, J. M. 2001, ApJ, 553, 341
Gangadhara, R. T. 2010, ApJ, 710, 29
Gould, D. M., & Lyne, A. G. 1998, MNRAS, 301, 235
Han, J. L., Demorest, P. B., van Straten, W., & Lyne, A. G. 2009, ApJS, 181, 557
Han, J. L., Manchester, R. N., van Straten, W., & Demorest, P. 2018, ApJS, 234, 11
Han, J. L., Manchester, R. N., Xu, R. X., & Qiao, G. J. 1998, MNRAS, 300, 373
Han, J. L., Wang, C., Wang, P. F., et al. 2021, RAA, 21, 107
Hankins, T. H., & Rankin, J. M. 2010, AJ, 139, 168
Hotan, A. W., van Straten, W., & Manchester, R. N. 2004, PASA, 21, 302
Jiang, P., Tang, N.-Y., Hou, L.-G., et al. 2020, RAA, 20, 064
Johnston, S., Hobbs, G., Vigeland, S., et al. 2005, MNRAS, 364, 1397
Johnston, S., & Karastergiou, A. 2019, MNRAS, 485, 640
Johnston, S., Karastergiou, A., Mitra, D., & Gupta, Y. 2008, MNRAS, 388, 261
Johnston, S., & Kerr, M. 2018, MNRAS, 474, 4629
Johnston, S., & Kramer, M. 2019, MNRAS, 490, 4565
Karastergiou, A., Johnston, S., & Manchester, R. N. 2005, MNRAS, 359, 481
Kijak, J., & Gil, J. 1997, MNRAS, 288, 631
Kramer, M., Xilouris, K. M., Lorimer, D. R., et al. 1998, ApJ, 501, 270
Li, X. H., & Han, J. L. 2003, A&A, 410, 253
Lommen, A. N., Zepka, A., Backer, D. C., et al. 2000, ApJ, 545, 1007

Lyne, A. G., & Manchester, R. N. 1988, MNRAS, 234, 477
Lyne, A. G., & Smith, F. G. 1968, Nature, 218, 124
Lyubarskii, Y. E., & Petrova, S. A. 1998, A&A, 333, 181
Maciesiak, K., Gil, J., & Melikidze, G. 2012, MNRAS, 424, 1762
Manchester, R. N. 1971, ApJS, 23, 283
Manchester, R. N., & Han, J. L. 2004, ApJ, 609, 354
Manchester, R. N., Han, J. L., & Qiao, G. J. 1998, MNRAS, 295, 280
Manchester, R. N., Hobbs, G. B., Teoh, A., & Hobbs, M. 2005, AJ, 129, 1993
McCulloch, P. M., Hamilton, P. A., Manchester, R. N., & Ables, J. G. 1978, MNRAS, 183, 645
McKinnon, M. M., & Stinebring, D. R. 2000, ApJ, 529, 435
Melrose, D. B., & Stoneham, R. J. 1977, Proceedings of the Astronomical Society of Australia, 3, 120
Mitra, D., Basu, R., Maciesiak, K., et al. 2016, ApJ, 833, 28
Mitra, D., & Rankin, J. M. 2011, ApJ, 727, 92
Nice, D. J., Splaver, E. M., & Stairs, I. H. 2001, ApJ, 549, 516
Noutsos, A., Sobey, C., Kondratiev, V. I., & et al. 2015, A&A, 576, A62
Ord, S. M., van Straten, W., Hotan, A. W., & Bailes, M. 2004, MNRAS, 352, 804
Posselt, B., Karastergiou, A., Johnston, S., et al. 2023, MNRAS, 520, 4582
Radhakrishnan, V., & Cooke, D. J. 1969, Astrophys. Lett., 3, 225
Rankin, J. M. 1983, ApJ, 274, 333
Rankin, J. M. 1990, ApJ, 352, 247
Rankin, J. M., & Benson, J. M. 1981, AJ, 86, 418
Rankin, J. M., & Ramachandran, R. 2003, ApJ, 590, 411
Rankin, J. M., Stinebring, D. R., & Weisberg, J. M. 1989, ApJ, 346, 869
Ruderman, M. A., & Sutherland, P. G. 1975, ApJ, 196, 51
Segelstein, D. J., Rawley, L. A., Stinebring, D. R., Fruchter, A. S., & Taylor, J. H. 1986, Nature, 322, 714
Serylak, M., Johnston, S., Kramer, M., et al. 2021, MNRAS, 505, 4483
Sobey, C., Johnston, S., Dai, S., et al. 2021, MNRAS, 504, 228
Sotomayor-Beltran, C., Sobey, C., Hessels, J. W. T., et al. 2013, A&A, 552, A58
Stinebring, D. R., Cordes, J. M., Rankin, J. M., Weisberg, J. M., & Boriakoff, V. 1984a, ApJS, 55, 247
Stinebring, D. R., Cordes, J. M., Weisberg, J. M., Rankin, J. M., & Boriakoff, V. 1984b, ApJS, 55, 279
Thorsett, S. E. 1991, ApJ, 377, 263
Thorsett, S. E., & Stinebring, D. R. 1990, ApJ, 361, 644
van Straten, W., & Bailes, M. 2011, PASA, 28, 1
van Straten, W., Manchester, R. N., Johnston, S., & Reynolds, J. E. 2010, PASA, 27, 104
von Hoensbroech, A., Kijak, J., & Krawczyk, A. 1998a, A&A, 334, 571
von Hoensbroech, A., Lesch, H., & Kunzl, T. 1998b, A&A, 336, 209
von Hoensbroech, A., & Xilouris, K. M. 1997, A&A, 324, 981
Wang, C., & Lai, D. 2007, MNRAS, 377, 1095
Wang, C., Lai, D., & Han, J. 2010, MNRAS, 403, 569
Wang, P. F., & Han, J. L. 2016, MNRAS, 462, 4416
Wang, P. F., Han, J. L., & Wang, C. 2013, ApJ, 768, 114
Wang, P. F., Wang, C., & Han, J. L. 2012, MNRAS, 423, 2464
Wang, P. F., Wang, C., & Han, J. L. 2014, MNRAS, 441, 1943
Wang, P. F., Wang, C., & Han, J. L. 2015, MNRAS, 448, 771
Weisberg, J. M., Cordes, J. M., Kuan, B., et al. 2004, ApJS, 150, 317
Weisberg, J. M., Cordes, J. M., Lundgren, S. C., et al. 1999, ApJS, 121, 171
Weltevrede, P., & Johnston, S. 2008, MNRAS, 391, 1210
Wu, X., Manchester, R. N., Lyne, A. G., & Qiao, G. 1993, MNRAS, 261, 630
Xilouris, K. M., Kramer, M., Jessner, A., et al. 1998, ApJ, 501, 286
Xilouris, K. M., Kramer, M., Jessner, A., Wielebinski, R., & Timofeev, M. 1996, A&A, 309, 481
Xu, J., Han, J. L., Wang, P. F., & Yan, Y. 2022, Science China Physics, Mechanics, and Astronomy, 65, 129704
Xu, R. X., Liu, J. F., Han, J. L., & Qiao, G. J. 2000, ApJ, 535, 354
Xu, R. X., Qiao, G. J., & Han, J. L. 1997, A&A, 323, 395
Yan, W. M., Manchester, R. N., van Straten, W., et al. 2011, MNRAS, 414, 2087
You, X.-P., & Han, J.-l. 2006, ChJAA (Chin. J. Astron. Astrophys.), 6, 237
Zepka, A., Cordes, J. M., Wasserman, I., & Lundgren, S. C. 1996, ApJ, 456, 305

Appendix A: PULSAR PROFILES

We have obtained the polarization profiles of 682 pulsars. Instead of the example pulsars in the main text, here we present all profiles. They are classified into 9 categories as in Section 3. Figure A.1 is for 96 pulsars with S-shaped PA curves, Figure A.2 for 136 pulsars with orthogonal modes, Figure A.3 for 45 pulsars with highly linear polarization, Figure A.4 for 9 pulsars with highly circular polarization, Figure A.5 for 28 conal double pulsars, Figure A.6 for 27 pulsars with inter pulses, Figure A.7 for 21 pulsars with

very wide profiles, Figure A.8 for 22 pulsars with obvious scattering tails, and Figure A.9 for the other 298 pulsars.

Appendix B: THE RVM SOLUTIONS

The RVM solutions of the fittings are presented for all the 190 pulsars. They are arranged in pulsar name, whose corresponding geometry parameters are listed in Table 5.

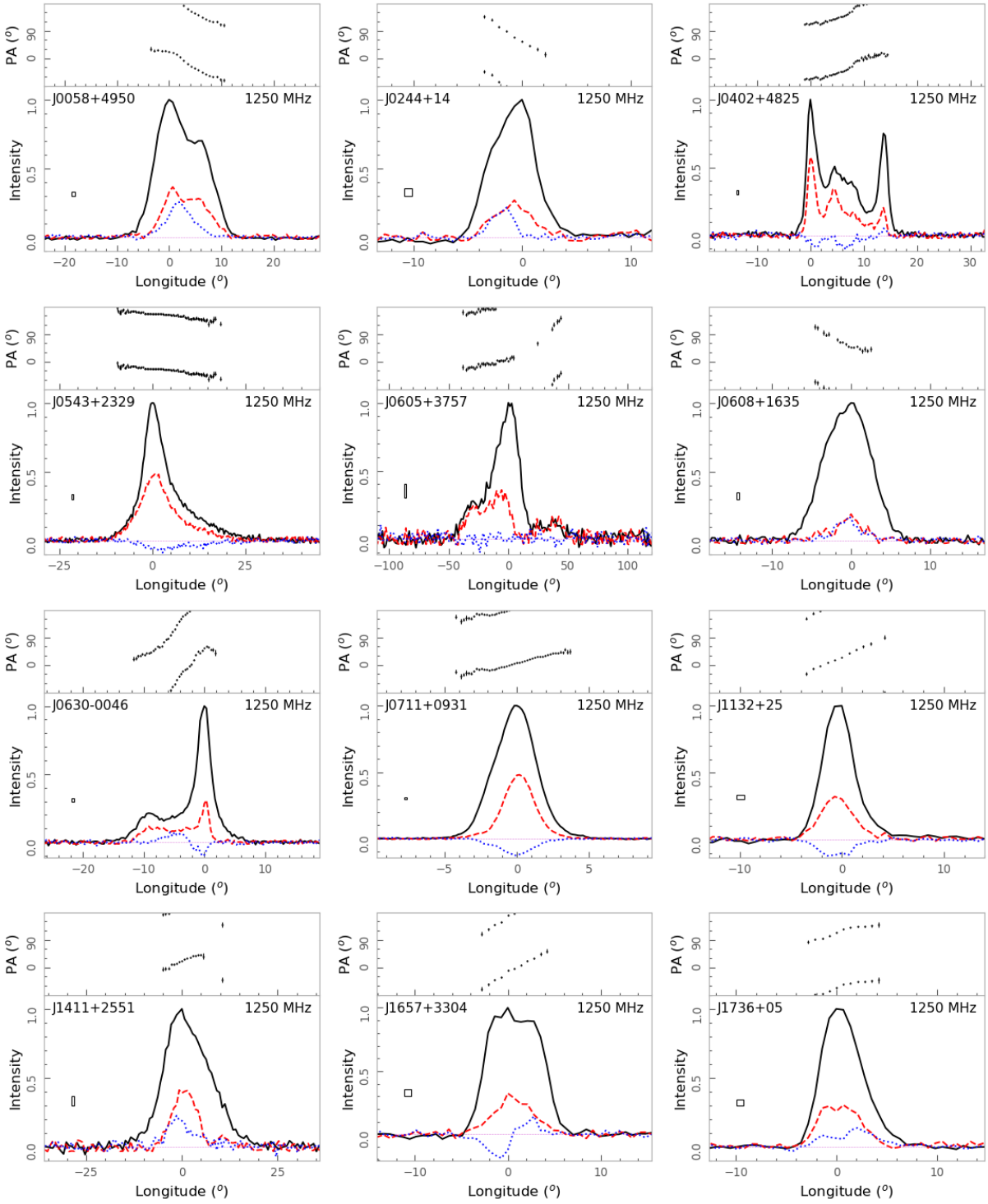

Fig. A.1 Polarization profiles with S-shaped PA curves for 96 pulsars here and 99 pulsars in other figures, including 46 pulsars with othogonal modes in Figure A.2, 14 pulsars with high linear polarization in Figure A.3, one pulsar with high circular polarization in Figure A.4, 22 conal double pulsars in Figure A.5, 13 pulsars with an interpulse in Figure A.6, and 3 pulsars with wide pulses in Figure A.7. For each pulsar, the total intensity, linear and circular polarization are represented by solid, dashed and doted lines in the bottom sub-panel. The left-hand circular polarization is defined to be positive. The bin size and 3σ are marked inside the sub-panel, here σ is the standard deviation of off-pulse bins. In the top panel, dots with error-bar are measurements of polarization position angles for linear polarization intensity exceeding 3σ line. – *to be continued*–

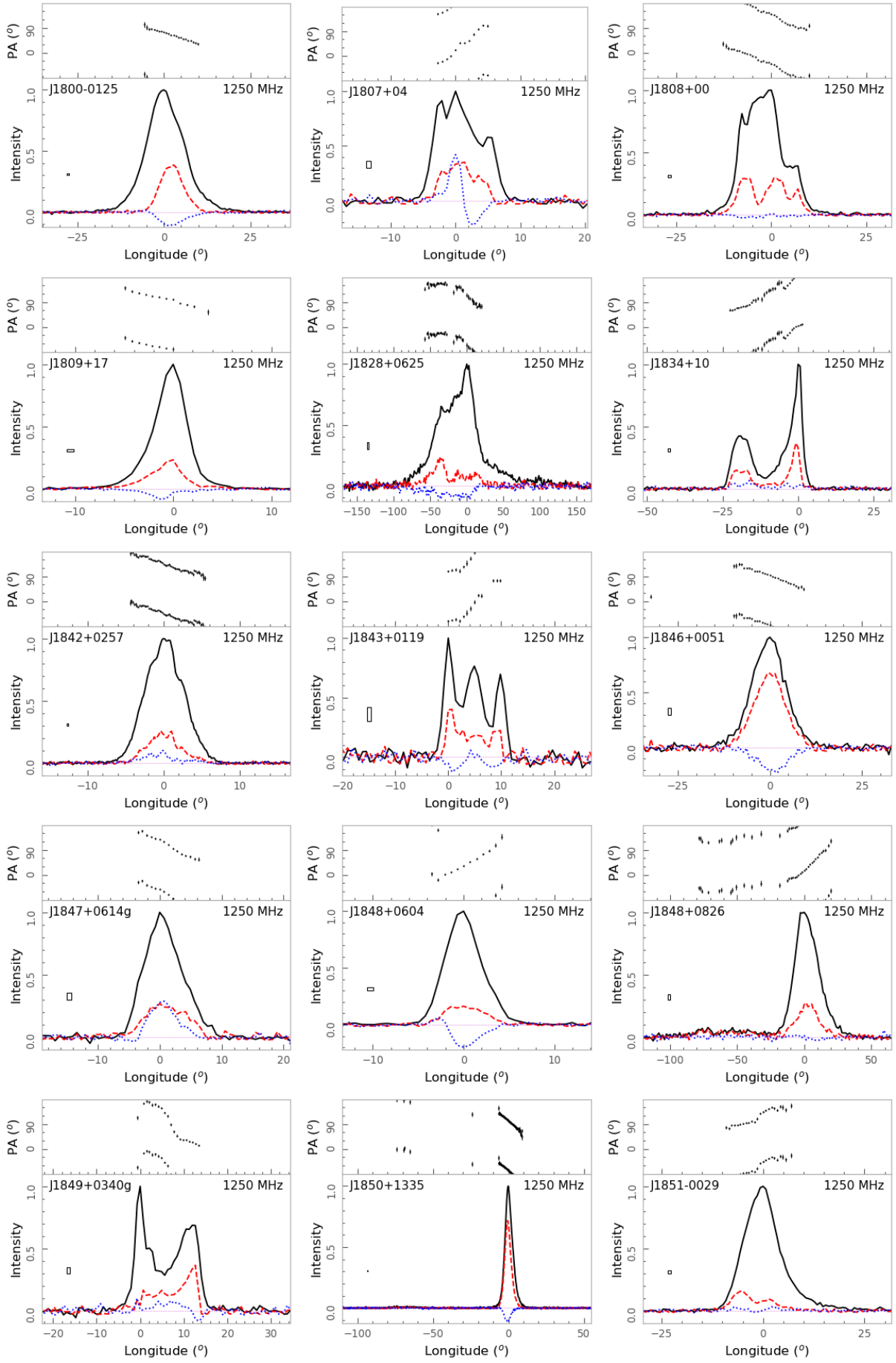

Fig. A.1 *–continued–*

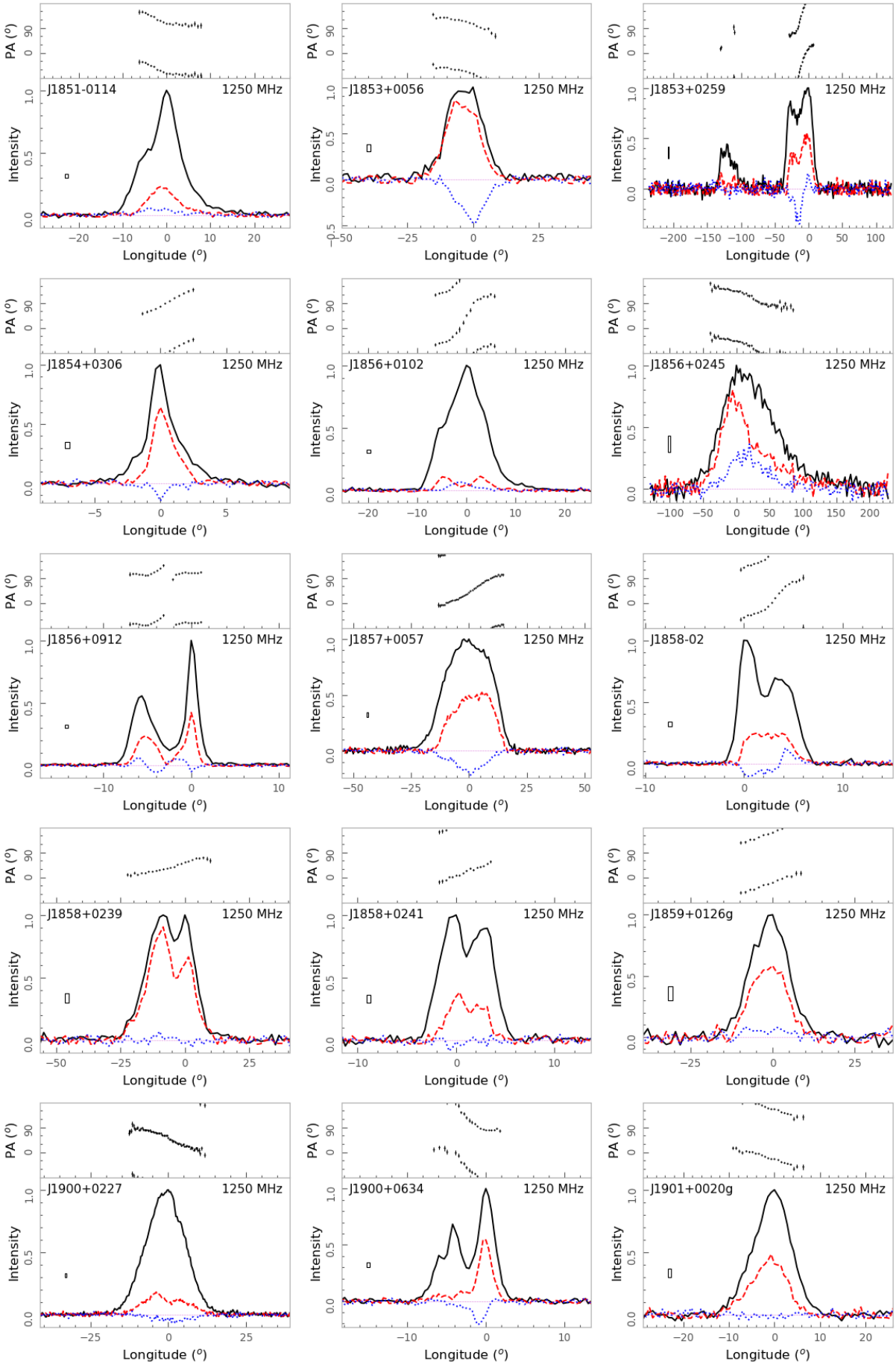

Fig. A.1 *–continued–*

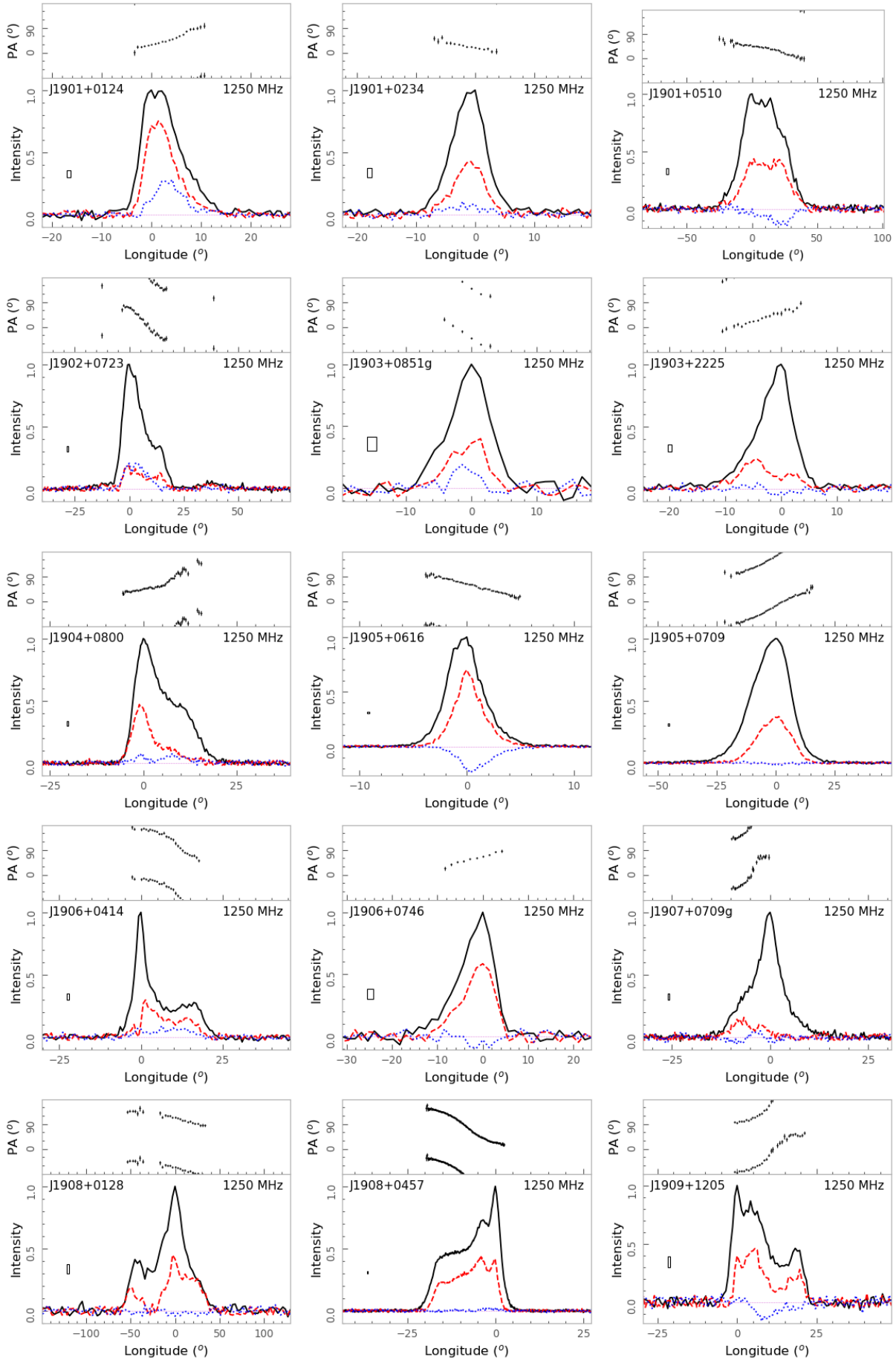

Fig. A.1 *–continued–*

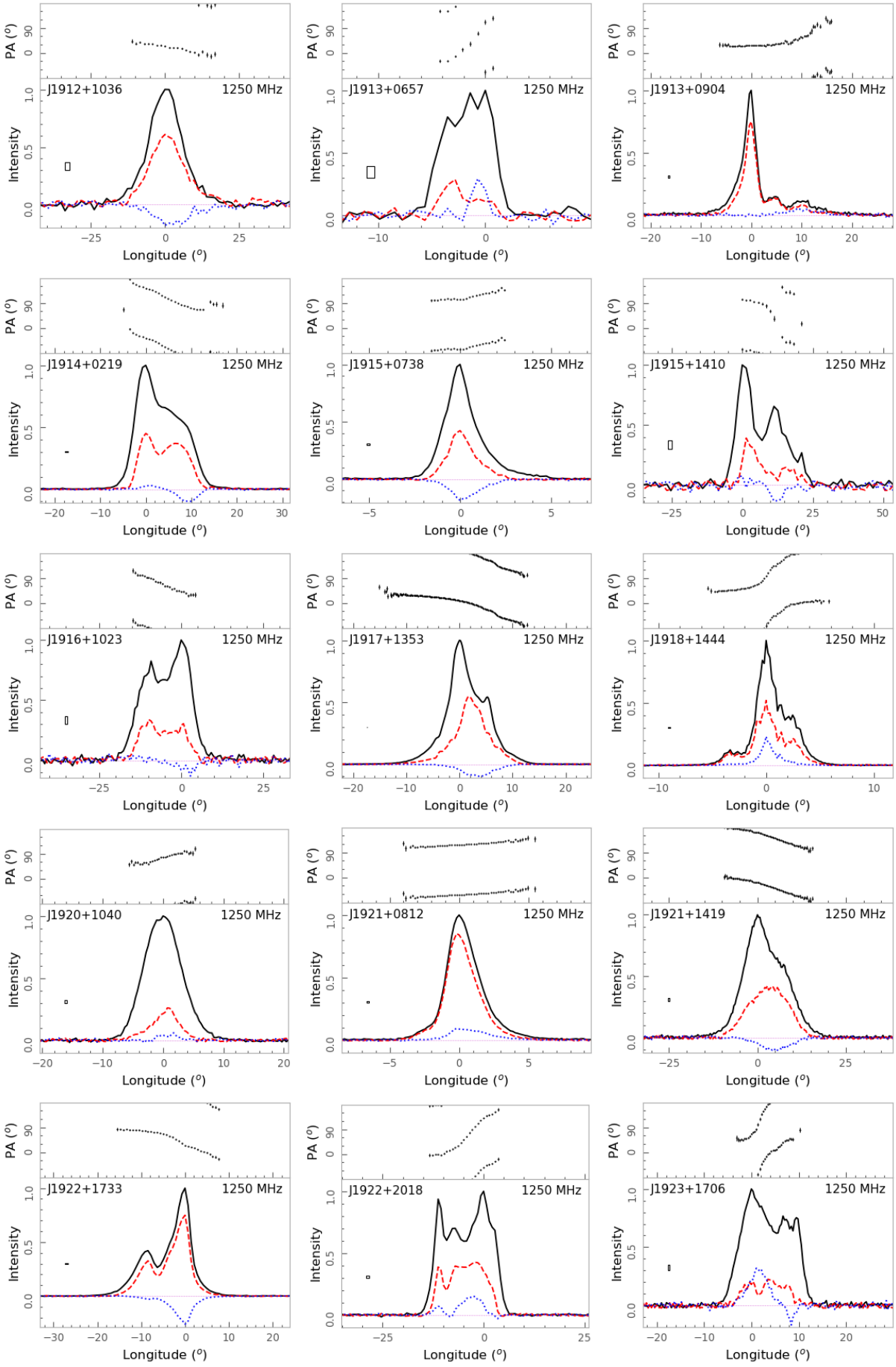

Fig. A.1 *–continued–*

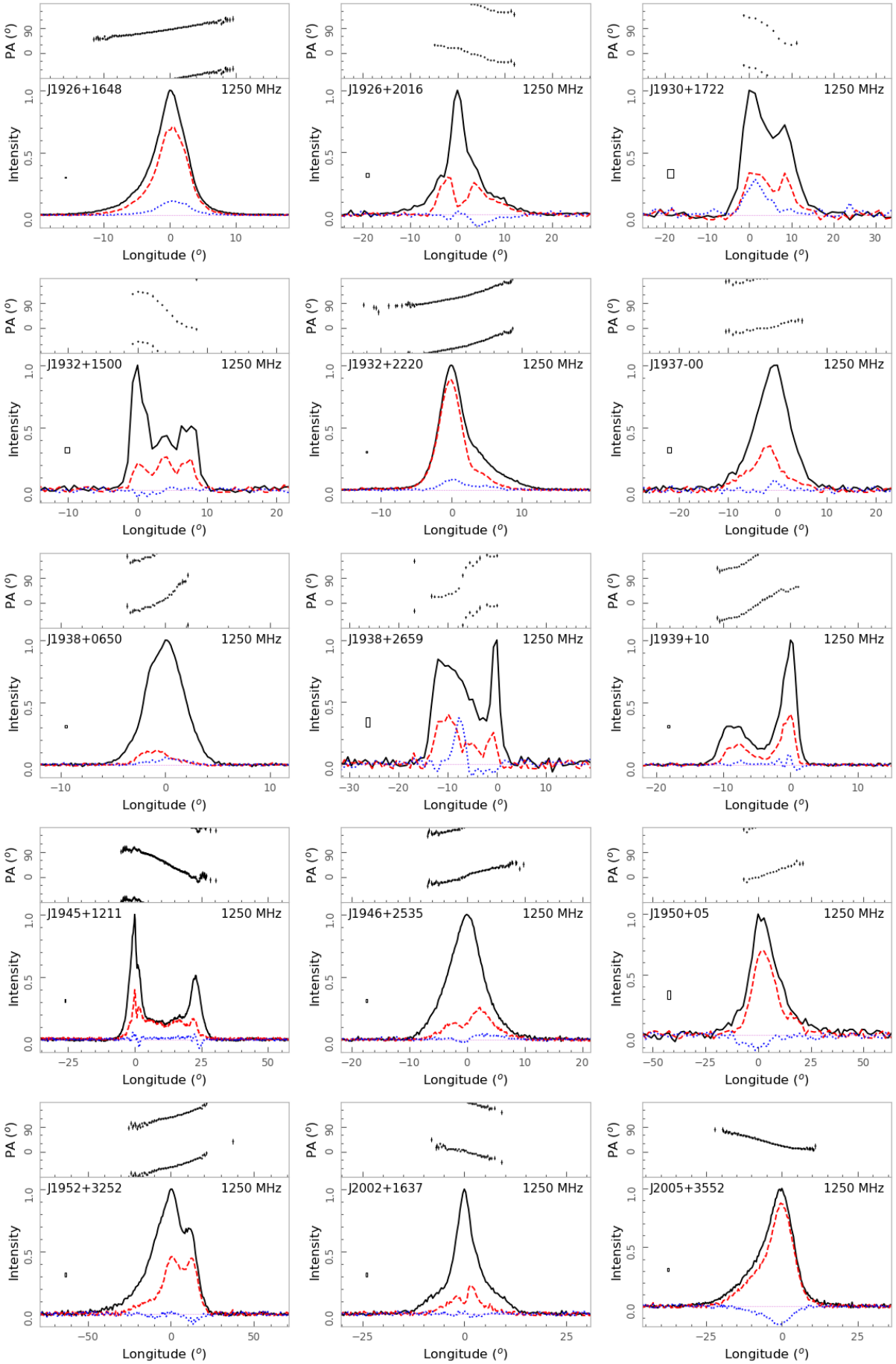

Fig. A.1 *–continued–*

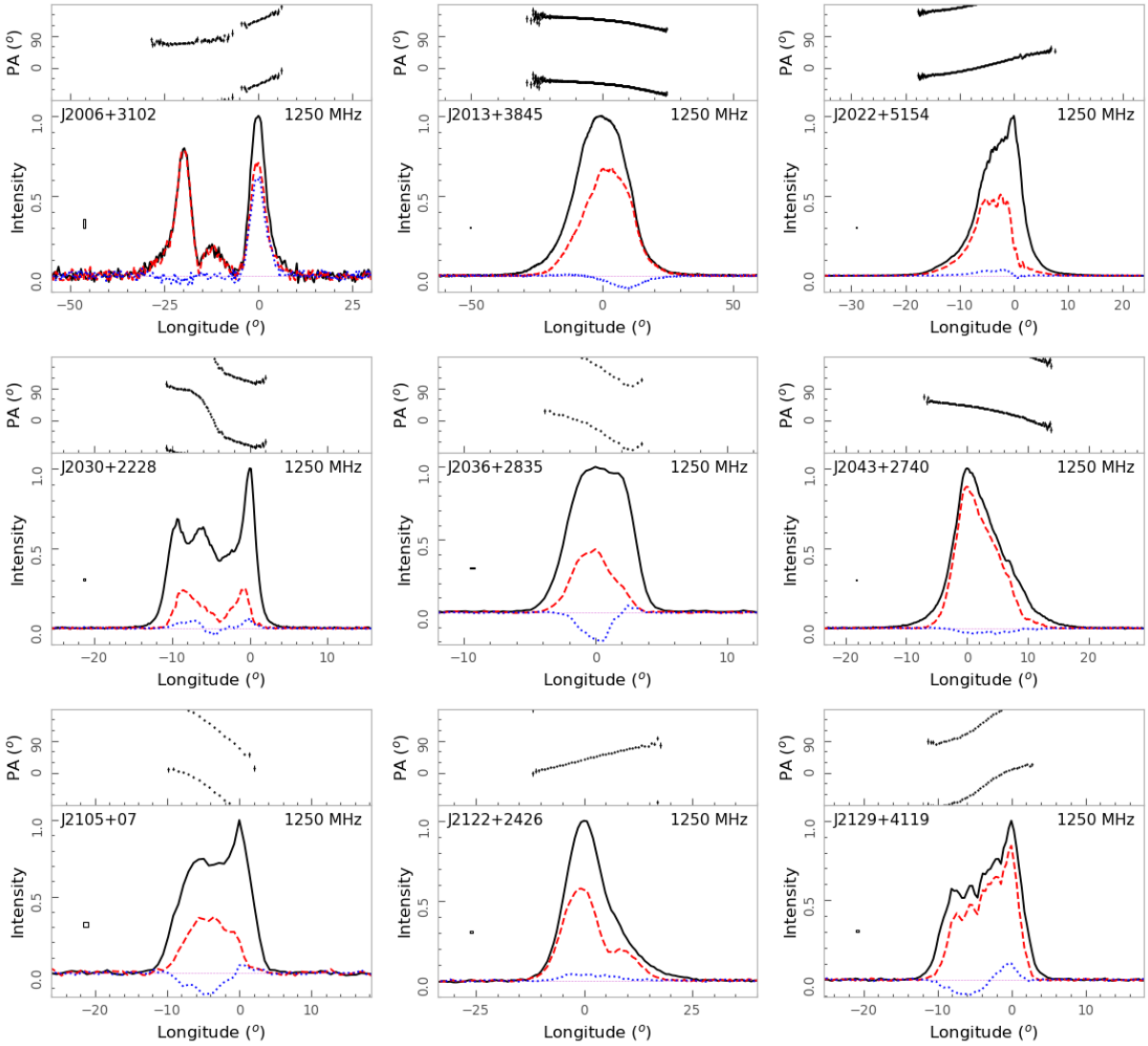
J2006+3102 1250 MHz
J2013+3845 1250 MHz
J2022+5154 1250 MHz
J2030+2228 1250 MHz
J2036+2835 1250 MHz
J2043+2740 1250 MHz
J2105+07 1250 MHz
J2122+2426 1250 MHz
J2129+4119 1250 MHz
PA (°)
Intensity
Longitude (°)

Fig. A.1 *–end.*

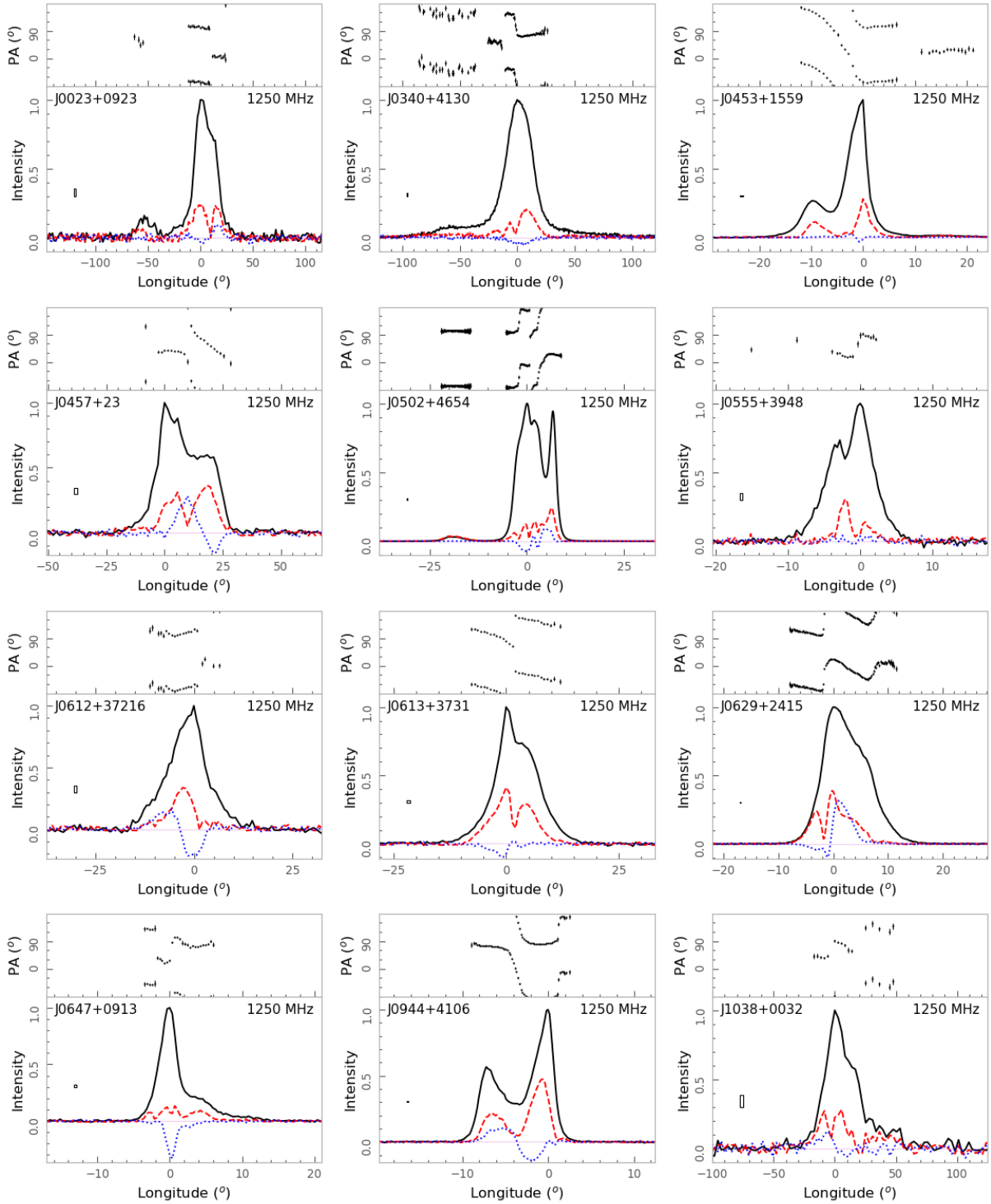

Fig. A.2 The same as Figure A.1 but for polarization profiles with orthogonal modes for 136 pulsars in this figure and for 35 pulsars in other figures (9 pulsars with highly linearly polarized components in Figure A.3, 5 conal double pulsars in Figure A.5, 6 pulsars with interpulse emission in Figure A.6, 13 pulsars with wide profiles in Figure A.7, and 2 pulsars affected by interstellar scattering in Figure A.8).– *to be continued*–

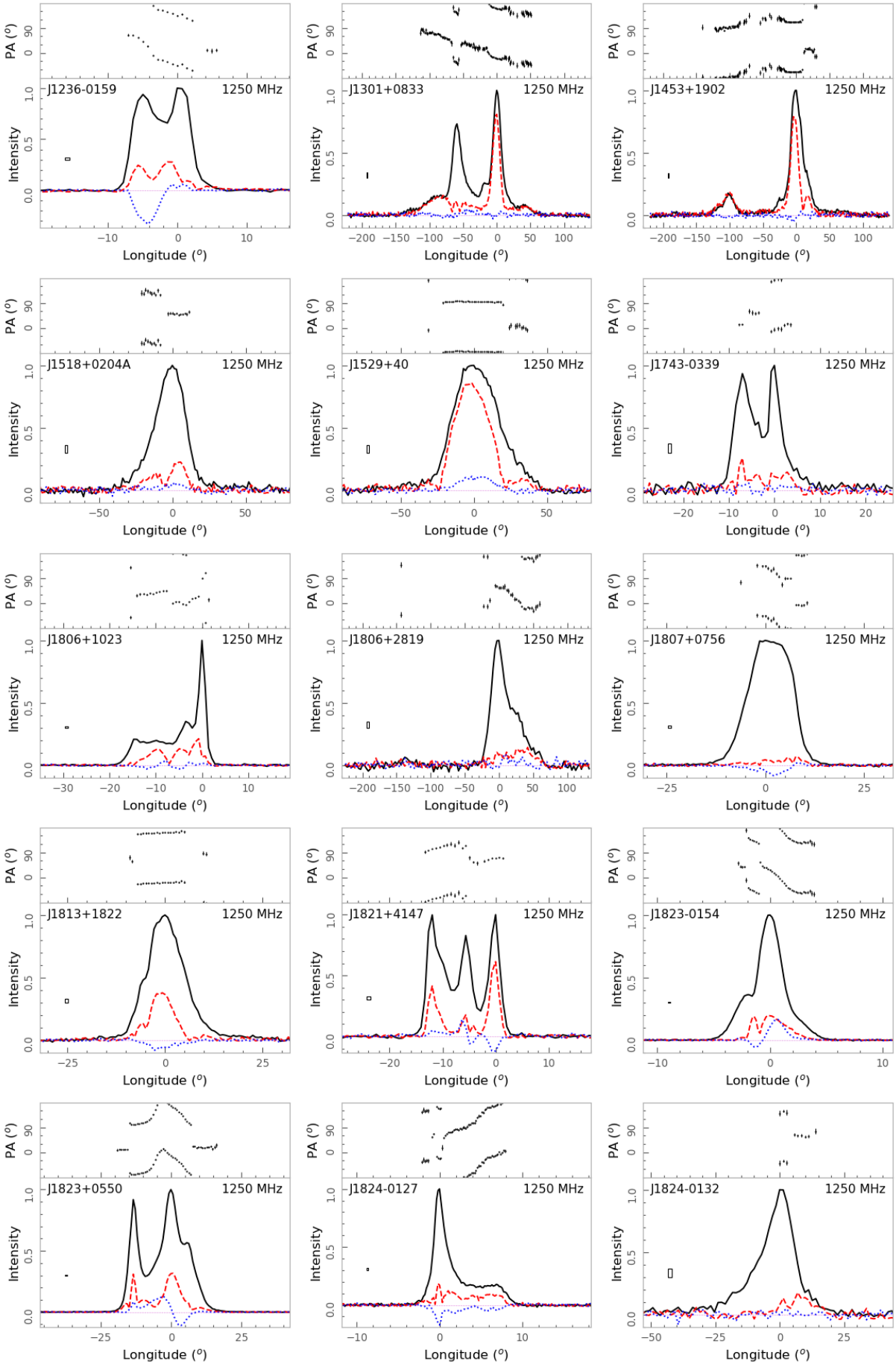

Fig. A.2 *–continued–*

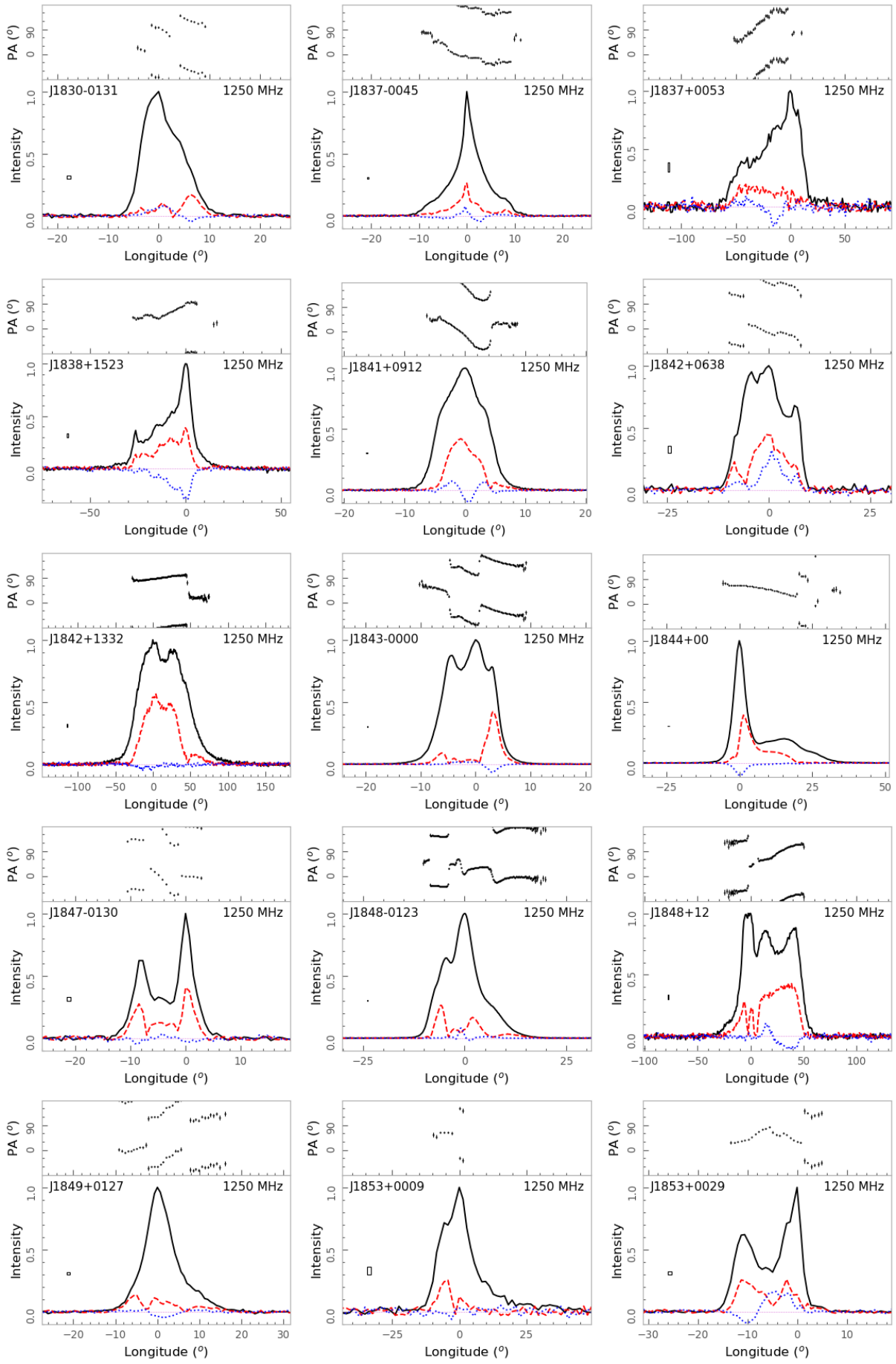

Fig. A.2 *–continued–*

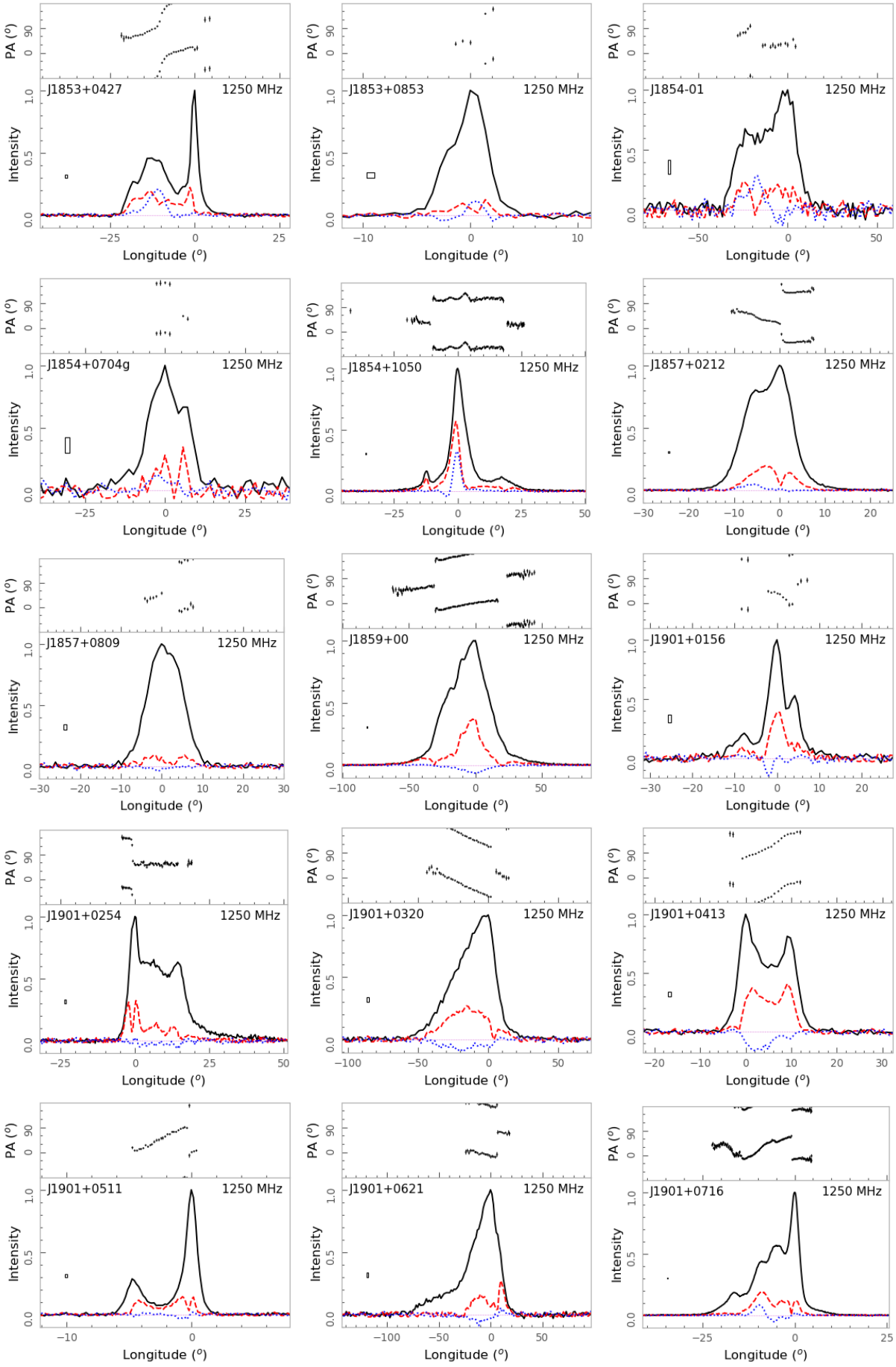

Fig. A.2 *–continued–*

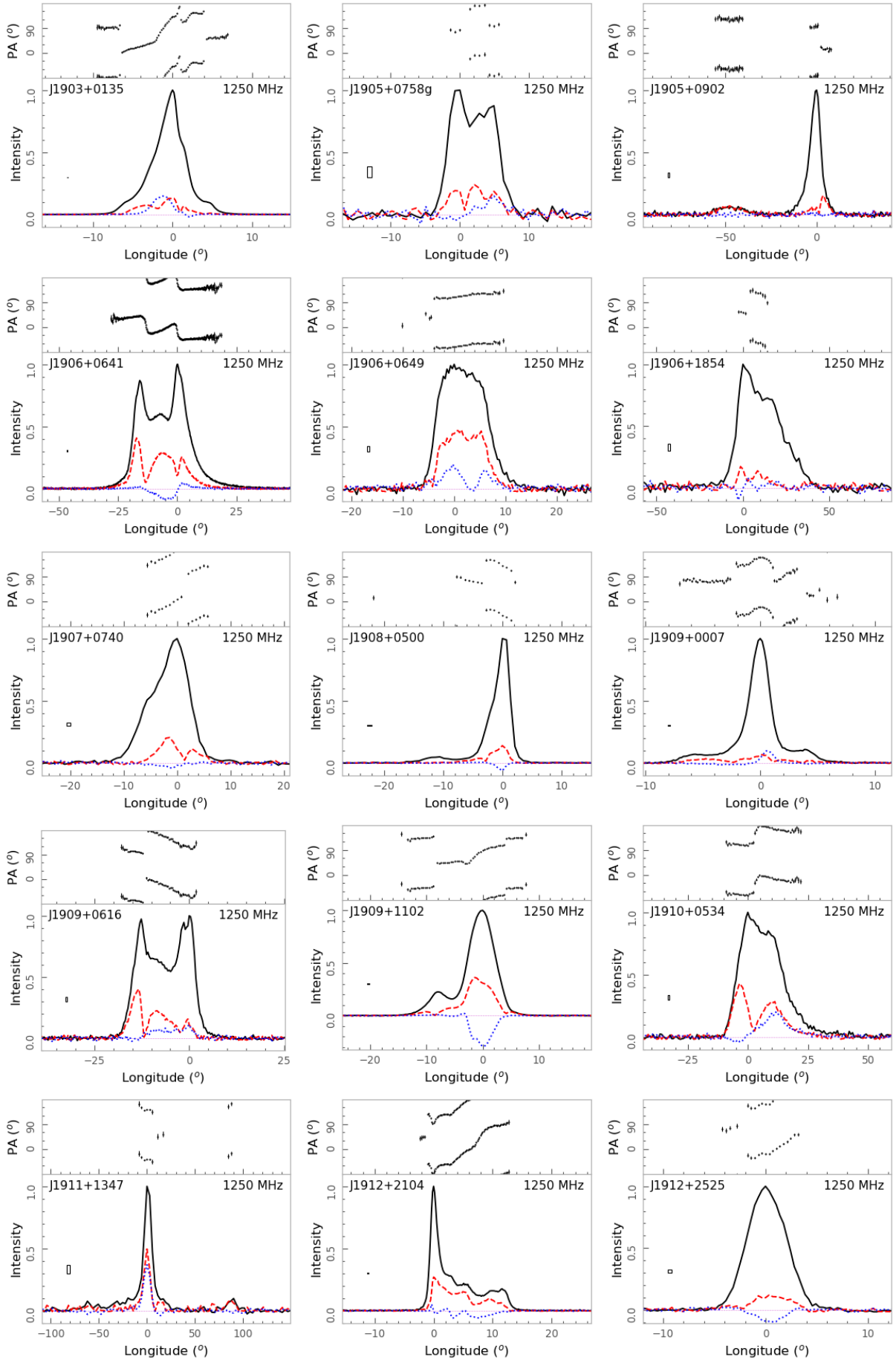

Fig. A.2 *–continued–*

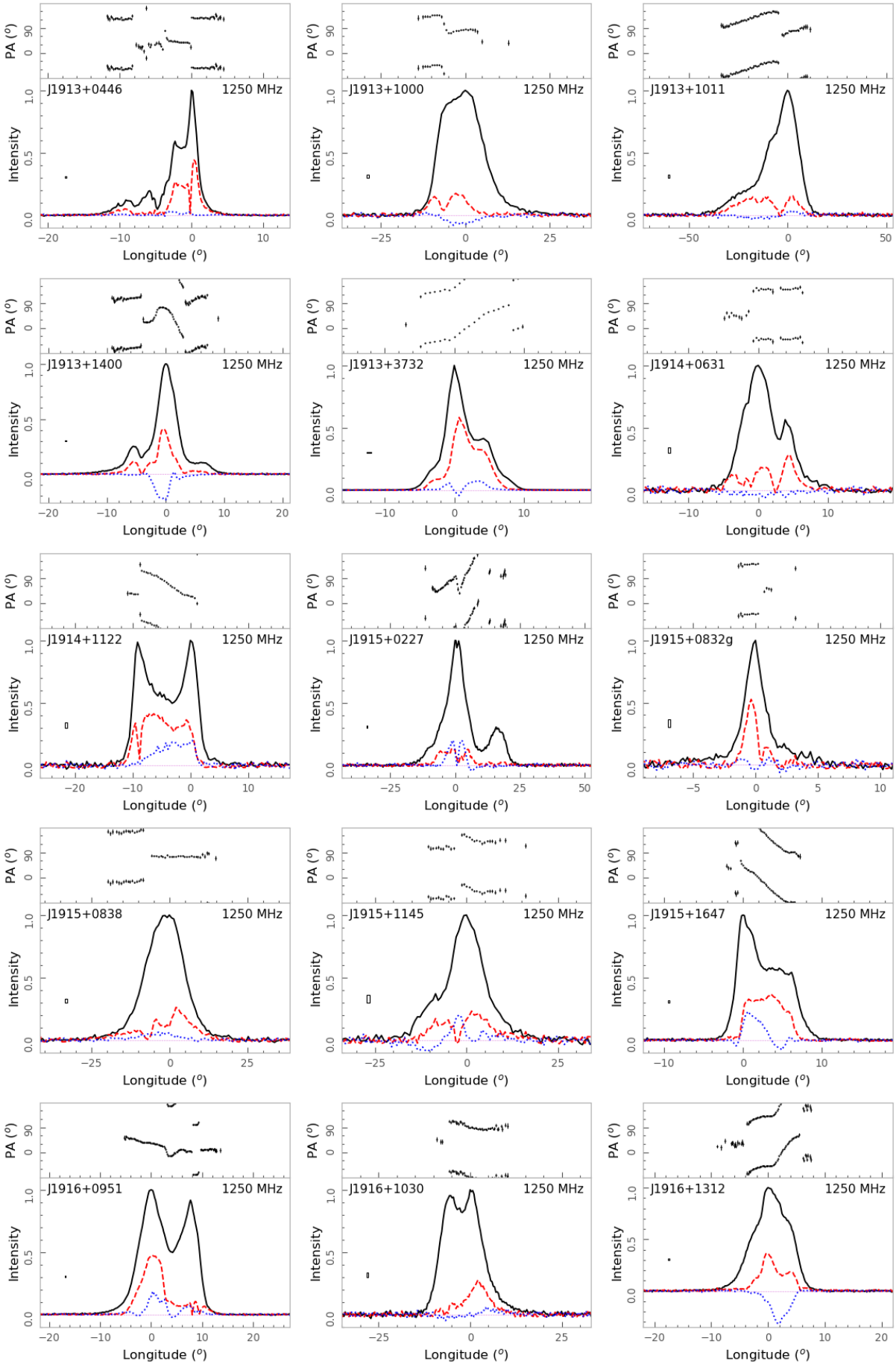

Fig. A.2 *–continued–*

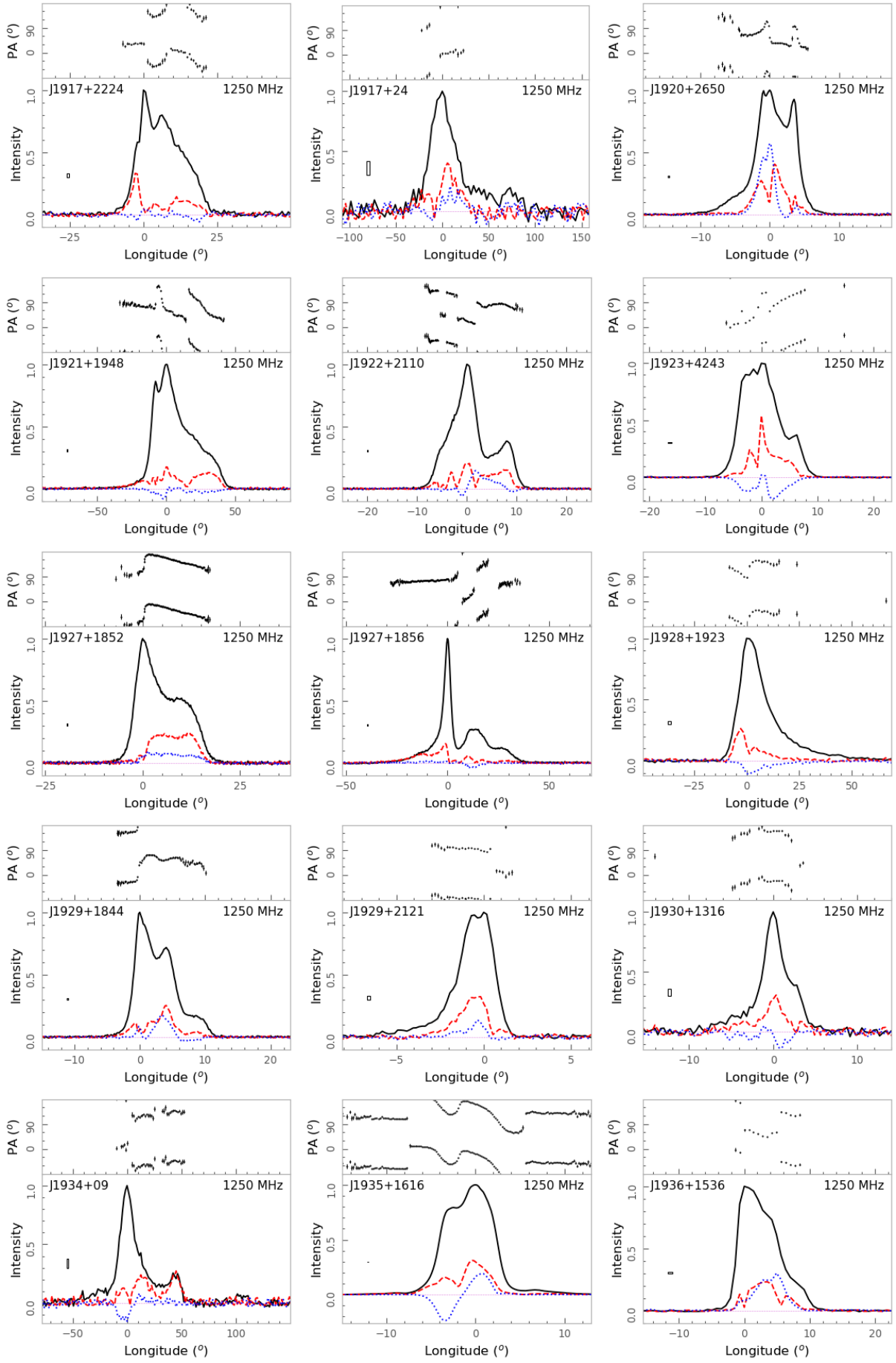

Fig. A.2 *–continued–*

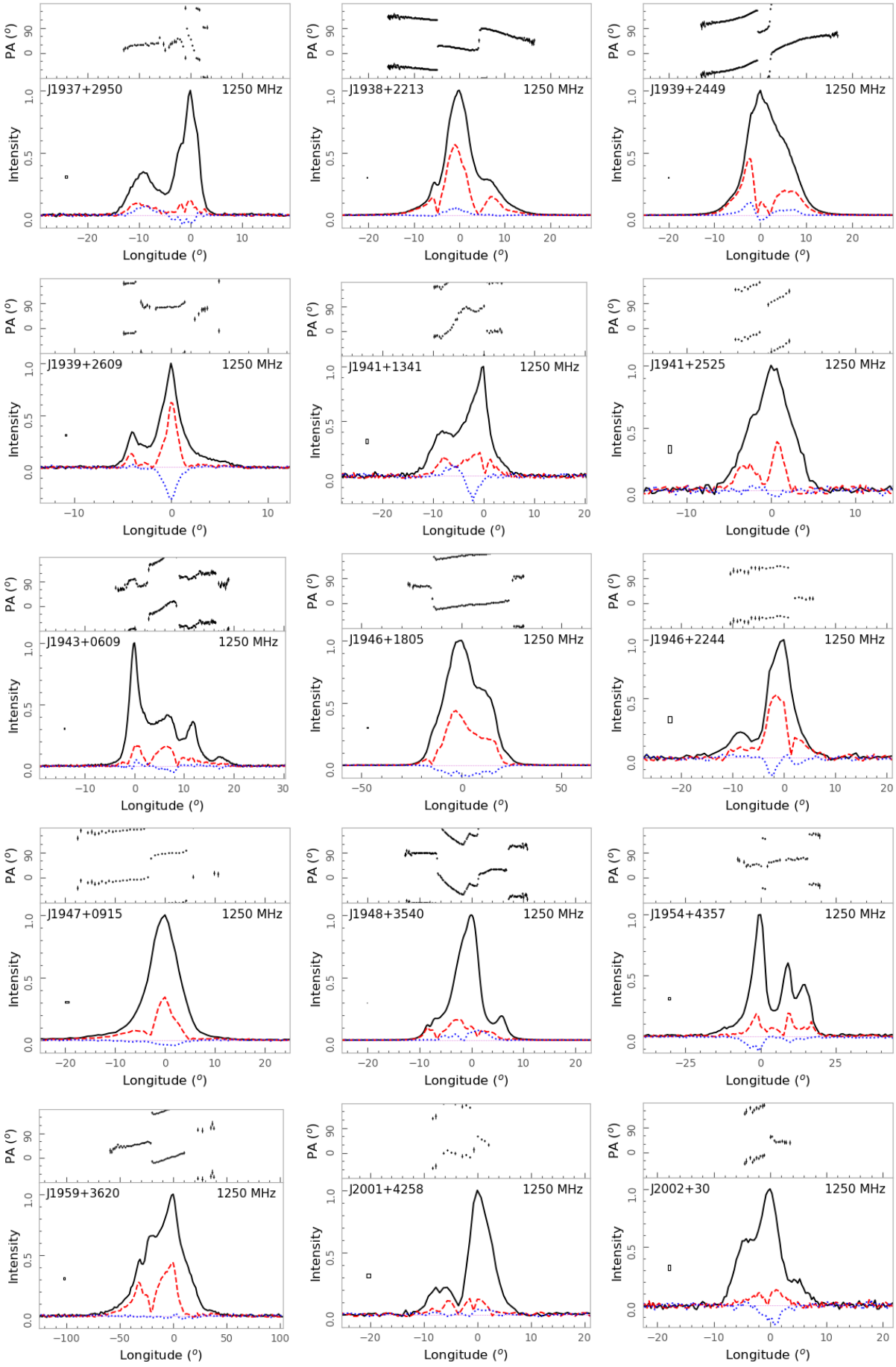

Fig. A.2 *–continued–*

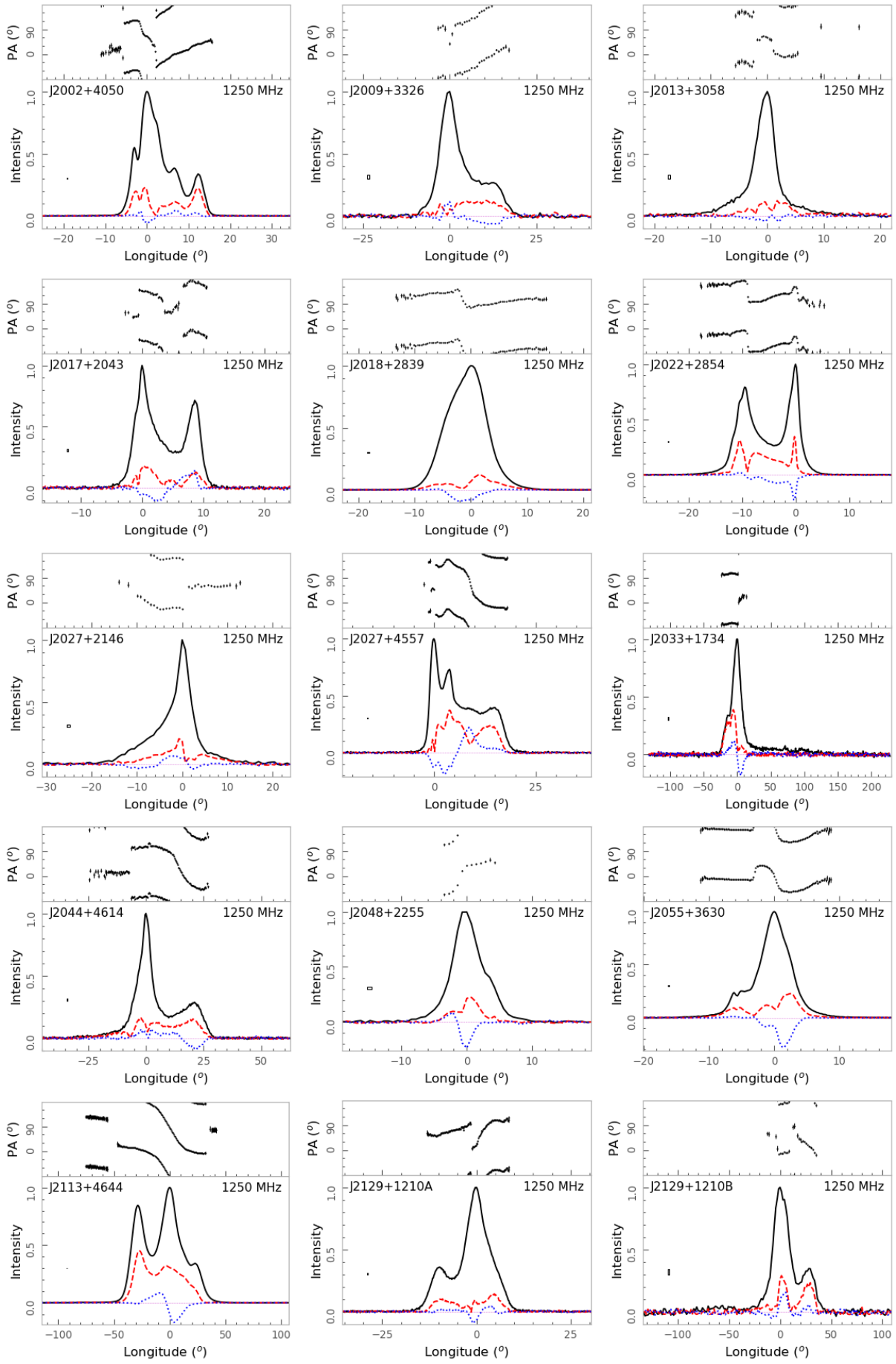

Fig. A.2 *–continued–*

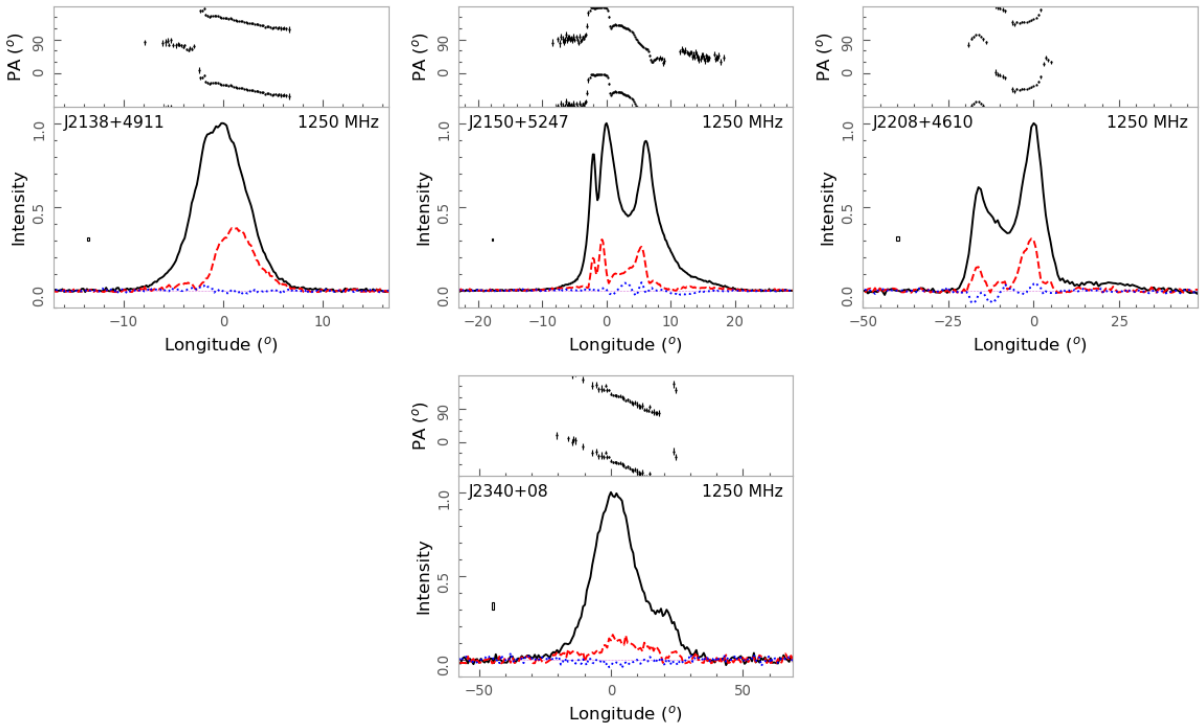
PA (°)
J2138+4911
1250 MHz
Intensity
Longitude (°)
J2150+5247
J2208+4610
J2340+08

Fig. A.2 *–end.*

(a) Pulsars with highly linearly polarized profiles.

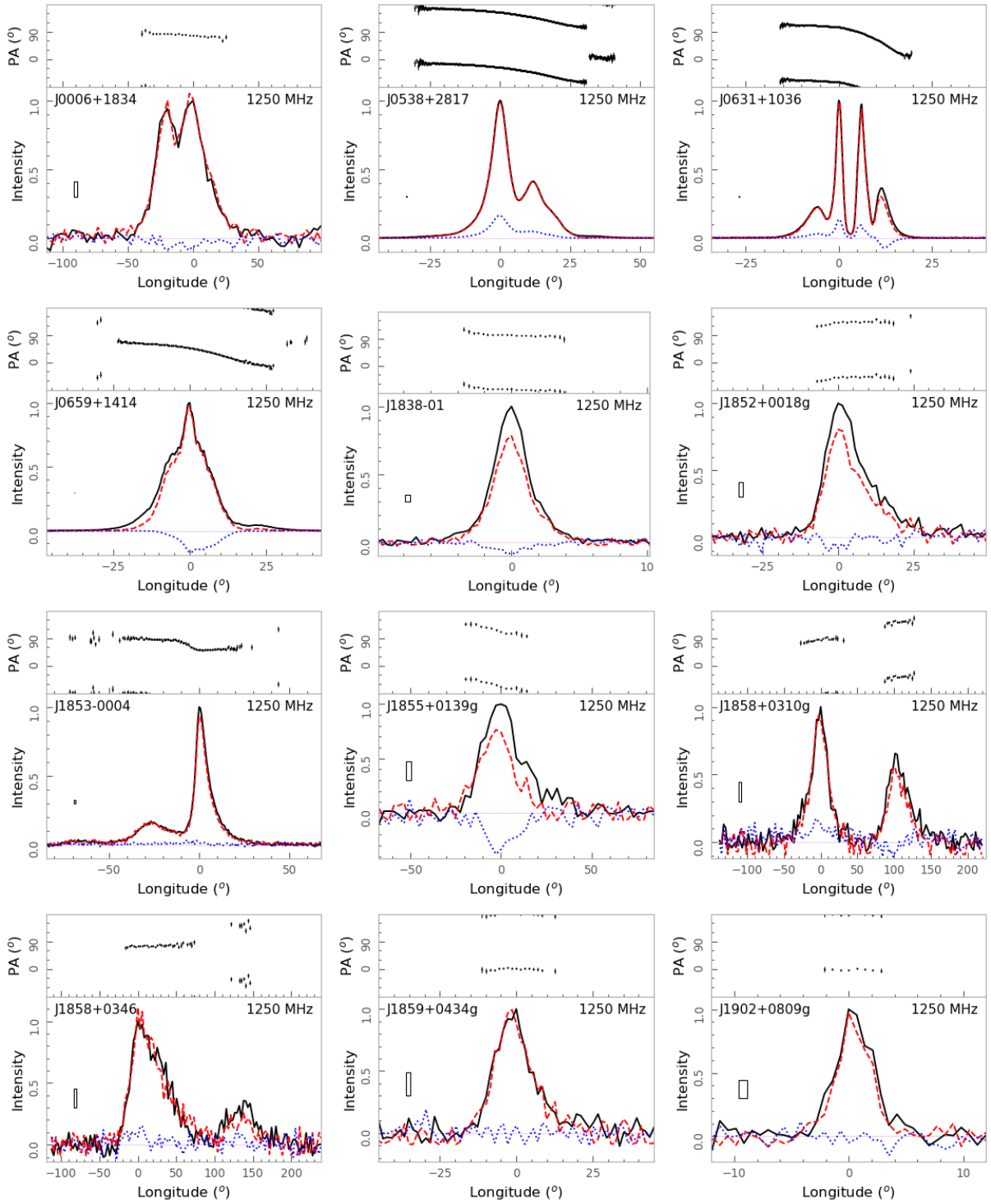

Fig. A.3 The same as Figure A.1 but for highly linearly polarized profiles of 45 pulsars in this figure and for 28 pulsars in other figures (13 pulsars with S-shaped position angles in Figure A.1, 2 pulsars with orthogonal modes in Figure A.2, 9 pulsars with interpulse emission in Figure A.6, 3 pulsars with wide profiles in Figure A.7, and one conal double pulsar in Figure A.5, as listed in Table 3). The highly linearly polarized emission can appear for (a) the whole profile, (b) the leading component, (c) the trailing component, and (d) both the leading and trailing components. – *to be continued*–

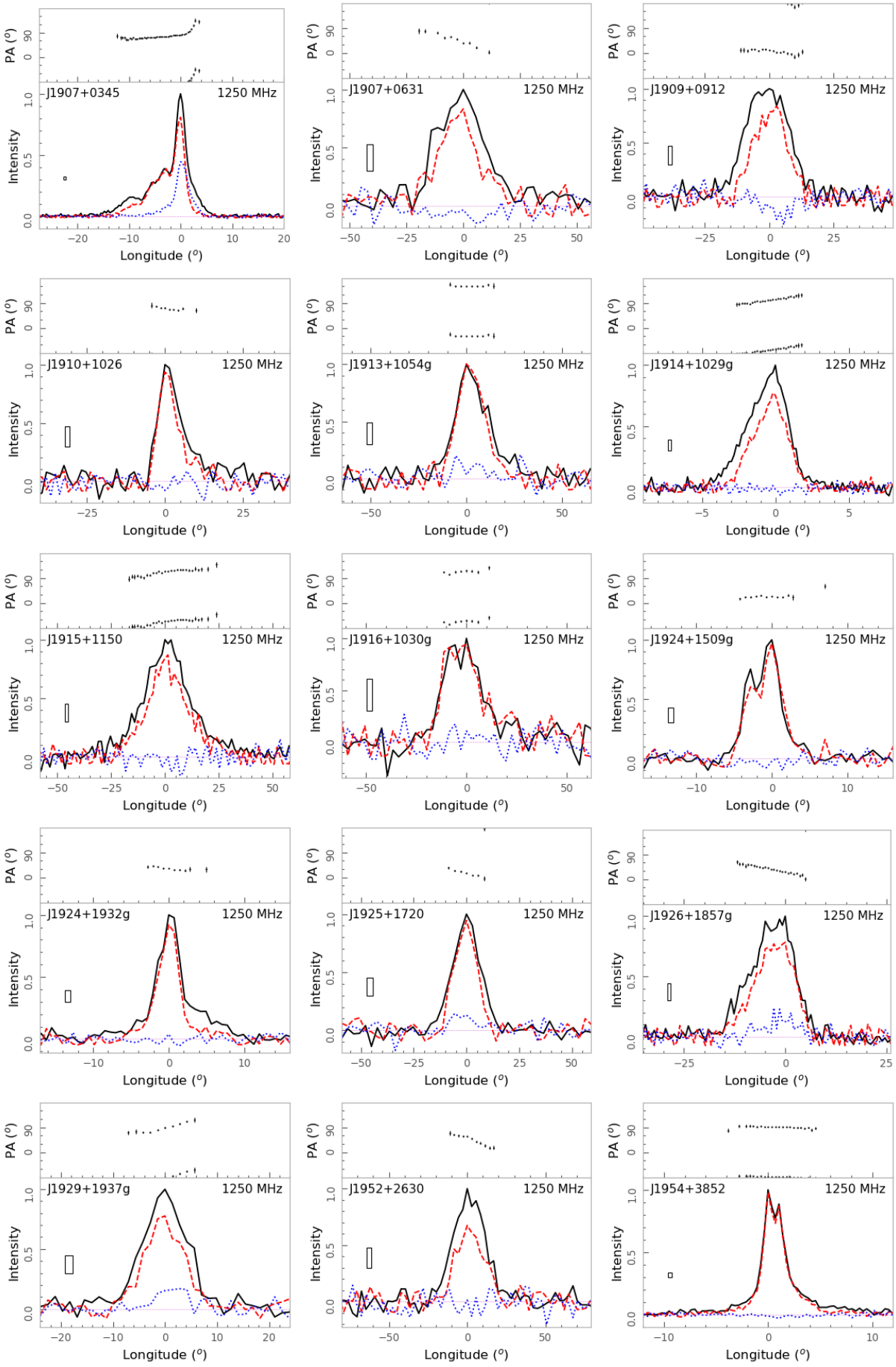

Fig. A.3 *– continued–*

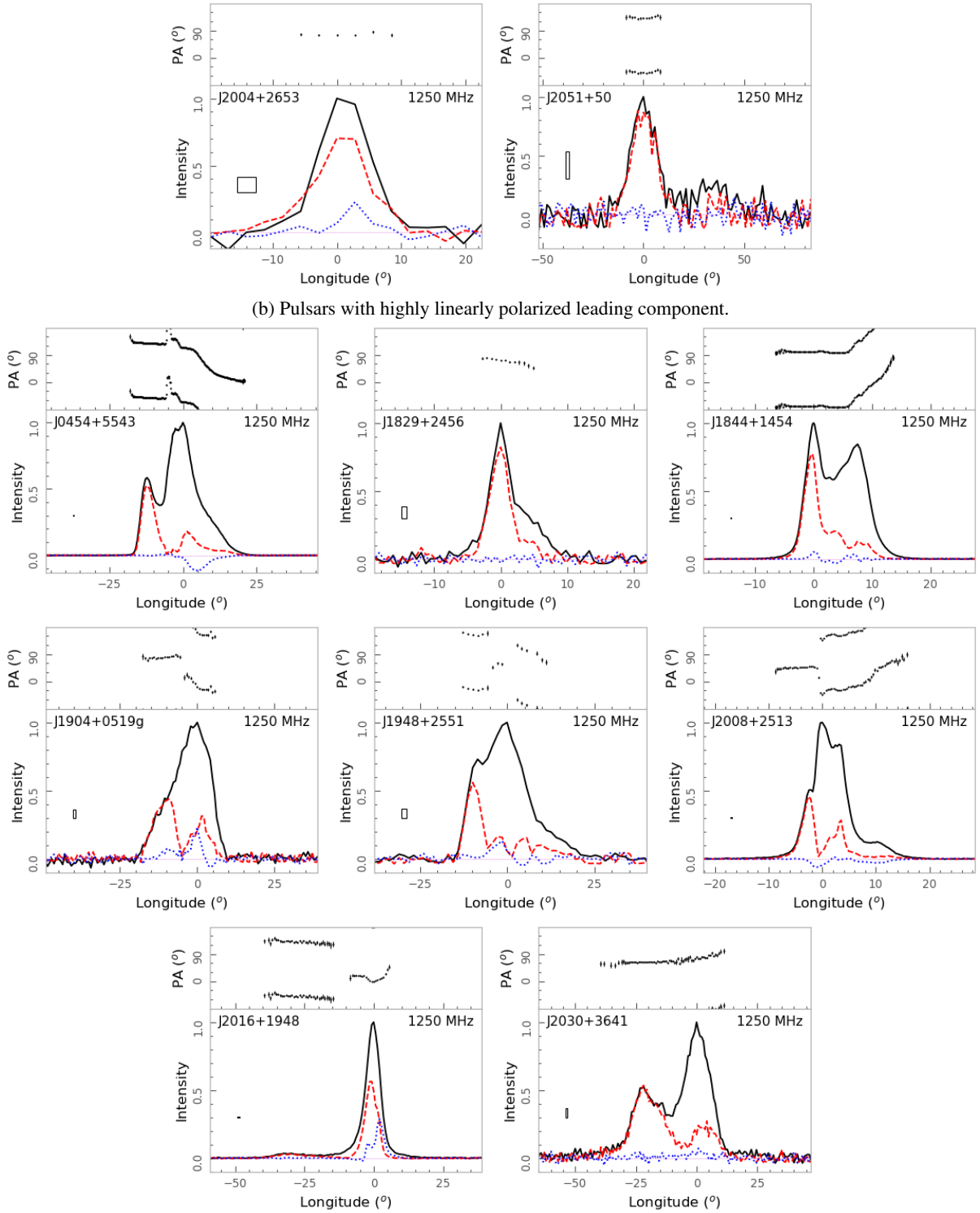

(b) Pulsars with highly linearly polarized leading component.

Fig. A.3 *– continued–*

(c) Pulsars with highly linearly polarized trailing component.

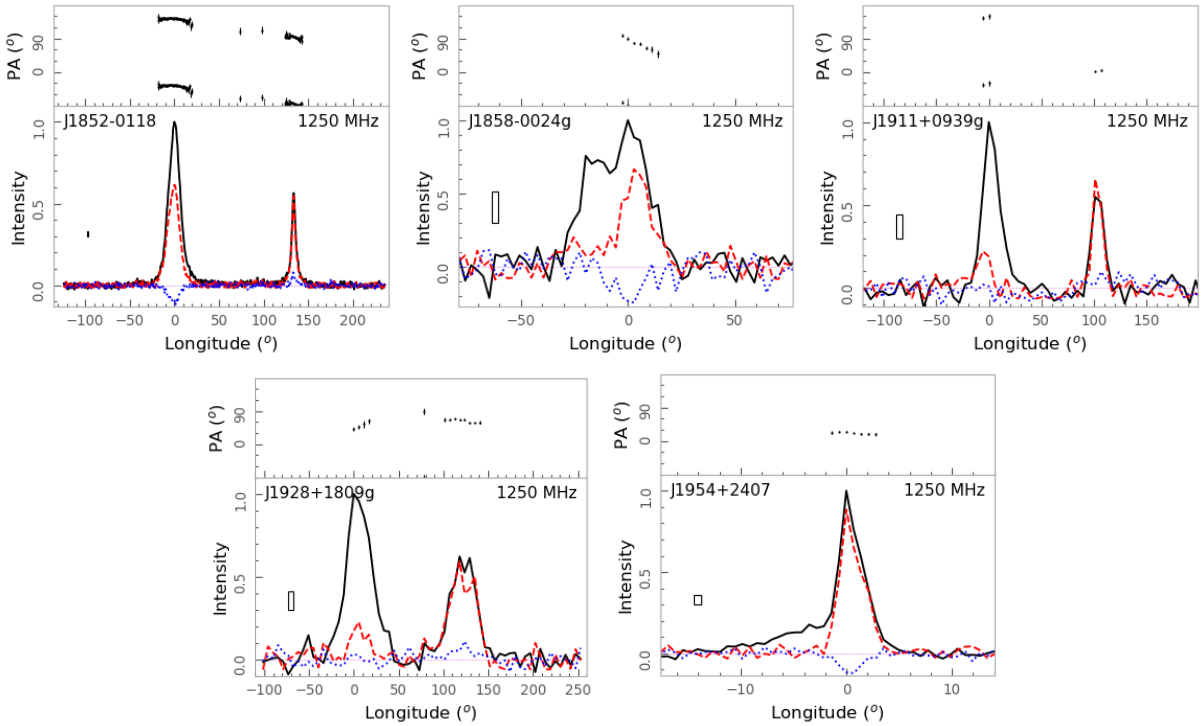

(d) Pulsars with highly linearly polarized leading and trailing components.

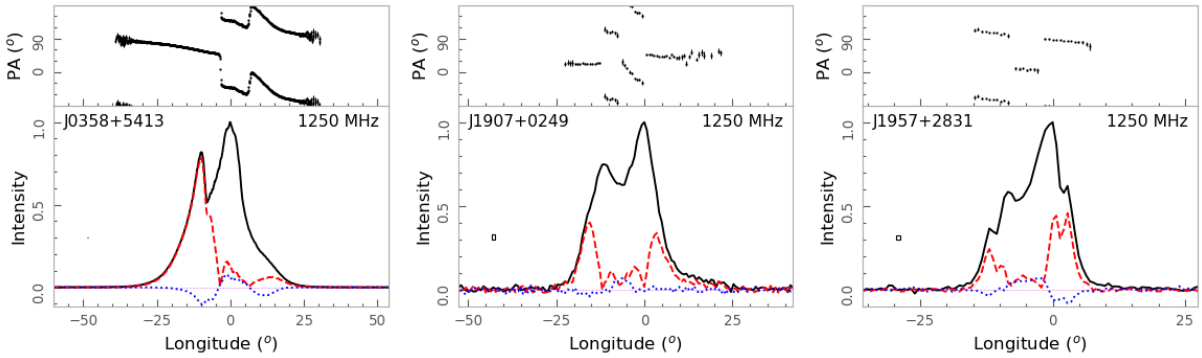

Fig. A.3 – *end.*

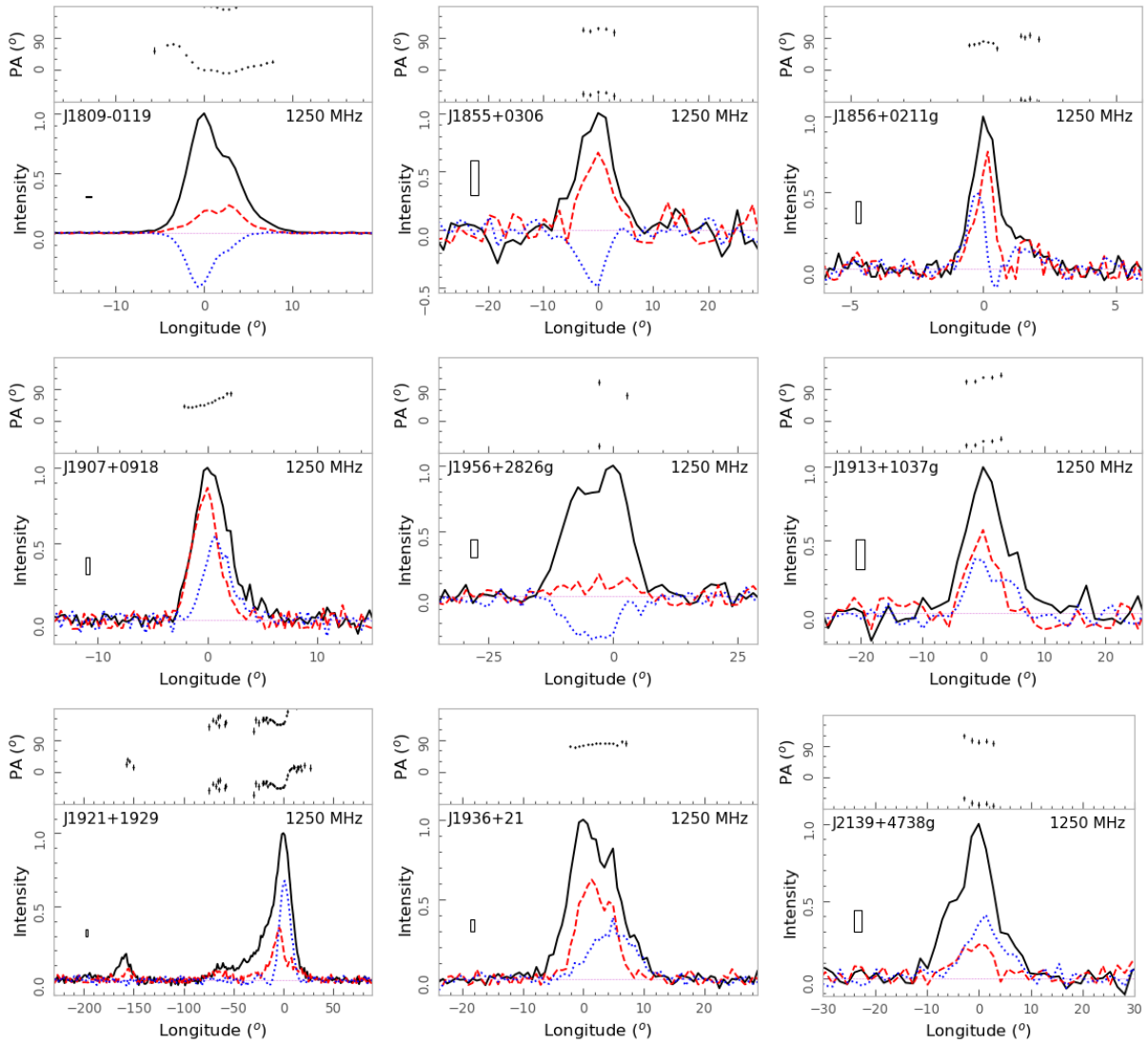

Fig. A.4 The same as Figure A.1 but for highly circularly polarized profiles ($|V|/I > 30\%$) of 9 pulsars here and 7 pulsars in other figures (PSRs J1853+0056 and J2006+3102 with S-shaped PA curves in Figure A.1, PSRs J1855+0139g and J1907+0345 with highly linearly polarized emission in Figure A.3, PSRs J1851+0118 and J1852+0056g with interpulse emission in Figure A.6, and PSR J1855+0527 affected by interstellar scattering in Figure A.8).

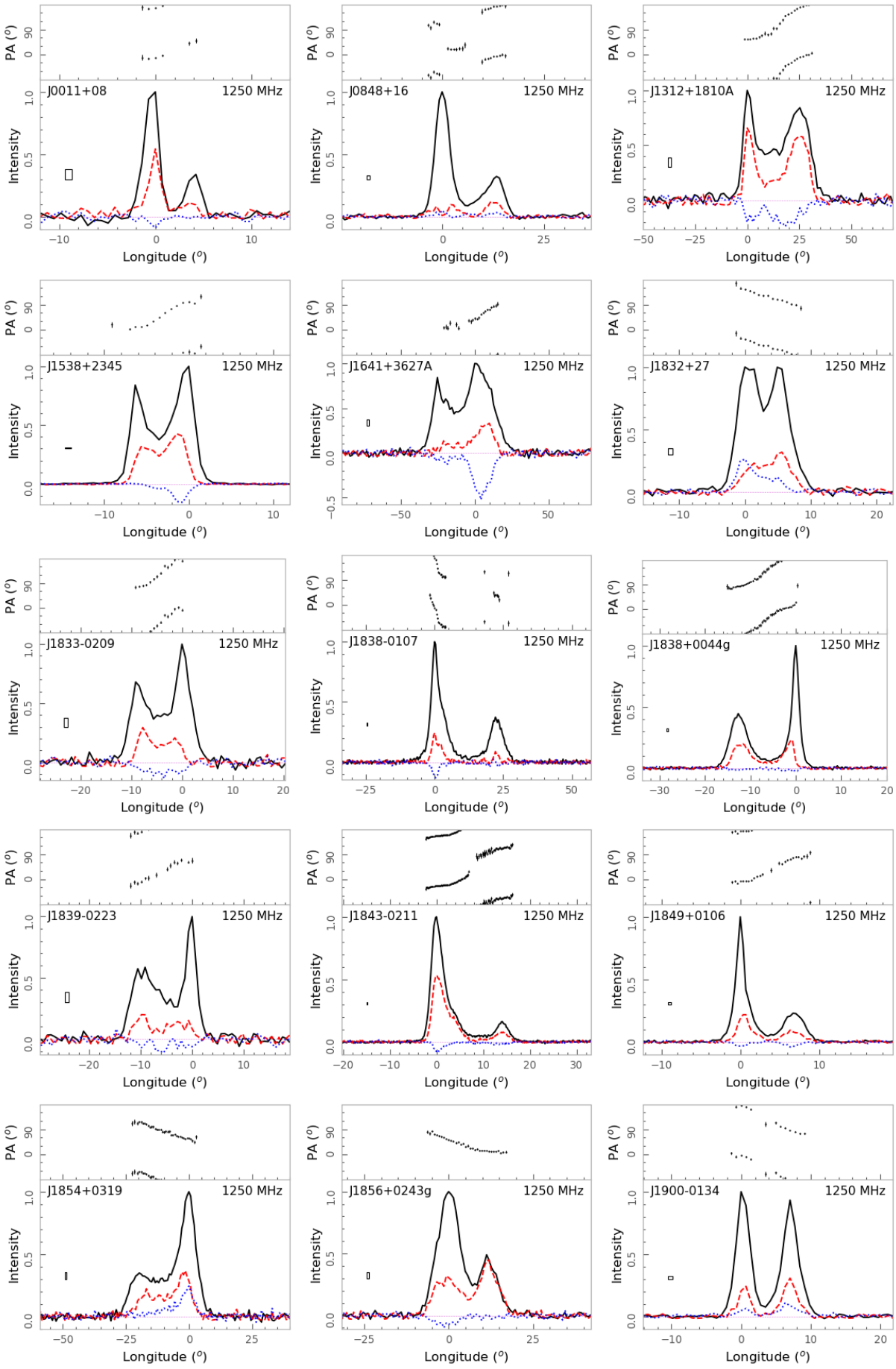

Fig. A.5 The same as Figure A.1 but for polarized pulse profiles of 28 conal double pulsars. – *to be continued.*

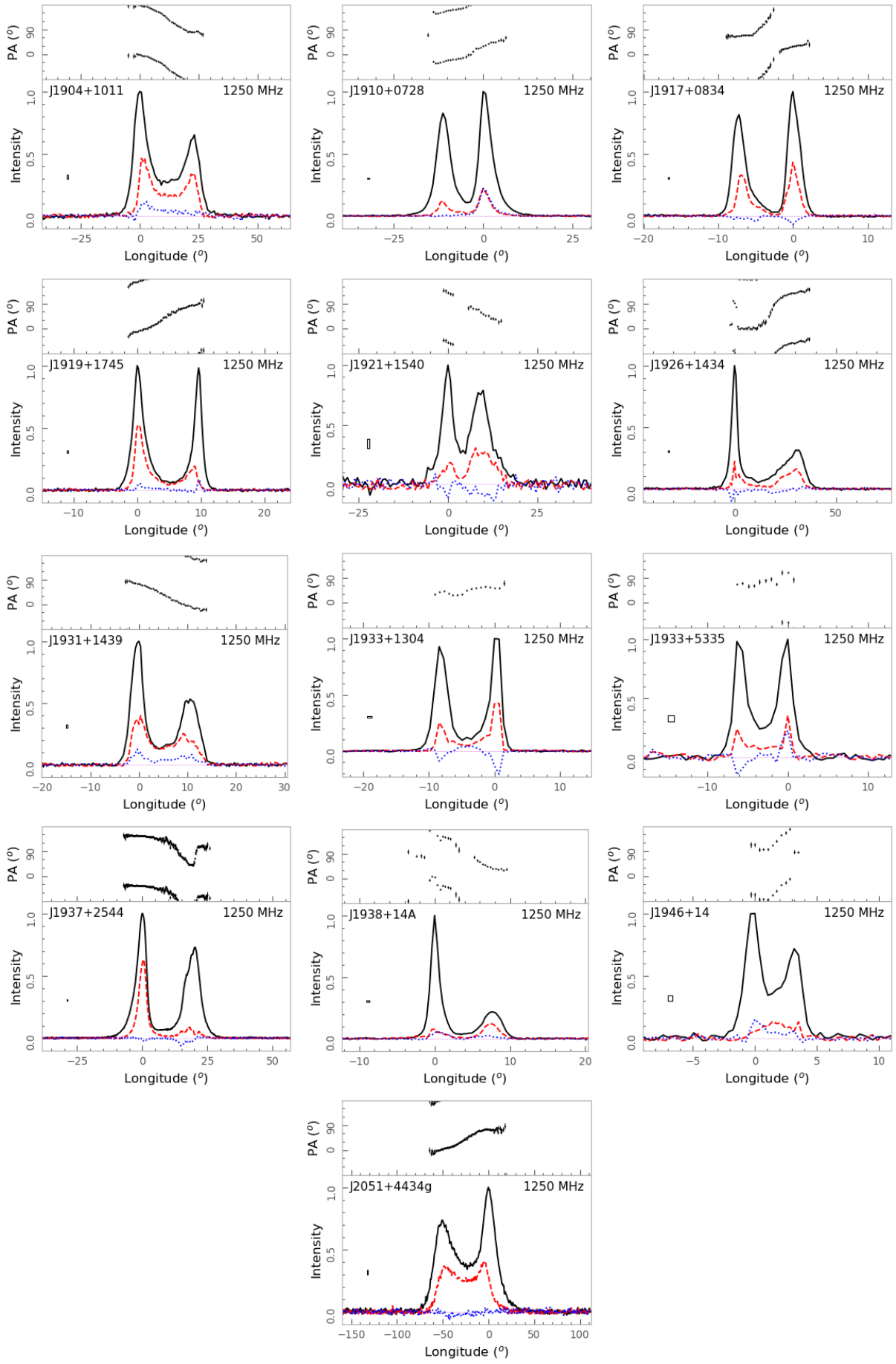
J1904+1011 1250 MHz
J1910+0728 1250 MHz
J1917+0834 1250 MHz
J1919+1745 1250 MHz
J1921+1540 1250 MHz
J1926+1434 1250 MHz
J1931+1439 1250 MHz
J1933+1304 1250 MHz
J1933+5335 1250 MHz
J1937+2544 1250 MHz
J1938+14A 1250 MHz
J1946+14 1250 MHz
J2051+4434g 1250 MHz
PA (°)
Intensity
Longitude (°)

Fig. A.5 *–end.*

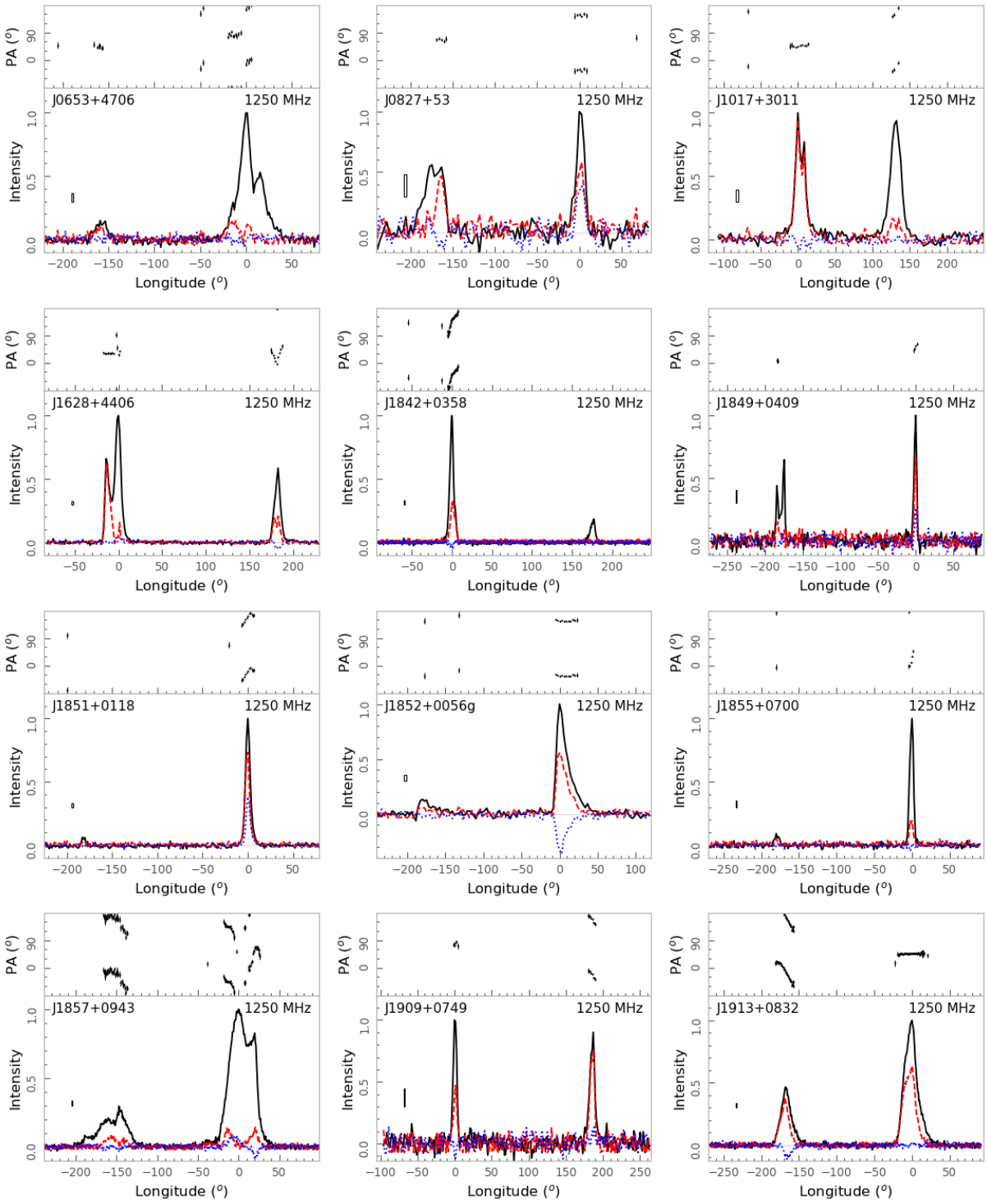

Fig. A.6 Polarized pulse profiles of 27 pulsars with interpulse emission. See the keys in Figure A.1. – *to be continued*.

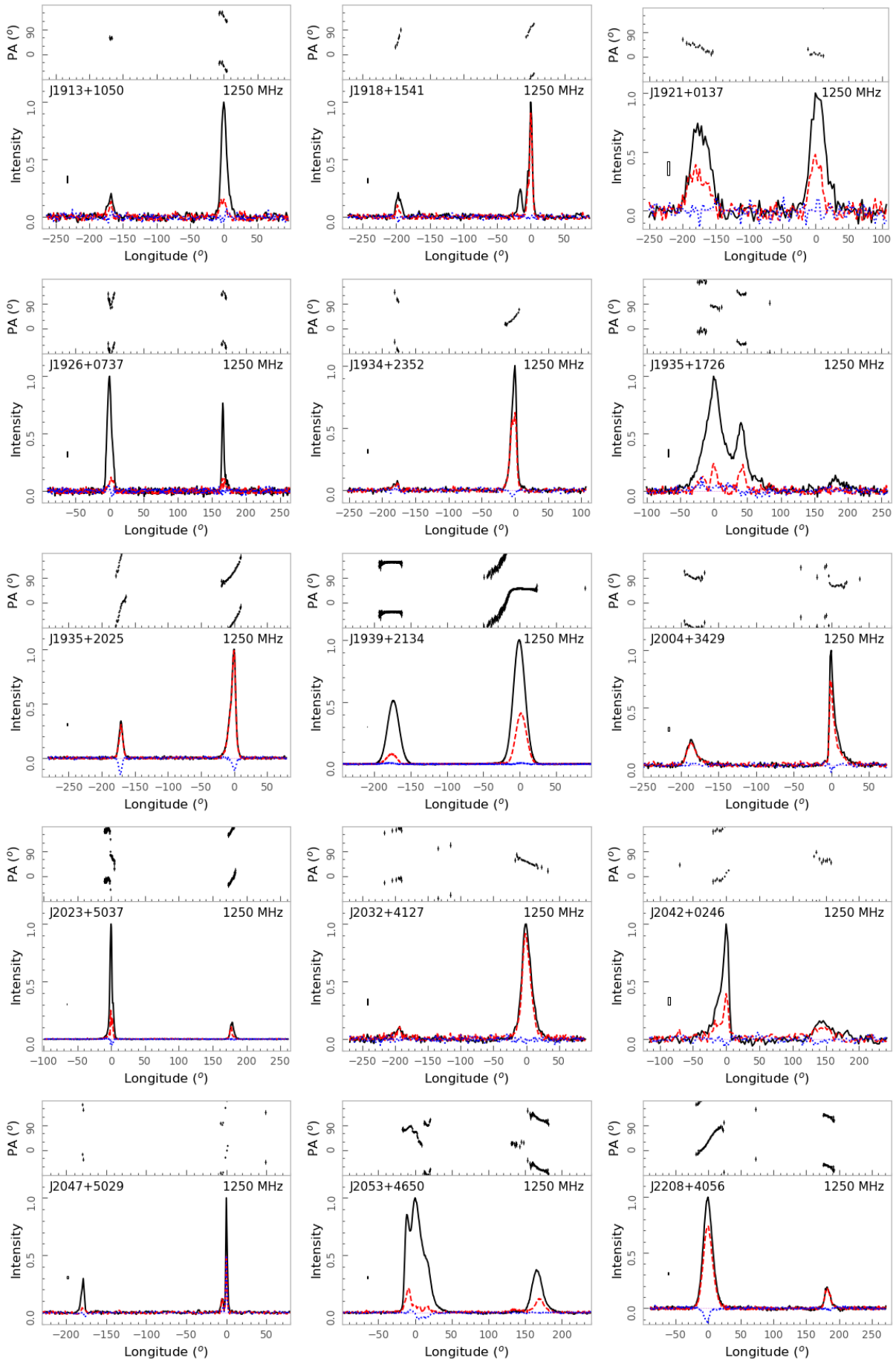
J1913+1050 1250 MHz
J1918+1541 1250 MHz
J1921+0137 1250 MHz
J1926+0737 1250 MHz
J1934+2352 1250 MHz
J1935+1726 1250 MHz
J1935+2025 1250 MHz
J1939+2134 1250 MHz
J2004+3429 1250 MHz
J2023+5037 1250 MHz
J2032+4127 1250 MHz
J2042+0246 1250 MHz
J2047+5029 1250 MHz
J2053+4650 1250 MHz
J2208+4056 1250 MHz
PA (°)
Intensity
Longitude (°)

Fig. A.6 – *end.*

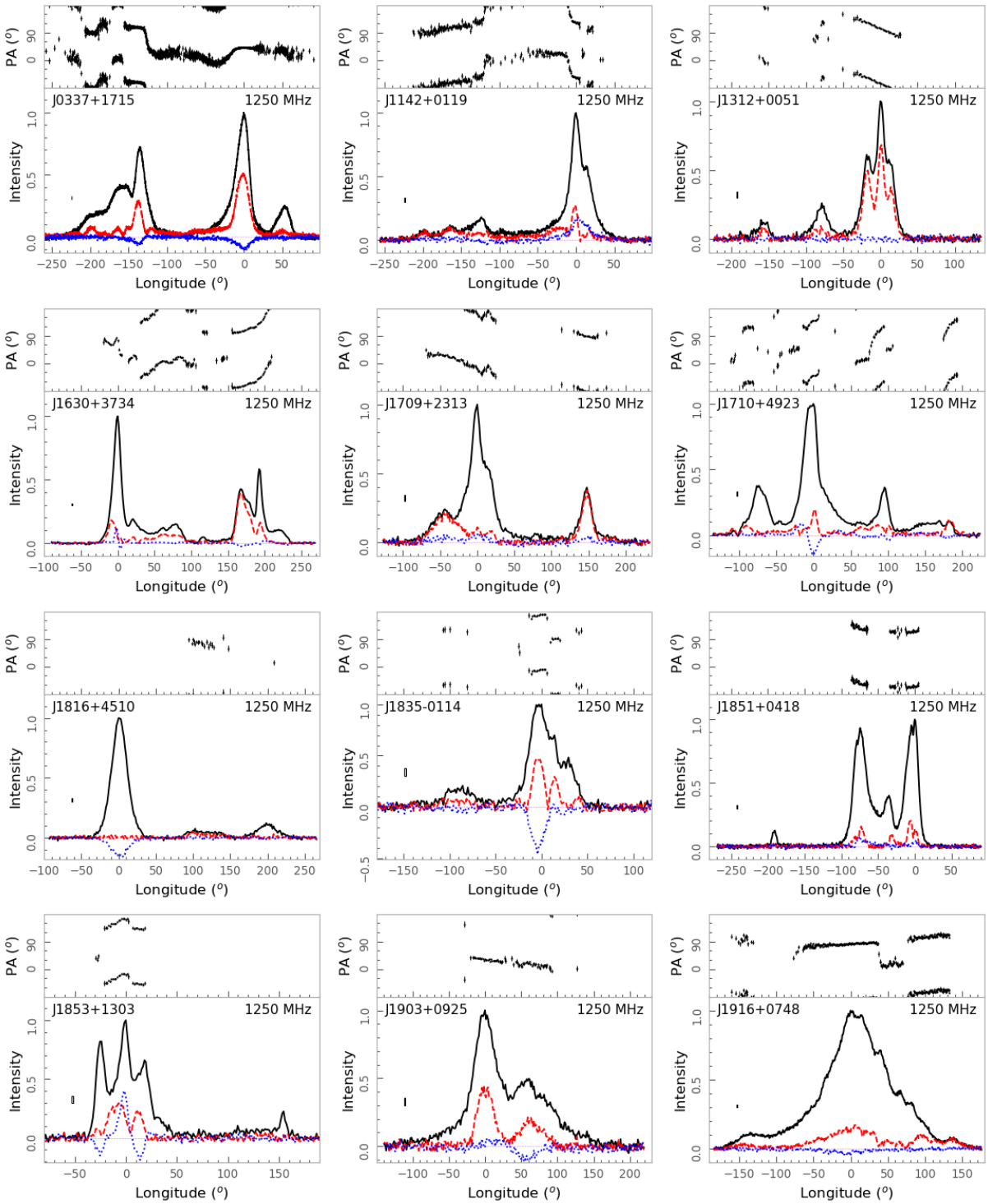

Fig. A.7 The same as Figure A.1 but for very wide profiles for 21 pulsars. PSRs J1851+0418, J1903+0925, J1916+0748 and J1932+1059 are normal pulsars, while others are millisecond pulsars. – *to be continued*.

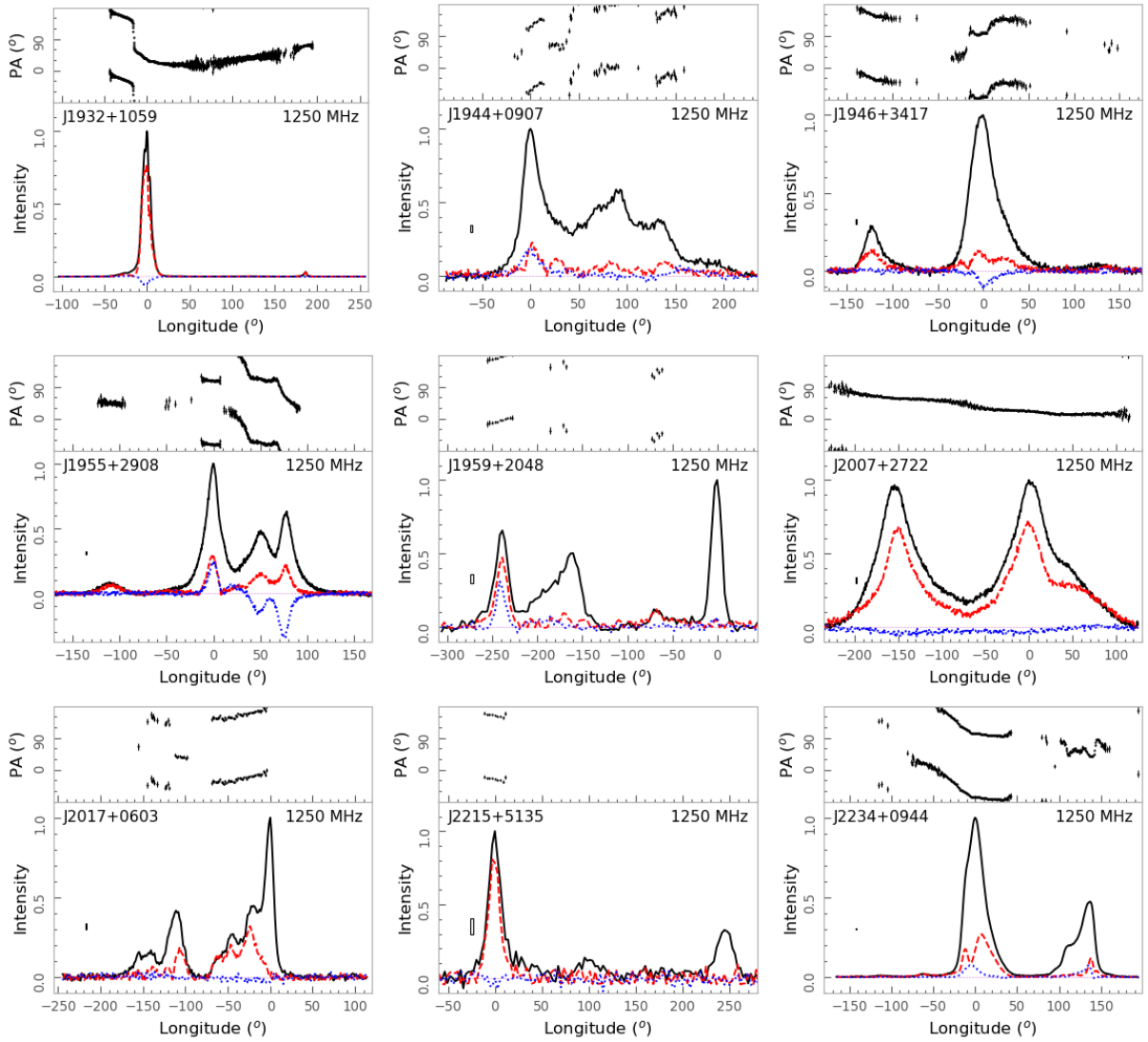
J1932+1059
1250 MHz
J1944+0907
1250 MHz
J1946+3417
1250 MHz
J1955+2908
1250 MHz
J1959+2048
1250 MHz
J2007+2722
1250 MHz
J2017+0603
1250 MHz
J2215+5135
1250 MHz
J2234+0944
1250 MHz
PA (°)
Intensity
Longitude (°)

Fig. A.7 – *end.*

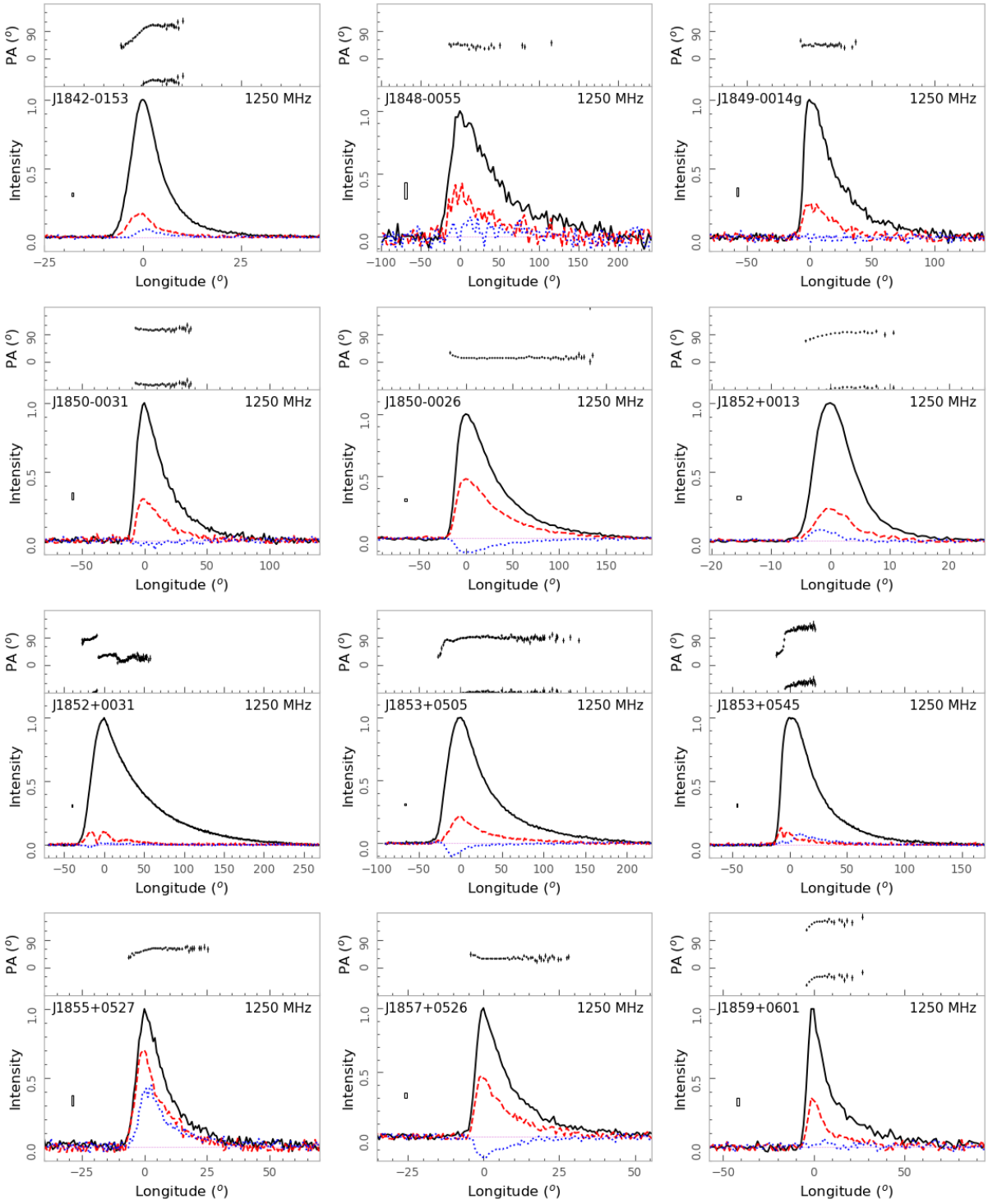

Fig. A.8 The same as Figure A.1 but for 22 pulsars with obvious scattering tails. – *to be continued*.

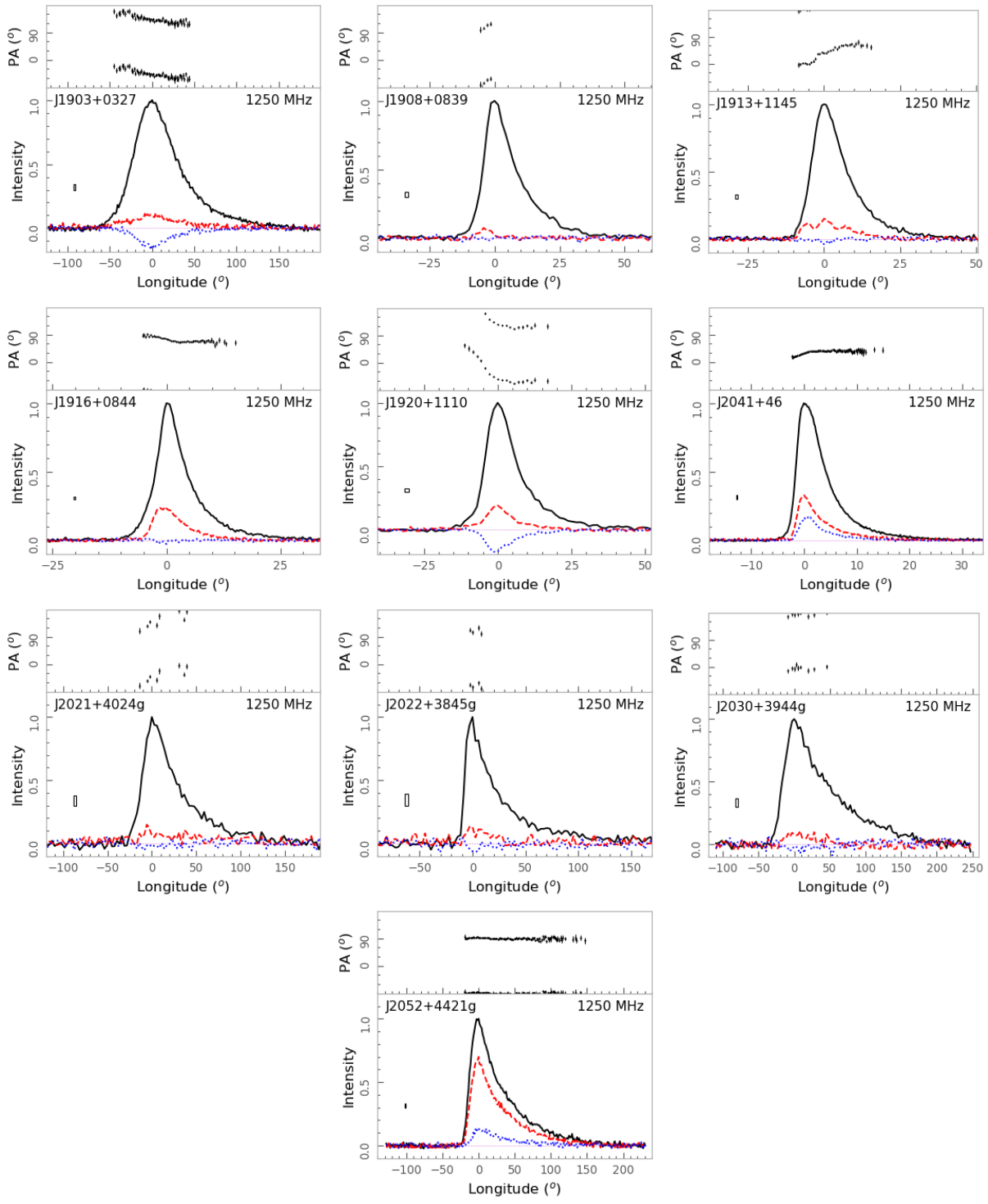
J1903+0327 1250 MHz
J1908+0839 1250 MHz
J1913+1145 1250 MHz
J1916+0844 1250 MHz
J1920+1110 1250 MHz
J2041+46 1250 MHz
J2021+4024g 1250 MHz
J2022+3845g 1250 MHz
J2030+3944g 1250 MHz
J2052+4421g 1250 MHz
PA (°)
Intensity
Longitude (°)

Fig. A.8 – *end.*

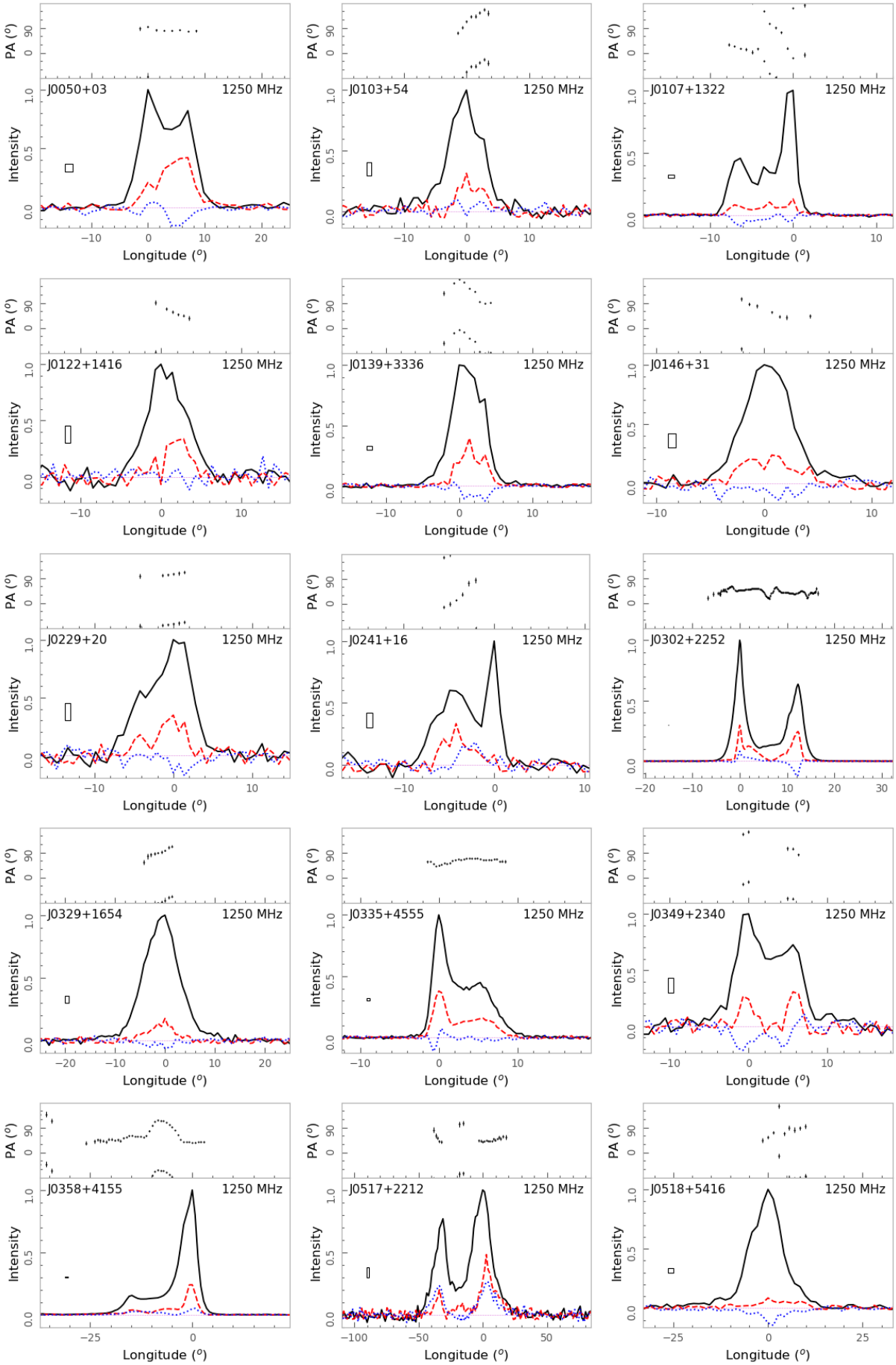

Fig. A.9 Polarized pulse profiles of the other 298 pulsars. See the keys in Figure A.1. – *to be continued* –

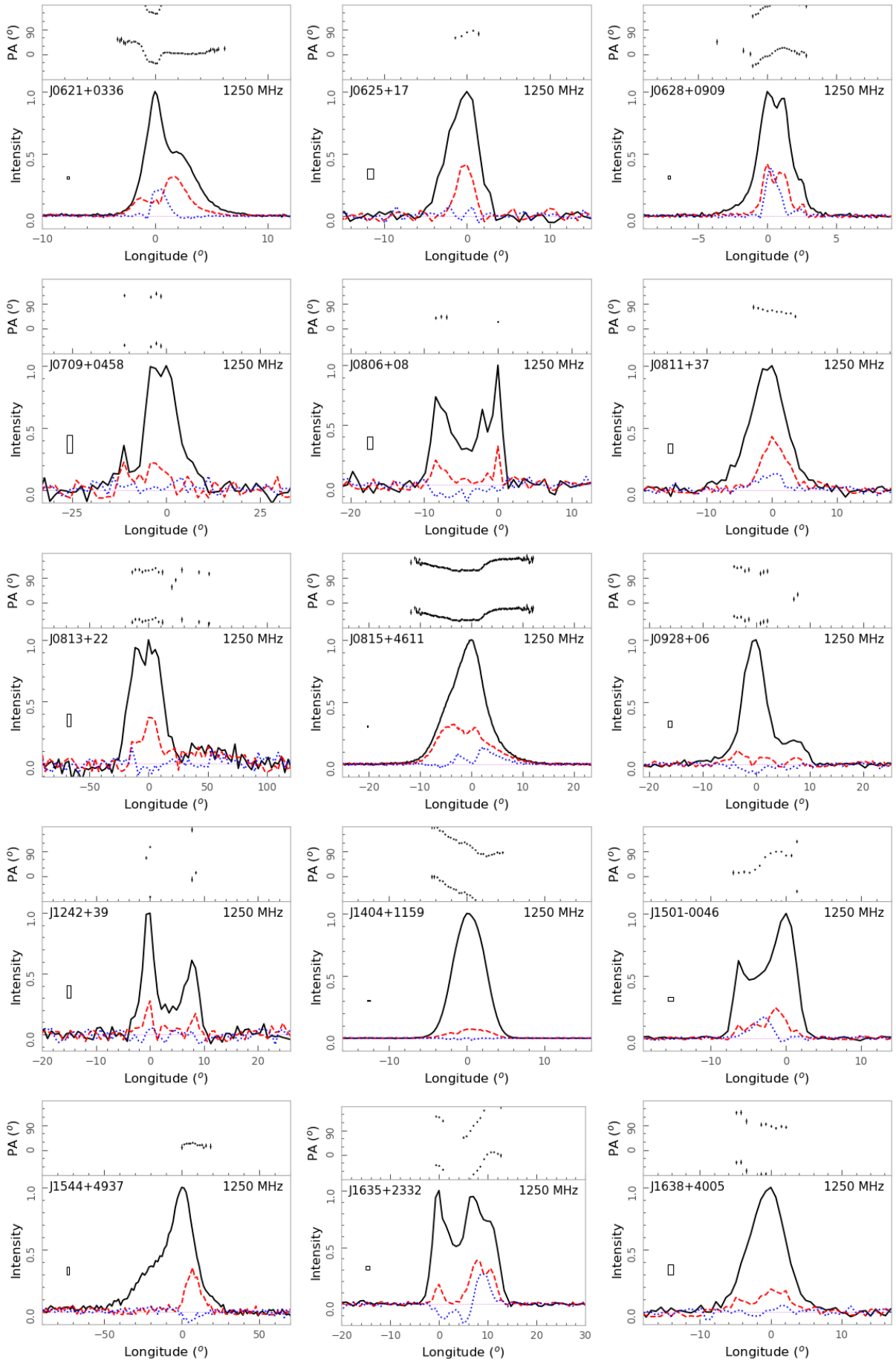

Fig. A.9 *– continued –*

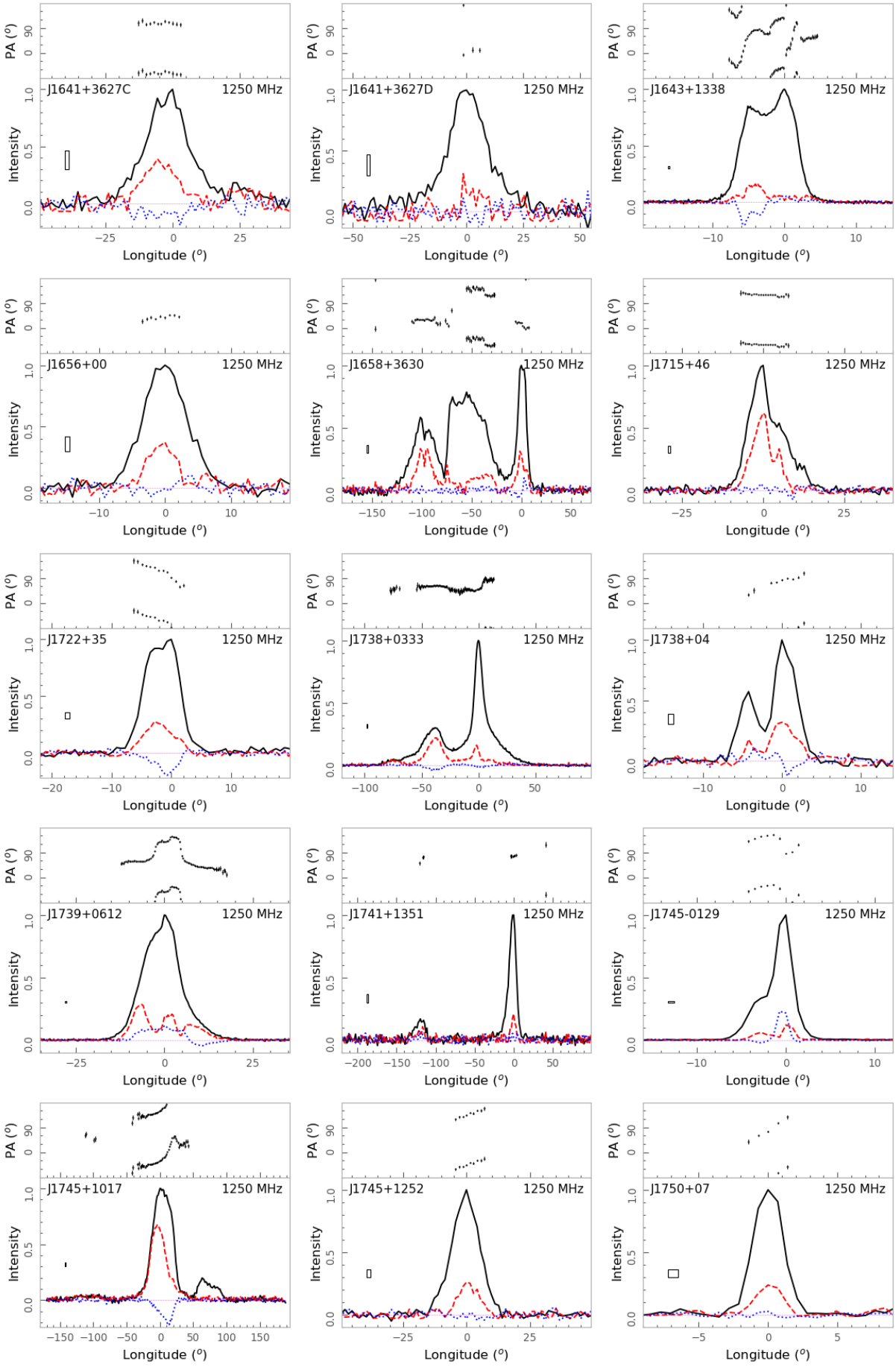

Fig. A.9 *– continued –*

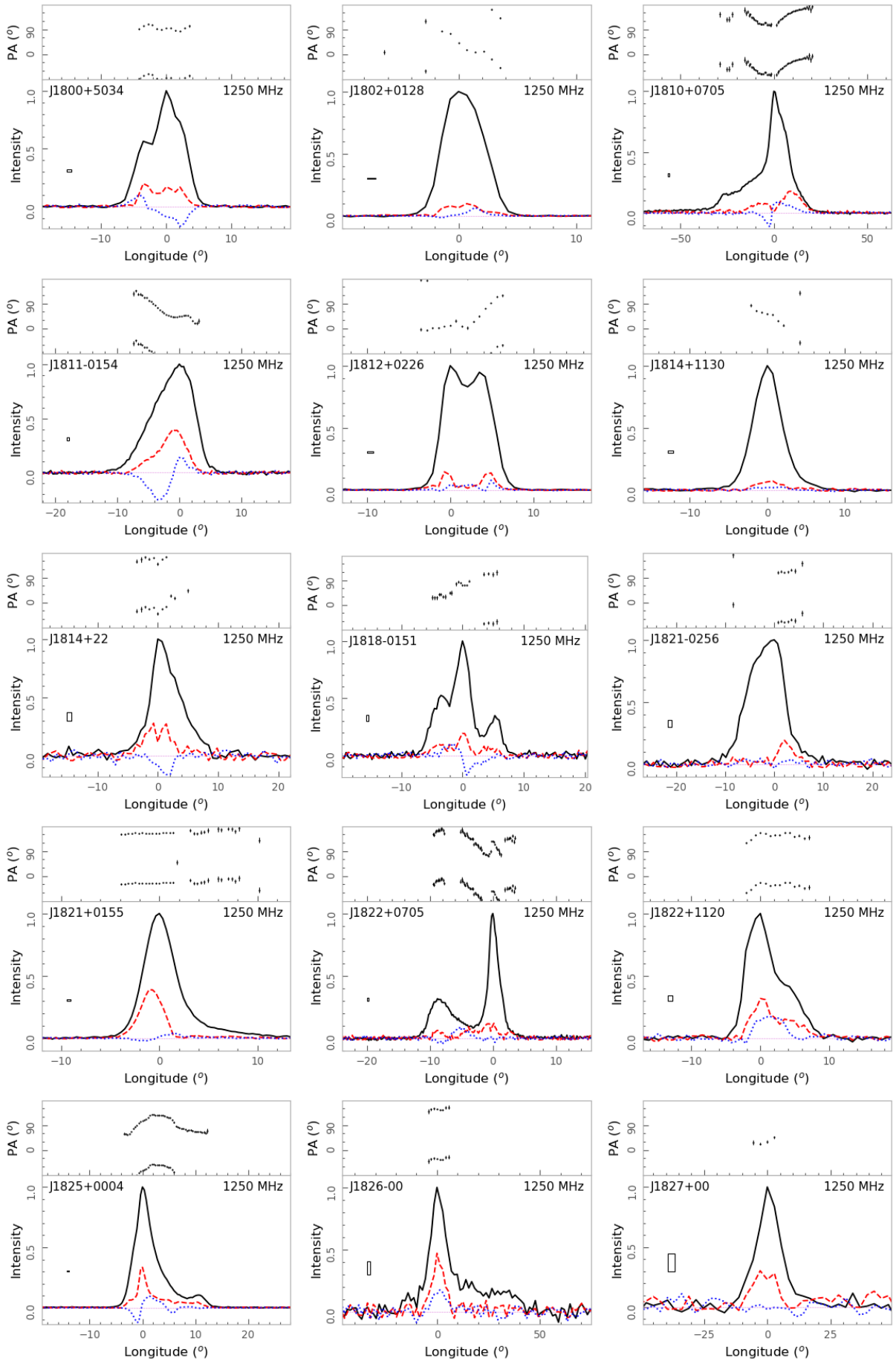

Fig. A.9 *– continued –*

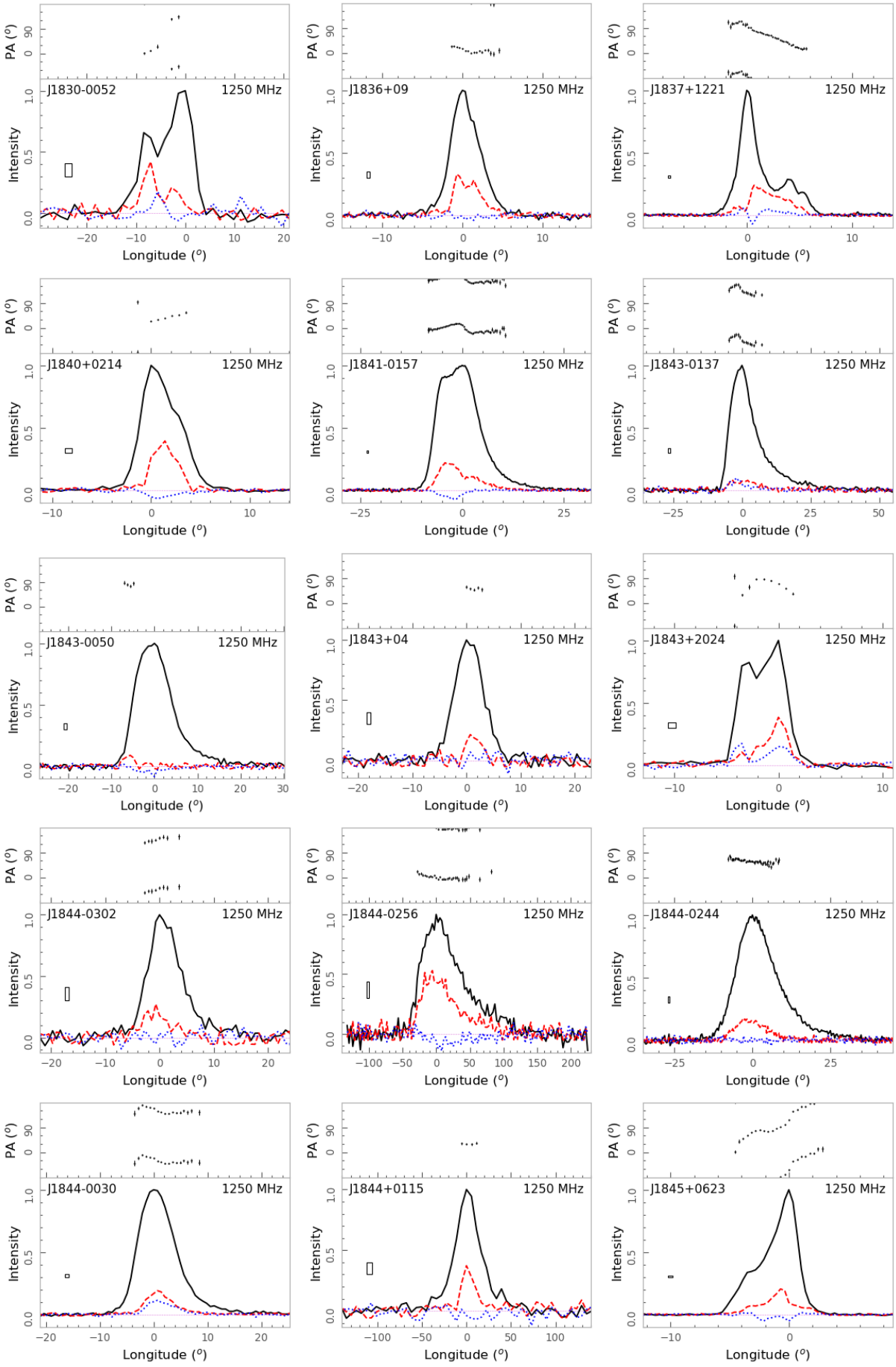

Fig. A.9 *– continued –*

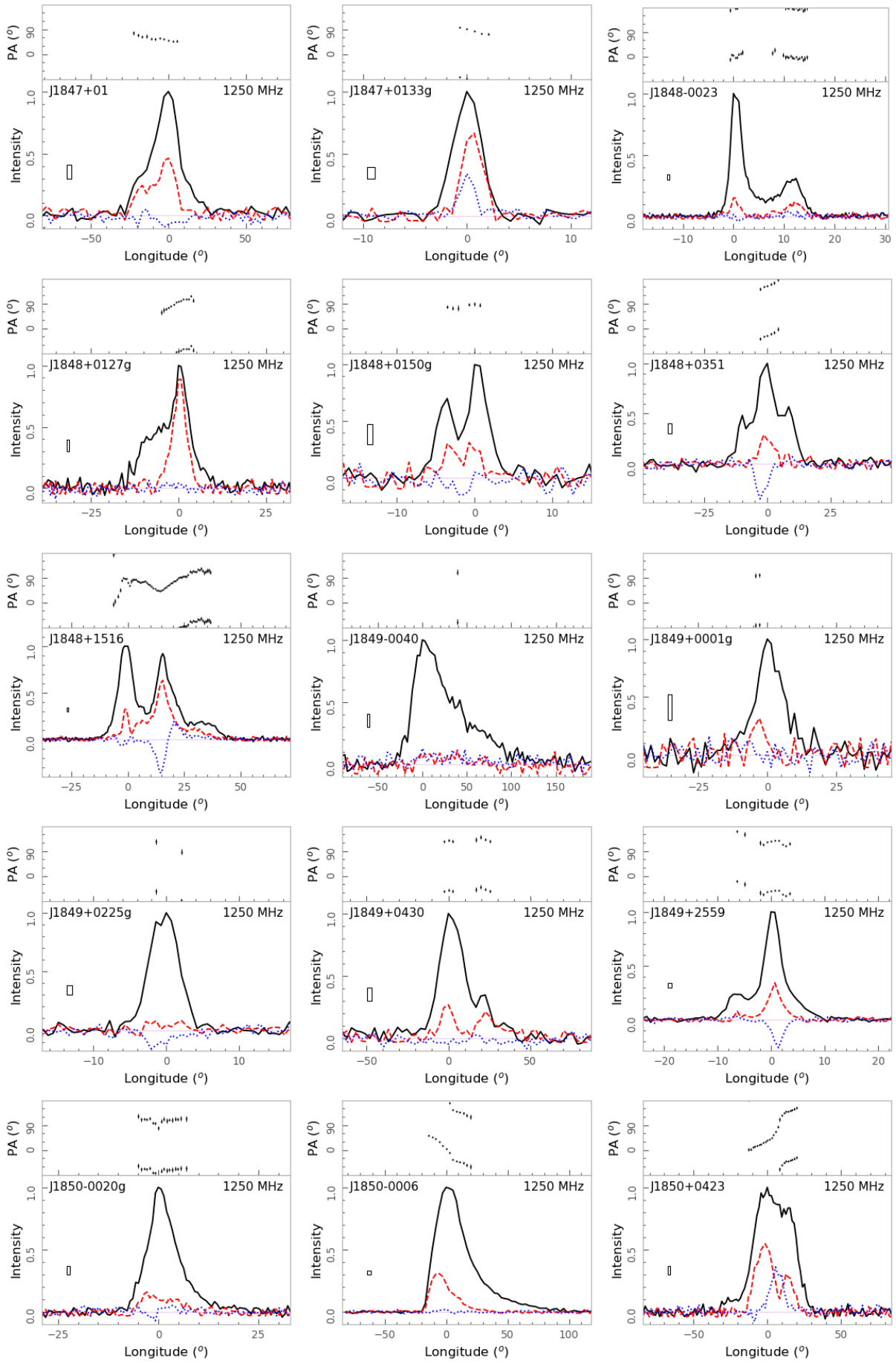

Fig. A.9 *– continued –*

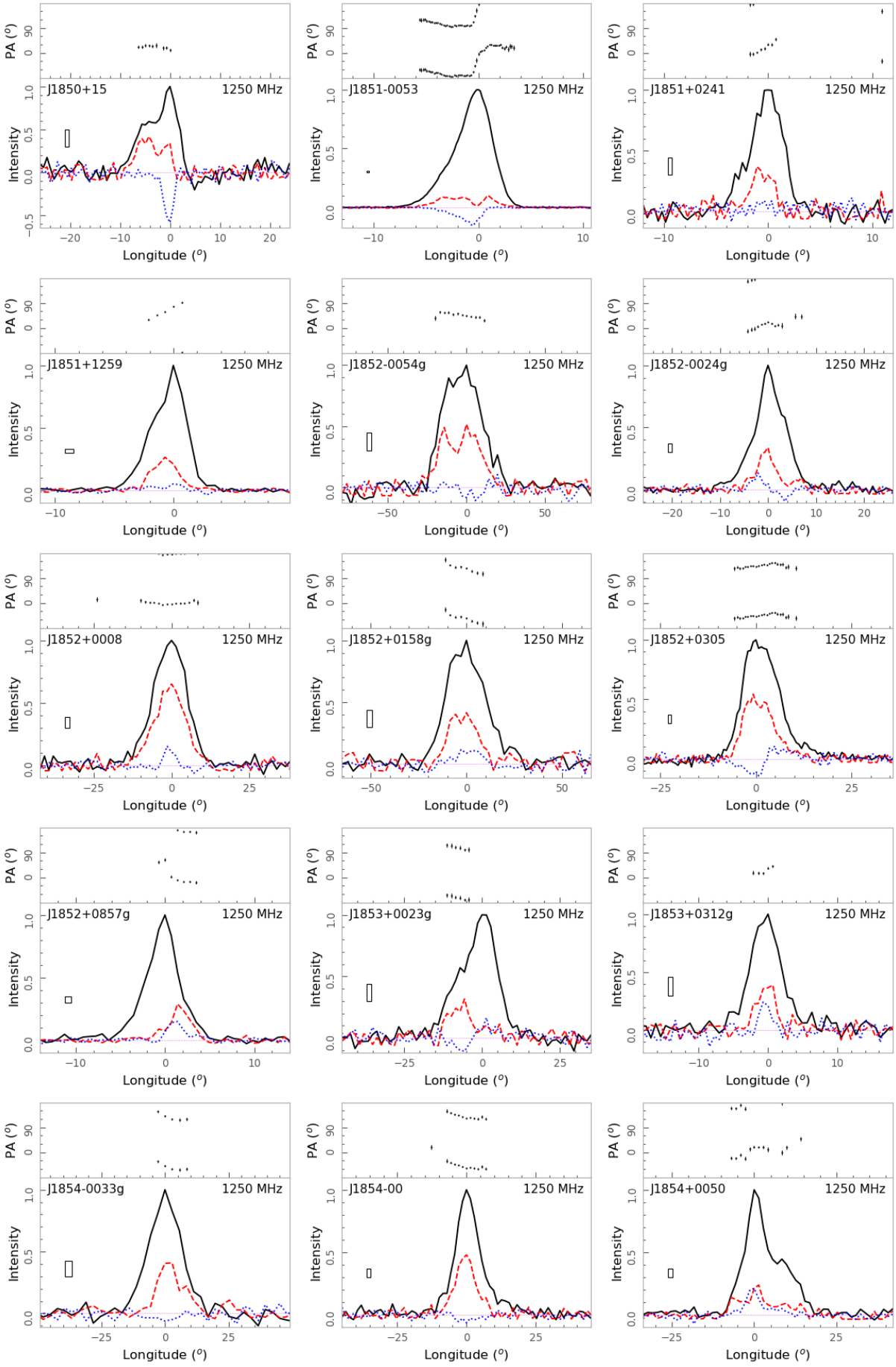

Fig. A.9 *– continued –*

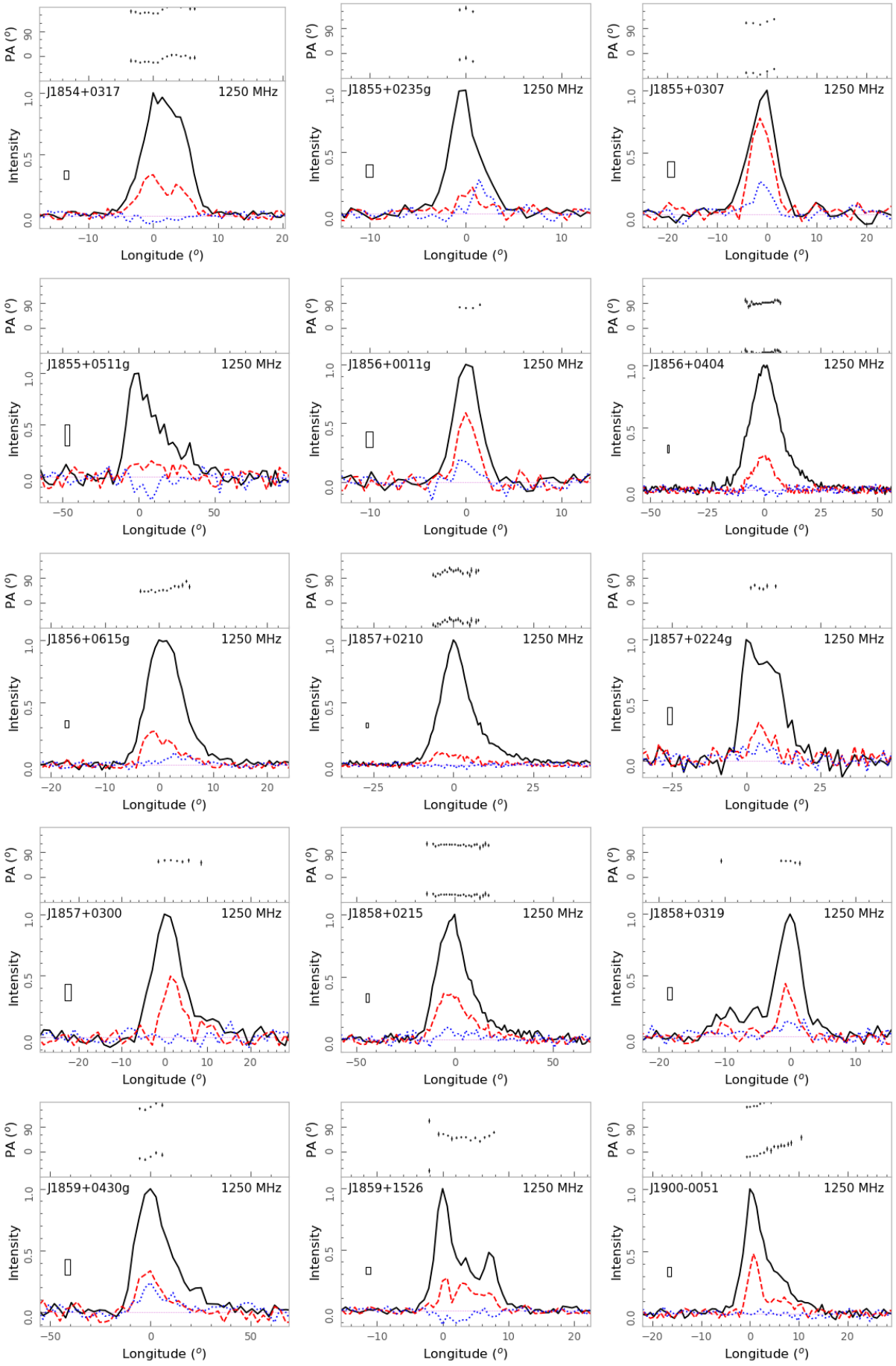

Fig. A.9 *– continued –*

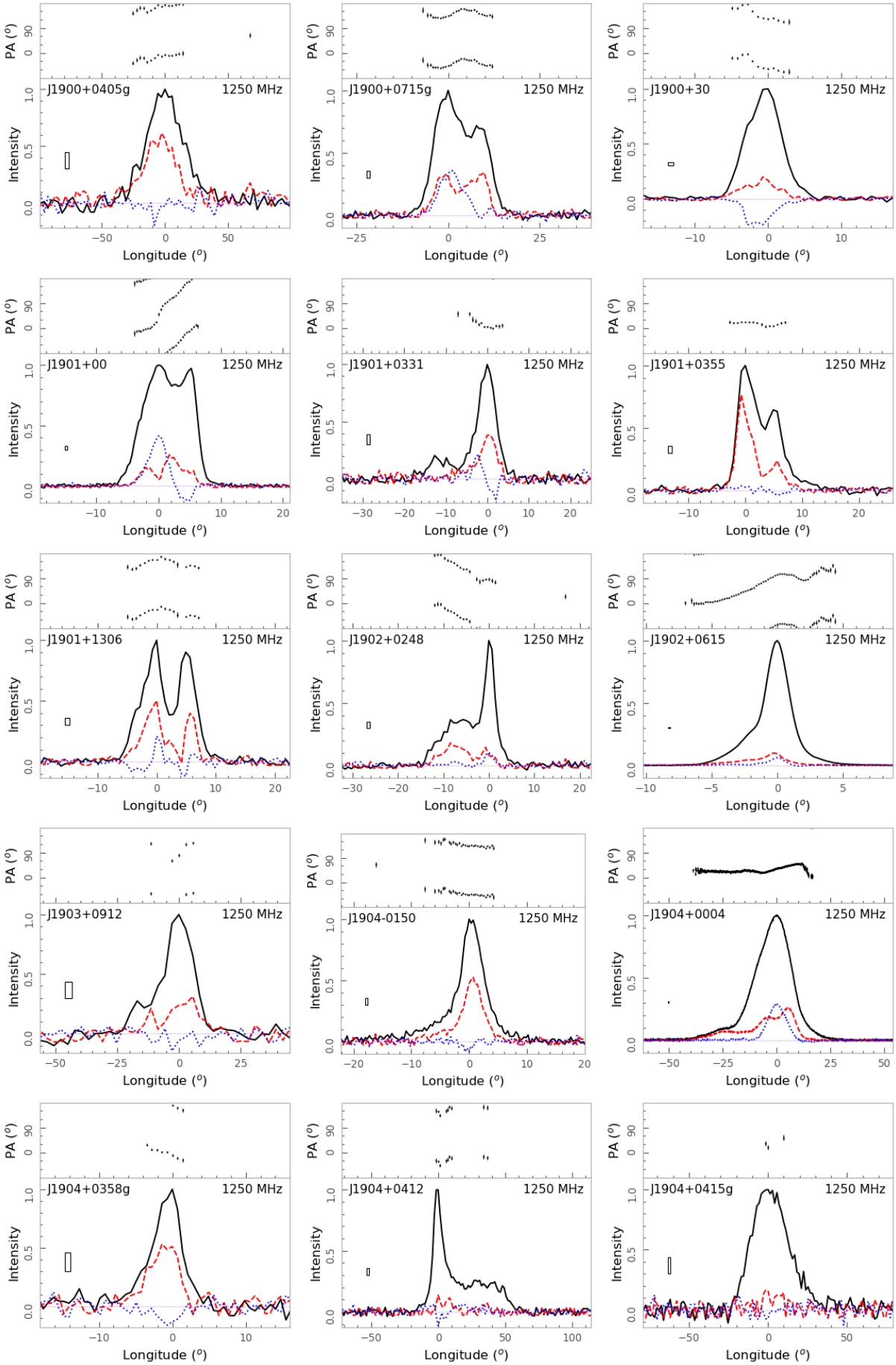

Fig. A.9 *– continued –*

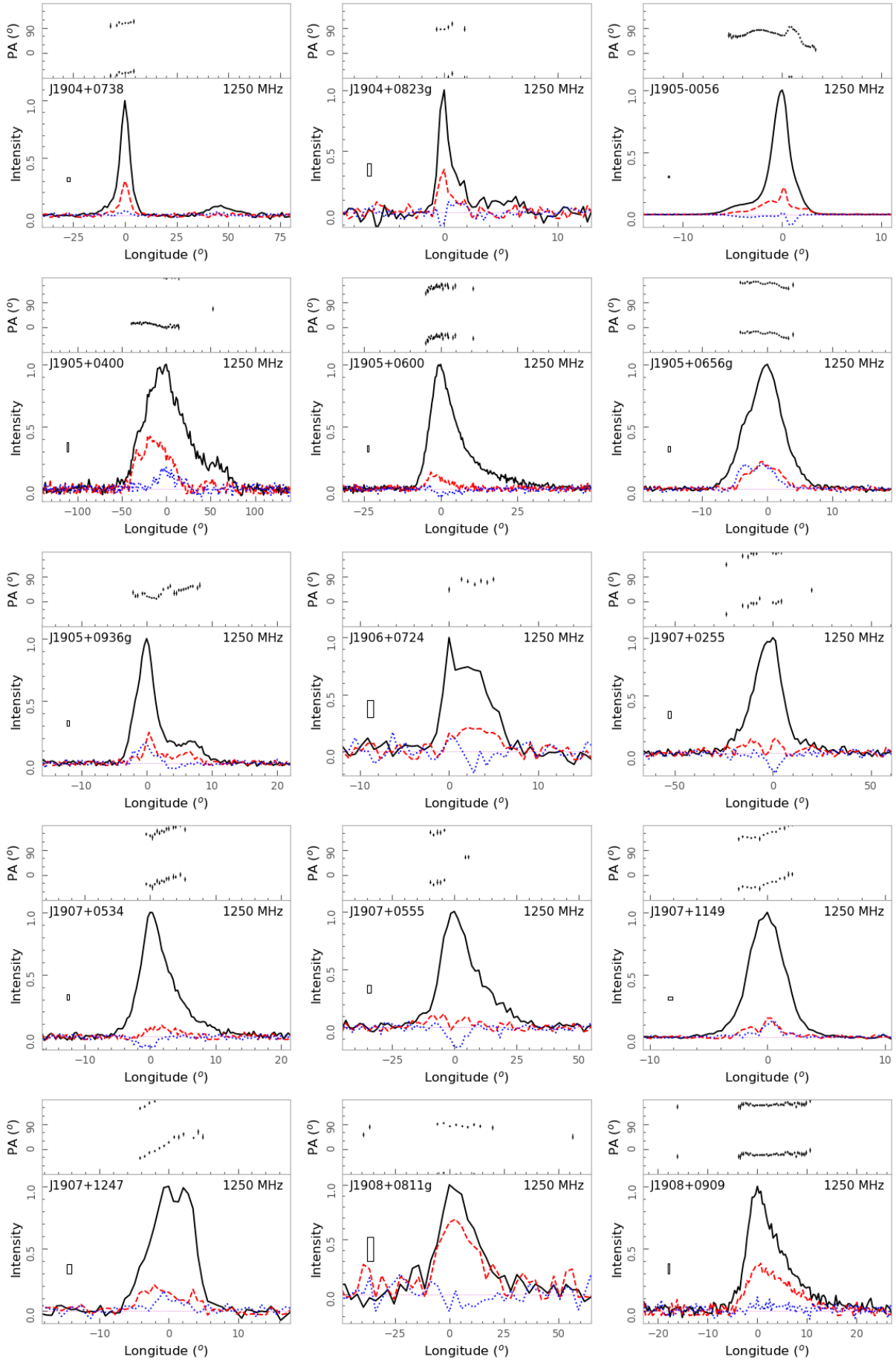

Fig. A.9 *– continued –*

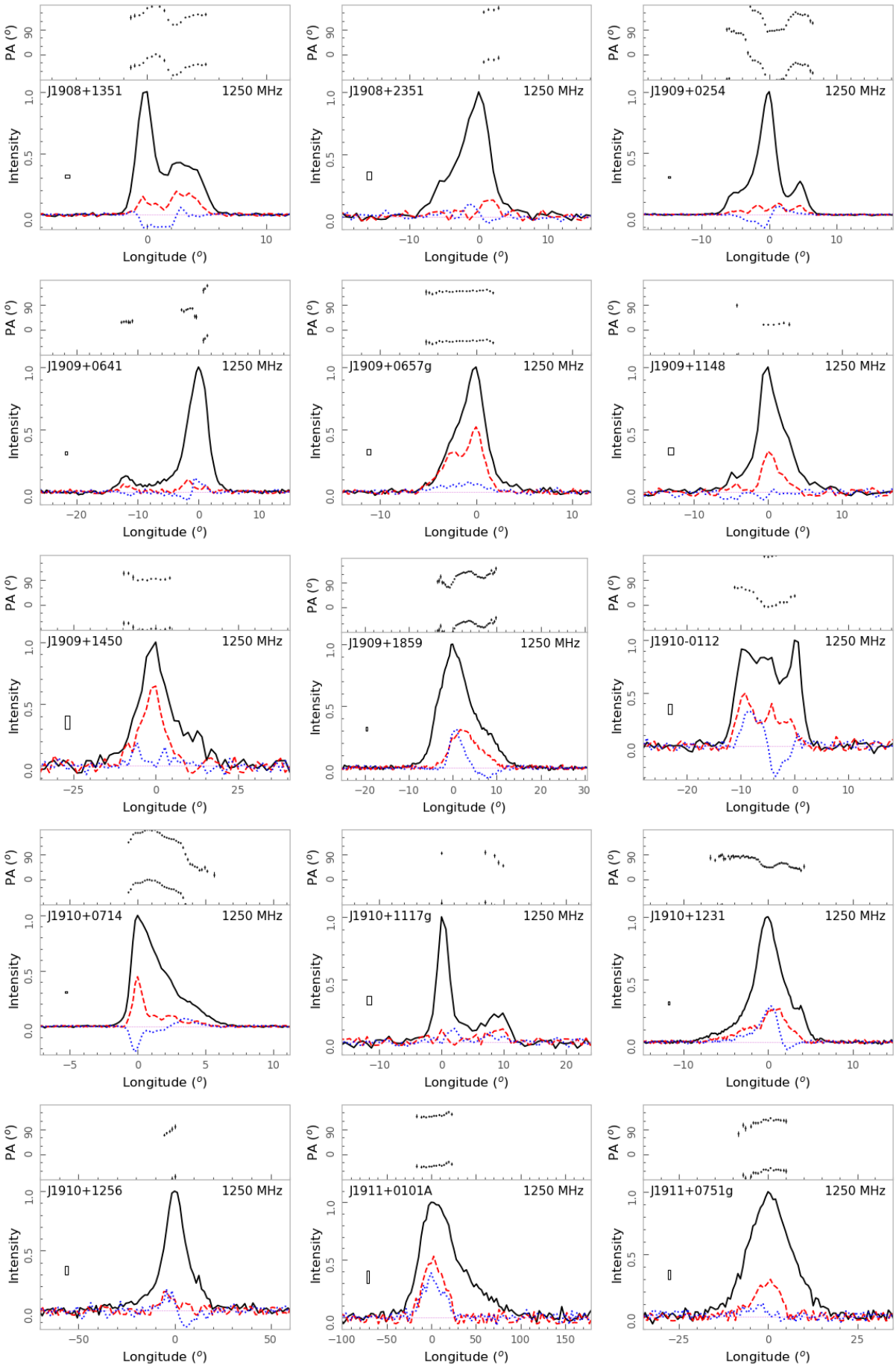

Fig. A.9 *– continued –*

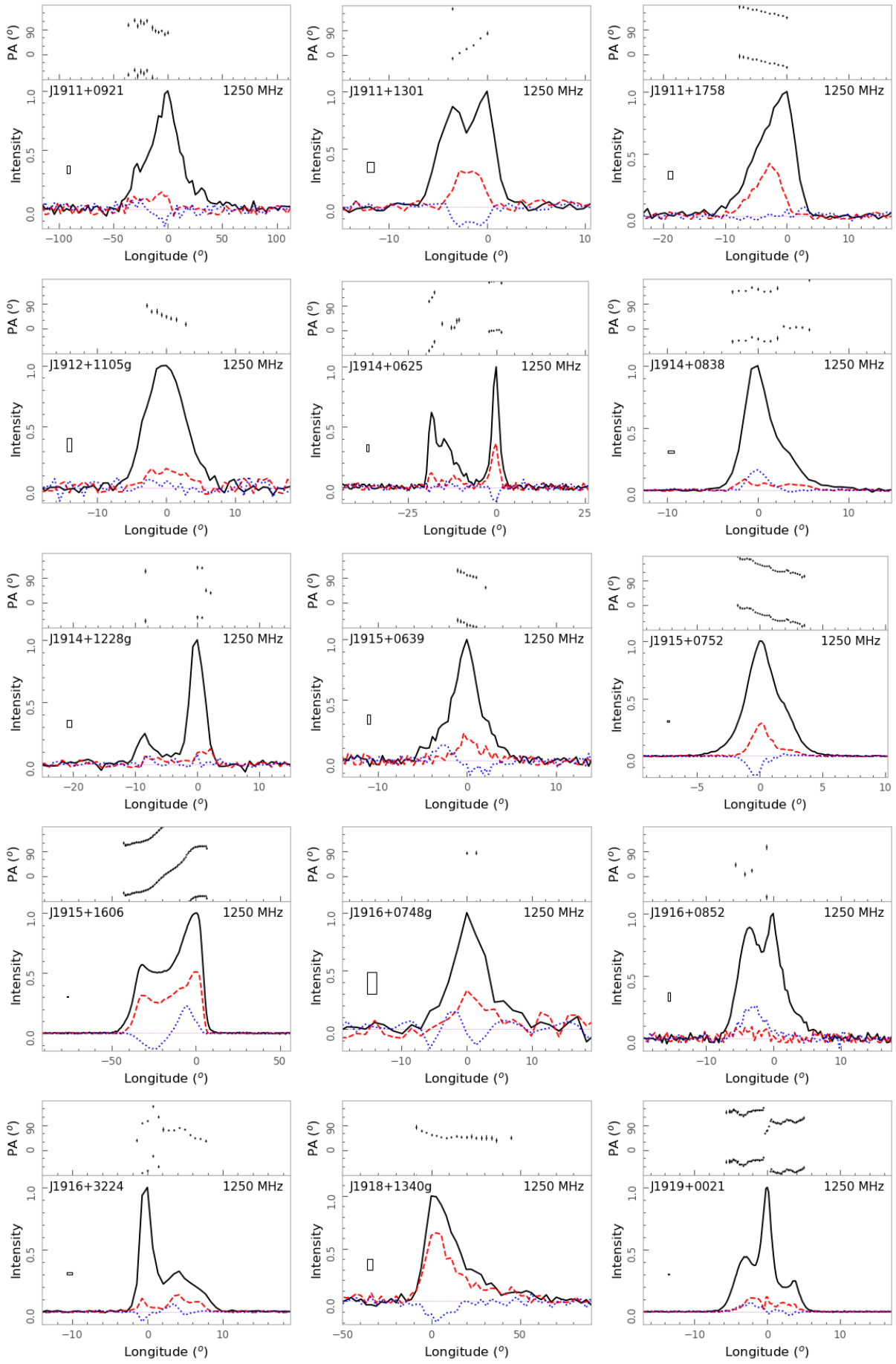

Fig. A.9 *– continued –*

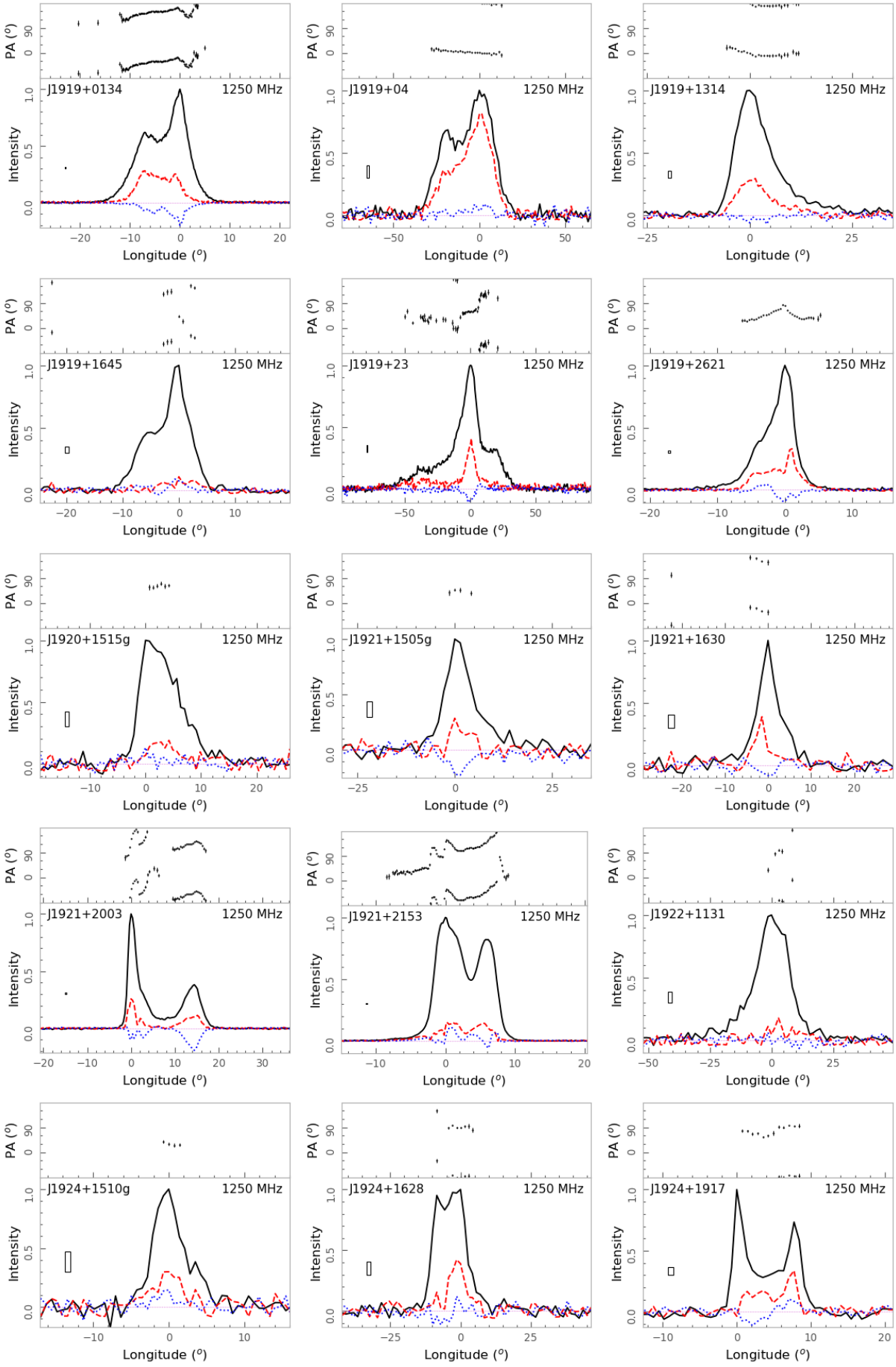

Fig. A.9 *– continued –*

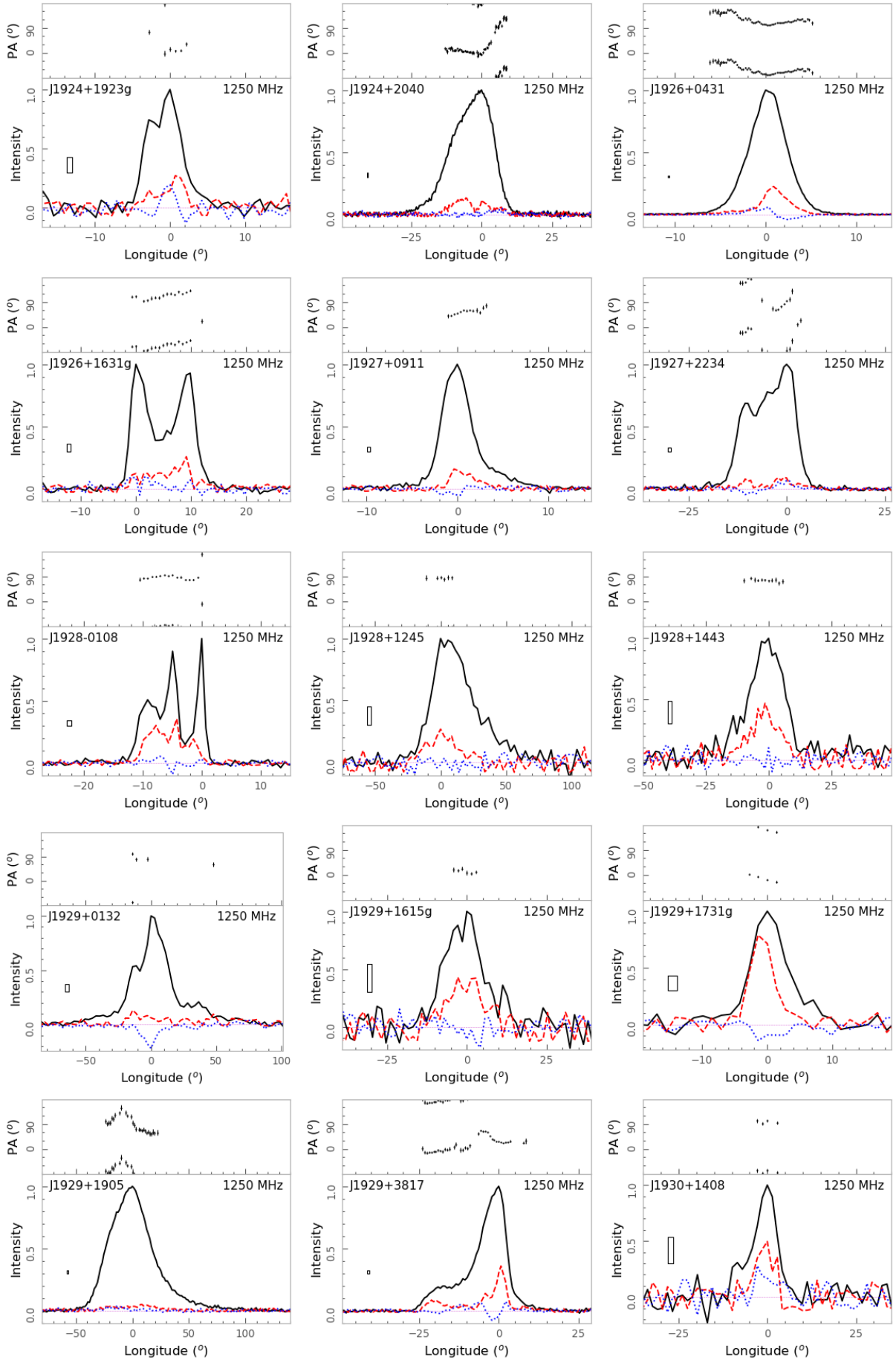

Fig. A.9 *– continued –*

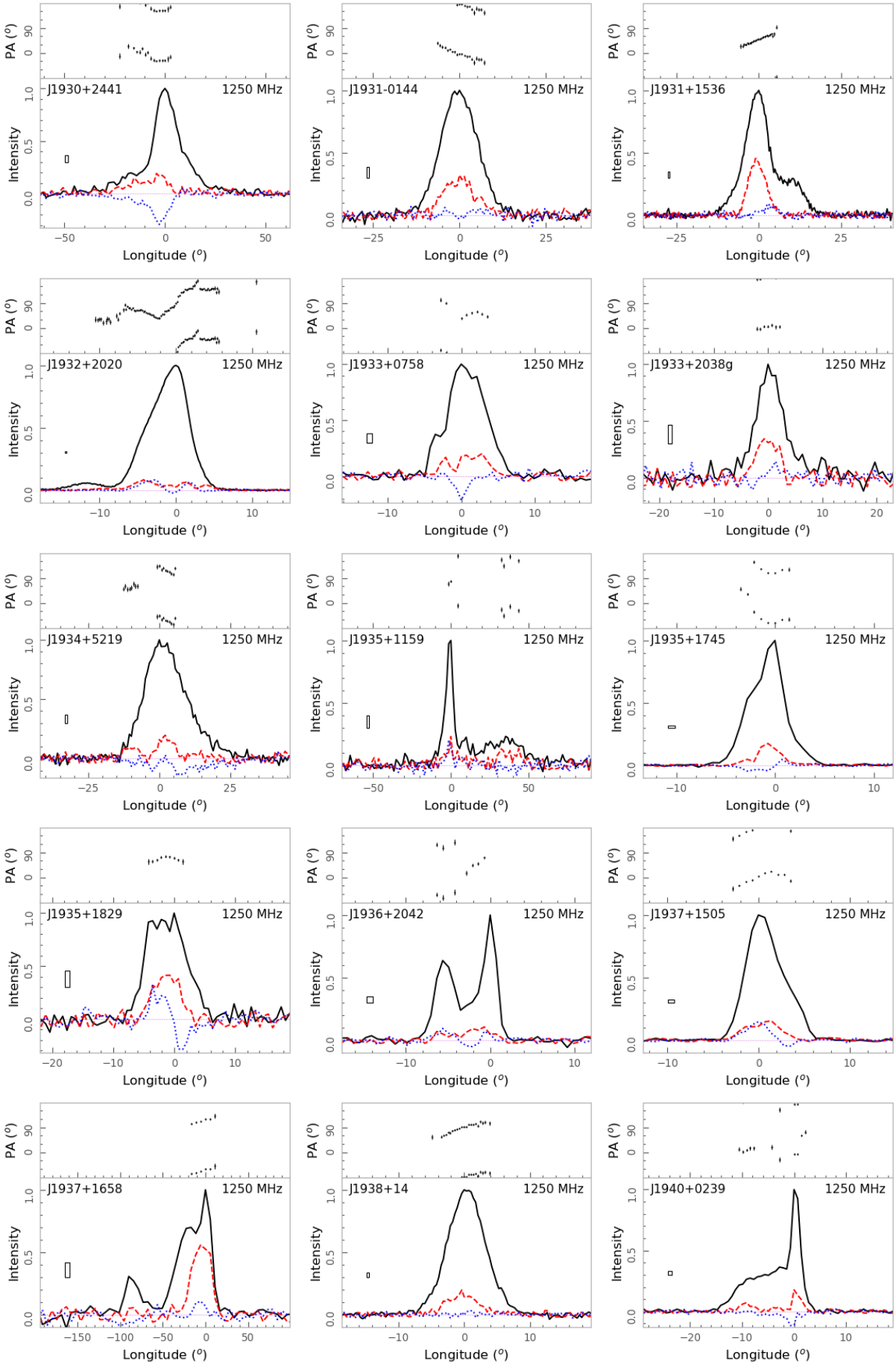

Fig. A.9 *– continued –*

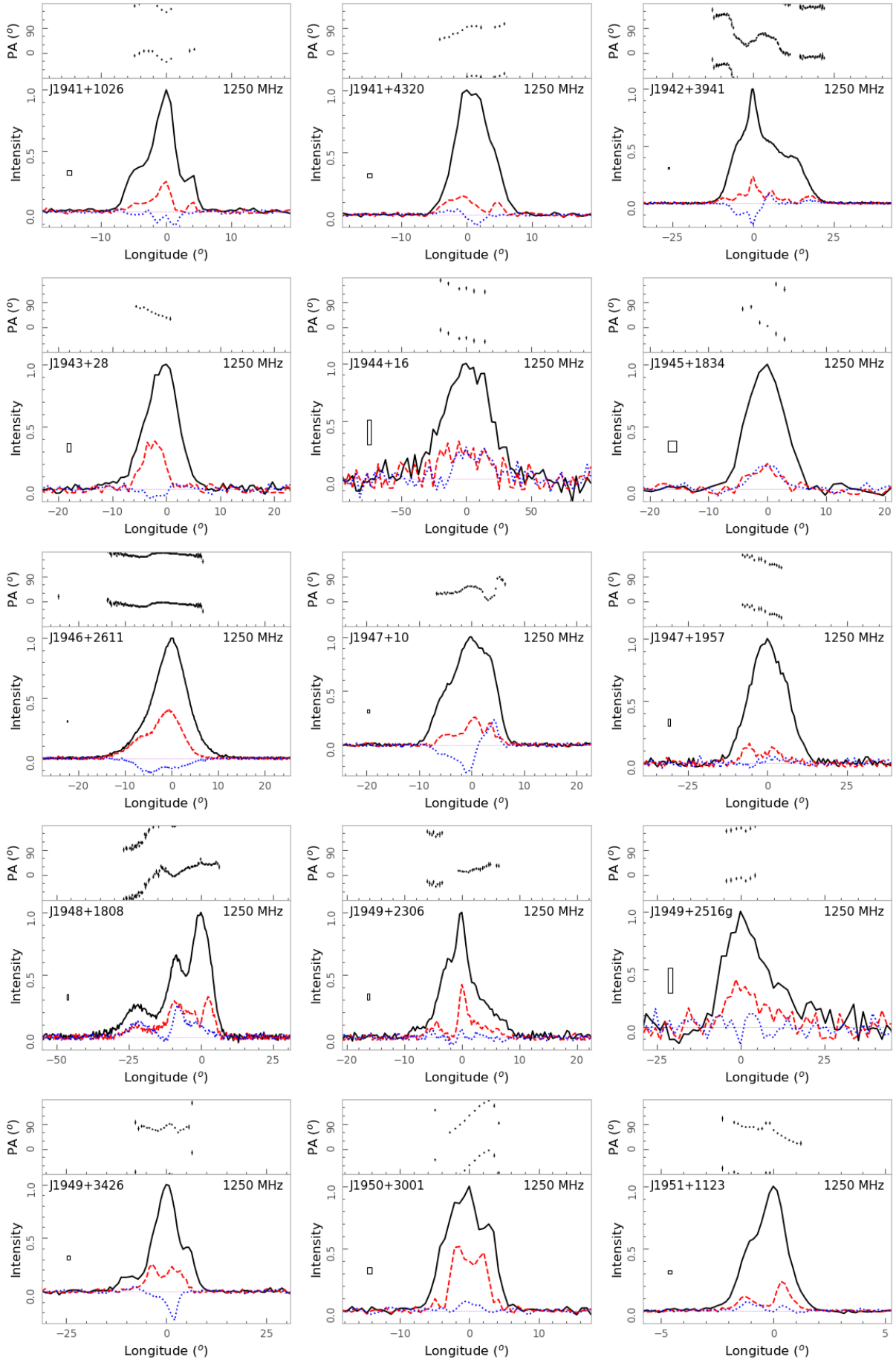

Fig. A.9 *– continued –*

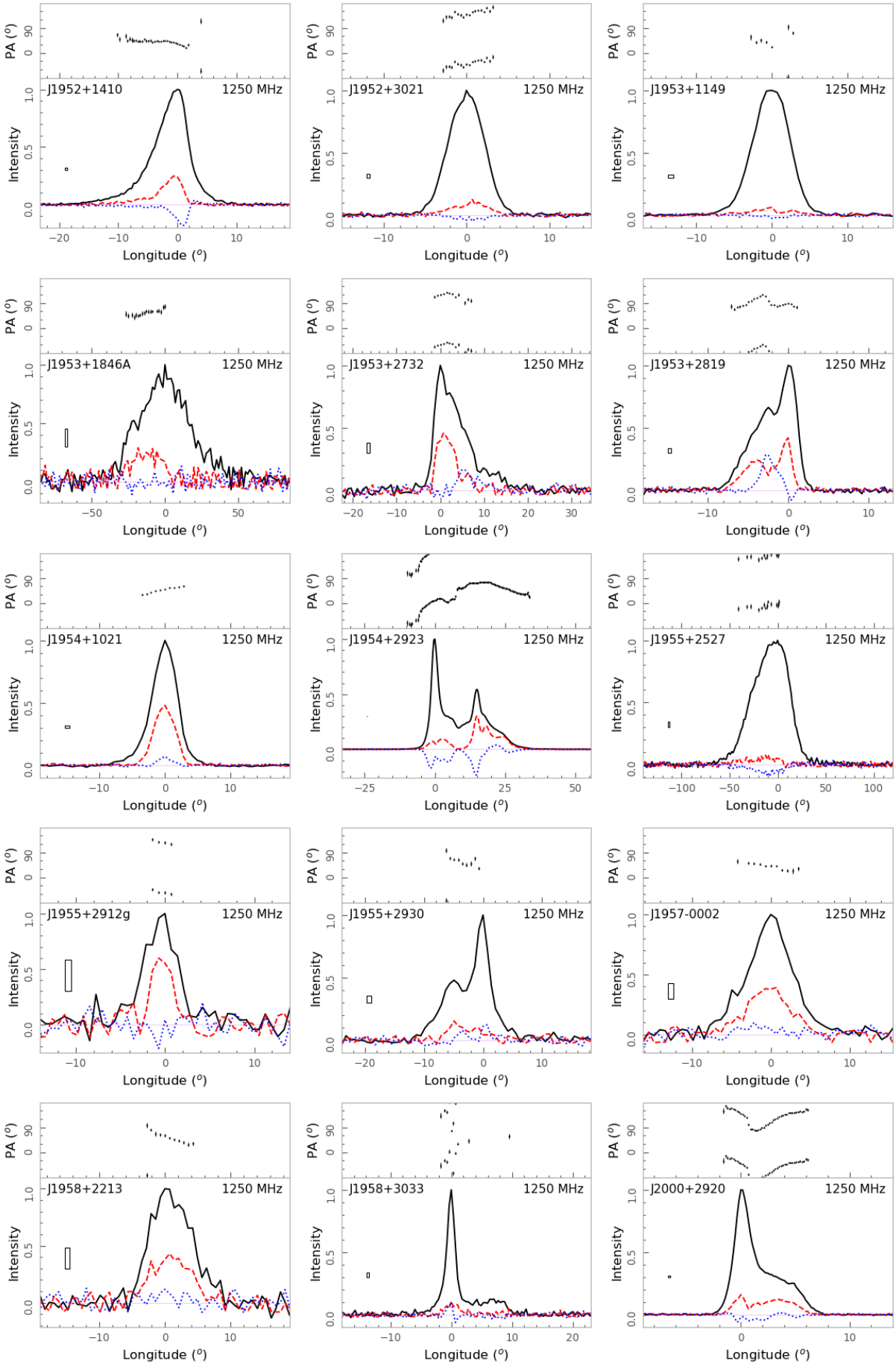

Fig. A.9 *– continued –*

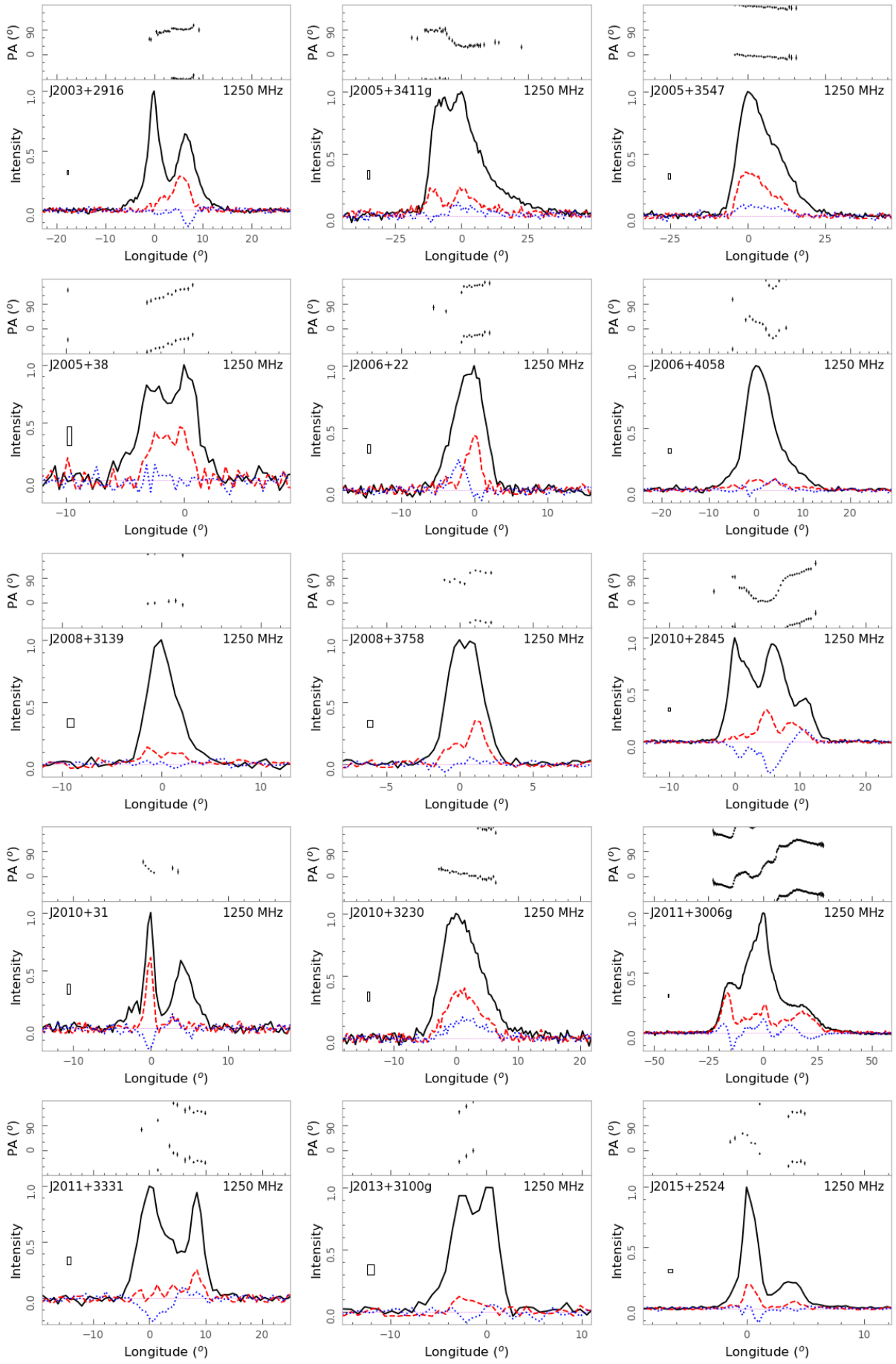

Fig. A.9 *– continued –*

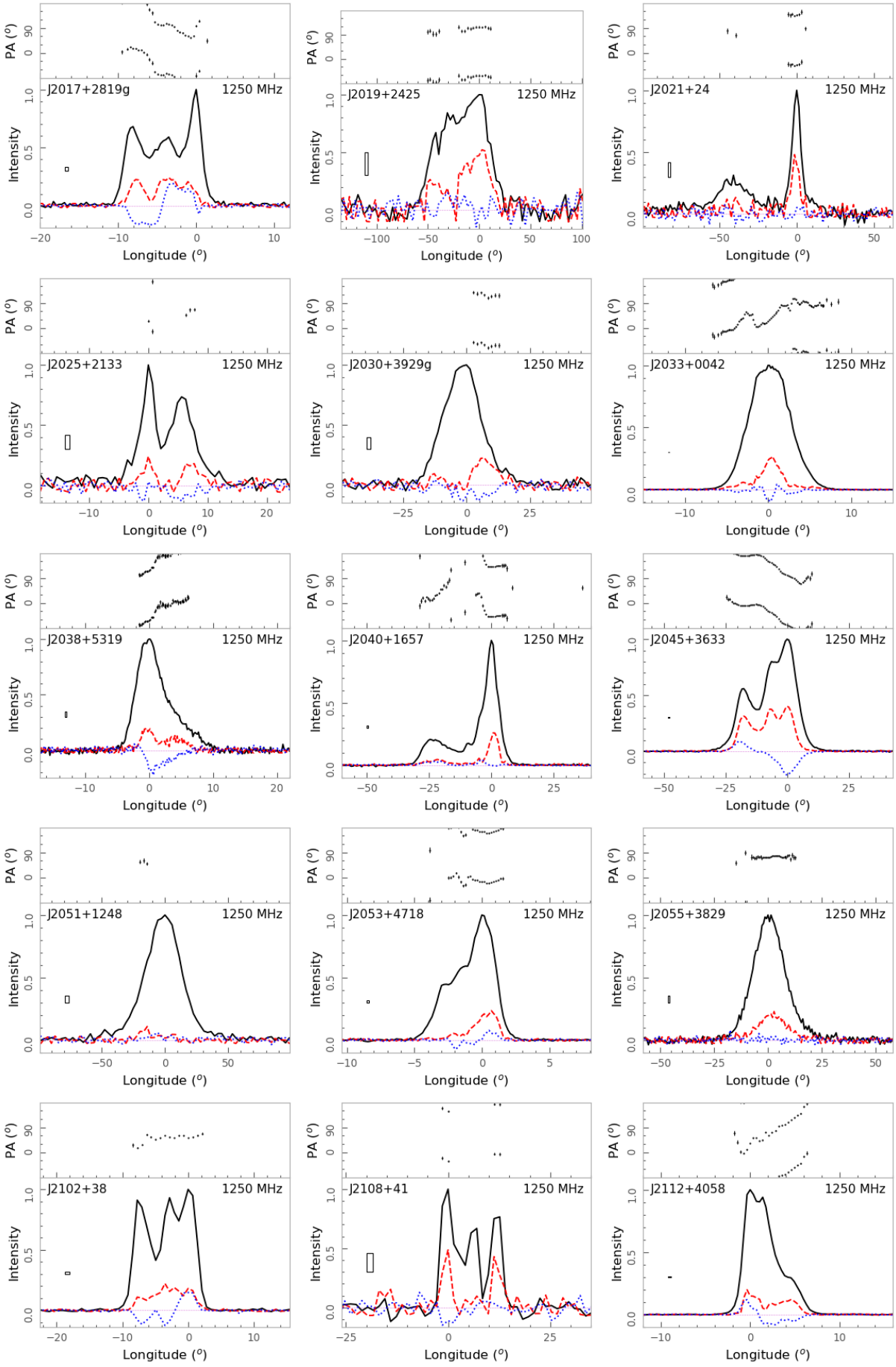

Fig. A.9 *– continued –*

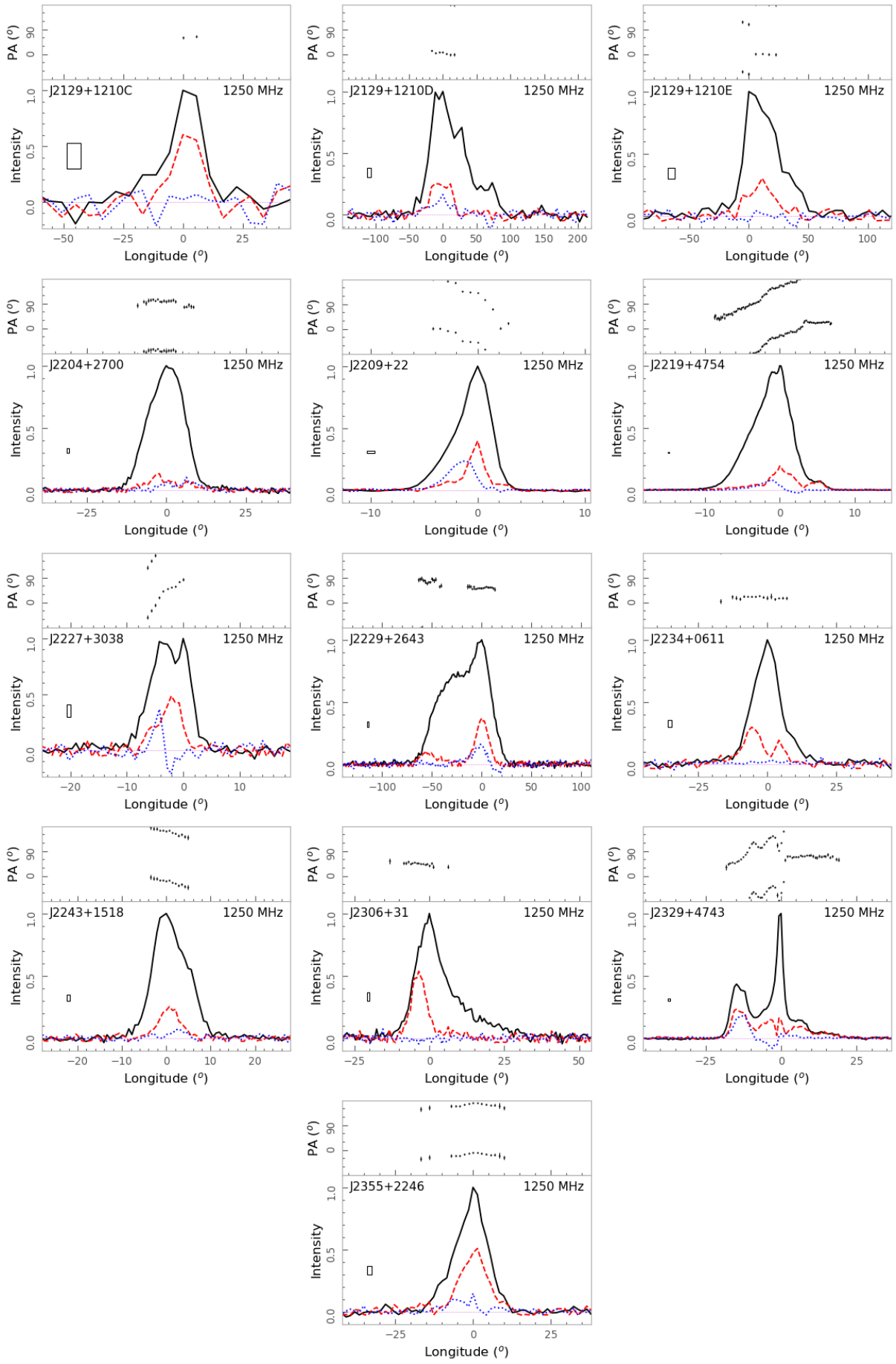
J2129+1210C 1250 MHz
J2129+1210D 1250 MHz
J2129+1210E 1250 MHz
J2204+2700 1250 MHz
J2209+22 1250 MHz
J2219+4754 1250 MHz
J2227+3038 1250 MHz
J2229+2643 1250 MHz
J2234+0611 1250 MHz
J2243+1518 1250 MHz
J2306+31 1250 MHz
J2329+4743 1250 MHz
J2355+2246 1250 MHz
PA (°)
Intensity
Longitude (°)

Fig. A.9 – *end.*

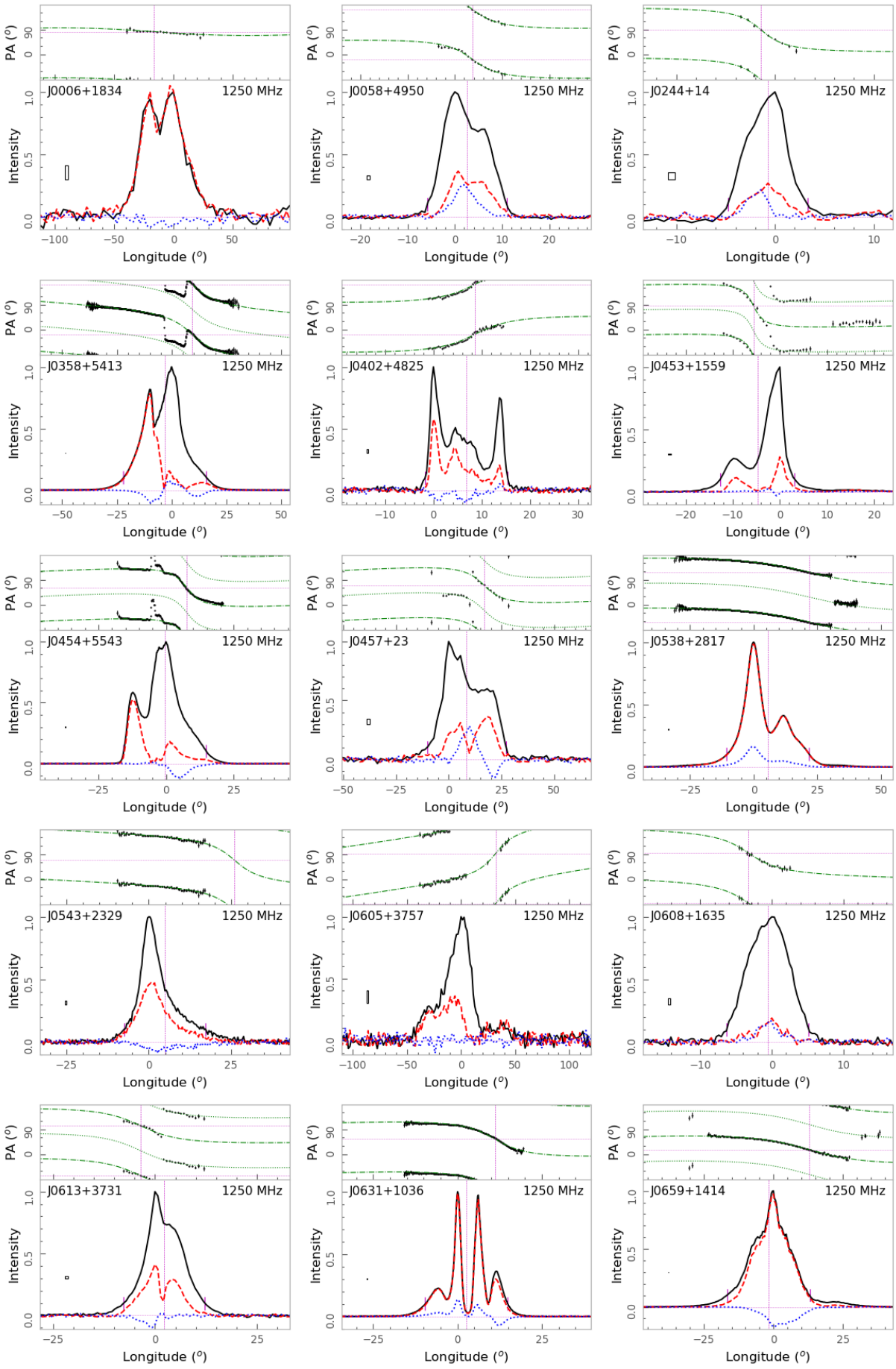

Fig. B.1 RVM fitting to the PA curves of 190 pulsars. See the keys in Figure 18. – *to be continued* –

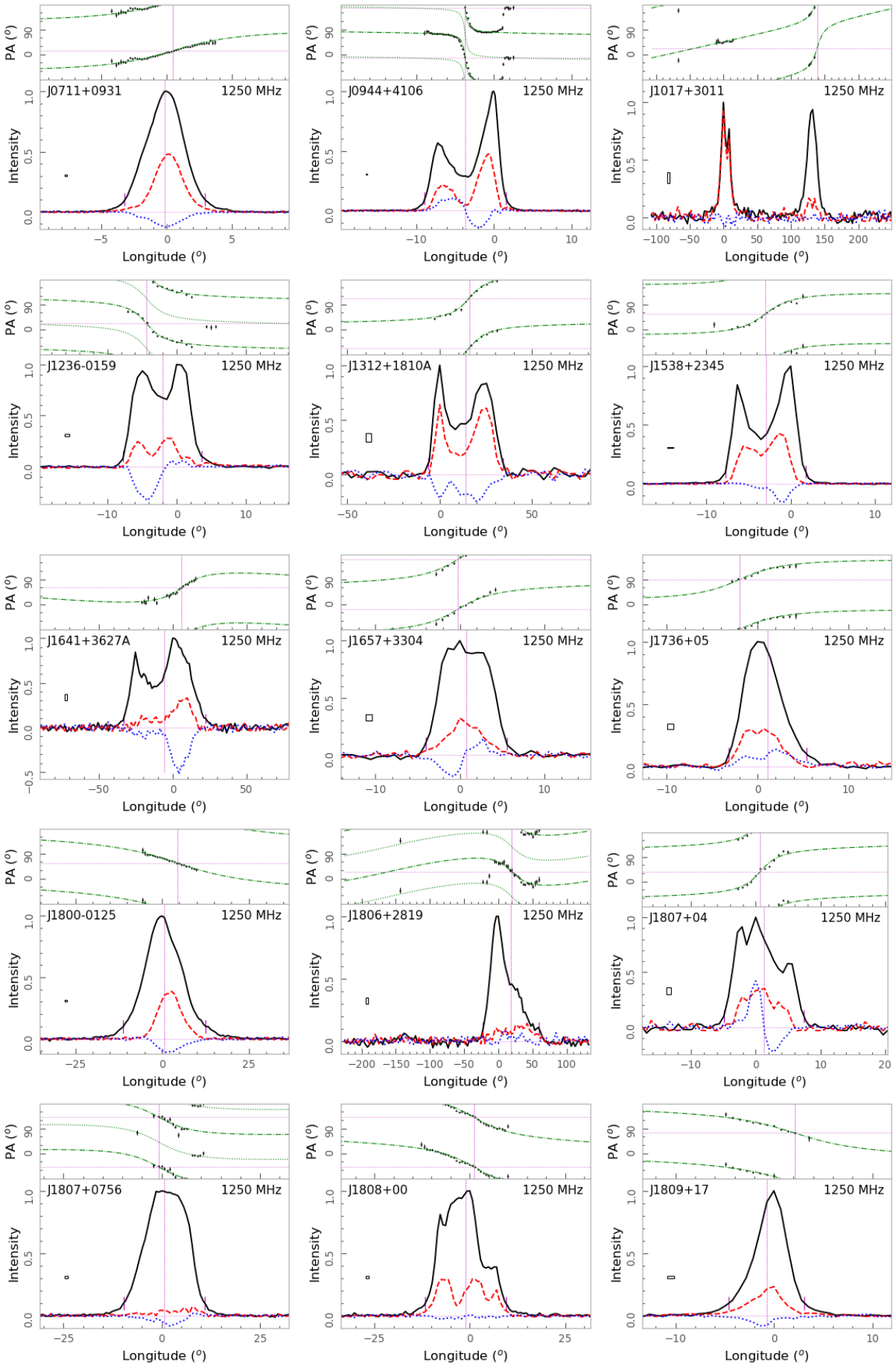

Fig. B.1 *– continued –*

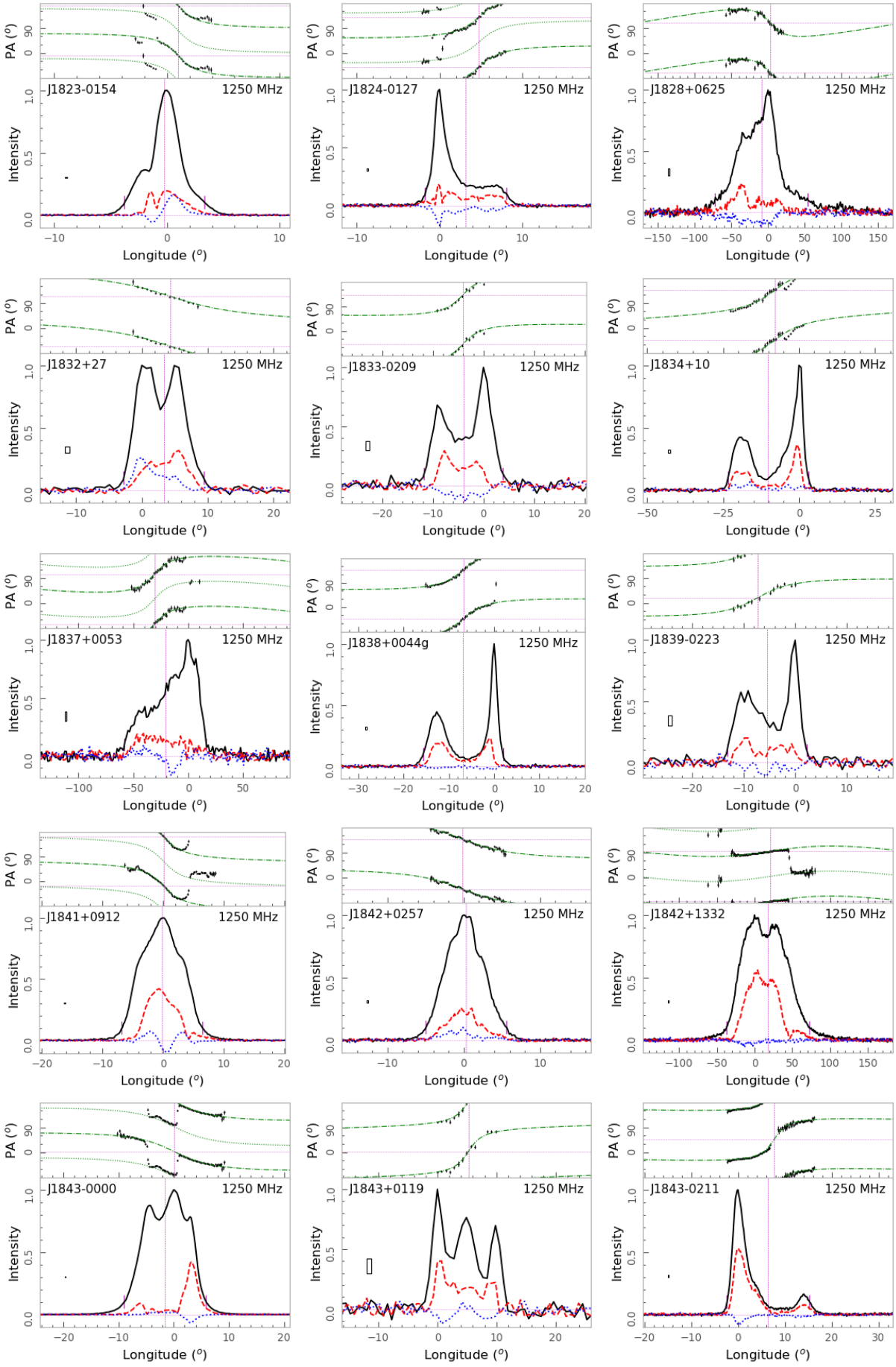

Fig. B.1 *– continued –*

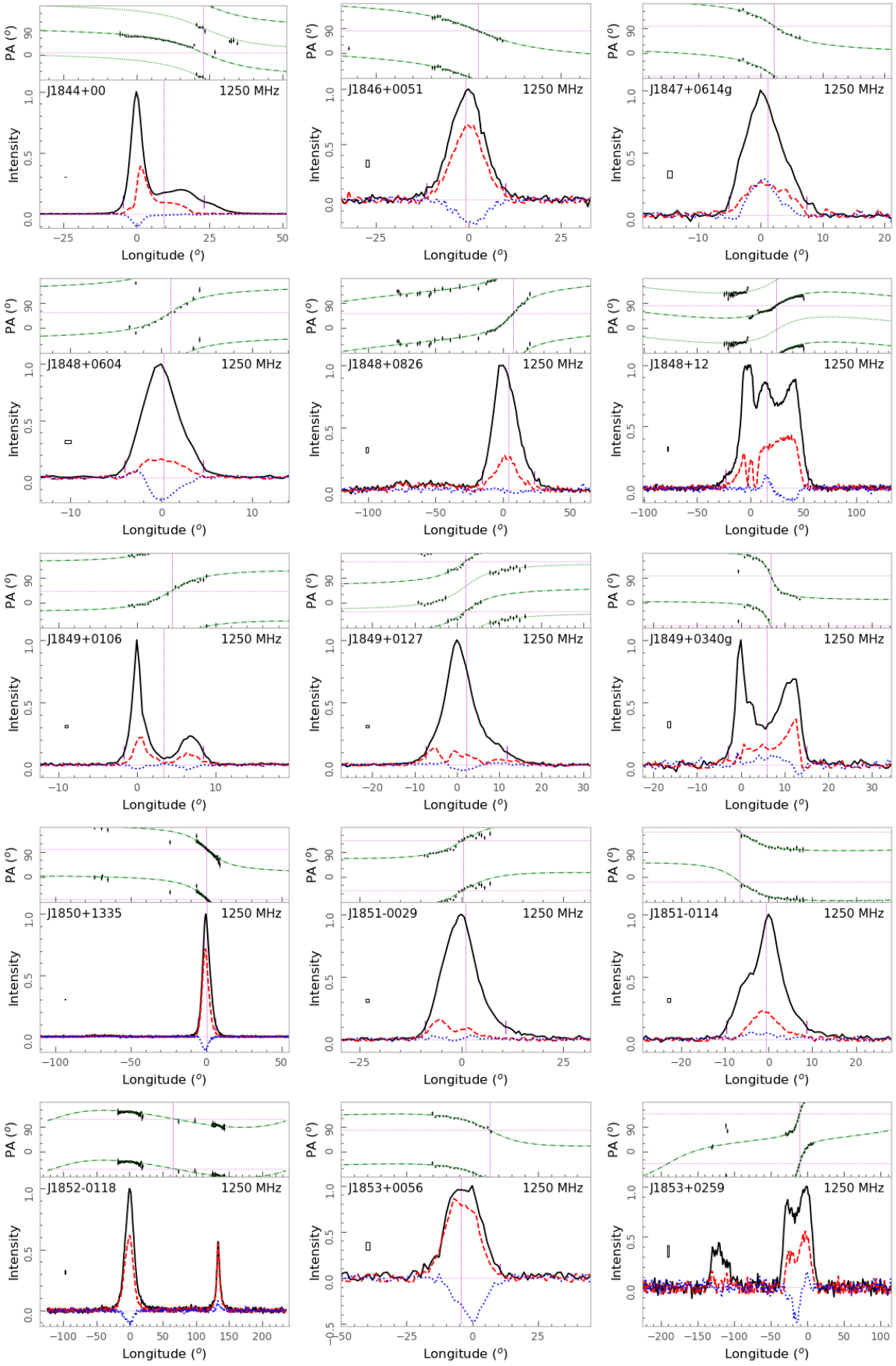

Fig. B.1 *– continued –*

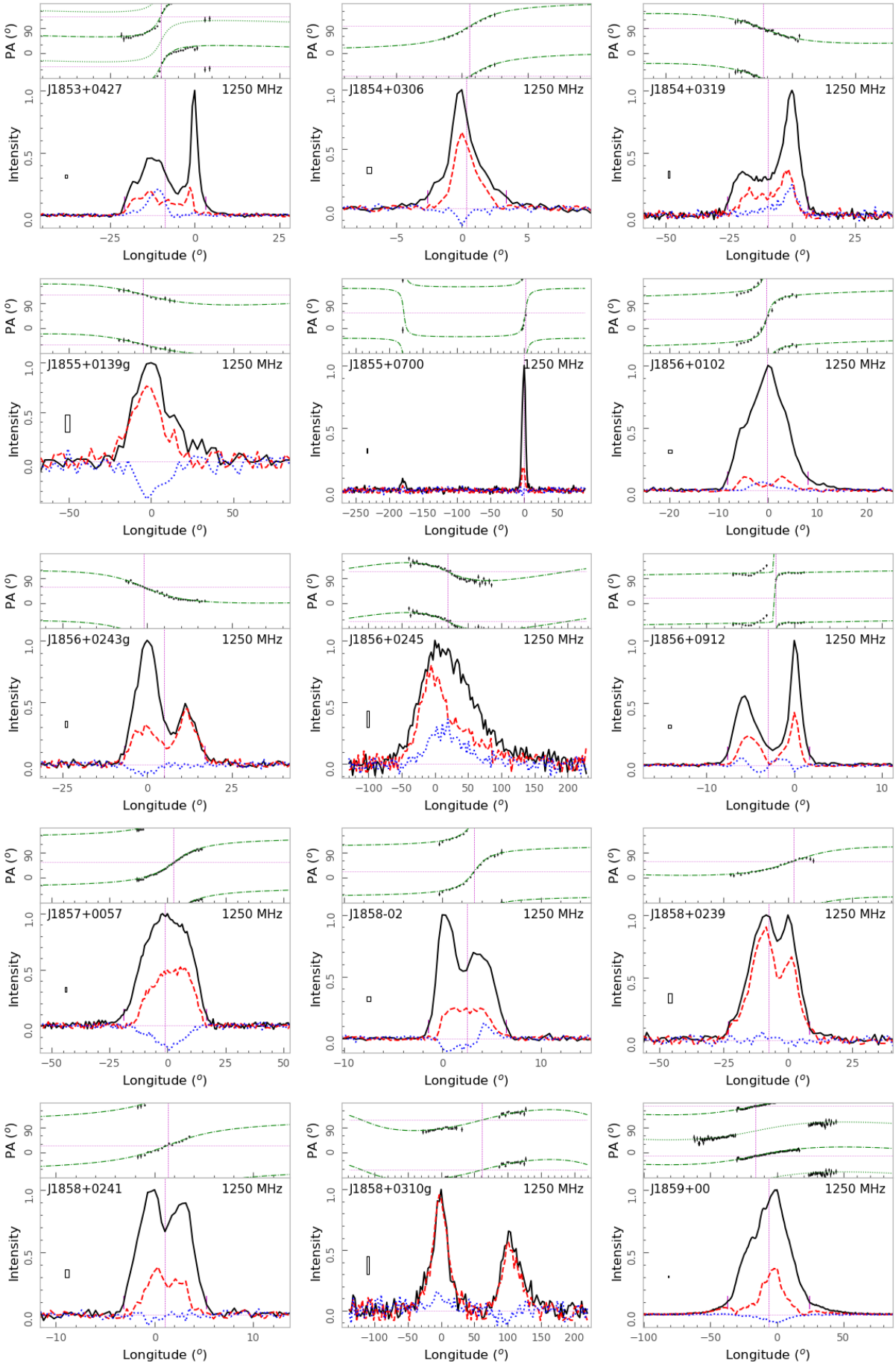

Fig. B.1 *– continued –*

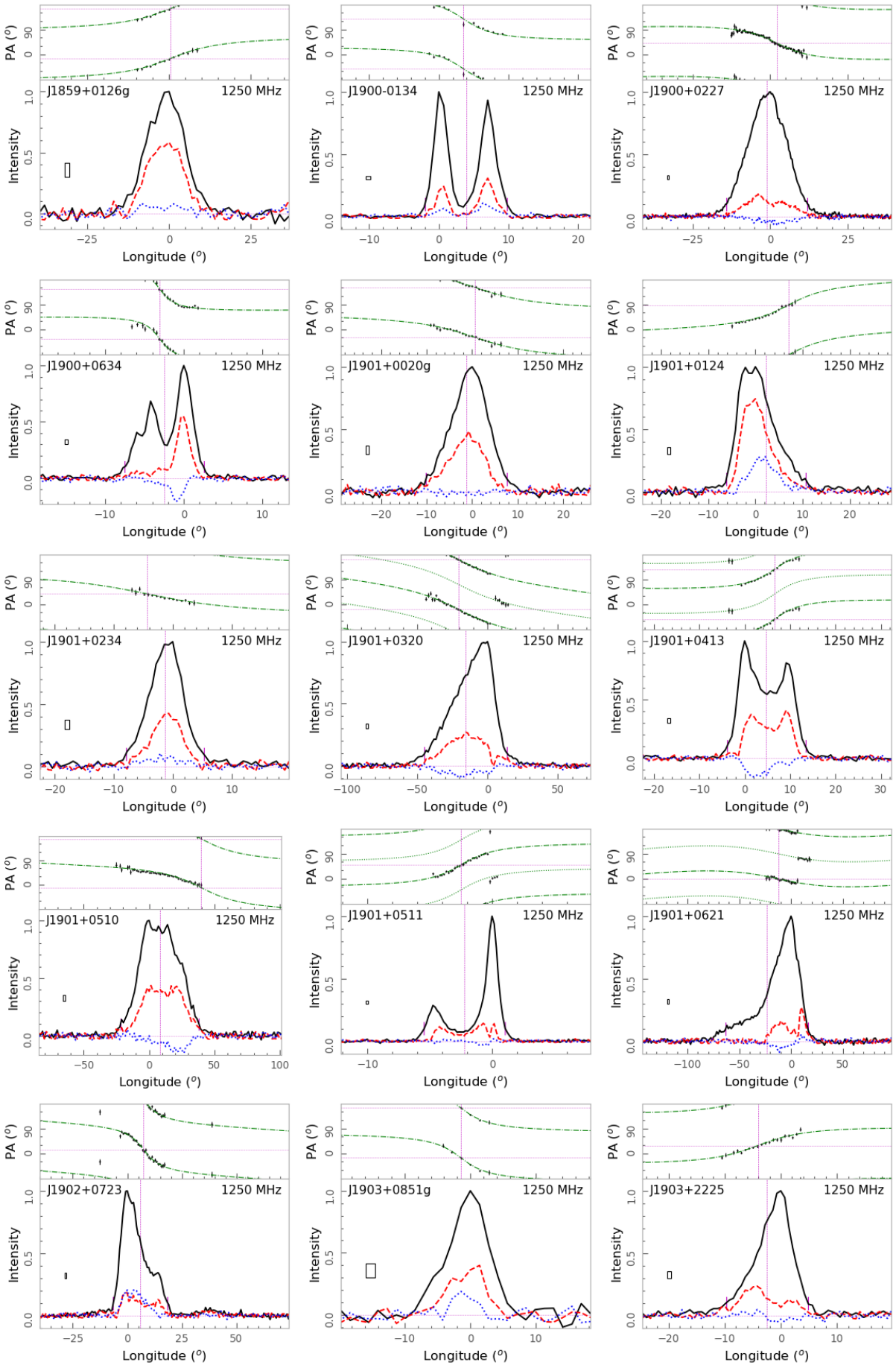

Fig. B.1 *– continued –*

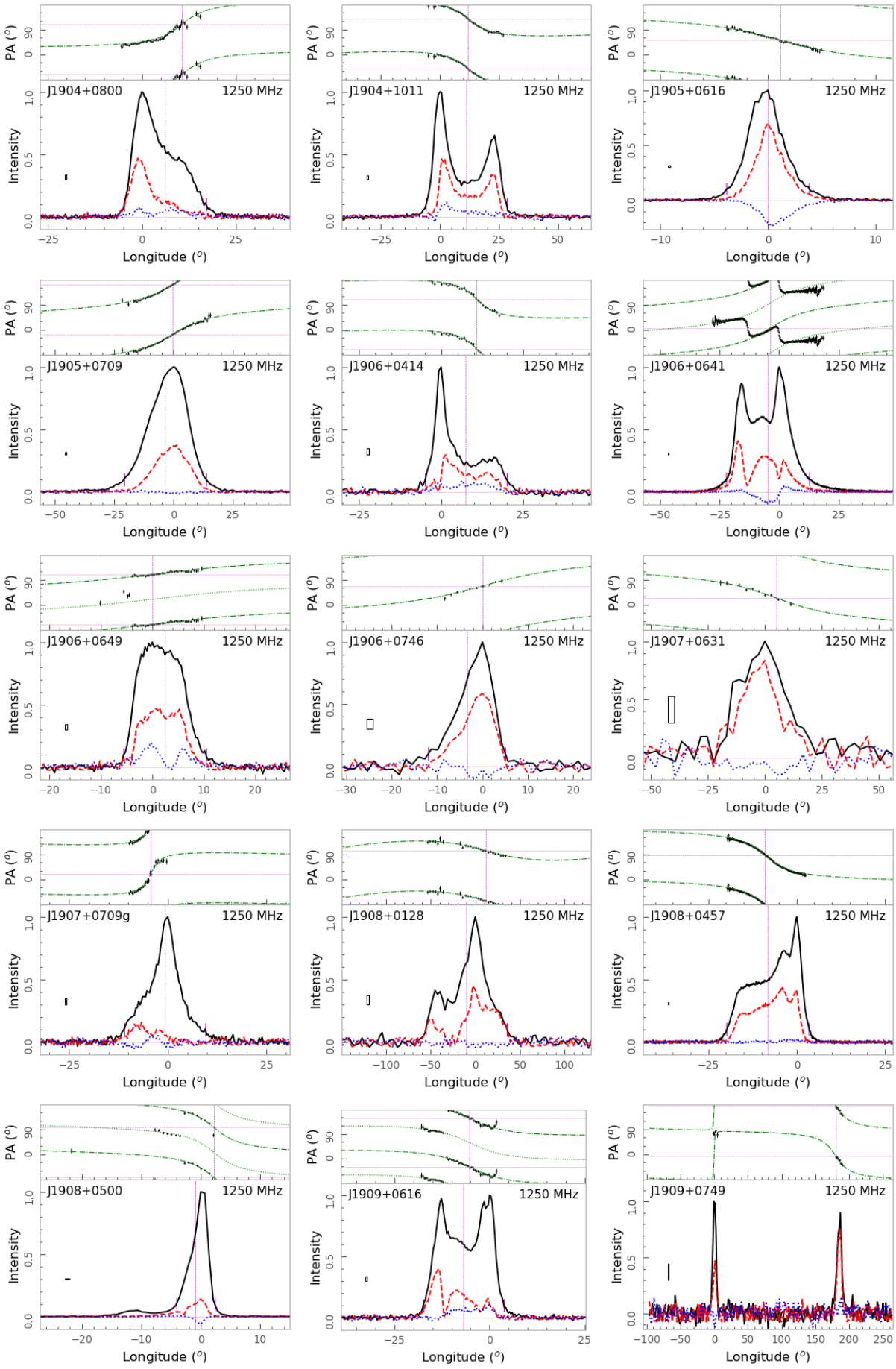

Fig. B.1 *– continued –*

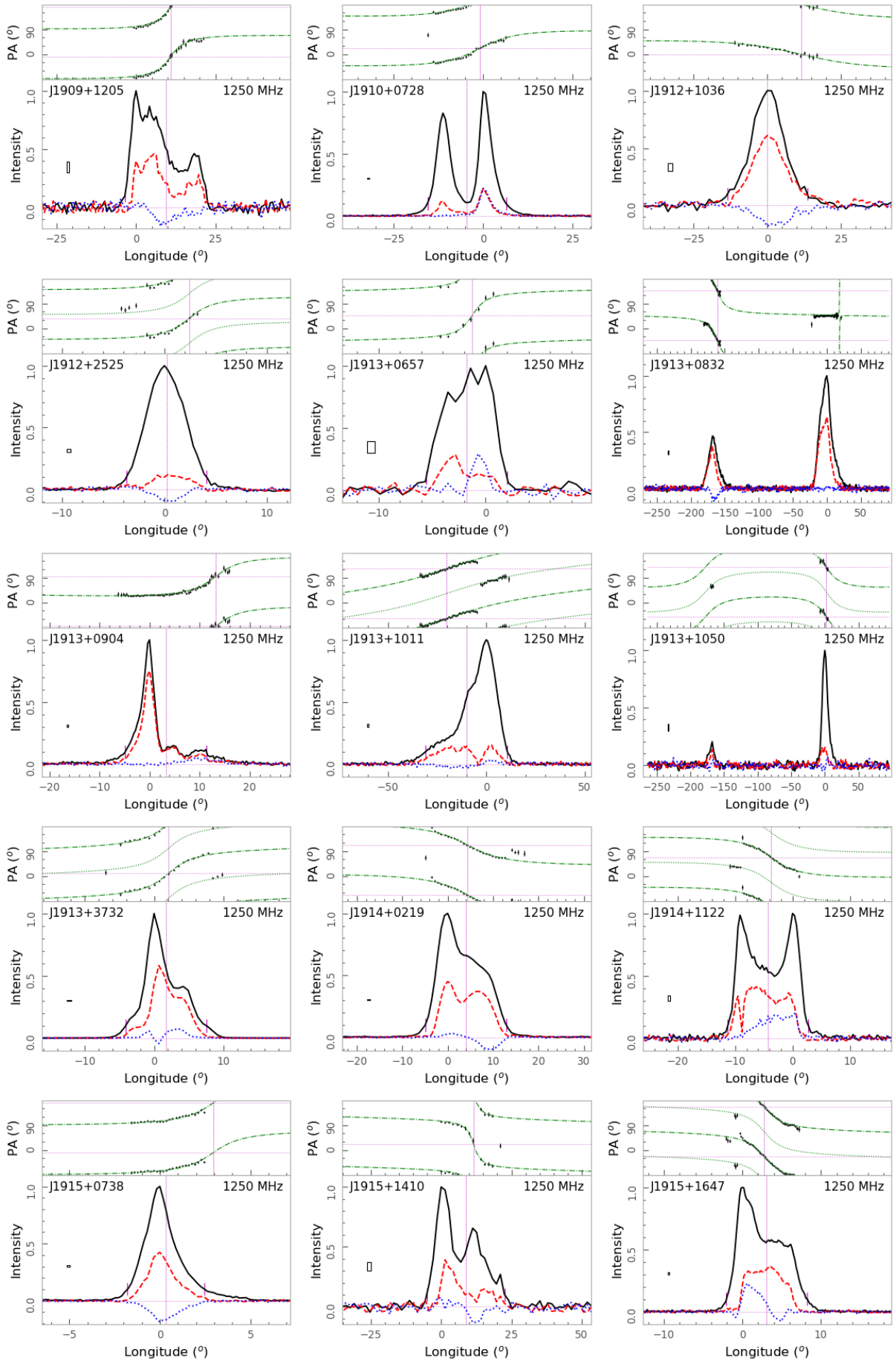

Fig. B.1 *– continued –*

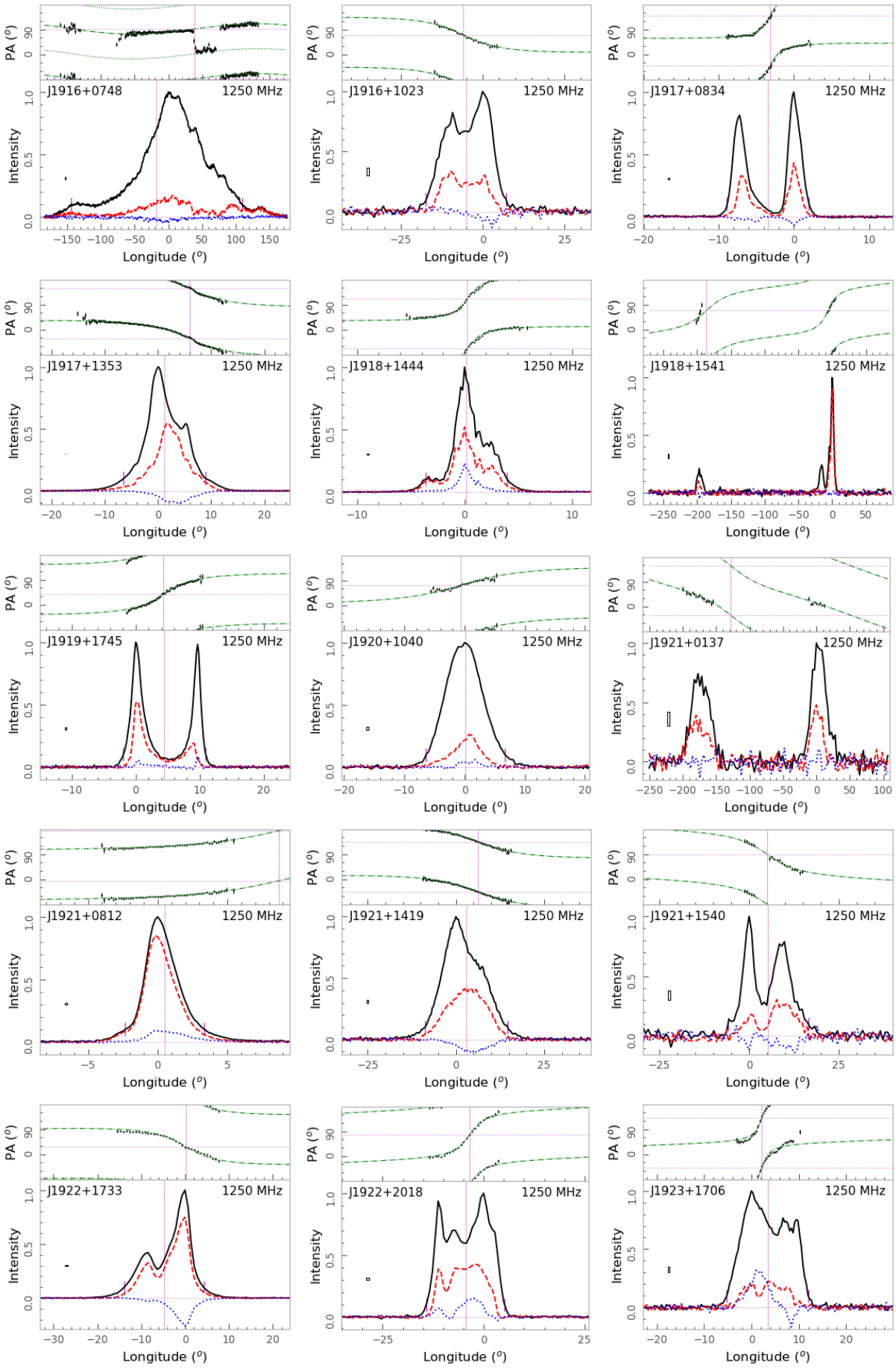

Fig. B.1 *– continued –*

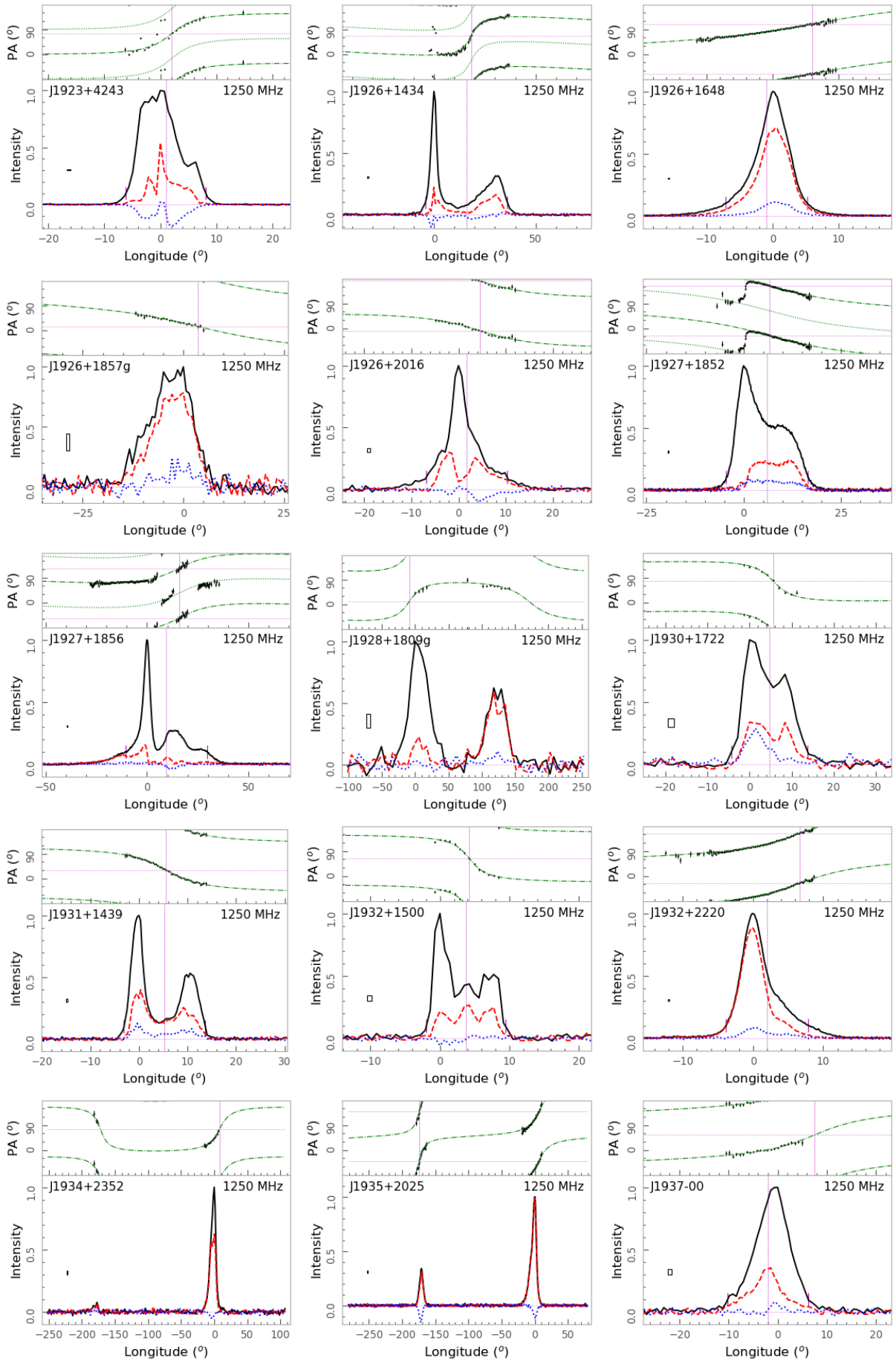

Fig. B.1 *– continued –*

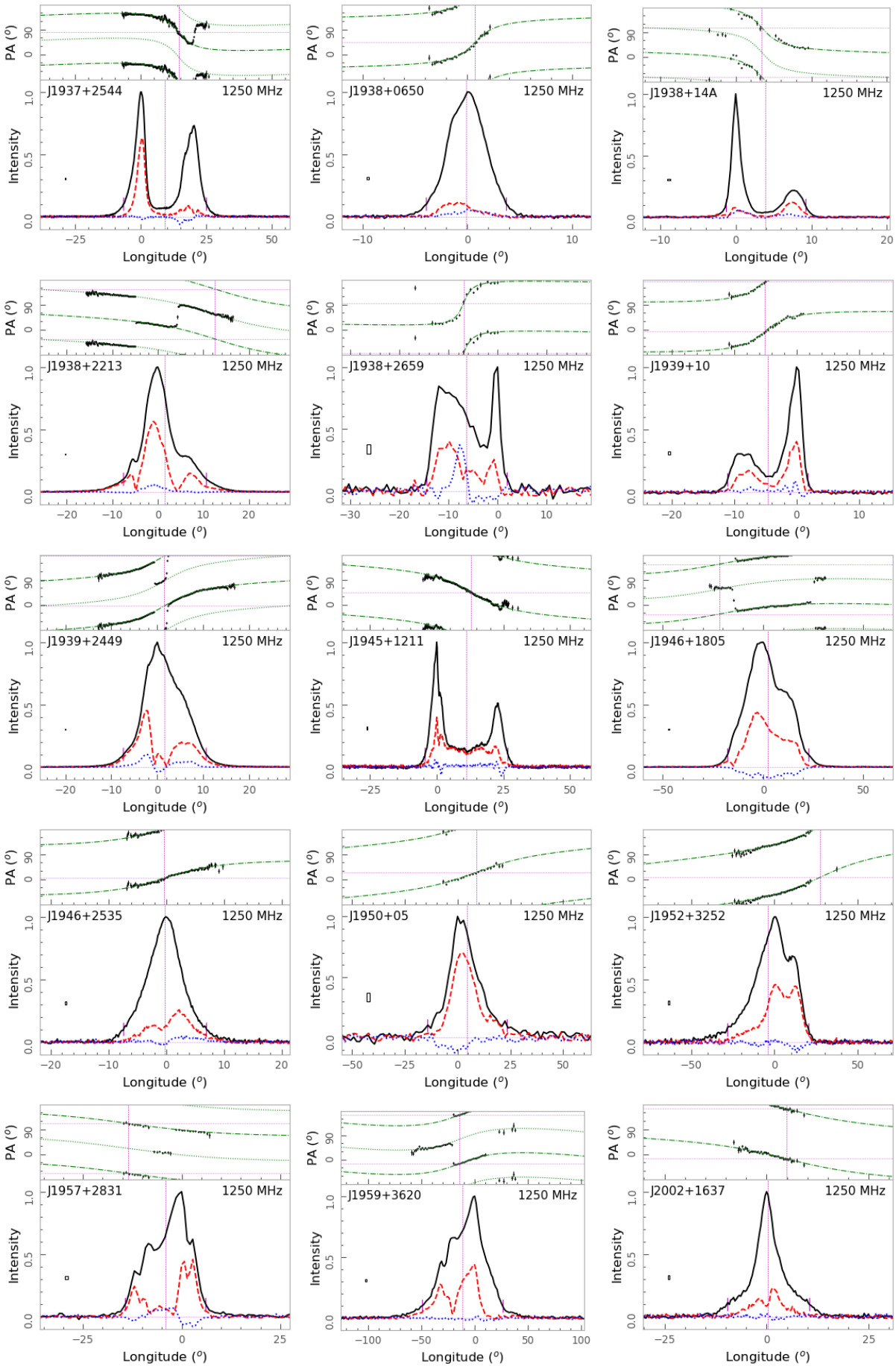

Fig. B.1 *– continued –*

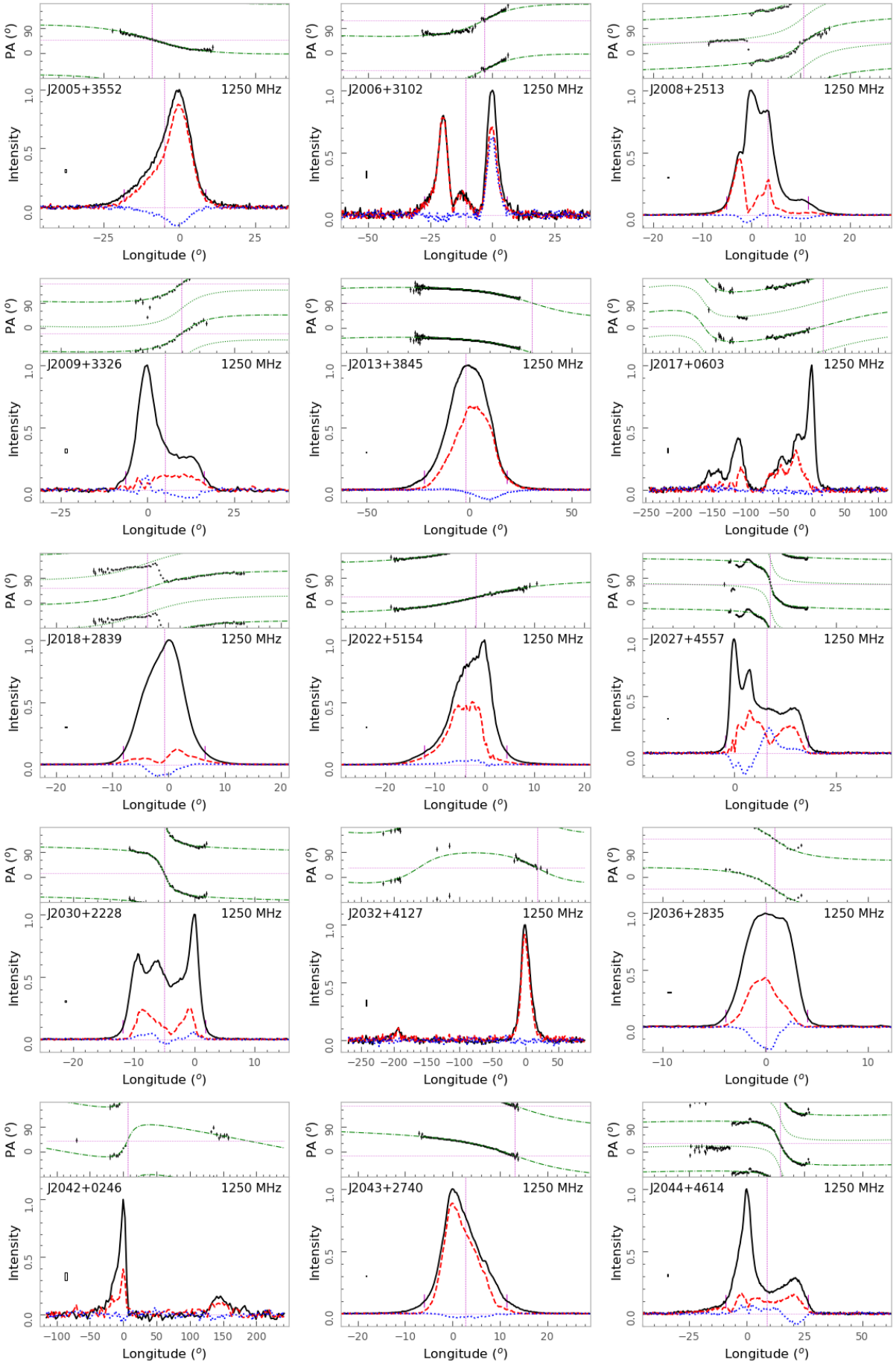

Fig. B.1 *– continued –*

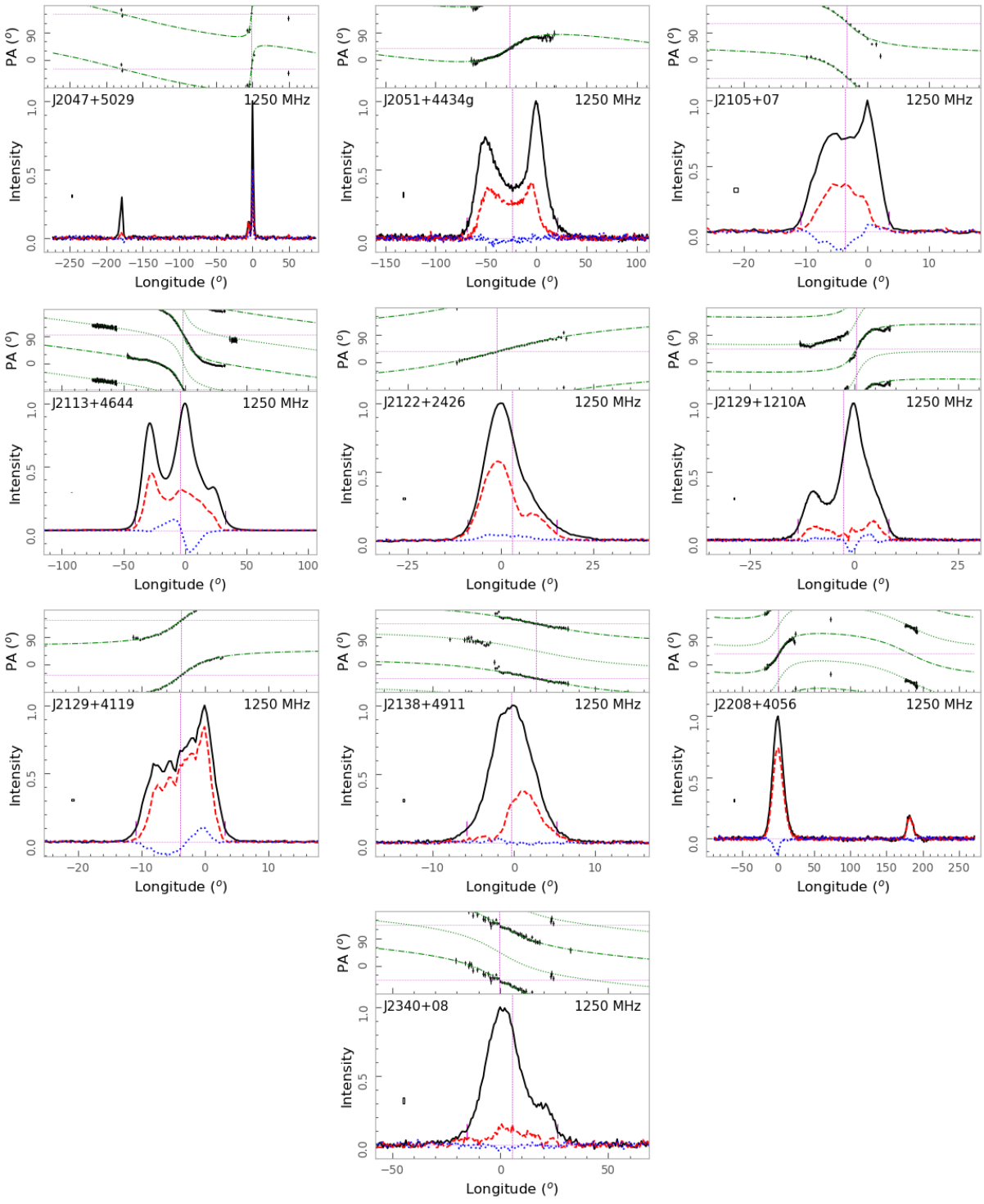
J2047+5029 1250 MHz
J2051+4434g 1250 MHz
J2105+07 1250 MHz
J2113+4644 1250 MHz
J2122+2426 1250 MHz
J2129+1210A 1250 MHz
J2129+4119 1250 MHz
J2138+4911 1250 MHz
J2208+4056 1250 MHz
J2340+08 1250 MHz
PA (°)
Intensity
Longitude (°)

Fig. B.1 – *end.*